Linking Porous Medium Physical Properties to Fluid and Tracer Transport Parameters

Pugliese, Lorenzo

Publication date:
2015

Document Version
Early version, also known as pre-print

Linking Porous Medium Physical Properties to Fluid and Tracer Transport Parameters

Ph.D. Dissertation

Effekt af Porøse Mediers Fysiske Egenskaber på Væske og Gas Transport Parametre

Ph.D. Afhandling

Lorenzo Pugliese

Department of Biotechnology, Chemistry and Environmental Engineering

Section of Environmental Engineering

Aalborg University

December 2013

Preface

The present dissertation, together with seven enclosed articles, is submitted in partial fulfilment of the requirements for obtaining the degree of Doctor of Philosophy (Ph.D.).

The work presented herein was mainly completed at Aalborg University, Department of Biotechnology, Chemistry and Environmental Engineering, where I have been enrolled as a Ph.D. student since December 2010. Laboratory measurements were all performed at the Environmental Engineering Laboratory. The work documented in two papers and the thesis was accomplished at Xi'an Jiaotong - Liverpool University (China), Department of Civil Engineering, during my three-month stay as a visiting Ph.D. student.

This three-year life-changing experience would not have been the same without the support and encouragement of a few pivotal figures. I am deeply indebted to my supervisor, Associate Professor Tjalfe G. Poulsen, for his immense understanding and unlimited help, from both the personal and scientific sides. He provided me with inspirational advice and valuable input, and made my stay in China and the attainment of this work possible. I gratefully acknowledge Assistant Professor Salvatore Straface for kindling the scientific interest in me, and for offering his collaboration in developing new and challenging research objectives. A sincere thanks also goes to the technician Helle Blendstrup, for the assistance in performing lab measurements, and to Kim Mørkholt, for technical support.

To my friends and colleagues, who accompanied me along the curvy paths of this fantastic adventure, I also offer my gratitude; thanks to Antonio, Diana, Elena, Gintare, Ludmilla, Martin, Özgün and Thomas, to Rune for the profitable discussions and fruitful cooperation, to Greta and Mads for assistance while I was abroad. Enormous and everlasting gratitude goes to my family, for constantly encouraging and believing in me. Last but not least, heartfelt thanks to Ania, the primary source of joy in my life.

Suzhou, December 2013

Lorenzo Pugliese

Summary

The need to improve existing concepts and/or investigate new fundamental characteristics of transport in porous media has long generated interest among the scientific community. The reasons for this interest lie in the broad applicability of these concepts for many engineering applications and not only. This Ph.D. project attempts to advance the current knowledge of advective and dispersive transport in granular porous media.

Physical media properties largely influence the transport and thus, a proper choice of medium, may ensure the achievement of specific objectives. Studies available in literature have often highlighted the influence of individual media properties on transport, neglecting therefore the effects generated from mutual linkage between properties. The objective of this study is to provide a better knowledge of the multi-linkage between transport and porous media physical properties. Analyses are performed using multiple granular materials mimicking single and dual porosity media, isotropic and anisotropic media, and media with different particle surface roughness and particle shape.

Pressure loss defines the resistance to fluid flow through porous media, and therefore represents an important physical property of the media. Two of the studies are devoted to investigate gas and water pressure loss in porous media. A new model concept for estimating gas pressure loss as a function of medium physical properties was proposed. In addition, an expression linking pressure loss for gas and water transport in coarse granular filter media, simply based on knowledge about the particle size distribution and particle shape for the medium in question, was presented.

Among the mechanisms governing transport in porous media, dispersion is one of the most important. In this work 4 different studies investigated gas and solute dispersion as related to porous medium properties. A simple model for estimating solute dispersivity from gas dispersivity was presented. In addition, an approach for predicting solute dispersivity using particle size distribution and particle shape, which reduces time consumption for solute measurements, was developed. Analysis of solute dispersion at low pore velocity yielded expressions for predicting solute dispersion as a function of medium properties in this velocity range. Finally, the link between dispersion, porous medium tortuosity, anisotropy ratio and media characteristics was examined.

Dansk resumé

Behovet for at forbedre eksisterende koncepter og/eller undersøge nye grundlæggende karakteristika ved transport i porøse medier har længe skabt interesse blandt forskere. Årsagerne til interessen ligger i den brede anvendelighed af denne viden i forbindelse med mange tekniske applikationer. Dette Ph.D. projekt forsøger at forbedre det nuværende kendskab til advektiv og dispersiv transport i granulære porøse medier.

Porøse mediers fysiske egenskaber har i meget høj grad indflydelse på transport og dermed valg af medie til opfyldelse af specifikke formål. De foreliggende undersøgelser i litteraturen har ofte fremhævet indflydelse af mediers individuelle karakteristika på transport, og har derfor til dels forsømt at undersøge de gensidige kombinations effekter genereret af flere egenskaber på en gang. Formålet med denne undersøgelse er derfor at give et bedre kendskab til disse effekter. Analyserne udføres ved på forskellige enkelt og dobbelt porøse materialer, isotrope og anisotrope materialer, og materialer med forskellig partikel overfladeruhed og partikel form.

Tryktab definerer modstanden mod strømning gennem porøse medier, og er derfor en vigtig fysisk egenskab. To undersøgelser er afsat til at undersøge gas og vand tryktab i porøse medier. Et ny modelkoncept for estimering gastryktabet som en funktion af forskellige fysiske egenskaber er foreslået. Desuden er der udviklet et udtryk som forbinder tryktab for gas og vand transport i grovkornedet filter medier, baseret udelukkende på viden om partikelstørrelsesfordeling og partikel form.

Blandt de mekanismer, der styrer transport i porøse medier, er dispersion en af de vigtigste. I dette arbejde er der via 4 forskellige studier udført undersøgelser af dispersion af gas og opløste stoffer og deres afhængighed af de porøse mediers egenskaber. En simpel model til estimering af dispersivitet for opløste stoffer ud fra gas dispersivitet blev præsenteret. Endvidere blev der udviklet en fremgangsmåde til at forudsige opløste stoffers dispersivitet ud fra partikelstørrelsesfordeling og partikelform, hvilket kan reducere tidsforbruget til målinger. Analysen af opløste stoffers dispersion ved lave pore hastigheder resulterede i et udtryk til at forudsige opløste stoffers dispersionen som funktion af mediets fysiske egenskaber i dette hastighedsområde. Endelig blev sammenhængen mellem dispersion, snoethed, anisotropi og partikelorientering undersøgt.

List of supporting papers

First-authored papers:

I. Pugliese, L., Poulsen, T. G., Andreasen, R. R. (2013). Biofilter media gas pressure loss as related to media particle size and particle shape. Journal of Environmental Engineering ASCE 139(12), 1424-1431.

II. Pugliese, L., Poulsen, T. G. (2014). Linking gas and liquid pressure loss to particle size distribution and particle shape in granular filter materials. Water Air and Soil Pollution 225(1), 1-13.

III. Pugliese, L., Poulsen, T. G., Straface, S. (2013). Gas-solute dispersivity ratio in granular porous media as related to particle size distribution and particle shape. Water Air and Soil Pollution 224(9), 1-12.

IV. Pugliese, L., Straface, S., Trujillo, B. M., Poulsen, T. G. (2015). Relating non-equilibrium solute transport and porous media physical characteristics. Water Air and Soil Pollution 226(3), 1-11.

V. Pugliese, L., Poulsen, T. G. (2014). Estimating solute dispersion coefficients in porous media at low pore water velocities. Soil Science 179(4), 175-181.

VI. Pugliese, L., Poulsen, T. G., Andreasen, R. R. (2012). Relating gas dispersion in porous media to medium tortuosity and anisotropy ratio. Water Air and Soil Pollution 223(7), 4101-4118.

In this dissertation the above papers will be referred to by their roman numerals.

Co-authored paper:

Andreasen, R. R., Pugliese, L., Poulsen, T. G. (2013). Water flow exchange characteristics in coarse granular filter media. Chemical Engineering Journal 221, 292-299.

Table of contents

1. Introduction

1.1 Overview

Transport of gaseous and dissolved compounds in granular porous media occurs in a large number of important applications, such as methane emissions from wetlands and landfills to the atmosphere, oxygen and carbon dioxide movement in passively aerated compost windrows, VOC contaminations, transport and removal of gaseous contaminants in filters for air cleaning, radon and volatile organic contaminant transport into buildings (**Paper VI**), removal of unwanted suspended materials, salt water intrusion into fresh water bodies, movement of minerals in soil, sequestration of CO_2 in saline aquifers, depletion of oil and gas reservoirs, and tracer use in petroleum engineering (Dullien, 1992; Brenner and Edwards, 1993; Sahimi, 1995). Understanding and quantifying the fundamental mechanisms of transport is therefore of utmost importance and essential for developing models able to analyse and optimize these processes.

Porous media typically exhibit a wide range in pore size due to variations in grain size, particle shape, particle orientation, and surface roughness. All these properties largely affect transport, and therefore, expressions must consider the physical characteristics of the particles which constitute the media (Bradford et al., 2002). For example both gas and solute dispersion generally increase with porous medium particle size range, anisotropy ratio, and pore system tortuosity as confirmed by several earlier studies, such as Delgado (2006), Gidda et al. (2006), Bromly et al. (2007), Poulsen et al. (2008), and Sharma and Poulsen (2010a) (**Paper III**). Effects of particle shape on dispersion have also been investigated, showing increasing particle sphericity with decreasing dispersion (Delgado, 2006). Differences of the diffusion coefficients and air permeability were noticed by Osozowa (1998), investigating four different textured soils. Results showed that diffusion is controlled by the air-filled pore space and pore network tortuosity, while the differences in terms of air permeability are caused by the soil pore size distribution and the continuity of large-pore networks. Hamamoto et al. (2009) investigated the effects of average particle size on the diffusion coefficient and on air permeability for six sandy soils under variable saturated conditions. Results showed that particle size markedly affects the effective diameter of the drained pores active in leading gas through the sample. For variable saturated conditions the same authors observed higher values of diffusion coefficient and of the air permeability, due to the rapid gas diffusion and advection through the less tortuous

large-pore network. Among the numerous studies investigating the hydraulic conductivity function, van Genuchten (1980) introduced a closed-form equation which considers the pore-size distribution of a soil. Arya et al. (1999) presented a model to compute the hydraulic conductivity directly from the particle size distribution of a soil. Results showed that the model parameters reflect the effect of pore size, shape, packing density and pore tortuosity. Moreover, in biofiltration by choosing a proper porous medium it is possible to increase active microbial biomass (De Oliveira et al., 2009) and contaminant removal capacity (Sakuma et al., 2006) and to reduce the energy consumption associated with the air flow resistance (Malhautier et al., 2005; Gadal-Mawart et al., 2010) (**Paper I**).

Studies of transport in coarse granular porous media during past decades have mostly been carried out using artificial media, such as glass and plastic spheres, Raschig rings, lead shot, porous pellets, and in general particles having simple spherical, cylindrical, cubic and parallelepiped shapes (Brusseau, 1993; Popovicova and Brusseau, 1997; Delgado, 2006). Thus, knowledge about transport in natural coarse porous media is somewhat limited.

1.2 Objectives

The overall objective of this work is to develop and verify expressions for estimating gas and solute transport parameters. The focal point of the full project is represented by the physical characteristics of the media involved in the studies, such as particle size distribution, particle shape, internal porosity and isotropy/anisotropy. Therefore, the investigation aims to link the media properties to the fundamental mechanisms governing the flow. At present, little is the knowledge available in literature, and a consistent effort is needed in this direction.

The objectives in details are:

- to link pressure loss to particle size and shape in isotropic media (**Paper I**, **Paper II**);
- to relate dispersion to particle size and shape in isotropic media (**Paper III**, **Paper IV**, **Paper V**);
- to describe pressure loss and dispersion in anisotropic media (**Paper VI**).

Chapter 2 contains an overview of the principal mechanisms controlling gas and liquid transport in porous media. To provide the reader with a brief and clear insight of the problem, the most commonly used equations are presented. The following chapter 3 outlines the research strategies,

and particularly the choice of the granular materials. Experimental procedures and results, for each of the six first-authored studies belonging to this thesis, are illustrated in details from chapter 4 to chapter 9. Chapter 10 contains the concluding remarks and a short discussion of the practical implications of these studies, while providing recommendation for further research.

2. Mechanisms controlling gas and liquid transport in porous media

An important issue in environmental science is to understand how chemical and biological substances are transported in porous media. Transport of dissolved or gaseous compounds in porous media is generally governed by three mechanisms: (1) advection caused by fluid pressure gradient within the medium, (2) molecular diffusion caused by concentration gradients, (3) mechanical dispersion caused by spatial variations in the fluid velocity and transport distances at the pore scale.

2.1 Advection

The term advection refers to the transport of a substance due to the fluid's motion, from points of higher to points of lower pressure. Therefore, the driving force is represented by the total pressure gradient, while resistance is caused by viscosity of the liquid and the permeability of the medium. The resistance to the fluid's motion is defined by the pressure loss.

If advection represents the only mechanism affecting the liquid transport into a homogeneous media, the tracer front would move assuming a distinct and sharp concentration. For solutes, differences of the front can be generated by the presence of bacteria or by the presence of negatively charged ions.

2.1.1 Pressure loss

Pressure loss (ΔP), through porous media at low flow velocities, is generally described by Darcy's law (1856), which in one dimension is expressed as:

$$\frac{\Delta P}{L} = \frac{\mu}{k} V \quad (1)$$

where L is the distance (length of the sample) over which the pressure loss takes place [L], k is the permeability of the medium [L^2], μ is the dynamic viscosity of the fluid [M L^{-1} T^{-1}], and V is the superficial flow velocity [L T^{-1}], also known as the Darcy velocity, expressed as:

$$V = \frac{Q}{A} \quad (2)$$

where Q is the volumetric flow [L^3 T^{-1}] and A is the medium cross-sectional area [L^2], perpendicular to the flow direction.

Equation (1) is only valid when inertial forces in the flow field are negligible (which is the case at low flow velocities). At higher flow velocities, when inertial forces are important, the relation between $\Delta P/L$ and V becomes non-linear and it is, in such cases, often described using the Forchheimer relationship (Forchheimer, 1901):

$$\frac{\Delta P}{L} = \frac{\mu}{k} V + \rho C_f V^2 \tag{3}$$

where ρ is the density [M L^{-3}] and C_f is a so-called form coefficient [L^{-1}].

Equation (3) applies for $1 < Re < 100$, where the flow is still laminar but inertial effects become increasingly important with increasing Re. Above Re = 100 (transition regime) Eq. (3) may be used to approximate the $\Delta P/L$ - V relationship although turbulent forces start appearing (Trussell and Chang, 1999; Andreasen and Poulsen, 2013).

Ergun (1952) introduced one of the most widely known and used Forchheimer-based equations, describing fluid flow in porous media. This semi-empirical equation is given as:

$$\frac{\Delta P}{L} = A \frac{(1-\varepsilon_{tot})^2}{\varepsilon_{tot}^p} D_{eq}^{-2} \mu V + B \frac{(1-\varepsilon_{tot})}{\varepsilon_{tot}^p} D_{eq}^{-1} \rho V^2 \tag{4}$$

where A, B and p are empirical constants [-], D_{eq} is an equivalent diameter [L] and ε_{tot} is the total porosity [m^3 m^{-3}]

Ergun (1952) suggested universal values of the empirical constants A, B and p, valid for any fluid and porous medium and equal to 150, 1.75 and 3, respectively. The universal applicability of these values was tested later by Macdonald et al. (1979), on a large set of flow-pressure data, who found that the constants depended on particle shape. Values of A, B and p equal to 180, 1.8 and 3.6 for smooth particles and 180, 4 and 3.6 for rough particles, were identified. Macdonald et al. (1979) used D_{eq} for spherical particles as:

$$D_{eq} = \frac{1}{\sum_i Y_i \left(6 \frac{V_{p,i}}{A_{p,i}}\right)^{-1}} \tag{5}$$

where Y_i, $V_{p,i}$ and $A_{p,i}$ are the volumetric fraction, the particle fraction and the particle surface area of the i´th particle, respectively. As Eq. (5) is only valid for spherical particles, an alternative and universal expression for estimating D_{eq} was considered (Macdonald et al., 1991):

$$D_{eq} = \left(\frac{M_2}{M_1}\right) \quad (6)$$

where M_1 and M_2 are the first and the second order moments of the particle size distribution [M L^2 T^{-2}].

Andreasen and Poulsen (2013) investigated gas $\Delta P/L$ - V relationships for a large set of coarse grained media with uniform particle size distributions originating from the same material (Leca®) using the Ergun (1952) equation. The authors observed that, in these media, $\Delta P/L$ was almost independent of air-filled porosity and therefore suggested that $\Delta P/L$ can be predicted as:

$$\frac{\Delta P}{L} = A{D_{eq}}^{-2}\mu V + B{D_{eq}}^{-1}\rho V^2 \quad (7)$$

where D_{eq} is expressed as:

$$D_{eq} = \frac{2}{\frac{1}{D_m} + \frac{1}{D_{min}}} \quad (8)$$

where D_m and D_{min} are the mean and minimum particle diameter [L].

2.2 Mechanical dispersion

Mechanical dispersion is caused by spatial variations in terms of velocities and distances in a medium. Faster flow characterizes shorter paths, larger pores and central passage of the molecules through the channels (less friction is involved). These differences generate mechanical dispersion, a mechanical mixing and dilution of the solute along the flow path. Particle surface roughness is an additional factor affecting dispersion. Increased surface roughness cause increased turbulence in a gas flow passing across the surface. This generates in turn greater mechanical mixing of the gas stream, which results in increased dispersion (**Paper VI**). Mixing occurring along the direction of the fluid flow is called longitudinal dispersion, while mixing taking place in a vertical place to the direction of the flow is termed transverse dispersion.

For one-dimensional transport, the mechanical dispersion coefficient (D_{mech}) can be expressed as:

$$D_{mech} = u\alpha \quad (9)$$

where α is the mechanical dispersivity in the mobile phase [L] and u is the pore velocity [L T^{-1}], calculated as:

$$u = -\frac{V}{\varepsilon_m} = -\frac{Q}{A\varepsilon_m} \quad (10)$$

where ε_m is the mobile filled porosity [L^3 L^{-3}]. At very low gas flow velocities flow dispersion is negligible and the linear relation (Eq. (9)) does not hold (Delgado, 2006).

Longitudinal dispersivity is generally assumed about 10 times larger than transverse dispersivity, due to the dominant velocity field in the direction of the flow. Delgado (2006) stated that for values of Reynolds number (*Re*) larger than 10, the dispersion coefficient in longitudinal direction is superior to the dispersion coefficient in radial direction by a factor of 5. For low values of *Re* (*Re* < 1), the two coefficients are approximately 0. Throughout this dissertation and all the papers carried out, α only refers to the longitudinal dispersivity.

The relationship between α and transport distance through the porous medium (scale) is often modeled using a power function type model, described as (Neuman, 1990; Schulze-Makuch, 2005):

$$\alpha = CL^e \quad (11)$$

where *C* [$L^{(1-e)}$] and *e* [-] are material specific constants. This means that if α at a given *L*, together with *C* and *e* for a given porous medium are known, values of α at any other *L* for that medium can be calculated. Schulze-Makuch (2005) indicated that *C* is on the order of 0.2 [$L^{(1-e)}$] while *e* varies between 0.5 and 1.

2.3 Molecular diffusion

Diffusion of a solute occurs in response to a concentration gradient, which mainly depends on temperature, viscosity of the solute and size of the particles. In response to this gradient there is a gradual mixing of the solute, which ends when the diffusive equilibrium is reached. Diffusion is typically described by Fick's law.

The importance of diffusion as a controlling parameter for chemical mobilization and transformations, and the important interactions between diffusion-controlled and convection-controlled transport domains have been acknowledged for both gaseous and liquid transport (van Genuchten and Wierenga, 1986; Brusseau, 1991; Moldrup et al., 2001). Consequently, a considerable number of models, predicting gas and solute diffusion coefficients (D_{mol}), have been introduced in literature (Moldrup et al., 2000a; 2000b; Olesen et al., 2001). Differences on these models are based on sieved, repacked and undisturbed soils, and dry or

wetted soils (for gas models). Moldrup et al. (2001) found that D_{mol} in repacked and undisturbed soil only differs a little, and it is typically lower in undisturbed soil, probably because of local-scale zones with higher bulk density (ρ_b) or water content that hinders the diffusive gas flux. For this reason D_{mol} is relatively easy and straight forward to obtain and can be corrected to account for soil tortuosity (τ). Additionally, gas diffusion is the only type of transport mechanism that occurs under isothermal and isobaric conditions making its identification, in different types of soil, less complicated to obtain from laboratory tests.

2.4 Transport modeling in porous media

Models presented in literature and used to describe transport in soil can be grouped in two main categories: (1) those based on an assumed or empirical distribution of pore water velocities and (2) those generated from a specific representation of the pore scale. The first group is the most widely used despite their parameters cannot be measured independently, as they often depend on the scale at which the experiments are carried out. Regarding solute transport, at present no attempts have been made to directly link the distribution of the pore velocity to the characteristics of the pore structure. Model parameters are in this case estimated inversely (Parker and van Genuchten, 1984), or inferred from the hydraulic conductivity/water content function (Scotter and Ross, 1994). Pore geometry models are instead not so widely used, despite the increasing level of attention they generated in recent publications (Perfect and Sukop, 2001).

Gas and solute transport of a tracer through porous media is traditionally described by the advection dispersion equation (ADE), the most widely used velocity distribution model. For one-dimensional transport of a conservative tracer in a column containing a homogeneous porous medium, under assumption of uniform flow and dispersion, in the presence of both a mobile and a stagnant (immobile) phase, the ADE is given as:

$$\frac{\partial C_m}{\partial t} = D_{tot}\frac{\partial^2 C_m}{\partial x^2} + u\frac{\partial C_m}{\partial x} + k(C_{im} - C_m) \tag{12}$$

where C_m and C_{im} are the tracer concentrations in the mobile and immobile fluid phases [M L^{-3}], respectively. D_{tot} is the overall dispersion-diffusion coefficient (L^2 T^{-1}) which takes into account effects of D_{mech}, D_{mol}, and fluid mixing (D_{mix}) in the tubing leading the tracer from the point of introduction to the porous medium column, and from the column to the point of tracer breakthrough

detection (Poulsen et al., 2008). k is the tracer mass transfer coefficient [T^{-1}] between the mobile and immobile phases, and x and t are the space [L] and time [T] variables, respectively.

Limitations of the ADE are represented by its inability to predict the late-time enhancement of tracer arrivals, the need to introduce scale-dependent coefficients (for example hydrodynamic dispersion) and the inability to predict the enhancement of tracer arrivals at early times (Hunt et al., 2011). Already in 1995, Berkowitz and Scher discussed in their work the inadequacy of considering a time-dependent dispersivity in the conventional ADE context, stating that it leads to incorrect solutions. Berkowitz et al. (2000) observed that the Continuous Time Random Walk (CTRW) theory may allow analysis of transport in porous media subject to complex heterogeneities at large scale, which may not be amenable to analysis using the ADE. Cortis and Berkowitz (2004) examined dispersion of a passive tracer in fully and partially saturated porous columns, noticing anomalous early arrival times and late time tailing, which was explained by CTRW theory. These problems are partly investigated in **Paper IV**.

2.5 Operation parameter – Reynolds number

Reynolds number (dimensionless) (*Re*) measures the ratio between the inertial and the viscous forces for given flow conditions. For a porous medium it is defined as:

$$Re = \frac{\rho V D_m}{\mu} \tag{13}$$

Following the classification of Trussell and Chang (1999), in their review of flow through porous media, there are four regimes of flow. The first regime, named Darcy regime, is limited to *Re* below approximately 1. This region is characterized by laminar flow and there is no inertial contribution. The second regime, named Forchheimer regime, is also strictly steady laminar but as the regime progresses, inertial forces become increasingly important. The third regime represents a transition flow, from more or less full inertial conditions to full statistical turbulence, and corresponds to a *Re* of approximately 100. At the lower end of this flow regime, turbulence is just beginning to appear in some of the cells of the porous media. At the upper end of this regime, turbulence is present in the bulk of those cells. Above this region is located the fourth region, which is characterized by full turbulence.

3. Research strategies

3.1 Choice of the materials

The Ph.D. study-focus is the effect of physical particle characteristics on transport in porous media, and particularly pressure loss and dispersion. A fairly large body of literature has been devoted to this issue, but the knowledge is generally limited to soils and, therefore, to small particle sizes. Moreover, investigations reproduced at lab scale are based on artificial media and the knowledge on natural media is somewhat limited.

To fully investigate these aspects and fulfil the research strategies, care was taken in choosing the appropriate materials. The identification was based on the following aspects:

- *particle size* as the applied media should have a particle size distribution which is easily reproducible with high accuracy, and which facilitates the packing that has to be done manually;
- *particle shape* as the applied media should have a particle shape that is representative of natural media;
- *porosity* as the applied media should represent a wide range of porous materials, which have a compact or an internal porous structure.

Most of the studies (except **Paper VI**) were carried out using media constituted by distinct grains, also known as granular media.

"*Granular materials are ubiquitous in nature*
and are the second-most manipulated material in industry (the first one is water)"
– Patrick Richard –

Overall, the following materials were used:

- *crushed granite*, characterized by an irregular and very angular particle shape, and a compact internal structure;
- *gravel*, constituted of rounded rock fragments with a compact internal structure;

- *Light Expanded Clay Aggregates* (Leca®), which has a spherical shape and exhibits an internal porous structure very much like soap foam;
- *pebbles*, characterized by spherical shape and a compact structure;
- *slate chips*, defined by parallelepiped shape and a compact structure;
- *wood chips (Pinus sylvestris*) which represent dual porosity aggregates and have an aggregate shape (parallelepiped) allowing for packing configurations with different tortuosity and anisotropy.

An overview of the particles used in all the papers is given in Fig. 1.

Figure 1. *Selected particles utilized in all the studies. From left to right: crushed granite, gravel, Leca®, pebbles, wood and slate chip.*

3.1.1 Particle size

A key aspect affecting transport in packed beds is the effect of the porous medium structure. In large particle size distributions, the small particles accumulate in the small interstices between the large particles, generating therefore lower porosity.

"*The grain size distribution of a soil*
determines the governing particle-level forces,
inter-particle packing and the ensuing macroscale behaviour"
– Santamaria and Cho –

Crusched granite, gravel and Leca® were initially sieved into 6 particle size fractions with uniform particle size distributions. Each of these fractions was characterized by a particle size range (R) of 2 mm, in the range between 2 and 14 mm. Particle diameters (D) were $2 \leq D < 4$, $4 \leq D < 6$, $6 \leq D < 8$, $8 \leq D < 10$, $10 \leq D < 12$, and $12 \leq D < 14$ mm corresponding to a D_m of 3, 5, 7, 9, 11, and 13 mm respectively. Additional fractions with R = 4 mm (D_m = 4, 6, 8, 10, 12 mm), R = 6 mm (D_m = 5, 7, 9, 11 mm), R = 8 mm (D_m = 6, 8, 10), R = 10 mm (D_m = 7, 9), and R = 12 mm (D_m = 8), with uniform particle distributions, were produced by combining appropriate quantities of the 6 R = 2 mm fractions. Uniform particle size distributions were chosen to ensure well defined distributions across all 63 particle size fractions (21 for each material) (**Paper I**).

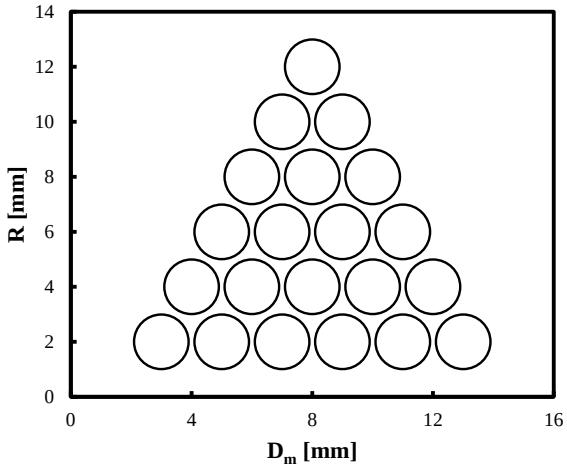

Figure 2. *Particle size range (R) and mean particle diameter (D_m) for the 21 particle size fractions used or partly used in all papers, except* ***Paper VI***.

Rounded pebbles, slate and wood chips were screened, and all particles able to pass an 18 mm but retained by a 10 mm sieve (average overall particle diameter 14 mm) were selected for the experiments. This specific particle size range was selected as a trade-off between facilitating ease of packing, which had to be done manually, one particle at a time, and having a particle size that

would still mimic relevant natural and man-made systems such as aggregated soils, weathered or fractured rock, various biofilters and building materials.

3.1.2 Particle shape

Particle shape influences many physical properties of porous materials such as void ratio, internal friction angle, and air permeability (Rouse et al., 2008; **Paper I**).

Particle shape irregularities are established at 3 different scales:

- the global form (sphericity rather than ellipticity or platiness);
- the scale of major surface features (roundness versus angularity);
- the scale of surface roughness (smoothness in opposition to roughness).

Sphericity is quantified as the diameter ratio between the largest inscribed and the small circumscribing sphere (Fig. 3). Roundness is defined as the average radius of curvature of surface relative to the radius of the maximum sphere that can be inscribed in the particle. Both properties can be estimated by visual comparison, using charts (Barrett, 1980). On the contrary, measurements of roughness are cumbersome. In fact the fractal nature of rough surfaces implies lack of characteristic scale (Santamarina and Cho, 2004).

In this work particle shape was taken into account by estimating roundness of the particles, following two very widely applied approaches: Pentland (1927) and Wadell (1935). This procedure was carried out only for crushed granite, gravel and Leca®.

Pentland (1927) defined the roundness as:

$$\varphi_p = \frac{\omega}{\omega_p} \tag{14}$$

where φ_p denotes the total degree of roundness [-] based on Pentland (1927) which cannot be greater than 1, ω is the cross-sectional or projection area of the grain [L^2] and ω_p is the area of the circle having the largest diameter of the grain [L^2]. The orientation of the particles was not definite.

Wadell (1935) defined the roundness as:

$$\varphi_w = \frac{N}{\sum_N \left(\frac{\mathcal{R}}{r_N}\right)} \tag{15}$$

where φ_w denotes the total degree of roundness [-] based on Wadell (1935), N is the number of corners in the given plane of the particle, $\mathcal{R}$ the radius of the largest inscribed circle [L] and r_N the radius of the inscribed circle [L] of the N^{th} corner of the particle in the plane.

For the evaluation of φ_p and φ_w, 30 particles were randomly selected from each of the three materials (5 particles for each of the 6 R = 2 mm fractions). For all granite and gravel, particle projections of particle shape onto a flat surface were carried out in three perpendicular planes. For Leca® projections were only carried out in one plane as particle shape was observed to be very similar in all planes. Values of ω and ω_p, and consequently φ_p (Eq. (14)) were subsequently determined from the projections. Values of $\mathcal{R}$ and r_N, and consequently φ_w (Eq. (15)), were determined by selecting the two sharpest corners of each projection (N = 2), and analysed using a circle scale (concentric circle protractor, Fig. 4) as proposed by Wadell (1935). Average values of φ_p and φ_w were then calculated for each material across the 6 R = 2 mm particle size fractions.

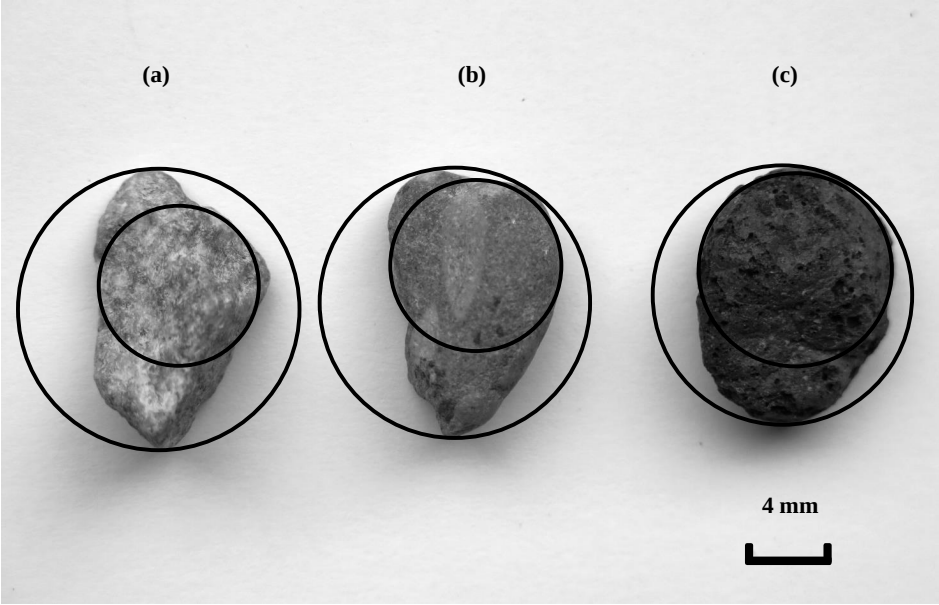

Figure 3. *The circumscribed and inscribed circles of the smallest and largest cross-sectional area, for* **(a)** *crushed granite,* **(b)** *gravel, and* **(c)** *Leca®.*

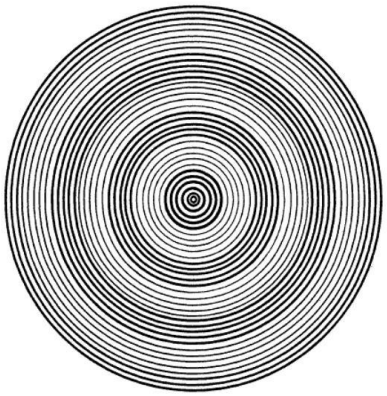

Figure 4. *Reproduction not in scale of Wadell's concentric circle protractor, with circle-scale of 2 mm (Riley, 1941).*

3.1.3 Particle orientation

Particle orientation assumes fundamental importance in the evaluation of anisotropy, and not only. Examples of anisotropic media are wood and soils, and also layered minerals such as slate. Being most of the porous materials anisotropic, particle orientation emerges as a significant parameter which needs a proper characterization. Therefore, part of our attention in this work is devoted to investigate the relationship between transport and particle orientation.

Coutelieris (2002) investigated the effect of geometry and axial orientation of spheroidal particles on the adsorption rate in a granular porous medium. The author found that the oblate geometry offers significant advantage for capturing the diluted mass compared with the prolate one, even in strongly convective environments. Baenninger et al. (2006) introduced a model which was able to use cross-sectional images of scattering media and to describe the effect of particle orientation.

Effects of particle orientation were analysed using only rounded pebbles, slate and wood chips (**Paper VI**). For slate and wood chips three separate columns were packed each with a different particle orientation. The columns were packed with the L_1, L_2 or L_3 dimensions being oriented vertically (in the direction of flow), while the other two particle dimensions were oriented randomly in the horizontal plane. Thus, the anisotropy tensor of the materials in each of the three columns

was two dimensional. The particle orientations were labelled A (particle dimension L_1 being vertical), B (dimension L_2 being vertical), and C (dimension L_3 being vertical). All columns were packed by manually placing each single particle, one at a time, with the correct spatial orientation. Three additional columns were packed using pebbles, slate and wood chips, respectively, with the particles randomly oriented in all three spatial dimensions (labelled D). These columns therefore contained isotropic media. For columns with particle orientation D, particles were not packed one at a time but instead poured into the column to achieve random orientation of particles in all spatial directions. All columns were packed taking care to achieve homogeneous packing and to reduce differences in ρ_b between particle orientations A, B, C, and D for each material as much as possible. An illustration of two selected particle orientations, for slate and wood chips, is given in Fig. 5.

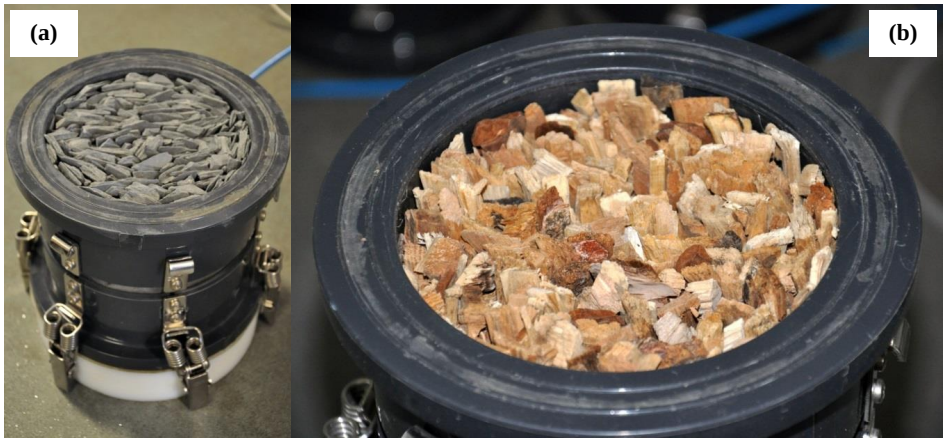

Figure 5. *Illustration of* **(a)** *slate chips, orientation B and* **(b)** *wood chips, orientation A.*

4. Gas pressure loss as related to coarse granular media particle size and particle shape

4.1 Experimental procedure

Measurements in **Paper I** were performed by packing each of the 21 particle size fractions for each of the three materials (crushed granite, gravel and Leca®) into a clear acrylic column of 100 cm in length and 14 cm inner diameter. This column size was chosen in order to avoid effects of preferential flow along the column walls, which may occur if column diameter is too small, compared to the average particle diameter. Great care was taken to achieve a uniform packing (especially along the length of the column), to reduce variations in ρ_b. Measurements of ΔP were carried out for each of the 63 particle size fractions following the approach of Pugliese et al. (**Paper VI**). Columns were fitted with a polyethylene lid and sealed with a rubber O-ring at the bottom. A stainless steel mesh with 2-mm openings and 1-mm thickness was installed to maintain a distance of 10 mm between the lid and the porous medium. The top of the column was kept open to the atmosphere while the bottom was connected to a supply of compressed atmospheric air via a valve and a precision ball flow meter (model P450; Porter Instruments). Soft Teflon tubing with an inner diameter of 4 mm was used to connect system components. Corresponding values of ΔP and V across the columns were measured for V = 0.005, 0.010, 0.016, 0.021, 0.032, 0.043, 0.054, 0.065 m s^{-1}, equal to Q = 5, 10, 15, 20, 30, 40, 50 and 60 l min^{-1} respectively. The relatively wide Q-range was chosen to get more reliable determination of the ΔP - V relationships for the different media. An Alnor AXD 560 digital manometer (Alnor, Ontario Canada), connected to the bottom and the top of the column, was used to measure ΔP. Measured ΔP values were corrected for the pressure drop across the empty column with the metal mesh in place. All experiments were carried out in duplicate.

4.2 Results

Measured $\Delta P/L$ - V relationships, for all materials and particle size investigated, follow a second order polynomial, thus, being consisted with Eq. (3). $\Delta P/L$ generally decreased with increasing average particle size with the 2-4 mm fractions having the highest ΔP, and the 12-14 mm fractions the lowest. This is a direct consequence of increasing pore size for the more coarse grained

materials. For identical particle size fractions, crushed granite generally yielded the highest *ΔP/L* while Leca® yielded the lowest values of *ΔP/L*, despite the fact that granite has a higher external (active) air-filled porosity compared to Leca® (Fig. 6). In fact for the three materials considered in this study, *ΔP/L* was inversely correlated with active air-filled porosity in contrast to Eq. (4).

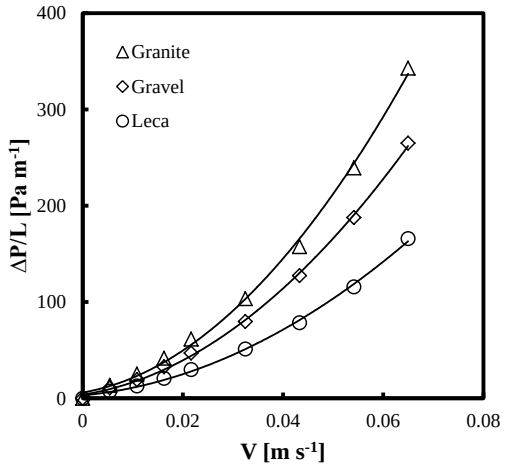

Figure 6. *Selected values of ΔP/L as a function of V for the 2-4 mm particle size fraction, for the three materials (crushed granite, gravel and Leca®) investigated in this study.*

This supports the findings of Andreasen and Poulsen (2013) who observed that *ΔP/L* was independent of active air-filled porosity across a wide range of Leca® particle size fractions. These authors, therefore, suggested to base models for predicting *ΔP/L* in coarse grained (2-18 mm) granular materials on *D* rather than air-filled porosity. This is likely because active porosity in fine grained materials (< 2 mm), for which Eq. (4) was originally developed, has a very different structure due to instance cracks and formation of aggregates compared to coarse grained materials such as those investigated here. Gravel exhibited intermediate *ΔP/L* compared to Leca® and crushed granite. The results for granite and gravel *ΔP/L* were 1.24 and 1.19 times larger than those for the Leca® on average across all particle size fractions, respectively. In general the relative differences

in $\Delta P/L$ between the three materials were most prominent for the fractions containing smaller particles.

The principal difference between the three materials considered in this study is their particle shape (as characterized by roundness). Therefore, the deviations in $\Delta P/L$ between the three materials likely result from the differences in φ, which was determined using Pentland (Eq. (14)) and Wadell (Eq. (15)) approaches. Flow in materials consisting of rounded particles (Leca®) should be expected to be more laminar and less subject to inertial forces than flow in materials consisting of more angular (less spherical) particles such as crushed granite. In **Paper VI** was observed that, in two materials with identical particle size distributions but different particle shapes (pebbles with high roundness and slate chips with low roundness), α diminished with decreasing particle roundness. This behaviour was, therefore, attributed to the difference in particle shape. It was further observed an inverse linear proportionality between α and $\Delta P/L$ under otherwise identical conditions. Thus, $\Delta P/L$ was observed to increase with decreasing particle roundness supporting that the differences in $\Delta P/L$, observed between the three materials used here, stems from differences in particle shape.

The model (Eq. (7)), suggested by Andreasen and Poulsen (2013) for predicting the $\Delta P/L$ - V relationships in materials with uniform particle size distributions (developed only for 36 Leca® particle size fractions) was tested against the $\Delta P/L$ - V values measured in this study, for all three materials (1008 data points). The test was performed by fitting Eq. (7) to the measured data using the model constants A and B as fitting parameters. The relative deviation between measured and fitted $\Delta P/L$ values as a function of the measured $\Delta P/L$ is upward concave such that the model tends to over predict at low and high values of $\Delta P/L$, and under predict at intermediate $\Delta P/L$. Figure 7 shows this behaviour for the 2-4 mm particle size fraction and for all three materials.

This behaviour was actually not seen only for the three data sets as a whole but also for the individual particle size fractions of each material, and tended to be most prominent for particle size fractions containing mainly small or large particles. The reason is that the model (Eq. (7)) is not able to fully capture the non-linear relationship between $\Delta P/L$ and V for the materials. As the curvature of the modeled $\Delta P/L$ - V relationship by Eq. (7) is not only controlled by the empirical constants, A and B, but also by the value of D_{eq}, it is likely that a more optimal choice of expression for D_{eq} may improve model results.

Andreasen and Poulsen (2013) proposed that D_{eq} may be predicted as the harmonic mean of D_{min} and D_m present in each particle size fraction (as given by Eq. (8)), thus D_{min} and D_m are weighted equally in the prediction of D_{eq}.

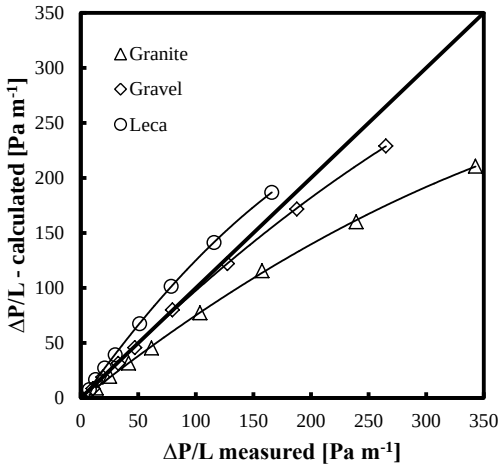

Figure 7. *Calculated (Eq. (7)) versus measured ΔP/L - V values, for the 2-4 mm particle size fraction and for all materials (crushed granite, gravel and Leca®) investigated in this study.*

Earlier studies, however, have suggested that the characteristics of granular materials might be predicted using the particle diameters corresponding to the 10% and 60% fractiles of the particle size distribution, D_{10} and D_{60}, respectively. These particle diameters will also be applicable to non-uniform particle size distributions, while this is not possible when using Eq. (8) as D_{min} is often not known for non-uniform particle size distributions. Thus, the choice of D_{min} and D_m (corresponding to D_0 and D_{50}) for predicting D_{eq} is likely not the optimal choice. It is also well-known that for a given medium consisting of a mixture of particles of different diameters, the smaller particles have a larger impact on $\Delta P/L$ than large particles. Therefore, weighting the two diameters equally in the D_{eq} prediction as done in Eq. (8) may not be the optimal approach.

Therefore, a new expression for D_{eq}, valid across different materials, was introduced:

$$D_{eq} = \frac{1}{\left(\frac{a}{D_{10}}+\frac{1-a}{D_{60}}\right)} \quad (16)$$

where a is a weighting factor $0 < a < 1$ and D_{10}, D_{60} [L] are the particle diameters at which 10% and 60% of the material mass consists of particles with a smaller diameter, respectively. Replacing Eq. (8) with Eq. (16) in Eq. (7) yields:

$$\frac{\Delta P}{L} = A\left(\frac{1}{\frac{a}{D_{10}}+\frac{1-a}{D_{60}}}\right)^{-2}\mu V + B\left(\frac{1}{\frac{a}{D_{10}}+\frac{1-a}{D_{60}}}\right)^{-1}\rho V^2 \quad (17)$$

Equation (17) was therefore fitted to the measured *ΔP/L* - *V* data for all three materials using A, B, and *a* as fitting parameters. Six different fitting approaches were tested: 1) values of A, B, and *a* were fitted individually for each of the three materials (a total of 9 fitting parameters), 2) A and B were fitted individually for each material while one common value of *a* across all three materials was used (7 fitting parameters), 3) A was fitted individually for each material while common values of B and *a* were used (5 fitting parameters), 4) B was fitted individually for each material while common values of A and *a* were used (5 fitting parameters), 5) *a* was fitted individually for each material while common values of A and B were used (5 fitting parameters), 6) Common values of A, B, and *a* were used (3 fitting parameters). Figure 8 shows predicted *ΔP/L* values using individual A, B, and *a* parameters for the different materials (Approach 1).

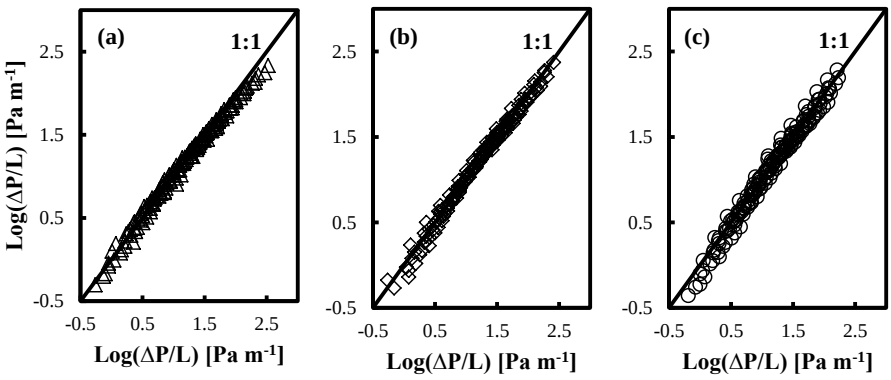

Figure 8. *Predicted (Eq. (17) with* A, B *and a fitted individually for each material) versus measured Log* (*ΔP/L*) *values, for* **(a)** *crushed granite,* **(b)** *gravel, and* **(c)** *Leca®.*

The results indicate that all three parameters A, B and a are related to φ, but it is likely not the only controlling factor or it may be that φ is not the optimal parameter for characterizing particle shape. The reason is that particles of different shapes may exhibit similar φ. It is also likely that particle characteristics such as surface roughness affects $\Delta P/L$ and thereby the values of A, B and a. Measurement of particle surface roughness on non-spherical particles remains a challenge due to the difficulty in distinguishing particle angularity and particle surface roughness as these two characteristics have similar impact on ΔP.

The data, for the 6 different approaches, indicate that despite the differences in particle shape among the three materials investigated here, it is not necessary to use individual values of A, B, and a for each material in order to avoid significant loss of accuracy. The results further indicate that a value of a = approximately 0.7 together with either individually calibrated values of A for each material or individually calibrated values of B do not result in significant loss of accuracy. Thus, effects of particle shape can be included via either A or B. This means that Eq. (17) with $2 + n$ empirical parameters appears sufficient to predict $\Delta P/L$ across different particle size fractions for n different materials with different particle shape, as long as the particle size distributions of the individual particle size fractions have the same shape. It is very likely that at least some of the empirical parameters A, B and a depend on the shape of the particle size distributions considered.

5. Linking gas and liquid pressure loss to particle size distribution and particle shape in granular filter materials

5.1 Experimental procedure

A total of 63 particle size fractions (21 for each material) were used in the analysis: crushed granite, gravel and Leca®. Air and water flow rates were selected to cover approximately the same range of Re ($0 \leq Re \leq 125$). All measured $\Delta P/L$ values were corrected for the empty column pressure loss (with the metal mesh in place).

Gas measurements of $\Delta P/L$ - V ($\Delta P_g/L$ - V_g), conducted using air, were taken from **Paper I**. Liquid measurements ($\Delta P_l/L$ - V_l), conducted using water and the same set-up as the one utilized in **Paper I**, were carried out in duplicate and under constant head conditions. The bottom of each column was connected to a constant-head water tank, in turn connected to a water reservoir via a pump (model E BS 5000 PT11 230V, Flojet, Hoddesdon, UK). The flow through the column was controlled by changing the elevation of the constant head tank. Prior to measurements columns were saturated from the bottom over a period of 30 minutes to achieve equilibrium. Values of V_l were determined by collecting the effluent water from the column over a given period of time followed by weighing. Corresponding values of $\Delta P_l/L$ were determined from the elevation of the water surface in the constant head tank. For each column one set of $\Delta P_l/L$ - V_l data, covering 8 water flow rates, was collected. Columns were subsequently drained and repacked, and another set of $\Delta P_l/L$ - V_l measurements was carried out. For Leca®, which has a very low ρ_b, a stainless steel mesh was also used at the top of the columns to prevent loss of material via the outlet.

5.2 Results

The $\Delta P/L$ - V and $\Delta P/L$ - Re relationships for both air and water flow all followed second order expressions, in agreement with Eq. (3). Selected $\Delta P/L$ - Re are shown in Fig. 9, for both air and water measurements. Values of Re range up to 60 and 125 for air and water measurements, respectively, covering the laminar ($Re < 1$), Forchheimer ($1 \leq Re < 100$) and part of the transition ($Re \geq 100$) flow regime (Trussell and Chang, 1999).

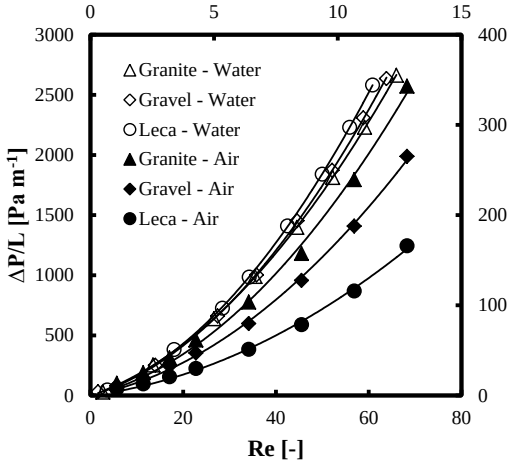

Figure 9. *Selected ΔP/L values as a function of Re for air measurements belonging to the 2-4 mm particle size fraction (filled in data points) and for water measurements belonging to the 2-14 mm particle size fraction (empty data points).*

As expected, $\Delta P/L$ decreases with increasing particle size for fixed values of *Re* (or *V*) across all three materials. For both fluids there is a tendency that $\Delta P/L$ depends on the material type. For air flow, granite (the most angular material) generally exhibits the highest $\Delta P/L$ values for fixed *Re* and particle size distribution (fixed *R* and D_m). For water flow, however, Leca® (the most rounded material) shows the highest values of $\Delta P/L$ although the tendency is much weaker than for the air flow data. The reason is likely that φ affects the flow field and thus $\Delta P/L$. Because the flow fields for air and water in the same medium are not identical (Schjonning, 1986; Riley and Ekeberg, 1989; Loll et al., 1999), particle shape does not affect the flow of the two fluids in the same manner, thus, the difference. That particle shape may affect fluid transport properties in porous media was documented by Pugliese et al. (**Paper VI)**, who observed a dependency between fluid dispersion and φ, thus, supporting the findings.

Individual values of D_{eq} for each of the 63 particle size fractions for both air and water, were determined by fitting Eq. (7) to the measured data using common optimized values of A and B across all materials, particle size fractions and fluids. For all six combinations of fluid and material

(particle shape), D_{eq} increases strongly with D_{10}, and to some degree also with D_{60} - D_{10} although this relation is much weaker than with D_{10}. This indicates that D_{eq} mainly depends on the diameter of the smallest particles in each medium and much less on the total range of particle diameters present in each of the 63 particle size fractions used. For air flow D_{eq} values range from 0.002 to 0.016 m, while for water flow values range from 0.002 to 0.003 m. This is in agreement with earlier findings of Schjonning (1986), Riley and Ekeberg (1989), and Loll et al. (1999) and supports the earlier discussed suggestion that the flow fields of the two fluids are different even under otherwise identical conditions. In general the water D_{eq} data exhibit more scatter, likely because $\Delta P_l/L$ - V_l relationships are more difficult to measure accurately.

Individual values of $D_{eq,l}$ were plotted against $D_{eq,g}$, showing the same general trend. Therefore, an exponential expression was chosen to model the $D_{eq,l}$ - $D_{eq,g}$ relationship as:

$$D_{eq,l} = b\left(1 - e^{(-c*D_{eq,g})}\right) \tag{18}$$

where b [L] and c [L^{-1}] are fitting parameters. As optimal values of b for all three materials were not significantly different, one common value of b but individual values of c for each of the three materials were used in the modeling. It is seen that the value of c is related to φ, such that the most rounded particles (Leca®) exhibit the lowest value of c. This again confirms that particle shape does have a marked influence on fluid flow through porous media.

Overall, Eq. (18) is able to achieve a good fit to the data as illustrated in Fig. 10, showing values of $D_{eq,l}$ versus corresponding values of $D_{eq,g}$. The data in Fig. 10 suggest that, if $D_{eq,g}$ for a given medium is known, it is possible to calculate the corresponding $D_{eq,l}$ using Eq. (18) and subsequently the $\Delta P_l/L$ - V_l relationship using Eq. (7).

The feasibility of predicting $\Delta P_l/L$ - V_l from the $\Delta P_g/L$ - V_g in the same medium was tested using six different approaches. All approaches are based on Eq. (7). However, different assumptions are made with respect to the estimation of parameters A, B, and D_{eq}. Approach 1 (Fig. 11(a)) strongly under predicts $\Delta P_l/L$ for almost all 63 media. There is a fair amount of scatter in the $\Delta P_g/L$ data and the approach has a tendency to overestimate $\Delta P_g/L$ for Leca® and underestimate for gravel and granite. This clearly shows that this approach is not capable of taking effects of fluid and medium properties into account. Approach 2 (Fig. 11(b)) improves prediction of $\Delta P_l/L$ somewhat, which result overestimated for the fine grained media but underestimated for the coarse grained media. For $\Delta P_g/L$ the prediction accuracy is somewhat lower than for approach 1.

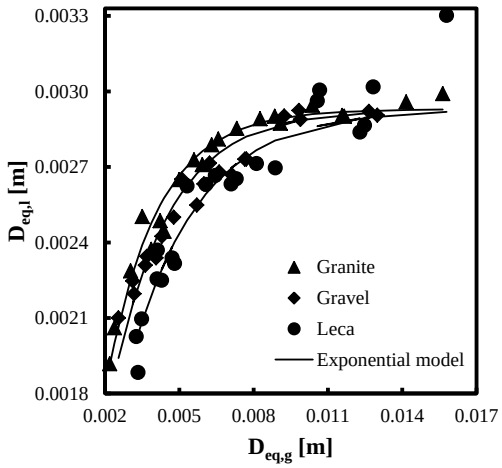

Figure 10. *Fitted values of $D_{eq,l}$ and $D_{eq,g}$ based on Eq. (18), for crushed granite, gravel and Leca®.*

Approach 3 (Fig. 11(c)), based on individually fitted values of D_{eq} for each medium and fluid combination, yields the best prediction accuracy for both $\Delta P_g/L$ and $\Delta P_l/L$. To use this approach in practice, knowledge of $D_{eq,g}$ and $D_{eq,l}$ for the medium in question plus the two empirical constants A and B are required as compared to three empirical constants (A, B, and *a*) for approach 1 and 2. Figure 11(c), however, does show the importance of accurate D_{eq} estimates for successful predictions of $\Delta P_g/L$ and $\Delta P_l/L$. Values of A, B can be established based on measurements of $\Delta P_g/L$ - V_g and/or $\Delta P_l/L$ - V_l in a limited set of media with a given φ. Hereafter estimates of any $\Delta P_g/L$ - V_g and $\Delta P_l/L$ - V_l value in any other medium with the same particle shape can be evaluated based on a limited set of $\Delta P_g/L$ - V_g and $\Delta P_l/L$ – V_l measurements in the medium of interest. Approach 4 (Fig. 11(d)) decreases the prediction accuracy somewhat compared to approach 3 as this approach only uses individually fitted values of $D_{eq\ g}$ together with 6 empirical constants (3 *c* values plus A, B and *b*). To use this approach in practice, knowledge of $D_{eq,g}$ as well as the empirical parameters A, B, *b* and *c* for the medium in question is required. Approach 5 (Fig. 11(e)) yields prediction accuracies that are comparable to approach 4, despite $\Delta P_g/L$ are somewhat higher than for approach 4. Larger values of $\Delta P_l/L$ are slightly overestimated although still grouped relatively close together. Approach 5 only uses 7 fitting parameters (A, B, *a, b* and three *c* values).

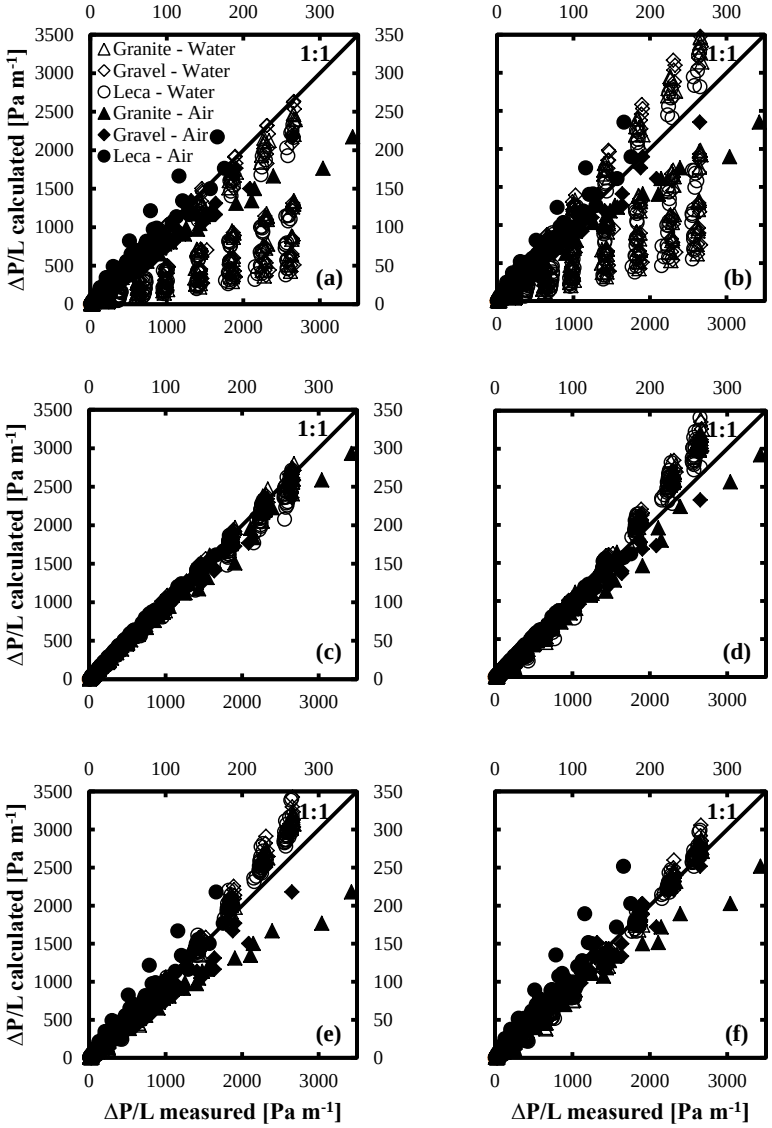

Figure 11. *Calculated (Eq. (7)) versus measured values of ΔP/L for air and water in all three materials (63 media), for* **(a)** *approach 1,* **(b)** *approach 2,* **(c)** *approach 3,* **(d)** *approach 4,* **(e)** *approach 5, and* **(f)** *approach 6.*

Approach 6 (Fig. 11(f)) is equivalent to approach 5 but based on fitting using the root mean square error (RMSE) rather than the relative square error (RSE). The advantage of using RMSE in the fitting is that the larger values of $\Delta P_l/L$ data are predicted more accurately (although the prediction of the small values is less accurate). For $\Delta P_g/L$ approach 6 has a weak tendency to overestimate for Leca® and underestimate for granite, indicating that $D_{eq,g}$ exhibits a weak dependency on the material properties (for example φ).

Altogether the data in Fig. 11 shows that it is possible to predict $\Delta P_l/L$ from measured $\Delta P_g/L$ data. The data also indicate that it may be possible to predict both $\Delta P_g/L$ and $\Delta P_l/L$ solely from the particle size distribution of the media although additional data are required to verify if this is viable. A dependency of the model constant c on the particle shape (but not the particle size distribution) of the media was also observed. In particular the fitted values of the c parameter for the three materials were inversely proportional to φ as defined by either Pentland (Eq. (14)) or Wadell (Eq. (15)). Thus, it seems that φ may be a useful parameter in the estimation of c and D_{eq} although additional data are needed to develop this further.

6. Gas-solute dispersivity ratio in granular porous media as related to particle size distribution and particle shape

6.1 Experimental procedure

The set-up dimensions for this study are identical to what was previously utilized in **Paper I** and **Paper II**. Measurements of D_{tot} were performed on three natural and commercially available media (crushed granite, gravel and Leca®). Different sets of flow rates were applied for both gas and solute dispersion experiments, in order to obtain comparable results for each fluid covering the same range of *Re* ($0.004 \leq Re \leq 2.13$). All experiments were carried out in duplicates.

Gas dispersion measurements were performed on 21 different particle size fractions and carried out only for granite, following the approach of Poulsen et al. (2008). Values of D_{tot} for gas transport in gravel and Leca® were taken from a previous study using an identical set-up and procedure (Sharma and Poulsen, 2010a). The inlet (at the bottom) end of each column was connected to an air/nitrogen supply via a three-way valve and a precision ball flow meter (model F150, Porter Instruments, Inc., Hatfield, PA) to control gas flow rate. The outlet lid was equipped with an oxygen sensor (KE-12 galvanic oxygen electrode, GS Yuasa Power Supply Ltd., Japan) with 5 seconds response time for determination of effluent oxygen concentrations. Readings from the oxygen sensor (sampling every 5 seconds) were recorded by a data logger (CR-1000, Campbell Scientific, Logan, UT). Atmospheric air and nitrogen were used as tracer gases. After saturating the columns with atmospheric air (78% N_2 and 21% O_2), the flow was adjusted to the desired values. Once the effluent O_2 concentration was stable, the inlet gas was switched to N_2. Care was taken to make sure that gas flow remained constant during the switch. A constant flow of N_2 was maintained until the effluent O_2 concentration reached zero. After that, the gas supply was switched back to atmospheric air and the flow maintained until a stable O_2 concentration was once again observed. Oxygen and nitrogen breakthrough curves (BTC's) were measured at gas flow rates of 0.2, 0.5, 1.0, 1.5, 2.0 and 2.3 l min^{-1}.

Solute dispersion measurements were performed for all three media, but using only 9 out of 21 particle size fractions for each material, as solute dispersion measurements are much more time consuming to carry out than gas dispersion measurements (about 12 times). Investigated particle size fractions are illustrated in Fig. 12.

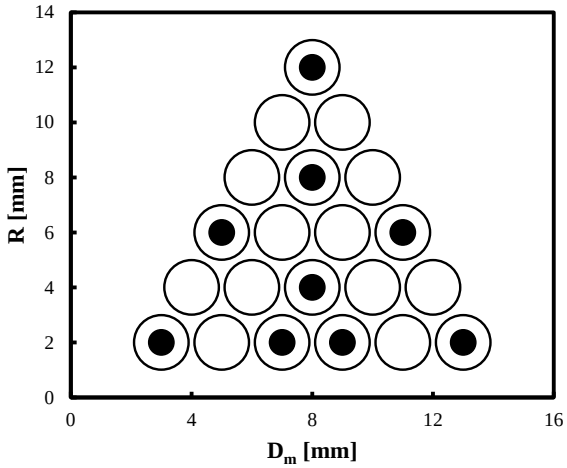

Figure 12. *Particle size range (R) and mean particle diameter (D_m) for the 21 particle size fractions. Black fully circles represent the particle size fractions for which water dispersion was investigated.*

The inlet (at the bottom) of the column was connected to a peristaltic pump (model PD 5101, Heidolf), while the outlet was connected to a measuring tube holding 12 ml of liquid, equipped with a TETRACON 325 conductometer. After saturating the columns with demineralized water, a NaCl solution of 5 g l^{-1} was injected continuously, at a specific flow rate. Effluent NaCl concentration was measured every 10 seconds. Experiments were carried out for all three materials at flow rates of 0.015, 0.05, 0.075, 0.1, 0.125, 0.15 l min^{-1}, and terminated when in and outlet NaCl concentrations were identical.

6.2 Results

For all particle size fractions and materials, values of D_{tot} (= D_{mol} + D_{mech} + D_{mix}) increased with u. Values of D_{tot} for a selected fraction (8-14 mm) are shown in Fig. 13. On average, values of D_{tot} for gas transport were 20-30 times higher compared to solute transport for identical values of *Re*.

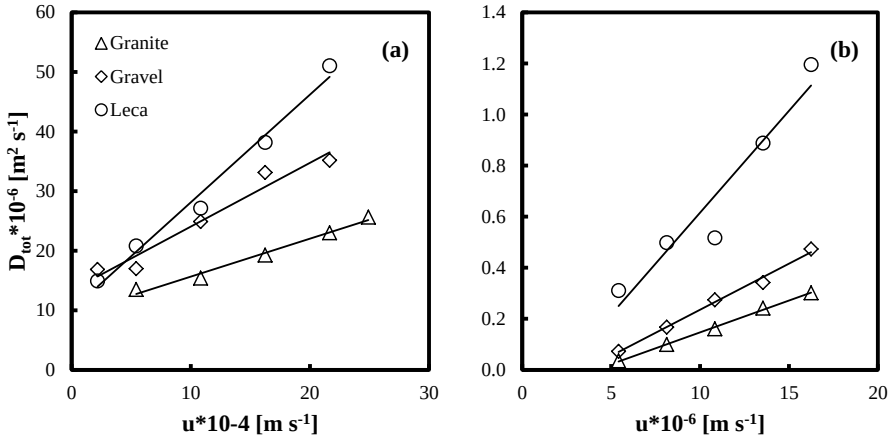

Figure 13. *Calculated values of dispersion (D_{tot}) as a function of pore fluid velocity (u), for* **(a)** *gas and* **(b)** *solute measurements using the 8-14 mm fraction size fraction.*

For gas dispersion, the D_{tot} - u relationship follow a consistent linear trend for $u > 5*10^{-4}$ m s^{-1}. Below this velocity the trend is less clear as there is considerable scatter in the gas dispersion data. This could be because the contribution by D_{mech} becomes small compared to D_{mol}, making it difficult to get a consistent and accurate determination of D_{mech}. For solute dispersion, the relationship between D_{tot} - u is also linear for $u > 5*10^{-5}$ [m s^{-1}]. Below this velocity, the measurements clearly show that the relationship does not follow the linear trend as the slope of the u - D_{tot} relationship approaches zero in this region. This may very well also be the case for gas dispersion, however, there is too much scatter in the data to assess if that is the case. The D_{tot} - u relationships for chloride measurements intercepts the D_{tot}-axis at a value close to zero, indicating that for the chloride transport D_{mol} is very small, which is in agreement with earlier literature.

Values of α were determined as the slopes of the linear parts of the D_{tot} - u relationships. α was generally highest for Leca®, lower for gravel and lowest for granite, indicating therefore, that particle shape does have a strong influence on it. It is seen that α generally increases with increasing φ, again suggesting that particle shape is important in controlling gas and solute α. Values of α for each of the three materials as a function of R and D_m are shown in Fig. 14, for both gas and solute dispersion.

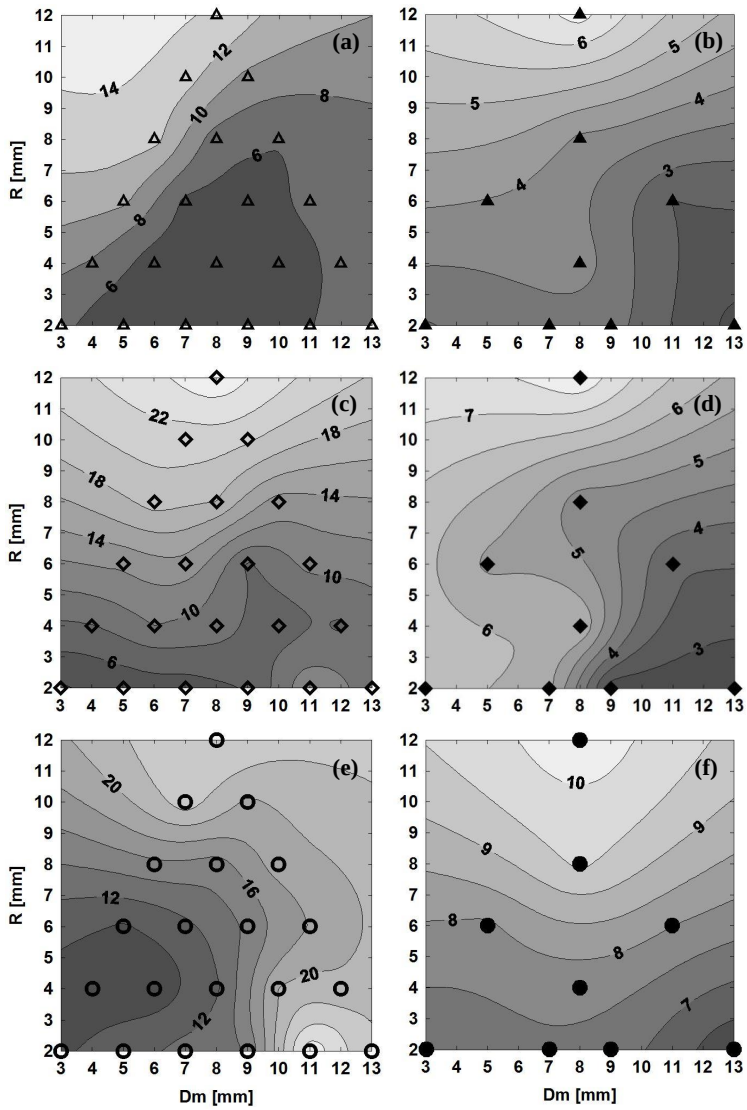

Figure 14. *Contour plots of dispersivity (α) as a function of particle size range (R) and particle diameter (D_m), for* **(a)** $\alpha_{g,granite}$, **(b)** $\alpha_{s,granite}$, **(c)** $\alpha_{g,gravel}$, **(d)** $\alpha_{s,gravel}$, **(e)** $\alpha_{g,Leca®}$,*and* **(f)** $\alpha_{s,Leca®}$.

Increasing α values are obtained for increasing values of R, in all materials. This suggests that increasing R causes an increasing variability of the length of pathways through the pore network, which in turn causes increasing dispersion as also discussed by Sharma and Poulsen (2010a) and in **Paper VI**. The α - D_m relationship is somewhat more complex across the six combinations of material and fluid, and there is no clear trend. For most of the combinations, α tends to be somewhat larger for small values of D_m (for fixed values of R), although this trend is relatively weak. Overall, the results indicate that α is strongly related to the width of the particle size distribution of the medium and the shape of the particles, while the impact of D_m is somewhat less marked.

Figure 15 shows the ratio between gas and solute dispersivity, α_g/α_s, as a function of R and D_m, for the three materials. In general, α_g/α_s tends to increase with increasing R and D_m, although the trends are relatively weak and there is considerable scatter in the data. The scatter is likely a result of the relatively few data points available. Overall, the ranges of α_g/α_s for the three materials are very similar and not significantly different on the 95% confidence level as tested using ANOVA. Thus, despite the strong dependency of both α_g and α_s on φ, their ratio appears independent of particle roundness.

As the ratio α_g/α_s depends on both R and D_m in a non-linear manner, it was chosen here to model this dependency using an empirical exponential relationship. Exponential functions are widely applied in science to describe a wide variety of relationships. The following empirical expression for modeling the dependency of α_g/α_s on R and D_m model was selected:

$$\frac{\alpha_g}{\alpha_s} = A(e^{BR} + e^{CD_m}) \tag{19}$$

where A, B and C are empirical constants.

Equation (19) was fitted to the α_g/α_s data for all three materials using 5 different approaches: 1) values of A, B and C were fitted individually for each material, 2) a common value of A across all three materials and individual values of B and C for each material were fitted, 3) common values of A and C across all three materials and individual values of B for each material were fitted, 4) common values of A and B across all three materials and individual values of C for each material were fitted, and 5) common values of A, B and C were fitted across all three materials. Fitted versus measured values of α_g/α_s using approach 1) are shown in Fig. 16.

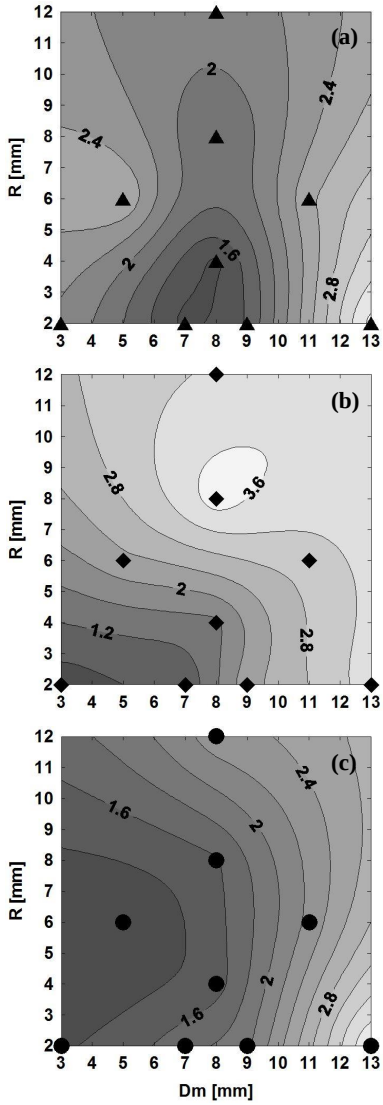

Figure 15. *Contour plots of dispersivity ratio (α_g/α_s) as a function of particle size range (R) and particle diameter (D_m), for* **(a)** *crushed granite,* **(b)** *gravel, and* **(c)** *Leca®.*

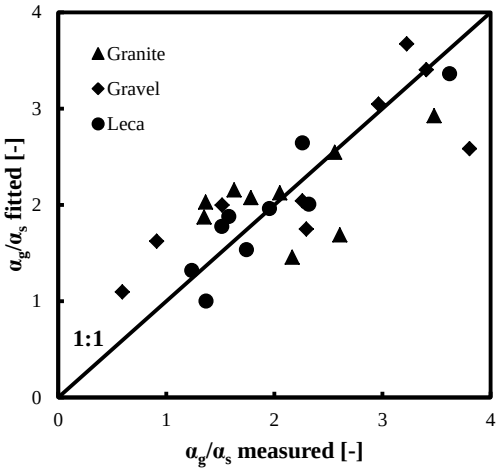

Figure 16. *Fitted (Eq. (19)) versus measured values of* α_g/α_s *using individual values of* A, B, *and* C *for each material investigated (approach 1).*

Fitting accuracy was quantified using the mean squared error (MSE). The MSE values are very similar for approaches 1 - 3, indicating that coefficients A and C are independent of the medium used. In contrast MSE increases by about 50% when using a common value of B indicating that this coefficient at least to some degree is medium dependent and, thus, different for each of three materials. Figure 16, however, indicates that most of the MSE is related to a limited number of measurements and that the fit in general is able to mimic the α_g/α_s - R - D_m relationship regardless of which of the 5 approaches that is used.

7. Relating non-equilibrium solute transport and porous media physical characteristics

7.1 Experimental procedure

Solute BTC's (324) used in this study were measured in **Paper III** using three commercially available materials: crushed granite, gravel and Leca®. A total of 27 particle size fractions (9 for each material) were investigated. Acrylic columns of 100 cm length and 14 cm inner diameter were used to contain the selected media, which was carefully placed to reduce inhomogeneities in packing density. Polyethylene lids sealed using rubber O-rings were used at both ends, while soft Teflon tubing with an inner diameter of 4 mm was used to connect each component of the system. Measurements were carried out in duplicates and performed at different flow rates equal to 0.015, 0.05, 0.075, 0.1, 0.125, 0.15 l min^{-1}. More details are given in chapter 6 (**Paper III**).

Measured BTC's were fitted using a mobile-immobile model (MIM), which accounts for early arrival and tailing during fluid transport in porous media. A set of equations was used to describe the dual region system, one for the tracer concentration in the mobile region (Eq. (12)) and one for the tracer concentration in the immobile region. The presence of non-connected or poorly connected pores (ε_{dead}), which have no solute mass exchange with the rest of the pore system, was also quantified. Optimization of D_{tot}, ε_m, ε_{dead} and k was carried out using an explicit finite difference method, corrected for numerical dispersion.

7.2 Results

A measured BTC for Leca®, at a solute flow rate of 0.125 l min^{-1} and for the 2-14 mm particle size is shown in Fig. 17. Shown is also the best fit curve for the MIM.

BTC's for all three materials exhibit the typical sigmoid shape characterising this type of process. In all three cases some tailing is evident, with granite showing the least and Leca® the most amount of tailing. The relatively little tailing exhibited by the granite data shows reduced solute exchange between the mobile and immobile phases, indicating a quasi-equilibrium condition between the two phases. Conversely, gravel and Leca® exhibit more tailing and thus have larger immobile water contents.

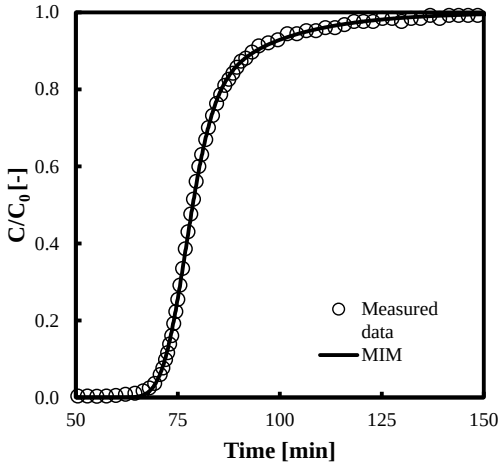

Figure 17. *Measured and fitted Leca® solute concentration for the 2-14 mm particle size fraction, at a flow rate of 0.125 l min^{-1}.*

Granite exhibits the lowest D_{tot} values, while gravel and Leca® the intermediate and the highest, respectively. In general the D_{mech} - u relationships follow a power function, expressed as:

$$D_{mech} = u\alpha^m \tag{20}$$

where m is a dimensionless exponent. Best fit values of α and m for each particle size fraction were determined by fitting Eq. (20) to the D_{tot} - u data, minimizing the sum of the squared errors. Granite generally exhibits the highest values of m, while intermediate and lowest m-values are exhibited by gravel and Leca®, respectively. This behavior was observed for all particle size fractions.

Similar relationships to D_{tot} - u was also observed between k and u. Leca® generally shows the highest k-values, while granite shows the lowest. This indicates that the more spherical the particles the greater is the transfer of tracer mass between the mobile and the immobile phases. This was also the case for the remaining BTC's and indicates that particle shape affects the flow field. Further analyses of the k - u data showed that k is also proportional to the mean diameter D_m, while particle size range, R, has a minimal effect on k.

It is well known from literature that D_{tot} increases with R, and that tends to be greater with packs of non-spherical particles than with packs of spherical particles of the same size (De Carvalho and

Delgado, 2003). This was later confirmed by Sharma and Poulsen (2010a) and Pugliese et al. (**Paper VI**), who found out that increasing R causes an increasing variability of the length of pathways through the pore network, which in turn increases dispersion. Analysis on the same media used in this study (**Paper III**) also proved the previous findings. Moreover, a marked dependency of transport on particle shape, φ, was documented, although α was not directly related to φ.

These observations suggest that in order to estimate α it may be advantageous to consider the contribution of each medium physical characteristic to α separately. It is therefore suggested to model α as a linear combination of contributions by the medium characteristics as:

$$\eta = p_1 * D_m + p_2 * R + p_3 * \varphi + p_4 \quad (21)$$

where η represents the parameter to be predicted (in this case α), p_1, p_2, p_3, and p_4 are empirical constants, whose dimensions depend on the parameter modeled.

Equation (21) was fitted to the calculated α data across all three materials. Fitted (Eq. (21)) versus calculated values of α are shown in Fig. 18.

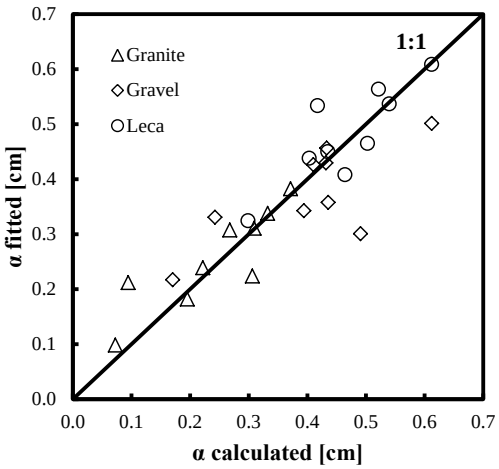

Figure 18. *Fitted (Eq. (21)) versus calculated (slopes of the D_{tot} - u trendlines) α values for all materials and particle size fractions with p_1 = -0.21 [-], p_2 = 0.18 [-], p_3 = 2.83 [mm], p_4 = 3.09 [mm]*.

One common set of values for p_1, p_2, p_3, and p_4 valid across all three materials is suggested to limit the number of fitting parameters used.

Observations of the D_{tot} - u and k - u relationship indicate that their slopes, α and β respectively, are related. Values of α versus β are therefore plotted in Fig. 19. The highest values of β are generally obtained for Leca®, while the lowest are obtained for granite. Thus, there seems to be a relationship between β and φ. Round particles such as Leca® seem to have higher mass transfer between the mobile and immobile phases (and thus higher β), than more angular particles such as granite.

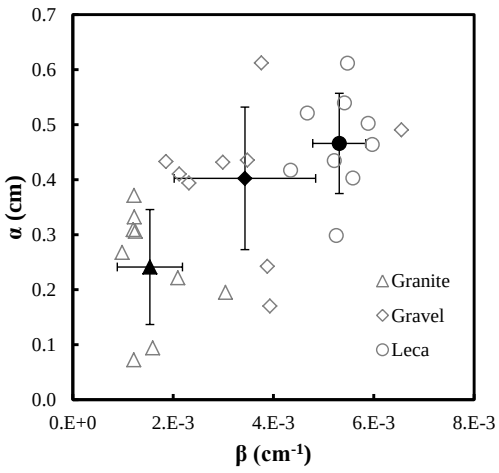

Figure 19. *Relationship between α and β, for all materials and particle size fractions. Grey and black data represent individual data points and average values, respectively. Error bars indicate one standard deviation.*

A reason for this behaviour could be the differences in the shape of local mobile and immobile pore regions at the pore scale and differences in the amount of interfacial area between the two phases. Despite some scatter in the data, especially for the gravel, Fig. 19 further indicates that α and β are proportional to some degree. This means that β likely depends on porous medium

characteristics in a manner similar to that of α. It was therefore chosen to describe β using Eq. (21) (with η now representing β). Analysis showed that p_2 and p_4 had little or no impact of the fitting accuracy and these parameters were therefore excluded from the analysis. Fitting of the β values (using Eq. (21)) was done based on β values, determined by best linear fit to the measured k - u relationships. Results are shown in Fig. 20.

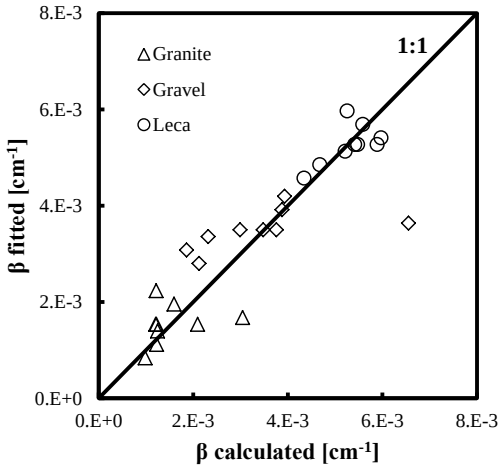

Figure 20. *Fitted (Eq. (21)) versus calculated (slopes of the k - u trendlines) β-values for all materials and particle size fractions with p_1 = 1.4e-5 [mm^{-2}], p_3 = 4.7e-4 [mm^{-1}].*

Again one common set of values for p_1 and p_3 in Eq. (21) valid across all three materials is suggested to limit the number of fitting parameters used.

Overall, the results indicate that α and β are related to porous medium particle size distribution and φ in a similar way and may be predicted from porous medium characteristics using the same type of expression. The results further suggest that accurate predictions of the tailing of solute breakthrough curves may be achieved using the MIM. Therefore, significant time can be saved while performing in-situ measurements.

8. Estimating solute dispersion coefficients in porous media at low pore water velocities

8.1 Experimental procedure

Assessment of the D_{mech} - u relationship was carried out using BTC's previously measured by Harleman and Rumer (1963), Hu and Brusseau (1994) and Pugliese et al. (**Paper III)**. Data for 29 porous media with very different particle shapes (ranging from almost spherical to very angular) and particle sizes (0.2 - 14 mm) at different velocities were used in the analyses.

Measurements, for crushed granite, gravel and Leca® were carried out in duplicate and performed at 6 different flow rates equal to 0.015, 0.05, 0.075, 0.1, 0.125, 0.15 l min^{-1}. A total of 324 BTC's were measured. More details on the experimental procedure are provided in **Paper III**. Two additional data sets (15 BTC's) taken from previous studies were also considered in the analysis (Harleman and Rumer, 1963; Hu and Brusseau, 1994). Harleman and Rumer (1963) performed the experiments using plastic spheres, having φ = 1 D_m = 0.96 mm and R = 0.2 mm. Hu and Brusseau (1994) used glass beads, with φ = 1 D_m = 0.256 mm and R = 0.088 mm.

8.2 Results

In general the D_{mech} - u relationships, based on the breakthrough data from Pugliese et al. (2013b), follow a power function. Crushed granite exhibit most curvature while Leca® exhibits the least. This was generally also the case for the D_{mech} - u relationships for the remaining 8 particle size fractions, for each of the three materials and throughout the u range investigated.

For all three materials Eq. (20) correctly estimates D_{mech} along all the u range investigated. Estimation procedure was carried out considering individual values of α and m for each particle size fraction and for crushed granite, gravel and Leca®. Leca® exhibits higher α values in agreement with previous studies carried out assuming m = 1 (**Paper III**), while gravel and granite exhibit the intermediate and lower α values, respectively. As the main difference between the three materials with respect to transport is φ, the results indicate that roundness is especially important when estimating α.

After developing a model for estimating α, the following equation was introduced:

$$\alpha = n_1(R^{n_2} - 1) + n_3\varphi^{n_4} \quad (22)$$

where α and R are given in cm and mm, respectively, and n_1, n_2, n_3, n_4 are empirical constants, which are identical for all particle size ranges and materials. Figure 21 shows α values fitted by Eq. (22) versus α values determined by Eq. (20), for all particle size fractions and materials. The results in Fig. 21 show that Eq. (22) provides a good accuracy across all five materials and 29 particle size fractions in fitting α values based on R, φ, and 4 empirical constants.

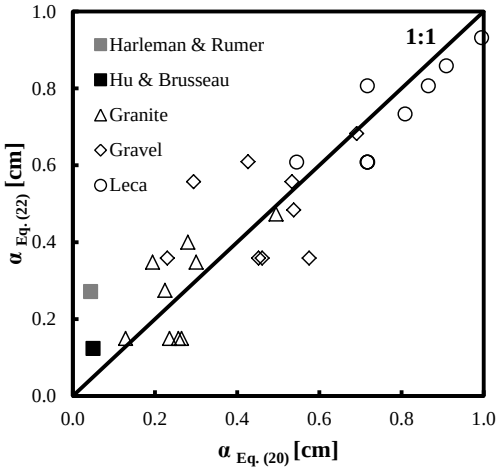

Figure 21. *Values of dispersivity (α) fitted by Eq. (22) versus α values determined by fitting D_{mech} (Eq. (20)), for all particle size fractions and materials. Values of the empirical constants are n_1 = 576 [-], n_2 = 0.0003 [-], n_3 = 0.56 [-], n_4 = 1.31 [-].*

D_m does not affect the estimation of α at very low pore velocities and this is in contrast with the behaviour of α at higher velocities, where D_m becomes important (De Carvalho and Delgado, 2003; Delgado, 2006; **Paper IV**). The results further indicate that Eq. (22) is applicable for almost all kinds of particle shapes and for particle sizes ranging between 0.2 and 20 mm.

In contrast to α, m is generally dependent on D_m but almost independent on R. Values of m are smallest for Leca®, intermediate for gravel and largest for granite. Values of m are thus inversely proportional to φ. This tendency is opposite to what was found for α, which is directly proportional to φ. Again, as roundness is the main difference between the three materials, this suggests that φ is very important when estimating m. The following expression was proposed:

$$m = n_1 {D_m}^{n_2} + \varphi^{n_3} \quad (23)$$

where m and D_m are given in cm and mm, respectively, and n_1, n_2, n_3 are empirical constants, which are identical for all particle size ranges and materials. Figure 22 shows m values fitted using Eq. (23) versus m values determined by fitting D_{mech} (Eq. (20)), for all particle size fractions and materials. Figure 22 shows that there is a good agreement between m values determined by Eq. (23) and Eq. (20).

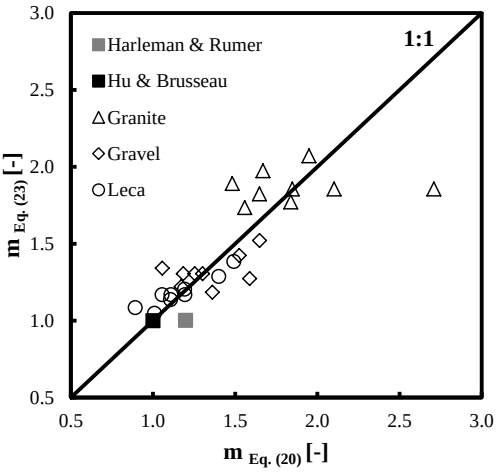

Figure 22. *Values of exponent (m) fitted by Eq. (23) versus m values determined by fitting D_{mech} (Eq. (20)), for all particle size fractions and materials. Values of the empirical constants are n_1 = 0.003 [-], n_2 = 1.89 [-], n_3 = -0.22 [-].*

9. Relating gas dispersion in porous media to medium tortuosity and anisotropy ratio

9.1 Experimental procedure

Assessment of the relations between gas phase α, tortuosity (τ) and anisotropy ratio (ξ) in porous media were carried out using three different commercially available materials: rounded pebbles (as an isotropic reference material), slate and wood chips. A specific particle size range (ranging from 10 to 18 mm) was selected as a trade-off between facilitating ease of packing, which had to be done manually, one particle at a time. Details about the packing procedure are given in paragraph 3.1.1 of this dissertation.

Prior to measurements all materials were dried for several weeks. Each of the materials was then packed into clear acrylic columns 15 cm in length and 14 cm inner diameter. This column size was chosen in order to avoid effects of preferential flow along the column walls, which may occur if column diameter is too small compared to the average particle diameter. All experiments were carried out in duplicate.

Determination of D_{tot} was carried out following the approach of Poulsen et al. (2008; **Paper III**). Oxygen and nitrogen BTC's were measured at Q = 0.5, 1.0, 1.5, 2.0 and 2.3 l min^{-1}.

Determination of D_{mol} was carried out using the same columns as used in the D_{tot} estimation. For D_{mol} determination, however, the top of each 15 cm column was connected to a 25 cm long empty column of the same diameter fitted with a KE-12 oxygen electrode, closed with a polyethylene lid (with a gas inlet) at the top, and sealed using rubber O-rings. The inlet was connected to the same air/nitrogen supply assembly as used for the D_{tot} determination. Soft Teflon tubing with an inner diameter of 4 mm was used to connect system components. The bottom of the 15 cm column was placed on a movable metal sheet such that the sheet could be slid out from under the column leaving it opened to the atmosphere without disturbing the gas inside the column. The connection between sheet and column was not tight but allowed gas to seep out of the column with the sheet in place, as long as the pressure inside the column was higher than outside. This allowed for saturating the column with N_2 prior to letting air diffuse into the column. The reason for having the bottom end open to the atmosphere rather than the top was to prevent effects of gravity driven gas flow as air

is slightly heavier than N_2. During measurements the experimental apparatus was placed in a closed chamber to reduce air movement around the apparatus and prevent disturbance to the diffusion process. Columns were initially saturated with N_2 via the inlet. The flow was then switched off and the metal sheet immediately removed from below the column, allowing air to diffuse back in.

Determination of gas permeability (k_g) for all nine media was carried out using the same 15 cm columns as used for the D_{tot} and D_{mol} measurements. The top of the column was kept open to the atmosphere while the bottom was connected to a supply of compressed atmospheric air via a valve and a precision ball flow meter (model P450, Porter Instruments, Inc., Hatfield, PA). Corresponding values of Q and ΔP across the columns were measured for Q ranging between 0 and 50 l min^{-1} using an Alnor AXD 560 digital manometer connected to the bottom and the top of the column. This relatively wide range of Q was used to get a more reliable determination of the Q - ΔP relationship for each medium. Measured ΔP values were corrected for the pressure drop across the empty column with the metal mesh in place.

9.2 Results

All measured O_2-N_2 BTC's for $u > 0$ exhibited the sigmoid shape expected for this type of experiments. Only a small amount of tailing was observed, indicating that the presence of an immobile gas phase in which gas exchange takes place was limited. This also means that no significant preferential flow along the column walls occurred as this will result in significant tailing of the BTC's. In all cases the (D_{mol} + D_{mech}) - u relationships are approximately linear in accordance with Eq. (9) except at low velocities (indicated by broken curve sections) where the slopes tend to decrease and intercept the y-axis at D_{mol}, as also discussed earlier. For a selected u, wood chips exhibit higher values of (D_{mol} + D_{mech}) compared to slate chips and pebbles. This could be because the surfaces of the wood chips are rougher than the slate chips and pebbles, and furthermore because this material is dual porous which, as discussed earlier, can result in larger D_{mech}. Also the wood chips have a much higher total porosity than slate chips (due to their high intra particle porosity) which result in larger values of D_{mol}. Linear regression lines were fitted to the (D_{mol} + D_{mech}) - u data for $u > 0$. Values of α, represented by the slopes of the regression lines (Eq. (9)), were determined. For both slate and wood chips α was highest for particle orientation A and lowest for particle orientation C. For the pebbles α was very close to the average α for all other materials and particle orientations combined (0.65 vs 0.63 cm, respectively). The α-value

for pebbles also corresponds well with earlier measurements of α in gravel materials of similar particle size by Sharma and Poulsen (2010a; 2010b) who observed α values of 0.3-0.9 cm.

Measured and fitted O_2-N_2 BTC's for u = 0 (only molecular diffusion taking place) asymptotically approach the atmospheric oxygen concentration over time. Diffusion was faster in materials with particle orientation A for both slate and wood chips (the curves approach atmospheric oxygen concentration faster) and slowest in material with particle orientation C. This is a direct consequence of τ being lowest for particle orientation A and highest for orientation C. Wood chips exhibited higher D_{mol} values than slate chips for identical particle orientation. Part of the reason is probably that the wood particles are porous, allowing for diffusion through the particles. This means that the total gas-filled porosity and thus the cross-sectional area available for diffusion, is larger in wood chips than in slate chips for the same particle orientation.

Values of k_g were highest for particle orientation A and lowest for orientation C for both slate and wood chips. Orientation D for both slate and wood chips as well as for pebbles showed intermediate k_g values. The reason is that, for particle orientation A, part of the pore system consists of large continuous highly conductive pores (channels parallel to the direction of flow) offering reduced flow resistance while, for orientation C, these channels are not present resulting in increased flow resistance. Thus as expected, k_g is directly controlled by particle orientation but less so by external porosity which is typically the case in homogeneous soils. Measurements of k_g can therefore be used to characterize the particle or aggregate orientation of aggregated or fractured porous media.

For each material and particle orientation τ was determined according to the following expression:

$$D_{mol} = \frac{\varepsilon_{tot}}{\tau} D_{void} \tag{24}$$

where D_{void} represents the molecular diffusion in a free gas volume [L^2 T^{-1}]. ξ was determined from corresponding values of k_g (labelled ξ_k) or D_{mol} (labelled ξ_D). For particle orientation A, $k_{g,perpendicular,A}$ was defined as the average of $k_{g,B}$ and $k_{g,C}$. A similar approach was used for the other particle orientations for both k_g and D_{mol}.

The data indicate a direct proportionality between k_g, D_{mol} and both ξ_D and ξ_k, while the shape factor (σ) is inversely related to ξ. This is to be expected as ξ and τ are dependent, and also because τ is defined based on the magnitude of D_{mol}, which is directly defined by the orientation

of the particles relative to the direction of transport. It also means that in media consisting of non-spherical particles or aggregates, D_{mol} is strongly dependent on particle or aggregate orientation. Data show that α is proportional to both k_g and D_{mol} for both slate and wood chips, which means that α also is strongly dependent on particle orientation. Thus, in anisotropic media it may be possible to predict α based on either D_{mol} or k_g, both of which are much easier to measure than α. It is noted that the k_g - D_{mol}, the k_g - α, and the D_{mol} - α relations, in addition to particle orientation, are also likely dependent on particle shape.

Figure 23 shows α as a function of τ (Fig. 23(a)), σ (Fig. 23(b)), ξ_D (Fig. 23(c)) or ξ_k (Fig. 23(d)) for all materials and particle orientations.

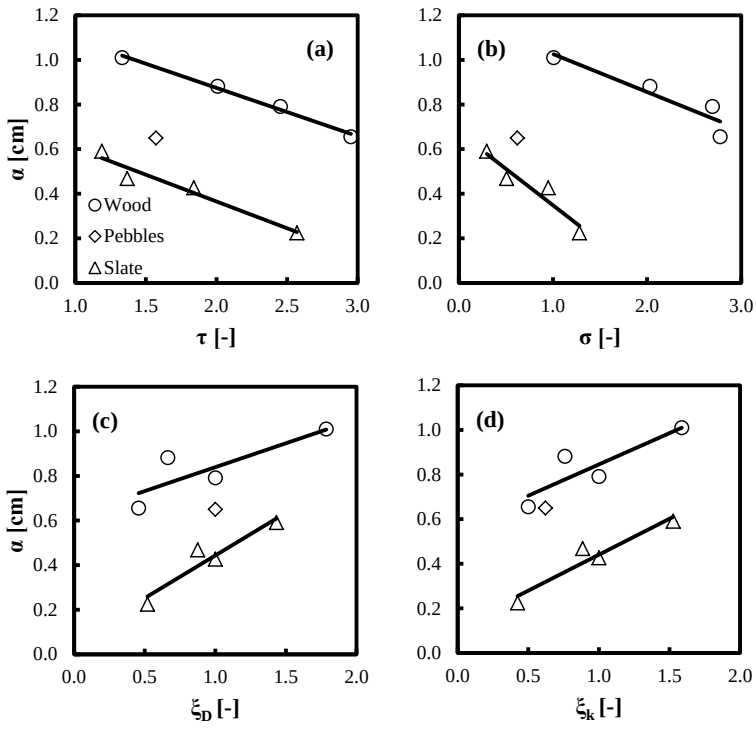

Figure 23. *Calculated values of α as a function of* **(a)** *tortuosity (τ),* **(b)** *shape factor (σ),* **(c)** *anisotropy ratio based on D_{mol} (ξ_D), and* **(d)** *anisotropy ratio based on k_g (ξ_k).*

For both slate and wood chips the relationships are approximately linear within the τ, σ or ξ ranges investigated, such that α decreases linearly with increasing τ and σ, and increases linearly with increasing ξ_D and ξ_k. In all four cases the pebbles fall within the region spanned by the wood and slate chips. Although the α - ξ_D and the α - ξ_k relationships are different, they are both strong, indicating that when developing models for predicting α from ξ, both relationships could be used as a starting point. Seen from an economic and time consumption perspective, ξ_k can with advantage be used as k_g is much simpler and faster to measure than D_{mol}.

The reason why α increases with ξ is that dispersion is caused by differences in the amount of time it takes for individual gas particles to pass through the porous medium. Transport time for a given gas particle, in turn, is controlled by the tortuosity of the individual pore (or succession of connected pores) through which it passes, the average velocity at which it moves through the pore, and the amount of turbulence and mixing within each pore. This means that α in a porous medium depends on both the distribution of tortuosities of the gas conducting pores and the distribution of gas velocities within these pores. The wider the range of transport times (the wider the range of gas conducting pore tortuosities and average pore gas flow velocities) the larger the value of α. In anisotropic media, the widest range in both pore tortuosity and gas pore velocity occur in the spatial direction corresponding to the largest average value of ξ. Consider for instance a medium consisting of layers of coarse and fine materials where the ranges of both individual α and u will be larger if gas flow occurs parallel to the layers (where different gas particles pass through different materials) compared to flow perpendicular to the layers (where all gas particles pass through the same materials).

Figure 24 shows the τ - ξ_k, τ - ξ_D, σ - ξ_k, and σ - ξ_D relationships for all three materials. Data indicate that τ decreases with increasing ξ_k and ξ_D (Fig. 24(a) and 24(b)) with slopes significantly smaller than zero. This shows that τ and ξ are strongly related and suggests the possibility for predicting τ from ξ or vice versa in anisotropic materials.

For both slate and wood chips σ is inversely proportional to ξ (Fig. 24(c) and 24(d)) as was also the case for τ. For the same ξ, wood chips exhibit larger values of σ although the data shows that the difference is not statistically significant. In fact the data suggest that the slopes of the relationships may be identical.

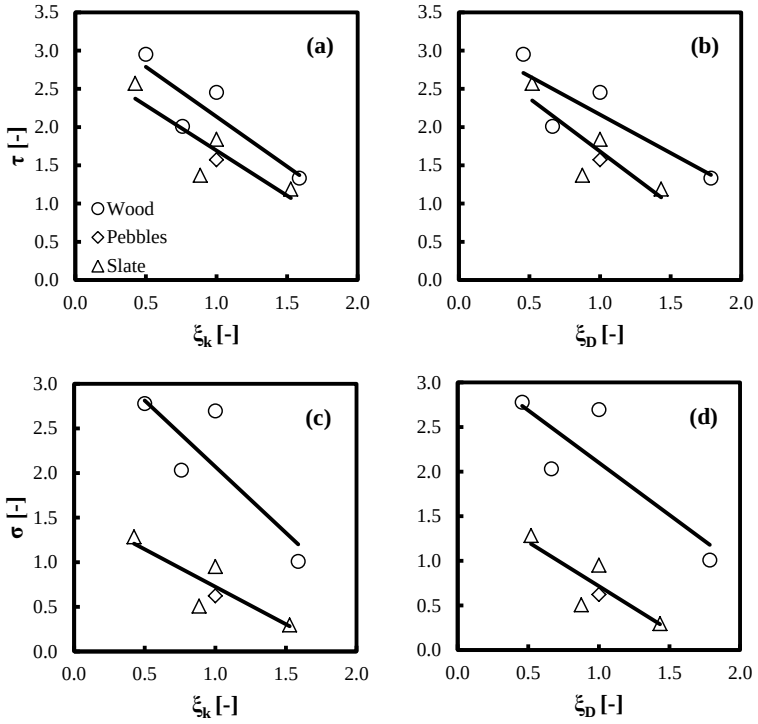

Figure 24. *Relationships between* **(a)** *tortuosity (τ) and anisotropy ratio based on* k_g *(*ξ_k*),* **(b)** *τ and anisotropy ratio based on* D_{mol} *(*ξ_D*),* **(c)** *shape factor (σ) and* ξ_k*, and* **(d)** *σ and* ξ_D*.*

10. Conclusions and perspectives

10.1 Conclusions

The relationships between transport of gases and dissolved compounds in porous media, and the physical media characteristics were investigated in the present work. Analysis was carried out across 6 different granular media exhibiting different particle shapes (roundness) and internal structure, having a diameter included in the range 2-18 mm.

The most relevant contributions of this work are:

Development of models predicting pressure loss in isotropic media. For both gas and liquid measurements, the relationship between pressure loss and velocity ($\Delta P/L$ - V) followed a second order polynomial in agreement with earlier literature. $\Delta P/L$ decreased with increasing particle size and increasing roundness (φ). In **Paper I** an existing model was tested again the measured gas data, performing relatively well although a tendency to over predict small and large values was noted. Thus, an improved model for predicting the relationship was proposed. Results from the modeling further indicated that the material specific empirical parameters were related to particle shape. In **Paper II** several existing approaches, based on previously published data for air flow, were evaluated to predict liquid $\Delta P/L$ from corresponding measurements performed using gas. Predictions of liquid $\Delta P/L$ were not found to be accurate, and a new exponential expression requiring only four empirical parameters was introduced. The link between the two equivalent particle diameters was estimated for particle sizes ranging from 2 to 14 mm. Results from the modeling indicated that some of the empirical parameters exhibited dependency on material particle shape.

Development of models predicting dispersion in isotropic media. Both gas and solute dispersion coefficients (D_{mech}) exhibited the well-known linear increase with fluid pore velocity (u), except at very low fluid velocities. Analysis of gas and liquid breakthrough curves (BTC's) was carried out in **Paper III**, showing that gas dispersion coefficients were generally larger than for solute. Results across all three media further indicate that dispersivity (α) is strongly related to the width of the particle size distribution (R) and to a lesser degree of the actual mean particle diameter (D_m). In contrast, the ratio between gas and solute α did not exhibit a strong relationship with φ, but instead depended on R and D_m. Based on these observations an empirical expression for

predicting the α ratio was suggested. This expression uses three empirical constants and the results indicate that at least two of the empirical constants are not medium dependent. In **Paper IV**, the possibility to estimate non-equilibrium solute transport parameters from porous medium physical properties, thus allowing considerable time savings when measuring solute BTC's, was investigated. Results indicated that the more spherical the particles (higher φ), the greater the mass transfer between the mobile and immobile phases. A simple linear expression for predicting the transport parameters from particle size distribution and particle shape characteristics was proposed. The D_{mech} – u relationship at low u was investigated in **Paper V** across five granular porous materials (crushed granite, gravel, Leca®, plastic spheres and glass beads). The analysis indicated that the classical assumption of dispersion coefficient, being equal to a constant times u to a power (m), well describes the measured data. Values of α were strongly dependent on φ, and showed a direct proportionality with φ. Results also indicated that α to some degree is proportional to R, but independent of D_m. The independency of D_m at low u is in contrast with earlier studies that show a dependency of α on D_m at high u. Values of m also showed a strong dependency on φ but were inversely proportional to φ. Results further showed that m to some degree is proportional to D_m but independent of R (in contrast to α). A set of equations, for predicting α and m from R, D_m and φ, were proposed.

Identification of the relationship between gas dispersion and pressure loss in anisotropic media. Measurements conducted in **Paper VI** showed that α is linearly related to gas permeability (k_g), molecular diffusion (D_{mol}) and anisotropy ratio (ζ) but inversely proportional (but still linearly related) to tortuosity ratio (τ) and particle shape. Higher α values are also generated from rougher surfaces, which generate increased gas turbulence and mixing. Values of the α ratio determined based on either k_g or D_{mol} were similar across the media investigated.

10.2 Perspectives

The research carried out in this work, has highlighted the importance of the particle characteristics in estimating the transport parameters. Throughout all the studies a significant improvement of existing models was gained in terms of prediction accuracy, on a large and different set of data. Moreover, new expression and new models were proposed and tested on the same data. Despite the good results, there is room for important future research within this area, especially when considering more realistic situations such as discussed below.

Important aspects for such future research are:

- *Investigation of both pressure loss and dispersion in media with different particle size distribution and shapes.* Each of the 6 different media utilized in this work was chosen to provide a certain representativeness of the different media characteristics. Therefore, the validation of the results for a unique characteristic may be affected somehow by the singular media investigated. Moreover, the approaches discussed here have only been tested against data for granular media, having uniform particle size distributions although the media represented a very wide range of uniform particle size distributions. Further measurements on other materials with a wider range of particle size distribution (uniform and non-uniform) and particle shapes, however, are required, to better understand the transport relationships for a given material and its particle size distribution and particle shape.
- *Investigation of dispersion at lower velocities.* The proposed model, introduced for describing the relationship between pore water velocity and mechanical dispersion, considered values of D_{mech} = 0 below a certain u. Despite the model yielded improved accuracy in comparison with the traditional linear model, it was seen that D_{mech} near 0 is not exactly 0. New experiments analysing D_{mech} at $u < 0.3$ cm min^{-1} may be valuable.
- *Investigation of anisotropy for a larger set of media and at a large scale.* The relationships between the anisotropy ratio, the media properties and the transport parameters were only investigated on a tiny set of media. Also in this case, the validation of the results for the anisotropy ratio may be affected somehow by the singular media investigated. These set of measurements were conducted using columns with certain length dimension (15 cm), to facilitate the packing procedure. In addition, investigation using longer columns would be useful to estimate the scale effect on the anisotropy ratio.

11. Nomenclature

A	medium cross sectional area [L^2]
C_f	form coefficient [L^{-1}]
C_{im}	immobile tracer concentration [$M\ L^{-3}$]
C_m	mobile tracer concentration [$M\ L^{-3}$]
D	particle diameter [L]
D_{eq}	equivalent diameter [L]
D_m	mean particle diameter [L]
D_{mech}	mechanical dispersion coefficient [$L^2\ T^{-1}$]
D_{min}	minimum particle diameter [L]
D_{mix}	fluid mixing [$L^2\ T^{-1}$]
D_{mol}	molecular diffusion coefficient [$L^2\ T^{-1}$]
D_{tot}	dispersion-diffusion coefficient [$L^2\ T^{-1}$]
D_{void}	molecular diffusion in a free volume [$L^2\ T^{-1}$]
$D_{10,\ 50,\ 60}$	particle diameter corresponding to the 10, 50, 60% fractile [L]
k	permeability [L^2]
k	mass transfer coefficient [T^{-1}]
L	length of the porous media in the flow direction [L]
m	dimensionless exponent [-]
M_1	first order moments of the particle size distribution [$M\ L^2\ T^{-2}$]
M_2	second order moments of the particle size distribution [$M\ L^2\ T^{-2}$]
Q	volumetric flow [$L^3\ T^{-1}$]
r	radius of the inscribed circle [L]
R	particle size range [L]

$\mathcal{R}$	radius of the largest inscribed circle [L]
Re	Reynolds number [-]
u	pore velocity [L T^{-1}]
V	superficial flow velocity [L T^{-1}]

Greek letters

α	longitudinal dispersivity [L]
α_g/α_s	mechanical dispersivity ratio [-]
ΔP	pressure loss [M L^{-1} T^{-2}]
ε_{dead}	dead porosity [L^3 L^{-3}]
ε_{im}	immobile filled porosity [L^3 L^{-3}]
ε_m	mobile filled porosity [L^3 L^{-3}]
ε_{tot}	total porosity [L^3 L^{-3}]
μ	dynamic viscosity [M L^{-1} T^{-1}]
ξ	anisotropy ratio [-]
ξ_D	anisotropy ratio calculated from D_{mol} [-]
ξ_k	anisotropy ratio calculated from k [-]
ρ	density [M L^{-3}]
ρ_b	bulk density [M L^{-3}]
σ	shape factor [-]
τ	tortuosity ratio [-]
φ_p	roundness defined by Pentland (1927) [-]
φ_w	roundness defined by Wadell (1935) [-]
ω	cross-sectional or projection area of the grain [L^2]
ω_p	area of the circle having the largest diameter of the grain [L^2]

12. References

Andreasen, R. R., Poulsen, T. G. (2013). Air flow characteristics in granular biofilter media. J. Environ. Eng.-ASCE 139(2), 196-204.

Arya, L. M., Leij, F. J., Shouse, P. J., van Genuchten, M. T. (1999). Relationship between the hydraulic conductivity function and the particle size distribution. Soil Sci. Soc. Am. J. 63(5), 1063-1070.

Baenninger, D., Lehmann, P., Fluehler, H. (2006). Modelling the effect of particle size, shape and orientation of light transfer through porous media. Eur. J. Soil Sci. 57(6), 906-915.

Barrett, P. J. (1980). The shape of rock particles, a critical review. Sedimentology 27(3), 291-303.

Berkowitz, B., Scher, H. (1995). On characterization of anomalous-dispersion in porous and fractures media. Water Resour. Res. 31(6), 1461-1466.

Berkowitz, B., Scher, H., Silliman, S.E. (2000). Anomalous transport in laboratory-scale, heterogeneous porous media. Water Resour. Res. 36(1), 149-158.

Bradford, S. A., Yates, S. R., Bettahar, M., Simunek, J. (2002). Physical factors affecting the transport and fate of colloids in saturated porous media. Water Resour. Res. 38(12), 1-12.

Brenner, H., Edwards, D. A. (1993). *Macrotransport processes*. Butterworth-Heinemann, Stoneham, MA.

Bromly, M., Hinz, C., Aylmore, L. A. G. (2007). Relation of dispersivity to properties of homogeneous saturated repacked soil columns. Eur. J. Soil Sci. 58(1), 293-301.

Brusseau, M. L. (1991). Transport of organic-chemicals by gas advection in structured or heterogeneous porous-media – development of a model and application to column experiments. Water Resour. Res. 27(12), 3189-3199.

Brusseau, M. L. (1993). The influence of solute size, pore water velocity, and intraparticle porosity on solute dispersion and transport in soil. Water Resour. Res. 29(4), 1071-1080.

Cortis, A., Berkowitz, B. (2004). Anomalous transport in “classical” soil and sand columns. Soil Sci. Soc. Am. J. 68(5), 1539-1548.

Coutelieris, F. A. (2002). The effect of geometry and axial orientation of spheroidal particles on the adsorption rate in a granular porous medium. Stud. Surf. Sci. Catal. 144, 745-751.

Darcy, H. (1856). *Les fontaines publiques de la ville de Dijon*. V. Dalmont, ed. Paris, 647.

De Carvalho, J. R. F. G., Delgado, J. M. P. Q. (2003). Effect of fluid properties on dispersion in flow through packed. AIChE J. 49(8), 1980-1985.

De Oliveira, L. L., Duarte, I. C. S., Sakamoto, I. K., Varesche, M. B. A. (2009). Influence of support material on the immobilization of biomass for the degradation of linear alkylbenzene sulfonate in anaerobic reactors. J. Environ. Manage. 90(2), 1261-1268.

Delgado, J. M. P. Q. (2006). A critical review of dispersion in packed beds. Heat Mass Transfer 42(4), 279-310.

Dullien, F. A. L. (1992). *Porous media. Fluid transport and pore structure*. Second edition, Academic Press, New York, 157.

Ergun, S. (1952). Fluid flow through packed columns. Chem. Engr. Prog. 48(2), 89-94.

Forchheimer, P. H. (1901). Wasserbewegung durch boden. *Zeitschrift ver deutscher ingenieure* 50, 1782-1788 (in German).

Gadal-Mawart, A., L. Malhautier, L., Renner, C., Fanlo, J. L. (2010). Physicochemical and hydrodynamic characterisation of various packing materials for biofiltration. Proceedings of the 2010 Duke-UAM Conference on Biofiltration for Air Pollution Control, Washington.

Gidda, T., Cann, D., Stiver, W. H., Zytner, R. G. (2006). Airflow dispersion in unsaturated soil. J. Contam. Hydrol. 82(1-2), 118-132.

Hamamoto, S., Moldrup, P., Kawamoto, K., Komatsu, T. (2009). Effect of particle size and soil compaction on gas transport parameters in variably saturated, sandy soils. Vadose Zone J. 8(4), 986-995.

Harleman, D. R. F., Rumer, R. R. (1963). Longitudinal and lateral dispersion in an isotropic porous medium. J. Fluid Mech. 16(3), 385-394.

Hu, Q. H., Brusseau, M. L. (1994). The effect of solute size on diffusive-dispersive transport in porous media. J. Hydrol. 158(3-4), 305-317.

Hunt, A. G., Skinner, T. E., Ewing, R. P., Ghanbarian-Alavijeh, B. (2011). Dispersion of solutes in porous media. Eur. Phys. J. B. 80(4), 411-432.

Loll, P., Moldrup, P., Schjonning, P., Riley, H. (1999). Predicting saturated hydraulic conductivity from air permeability: application in stochastic water infiltration modeling. Water Resour. Res. 35(8), 2387-2400.

Macdonald, I. F., Elsayed, M. S., Mow, K., Dullien, F. A. L. (1979). Flow through porous-media - Ergun equation revisited. Ind. Eng. Chem. Fund. 18(3), 199-208.

Macdonald, M. J., Chu, C. F., Guilloit, P. P., Ng, K. M. (1991). A generalized blake-kozeny equation for multisized spherical-particles. AIChE J. 37(10), 1583-1588.

Malhautier, L., Khammar, N., Bayle, S., Fanlo, J. L. (2005). Biofiltration of volatile organic compounds. Appl. Microbiol. Biot. 68(1), 16-22.

Moldrup, P., Olesen, T., Schjonning, P., Yamaguchi, T., Rolston, D. E. (2000a). Predicting the gas diffusion coefficient in undisturbed soil from soil water characteristics. Soil Sci. Soc. Am. J. 64(1), 94-100.

Moldrup, P., Olesen, T., Gamst, J., Schjonning, P., Yamaguchi, T., Rolston, D. E. (2000b). Predicting the gas diffusion coefficient in repacked soil: Water-induced linear reduction model. Soil Sci. Soc. Am. J. 64(5), 1588-1594.

Moldrup, P., Olesen, T., Komatsu, T., Schjonning, P., Rolston, D. E. (2001). Tortuosity, diffusivity, and permeability in the soil liquid and gaseous phases. Soil Sci. Soc. Am. J. 65(3), 613-623.

Neuman, S. P. (1990). Universal scaling of hydraulic conductivities and dispersivities in geologic media. Water Resour. Res. 26(8), 1749-1758.

Olesen, T., Moldrup, P., Yamaguchi, T., Rolston, D. E. (2001). Constant slope impedance factor model for predicting the diffusion coefficient in unsaturated soil. Soil Sci. 166(2), 89-96.

Osozowa, S. (1998). A simple method for determining the gas diffusion coefficient in soil and its application to soil diagnosis and analysis of gas movement in soil. Natl. Inst. Of Agro-Environ. Sci., Ibaraki, Japan.

Parker, J. C., van Genuchten, M. T. (1984). Determining transport parameters from laboratory and field tracer experiments. VA Agr. Exp. Stat. B. 84-3, 1-96.

Pentland, A. (1927). A method of measuring the angularity of sands. Royal Soc. Canada, Proc. and Trans. 21(3), Appendix C.

Perfect, E., Sukop, M. C. (2001). Models relating solute dispersion to pore space geometry in saturated media: a review. Physical and chemical processes of water and solute transport/retention to soils, proceedings 56, 77-146.

Popovicova, J., Brusseau, M. L. (1997). Dispersion and transport of gas-phase contaminants in dry porous media: effect of heterogeneity and gas velocity. J. Contam. Hydrol. 28(1-2), 157-169.

Poulsen, T. G., Suwarnarat, W., Hostrup, M. K., Kalluri, P. N. V. (2008). Simple and rapid method for measuring gas dispersion in porous media: methodology and applications. Soil Sci. 173(3), 169-174.

Riley, N. A. (1941). Projection sphericity. J. Sediment Petrol. 11(2), 94-97.

Riley, H., Ekeberg, E. (1989). Ploughless tillage in large-scale trials. Norsk Landbruksforskning 3, 107-115.

Rouse, P. C., Fannin, R. J., Shuttle, D. A. (2008). Influence of roundness on the void ratio and strength of uniform sand. Geotechnique 58(3), 227-231.

Sahimi, M. (1995). *Flow and transport in porous media and fractured rock: from classical methods to modern approaches*. John Wiley, New York.

Sakuma, T., Hattori, T., Deshusses, M. A. (2006). Comparison of different packing materials for the biofiltration of air toxics. J. Air Waste Manage. 56(11), 1567-1575.

Santamarina, J. C., Cho, G. C. (2004). Soil behavior: the role of particle shape. Proc. Skempton Conf. London.

Schjonning, P. (1986). Soil permeability by air and water as influenced by soil type and incorporation of straw. *Tidsskrift for planteavl* (Special issue).

Schulze-Makuch, D. (2005). Longitudinal dispersivity data and implications for scaling behaviour. Ground Water 43(3), 443-456.

Scotter, D. R., Ross, P. J. (1994). The upper limit of solute dispersion and soil hydraulic properties. Soil Sci. Soc. Am. J. 58(3), 659-663.

Sharma, P., Poulsen, T. G. (2010a). Gas dispersion and immobile gas content in granular porous media: effect of particle size nonuniformity. Soil Sci. 175(9), 426-431.

Sharma, P., Poulsen, T. G. (2010b). Gas dispersion and immobile gas volume in solid and porous particle biofilter materials at low air flow velocities. J. Air Waste Manage. 60(7), 830-837.

Trussell, R. R., Chang, M. (1999). Review of flow through porous media as applied to head loss in water filters. J. Environ. Eng.-ASCE 125(11), 998-1006.

van Genuchten, M. T. (1980). A closed-form equation for predicting the hydraulic conductivity of unsaturated soils. Soil. Sci. Soc. Am. J. 44(5), 892-898.

van Genuchten, M. T., Wierenga, P. J. (1986). *Solute dispersion coefficients and retardation factors. Methods of soil analysis.* ASA and SSSA, Madison, New York, 1025-1054.

Wadell, H. (1935). Volume, shape and roundness of quartz particles. J. Geol. 43(3), 250-280.

13. Supporting papers

Paper I

Biofilter Media Gas Pressure Loss as Related to Media Particle Size and Particle Shape

Lorenzo Pugliese[1]; Tjalfe G. Poulsen[2]; and Rune R. Andreasen[3]

Abstract: Pressure loss (ΔP) is a key parameter for estimating biofilter energy consumption. Accurate predictions of ΔP as a function of air velocity (V) are, therefore, essential to assess energy consumption and minimize operation costs. This paper investigates the combined impact of medium particle size and shape on the V-ΔP relationship. The V-ΔP measurements were performed using three commercially available materials with different particle shapes: crushed granite (very angular particles), gravel (particles of intermediate roundness), and lightweight clay aggregrate (almost spherical particles). A total of 21 different particle-size fractions, with particle sizes ranging from 2 to 14 mm, were considered for each material. As expected, ΔP decreased with increasing particle size in agreement with earlier findings. The value of ΔP, however, also showed a tendency to decrease with increasing particle roundness especially for fractions containing smaller particles. A new model concept for estimating V-ΔP across different particle-size fractions and shapes was proposed. This model yielded improved prediction accuracy in comparison with existing prediction approaches. **DOI: 10.1061/(ASCE)EE.1943-7870.0000771.** © *2013 American Society of Civil Engineers.*

CE Database subject headings: Air flow; Granular media; Permeability; Particle size distribution; Moisture; Filtration.

Author keywords: Air flow; Granular media; Permeability; Pressure loss; Particle-size distribution; Particle shape; Moisture; Filtration.

Introduction

Biofiltration is one of the most widely employed technologies for removal of organic pollutants (including malodorous compounds) in air streams originating from industrial and commercial activities (Goldstein 1996; Nicolai and Janni 2000). The filtration process is carried out by the use of microorganisms that are immobilized in a biofilm attached to a porous packing (carrier) material such as straw, wood chips, pebbles, or various artificial materials. Removal of the contaminants then occurs as a consequence of the microbial metabolism where the contaminants are degraded to yield carbon and energy for microbial growth. Biofiltration cost efficiency is generally defined as the quantity of air cleaned to a required level per amount of operation costs. Filter cleaning capacity depends on the quantity of active biomass in the filter, which in turn depends on the active specific surface of the packing material. Operation costs are for a large part connected with the energy consumption of the filter, which in turn is mainly associated with the pressure loss across the filter. Thus material physical properties, such as specific surface area and airflow resistance, are key parameters to consider when assessing biofilter performance (Wani et al. 1997; McNevin and Barford 1998; Kim et al. 2000; Elias et al. 2003; Barona et al. 2004). By choosing a proper porous medium, it is possible to increase active microbial biomass (De Oliveira et al. 2009) and contaminant removal capacity (Sakuma et al. 2006) and to reduce the energy consumption associated with the airflow resistance of the biofilter (Malhautier et al. 2005; Gadal-Mawart et al. 2010).

Filter pressure loss (ΔP) is a key parameter for estimating biofilter energy consumption. Accurate predictions of ΔP are, therefore, necessary when designing biofilters, selecting biofilter packing materials, and estimating economic costs. Darcy (1856) proposed a linear expression relating ΔP with packing material properties (permeability) based on studies of water flow in filter sand. Several studies have subsequently investigated the relationship between permeability, particle size, and porosity for porous media (Kozeny 1927; Fair and Hatch 1933; Carman 1937; Scheidegger 1960; Sorrentino and Anlauf 1999; Sperl and Trckova 2008; Hamamoto et al. 2009).

Forchheimer (1901) observed that in porous media at high fluid flow velocity (V), the relationship between V and ΔP was not linear as predicted by Darcy's law but instead followed a second-order relationship. Therefore a quadratic V term was added to the Darcy equation to take the effects of inertial forces and turbulence into account. Ergun (1952) proposed a Forchheimer-based expression that essentially links the ΔP to fluid-filled porosity (ε), a medium particle specific characteristic length (D_{eq}) and a set of empirical constants that were supposed to be universal across different porous materials. Ahmed and Sunada (1969) proposed a rearrangement of the Forchheimer equation using the Navier-Stokes equations. The new relationship showed that the empirical constants were related to the properties of the fluid and the porous media by the intrinsic permeability and a proportionality factor (Chin et al. 2009). Ward (1966) derived the same equation by using a dimensional analysis.

Macdonald et al. (1979) evaluated the accuracy of the Ergun equation. A large number of experimental data from different porous media were used. The results of Macdonald et al. (1979) showed that the empirical constants in the equation were not independent of porous medium properties, thus, complicating the use of

[1]Ph.D. Student, Dept. of Chemistry and Biotechnology, Aalborg Univ., Sohngaardsholmsvej 57, Alborg DK-9000, Denmark (corresponding author). E-mail: lp@bio.aau.dk

[2]Associate Professor, Dept. of Chemistry and Biotechnology, Aalborg Univ., Sohngaardsholmsvej 57, Aarhus DK-9000, Denmark. E-mail: tgp@bio.aau.dk

[3]Postdoctoral Researcher, Dept. of Agroecology, Aarhus Univ., Blichers Allé 20, Aarhus DK-8830, Denmark. E-mail: RuneR.Andreasen@agrsci.dk

Note. This manuscript was submitted on March 20, 2013; approved on August 10, 2013; published online on August 13, 2013. Discussion period open until May 1, 2014; separate discussions must be submitted for individual papers. This paper is part of the ***Journal of Environmental Engineering***, Vol. 139, No. 12, December 1, 2013. © ASCE, ISSN 0733-9372/2013/12-1424-1431/$25.00.

the Ergun equation across different types of porous media. Trussell and Chang (1999) analyzed the validity of the Forchheimer and the derived relations on a large set of data (glass beads, anthracite, sand, potter's beads, marbles, and fragments of crushed dolerite) with respect to impact of medium particle size on ΔP. The results pointed out difficulties in determination of the empirical model parameters, thus, leading to prediction errors. Andreasen and Poulsen (2013) investigated ΔP in a set of coarse-grained porous materials (with a particle diameter greater than or equal to 2 mm) relevant for biofiltration and found that ΔP was only weakly dependent on air-filled porosity (ε) for this type of media. These authors, therefore, proposed a simplified model concept for predicting ΔP based on particle-size distribution and particle diameter rather than on material air-filled porosity as traditionally done. The model, developed and tested using a set of media with a wide range of particle sizes, yielded predictions equivalent to 90% reduction in prediction error compared to the Ergun equation. The media tested, however, all belonged to the same material [Leca (Weber A/S, Denmark), a granular material used for insulation and biofiltration consisting of porous rounded particles] and there is thus, a need to verify if this model concept is applicable for others types of porous materials, including materials with different particle shapes.

Particle shape influences many physical properties of porous materials such as void ratio, internal friction angle, and air permeability (Witt and Brauns 1983; Shinohara et al. 2000; Rouse et al. 2008). Studies by Connell et al. (1999), Endo et al. (2001), and Pugliese et al. (2012) indicate that particle shape does have an impact on the V-$\Delta P/L$ relationship, although at present very little is known about how particle shape affects ΔP in porous media.

The aim of this study is, therefore, to investigate the effects of particle shape on the V-$\Delta P/L$ relationship across porous materials with different particle shapes and particle-size distributions relevant for biofiltration. The investigation will be based on measurement of ΔP in three different commercially available granular materials, which have very different particle shapes: crushed granite (very angular particles), gravel (particles of intermediate roundness), and Leca (almost spherical particles). A total of 21 different particle-size fractions, with particle sizes ranging from 2 to 14 mm were considered for each of the three materials.

Theory

At low V, the ΔP of a fluid flowing through a porous medium can be described by Darcy's law (Darcy 1856) which, however, is only valid for Reynolds numbers (R) (Andreasen et al. 2012) below approximately 1, when flow conditions are laminar and the inertial forces in the flow field are negligible. At R greater than 1 (higher flow V), inertial forces are important, the V-ΔP relationship becomes nonlinear and Darcy's law no longer applies. Several nonlinear equations for relating V and ΔP in this region of R have been presented (Green and Duwez 1951; Cornell and Katz 1953; Geertsma 1974; Antohe et al. 1997; Lage et al. 1997; Trussell and Chang 1999) but the most widely used is the second-order Forchheimer relationship (Forchheimer 1901). This relationship was originally developed for $1 < \mathsf{R} < 100$, but it can also be used to approximate the V-ΔP relationship above $\mathsf{R} = 100$ (Trussell and Chang 1999; Andreasen and Poulsen 2013).

Among the expressions describing fluid flow through packed beds following the Forchheimer relationship, the Ergun equation (Ergun 1952) is perhaps the most widely used. This equation uses an equivalent particle diameter (D_{eq}) and three empirical constants for which Ergun suggested universal values. Macdonald et al. (1979) later tested the Ergun equation against a large set of flow-pressure data from several porous media and found that the empirical constants depended on the physical properties of the media. Macdonald et al. (1991) proposed an expression for estimating D_{eq}, using the first- and the second-order moments of the particle-size distribution. A more thorough presentation of the preceding theory and the equations involved can be found in Andreasen et al. (2012), Andreasen and Poulsen (2013), and Andreasen et al. (2013).

A simpler expression to evaluate D_{eq} was proposed by Andreasen and Poulsen (2013). Based on measurements for a large set of porous media with uniform particle-size distributions originating from the same material (Leca, with diameters ranging from 2 to 18 mm) D_{eq}, for materials with uniform particle-size distributions, was estimated as a harmonic mean of the mean particle diameter (D_m) and the minimum particle diameter (D_{min}) for each medium as

$$D_{\text{eq}} = \frac{2}{\frac{1}{D_m} + \frac{1}{D_{\text{min}}}} \tag{1}$$

Andreasen and Poulsen (2013) further observed that ΔP in these media was almost independent of air-filled porosity and therefore suggested that ΔP can be predicted as

$$\frac{\Delta P}{L} = A\left(\frac{2}{\frac{1}{D_m} + \frac{1}{D_{\text{min}}}}\right)^{-2} \mu V + B\left(\frac{2}{\frac{1}{D_m} + \frac{1}{D_{\text{min}}}}\right)^{-1} \rho V^2 \tag{2}$$

where ΔP = the pressure drop across the medium (Pa); L = the distance over which the pressure drop takes place (m); μ = the air viscosity (Pa s); ρ = the air density (kg/ m^3); V = the superficial air velocity (m/s); and A and B = empirical constants. Based on this study, the authors concluded that a likely dependency of $\Delta P/L$ on particle shape was expected. The authors also suggested that instead of defining D_{eq} based on the smallest and largest particle diameter, improved predictions might be achieved by using alternative values.

Particle shape is often characterized by particle roundness, which is the ratio between the diameters of the largest inscribed and the smallest circumscribing spheres (Santamarina and Cho 2004). Earlier studies (Krumbein 1941; Meloy 1977; Barret 1980; Bowman et al. 2001) have concluded that the projection sphericity (equivalent to roundness) (Cox 1927; Pentland 1927; Tickell 1931; Wadell 1935) represents the best way to analyze effects of particle shape on transport in porous media. Two very widely applied approaches are those of Pentland (1927) and Wadell (1935). Pentland (1927) defined the roundness as

$$\varphi_p = \frac{\omega}{\omega_p} \tag{3}$$

where φ_p = the total degree of roundness (dimensionless) based on Pentland (1927) which cannot be greater than 1; ω = the cross-sectional or projection area of the grain (m^2); and ω_p = the area of the circle having the largest diameter of the grain (m^2). The orientation of the particles was not definite.

Wadell (1935) defined the roundness as

$$\varphi_w = \frac{N}{\sum_N \left(\frac{\mathcal{R}}{r_N}\right)} \tag{4}$$

where φ_w = the total degree of roundness based on Wadell (1935) (dimensionless); N = the number of corners in the given plane of the particle; $\mathcal{R}$ = the radius of the largest inscribed circle (m); and r_N = the radius of the inscribed circle of the Nth corner of the particle in the plane (m).

Materials and Methods

Measurements of ΔP were conducted using three commercially available materials: crushed granite, gravel, and Leca (light expanded clay aggregates). An irregular and very angular particle shape characterizes the crushed granite; gravel consists of somewhat rounded rock fragments and Leca consists of rounded particles. Granite and gravel do not have any internal porosity (inside the particles) while Leca consists of highly porous particles; although this internal porosity is inaccessible by air as it consists of closed vesicles very much like soap foam. Fig. 1 shows the three materials.

All three materials were initially sieved into six particle-size fractions with uniform particle-size distributions. Each of these fractions was characterized by a particle-size range (R) of 2 mm in the range between 2 and 14 mm. Particle diameters (D) were $2 \le D < 4$, $4 \le D < 6$, $6 \le D < 8$, $8 \le D < 10$, $10 \le D < 12$, and $12 \le D < 14$ mm corresponding to mean particle diameter (D_m) of 3, 5, 7, 9, 11, and 13 mm, respectively. Additional fractions with $R = 4$ mm ($D_m = 4$, 6, 8, 10, 12 mm); $R = 6$ mm ($D_m = 5$, 7, 9, 11 mm); $R = 8$ mm ($D_m = 6$, 8, 10); $R = 10$ mm ($D_m = 7$, 9); and $R = 12$ mm ($D_m = 8$), with uniform particle distributions, were produced by combining appropriate quantities of the six $R = 2$ mm fractions. Uniform particle-size distributions were chosen to ensure well-defined particle-size distributions across all particle-size fractions used. A total of 63 particle-size fractions were produced (21 for each material).

For granite, ρ_b for each particle size fraction was measured by packing the material into a known volume followed by weighing. The external porosity (ε_{ex}), which for granite equals ε_{tot}, was calculated from ρ_b using a solid density of 2.75 g/cm^3 (Hausrath et al. 2009; Omosanya et al. 2012). Corresponding values of ρ_b and $\varepsilon_{ex}(\varepsilon_{tot})$ for gravel and Leca were obtained from Sharma and Poulsen (2010) and Andreasen and Poulsen (2013), respectively. For determination of roundness, φ_p and φ_w, 30 particles were randomly selected from each of the 3 materials (5 particles for each of the 6 $R = 2$ mm fractions). For all granite and gravel particles, projections of particle shape onto a flat surface were carried out in three perpendicular planes. For Leca, projections were only carried out in one plane as particle shape was observed to be very similar in all planes. Values of ω and ω_p, and consequently φ_p [Eq. (3)] were subsequently determined from the projections. Values of $\mathcal{R}$ and r_N and consequently φ_w [Eq. (4)] were determined by selecting the two sharpest corners of each projection ($N = 2$) and analyzed using a circle scale as proposed by Wadell (1935). Average values of φ_p and φ_w were then calculated for each material across the 6 $R = 2$ mm particle-size fractions (five particles for each). All measurements were carried out in duplicate. An overview of the media properties is given in Table 1.

Each experiment was performed by packing each of the 21 particle-size fractions for each of the 3 materials into a clear acrylic column of 100 cm in length and 14 cm inner diameter. This column size was chosen in order to avoid effects of preferential flow along the column walls, which may occur if column diameter is too small, compared to the average particle diameter (Pugliese et al. 2012). Great care was taken to achieve a uniform packing (especially along the length of the column), to reduce variations in ρ_b. Measurements of ΔP were carried out for each of the 63 particle size fractions following the approach of Pugliese et al. (2012). Columns were fitted with a polyethylene lid and sealed with a rubber O-ring at the bottom. A stainless steel mesh with 2-mm openings and 1-mm thickness was installed to maintain a distance of 10 mm between the lid and the porous medium. The top of the column was kept open to the atmosphere while the bottom was connected to a supply of compressed atmospheric air via a valve and a precision ball flowmeter (Model P450) (Porter Instrument Div., Hatfield, PA). Soft Teflon tubing with an inner diameter of 4 mm was used to connect system components. Corresponding values of V and ΔP across the columns were measured for $V = 0.005$, 0.010, 0.016, 0.021, 0.032, 0.043, 0.054, and 0.065 m/s, equal to $Q = 5$, 10, 15, 20, 30, 40, 50, and 60 l/min, respectively. The relatively wide Q-range was chosen to get more reliable determination of the V-ΔP relationships for the different media. An Alnor AXD 560 digital manometer (Alnor, Ontario, Canada), connected to the bottom and the top of the column, was used to measure ΔP. Measured ΔP values were corrected for the pressure drop across the empty column with the metal mesh in place. All experiments were carried out in duplicate. A schematic of the experimental setup is shown in Fig. 2.

Results and Discussion

Measured V-$\Delta P/L$ relationships for selected particle-size fractions for all three materials are shown in Fig. 3.

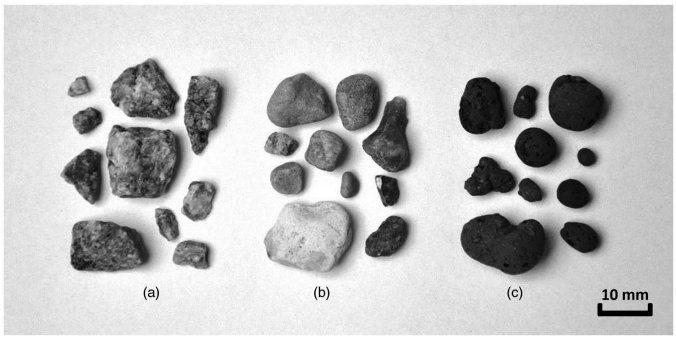

Fig. 1. Porous materials used in the tracer experiments: (a) granite; (b) gravel; (c) Leca

Table 1. Physical Properties of the Three Porous Materials (Granite, Gravel, and Leca) and 63 Particle-Size Fractions

	Granite			Gravel			Leca		
	ρ_p (g/cm^3)	φ_p	φ_W	ρ_p (g/cm^3)	φ_p	φ_W	ρ_p (g/cm^3)	φ_p	φ_W
Size range	2.75	0.64	0.09	2.65	0.65	0.51	0.40	0.80	0.89
(mm)	ρ_b (g/cm^3)	$\varepsilon_{tot} = \varepsilon_{ex}$ (cm^3/cm^3)		ρ_b (g/cm^3)	$\varepsilon_{tot} = \varepsilon_{ex}$ (cm^3/cm^3)		ρ_b (g/cm^3)	ε_{ex} (cm^3/cm^3)	ε_{tot} (cm^3/cm^3)
2–4	1.51	0.45		1.55	0.42		0.33	0.28	0.88
4–6	1.55	0.44		1.54	0.42		0.29	0.39	0.89
6–8	1.52	0.45		1.54	0.42		0.25	0.37	0.91
8–10	1.48	0.46		1.55	0.41		0.25	0.37	0.91
10–12	1.46	0.47		1.55	0.41		0.24	0.36	0.91
12–14	1.47	0.47		1.55	0.41		0.23	0.33	0.91
2–6	1.53	0.44		1.54	0.42		0.31	0.33	0.88
4–8	1.50	0.45		1.53	0.42		0.27	0.37	0.90
6–10	1.53	0.44		1.54	0.42		0.25	0.37	0.91
8–12	1.49	0.46		1.56	0.41		0.24	0.37	0.91
10–14	1.46	0.47		1.55	0.42		0.24	0.35	0.91
2–8	1.55	0.44		1.56	0.41		0.29	0.34	0.89
4–10	1.50	0.45		1.54	0.42		0.26	0.37	0.90
6–12	1.48	0.46		1.55	0.42		0.24	0.37	0.91
8–14	1.49	0.46		1.56	0.41		0.24	0.34	0.91
2–10	1.54	0.44		1.59	0.40		0.27	0.36	0.90
4–12	1.52	0.45		1.58	0.41		0.26	0.37	0.90
6–14	1.52	0.45		1.56	0.41		0.24	0.35	0.91
2–12	1.55	0.44		1.58	0.40		0.27	0.35	0.90
4–14	1.53	0.44		1.59	0.40		0.25	0.36	0.91
2–14	1.54	0.44		1.61	0.39		0.26	0.35	0.90

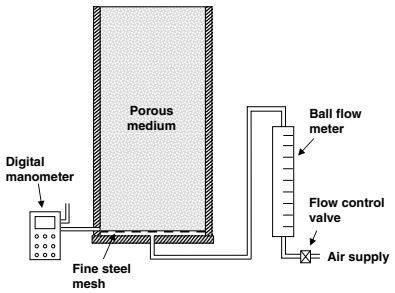

Fig. 2. Experimental setup for measuring pressure loss (ΔP) in porous filter media

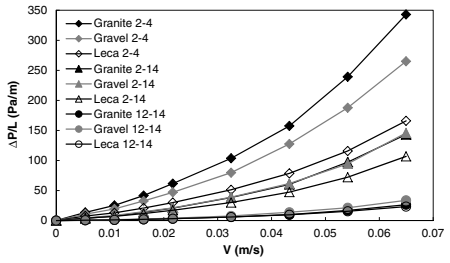

Fig. 3. Measured values of $\Delta P/L$ as a function of V for three selected fractions (2–4, 2–14, 12–14 mm) for the three materials (granite, gravel, Leca) considered in this study

The V-$\Delta P/L$ relationships follow a second-order polynomial in all cases, thus, being consisted with Eq. (2). This was the case for all materials and particle-size fractions investigated. Values of R range up to 60, covering therefore both the Darcy and Forchheimer flow domains. $\Delta P/L$ generally decreased with increasing average particle size. The reason is that smaller particles means smaller pores and, thus, increasing resistance to flow. The smallest pores of the media considered here characterize the 2–4 mm fractions (average particle size equal to 3 mm) and, therefore, this medium has the greatest ΔP. In contrast, the lowest values of $\Delta P/L$ were obtained for the 12–14 mm particle size fraction that has the largest average particle diameter (13 mm) and, therefore, also the largest pores.

For identical particle-size fractions, the crushed granite generally yielded the highest $\Delta P/L$ while Leca yielded the lowest values of $\Delta P/L$ despite the fact that granite has a higher external (active) air-filled porosity compared to Leca (Table 1). In fact, for the three materials considered in this study, $\Delta P/L$ was inversely correlated with active air-filled porosity. This supports the findings of Andreasen and Poulsen (2013) who observed that $\Delta P/L$ was independent of active air-filled porosity across a wide range of Leca particle-size fractions. These authors, therefore, suggested to base models for predicting $\Delta P/L$ in coarse-grained (2–18 mm) granular materials on particle diameter rather than air-filled porosity. This is likely because active porosity in fine-grained materials (less than 2 mm) for which Eq. (2) was originally developed, has a very different structure due to for instance cracks and formation of aggregates compared to coarse-grained materials such as those investigated here. Gravel exhibited intermediate ΔP compared to Leca

and crushed granite. The granite and gravel $\Delta P/L$ were 1.24 and 1.19 times larger than those for the Leca on average across all particle-size fractions, respectively. In general, the relative differences in $\Delta P/L$ between the three materials were most prominent for the fractions containing smaller particles.

Values of particle roundness for the three materials as calculated by Pentland (1927) [Eq. (3)] and Wadell (1935) [Eq. (4)] were lowest for granite and highest for Leca. As the principal difference between the three materials considered here is their particle shape (as characterized by roundness), the deviations in ε_{ex} and ρ_b, and $\Delta P/L$ between the three materials likely result from the differences in roundness. Flow in materials consisting of rounded particles (Leca) should be expected to be more laminar and less subject to inertial forces than flow in materials consisting of more angular (less spherical) particles such as crushed granite. Pugliese et al. (2012) observed that, in two materials with identical particle-size distributions but different particle shapes (pebbles with high roundness and crushed slate with low roundness), dispersivity decreased with decreasing particle roundness. This behavior was therefore attributed to the difference in particle shape. The same authors further observed an inverse linear proportionality between dispersivity and $\Delta P/L$ under otherwise identical conditions. Thus $\Delta P/L$ was observed to increase with decreasing particle roundness supporting that the differences in $\Delta P/L$ observed between the three materials used here mainly stems from differences in particle shape. In general the results discussed earlier show that among the three factors (particle size, particle shape, and porosity) particle size is the most important for controlling $\Delta P/L$ (a well-known fact) followed by particle shape, while porosity has little or no impact on $\Delta P/L$ in coarse-granular materials.

The model [Eq. (2)], suggested by Andreasen and Poulsen (2013) for predicting the V-$\Delta P/L$ relationships in materials with uniform particle-size distributions (developed based on data for 36 Leca particle-size fractions), was tested against the V-$\Delta P/L$ values measured in this study for all three materials (1,008 data points). The test was performed by fitting Eq. (2) to the measured data using the model constants A and B as fitting parameters. Optimal values of A and B for each of the three materials were identified by minimizing the sum of the relative squared errors (RSE) between measured and fitted ΔP values, calculated as

$$\mathrm{RSE} = \sum_{i=1}^{N} \left[\frac{\Delta P/L_{\mathrm{measured}}(i) - \Delta P/L_{\mathrm{predicted}}(i)}{\Delta P/L_{\mathrm{measured}}(i)} \right]^2 \quad (5)$$

where $\Delta P/L_{\mathrm{measured}}$ (i) and $\Delta P/L_{\mathrm{predicted}}$ (i) = the observed and predicted (by the model) pressure gradients, respectively; while N = the total number of measurements.

The optimal values of A and B for the three materials are given in Table 2 and the fitted versus measured values of $\Delta P/L$ by Eq. (2) with the A and B values from Table 2 are shown in Fig. 4 for the three materials.

Values of A and B for Eq. (2) are relatively similar across the three materials with averages of 443 (±9%) and 56 (±15%), respectively, with numbers in parentheses indicating one standard deviation. In general the model is able to fit the data relatively well with relative RSE values ranging from 0.17 to 0.21 indicating that the average squared error in fitting individual values of $\Delta P/L$ is 0.19 on average.

Fig. 4 shows that it is possible to get a relatively close fit of Eq. (2) to the measured $\Delta P/L$ values especially considering that the $\Delta P/L$ varies over three orders of magnitude. The plots, however, also show that Eq. (2) has a tendency to underpredict small $[-0.5 < \log(\Delta P/L) < 0.5]$ and large $[2.0 < \log(\Delta P/L) < 2.5]$ $\Delta P/L$ values. This behavior is actually not seen only for the three data sets as a whole but also for the individual particle-size fractions for each material.

This is illustrated in Fig. 5 that shows the relative deviation between measured and fitted $\Delta P/L$ values [calculated using Eq. (2)] as a function of the measured $\Delta P/L$ for selected

Table 2. Different Approaches and Related Optimal Values of A, B, and a in Terms of Relative Squared Errors for the Three Different Materials

Approach	Equation	A_{granite}	A_{gravel}	A_{Leca}	B_{granite}	B_{gravel}	B_{leca}	a_{granite}	a_{gravel}	a_{Leca}	$\mathrm{RSE}_{\mathrm{granite}}$	$\mathrm{RSE}_{\mathrm{gravel}}$	$\mathrm{RSE}_{\mathrm{Leca}}$	$\mathrm{RSE}_{\mathrm{Tot}}$
Andreasen et al. (2013)	Eq. (2) A, B	481	444	405	53	65	49				0.18	0.17	0.21	0.19
1	Eq. (7) A, B, a	587	604	509	49	63	47	0.72	0.62	0.68	0.15	0.13	0.18	0.15
2	Eq. (7) A, B	599	565	498	49	63	47	0.70	0.15	0.14	0.18	0.16		
3	Eq. (7) A, a	597	642	480	51	0.68	0.15	0.15	0.18	0.16				
4	Eq. (7) B	560	51	63	43	0.73	0.15	0.13	0.18	0.16				
5	Eq. (7) a	560	51	0.73	0.76	0.57	0.15	0.16	0.19	0.17				
6	Eq. (7)	562	51	0.68	0.15	0.17	0.20	0.18						

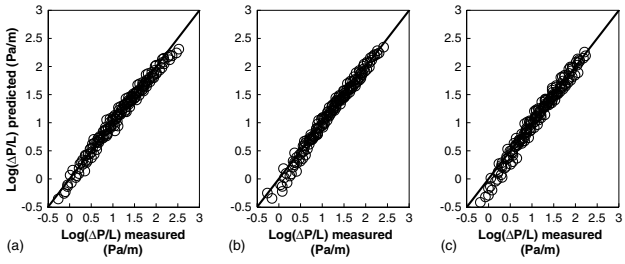

Fig. 4. Fitted [using Eq. (2)] versus measured values of Log $(\Delta P/L)$ for (a) granite; (b) gravel; (c) Leca

particle-size fractions for each of the three materials. In all six cases shown in Fig. 5, the relative deviation between measured and fitted $\Delta P/L$ values as a function of the measured $\Delta P/L$ shows an upward concave relationship. This means that on average the model tends to over predict $\Delta P/L$ at low and high values of $\Delta P/L$ and underpredict at intermediate $\Delta P/L$. This tendency was also observed for all other particle-size fractions across all three materials but tended to be most prominent for particle-size fractions containing mainly small or large particles. The reason is that the model [Eq. (2)] is not able to fully capture the nonlinear relationship between $\Delta P/L$ and V for the materials. As the curvature of the modeled V-$\Delta P/L$ relationship by Eq. (2) is not only controlled by the empirical constants, A and B, but also by the value of D_{eq}, it is likely that a more optimal choice of expression for D_{eq} may improve model results. Andreasen and Poulsen (2013) proposed that D_{eq} might be predicted as the harmonic mean of the smallest and the mean particle diameter present in each particle size fraction [as given by Eq. (1)], thus the smallest and the mean particle sizes are weighted equally in the prediction of D_{eq}. Earlier studies, however, have suggested that the characteristics of granular materials might be predicted using the particle diameters corresponding to the 10 and 60% fractiles of the particle-size distribution, D_{10} and D_{60}, respectively. These particle diameters will also be applicable to nonuniform particle-size distributions while this is not possible when using Eq. (1) as D_{min} is often not known for nonuniform particle-size distributions. Thus, the choice of D_{min} and D_m (corresponding to D_0 and D_{50}) for predicting D_{eq} is likely not the optimal choice. It is also well known that for a given medium consisting of a mixture of particles of different diameters, the smaller particles have a larger impact on $\Delta P/L$ than large particles. Therefore, weighting the two diameters equally in the D_{eq} prediction as done in Eq. (1) may not be the optimal approach.

We, therefore, propose that the following expression for predicting D_{eq} across different materials:

$$D_{eq} = \frac{1}{\left(\frac{a}{D_{10}} + \frac{1-a}{D_{60}}\right)} \tag{6}$$

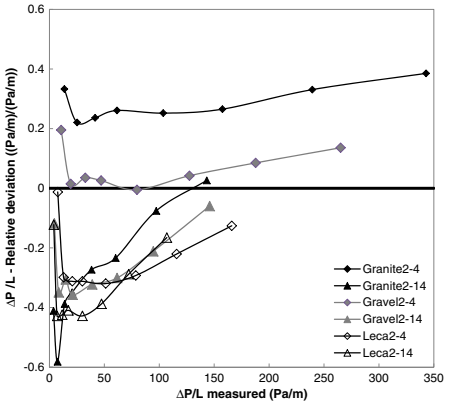

Fig. 5. Relative deviations between fitted [using Eq. (2)] and measured values of $\Delta P/L$ as a function of the measured $\Delta P/L$ for selected particle-size fractions from the three materials considered in this study

where a = a weighting factor $0 < a < 1$; and D_{10} and D_{60} (m) = the particle diameters at which 10 and 60% of the material mass consists of particles with a smaller diameter, respectively. Replacing Eq. (1) with Eq. (6) in Eq. (7) yields

$$\frac{\Delta P}{L} = A\left(\frac{1}{\frac{a}{D_{10}} + \frac{1-a}{D_{60}}}\right)^{-2} \mu V + B\left(\frac{1}{\frac{a}{D_{10}} + \frac{1-a}{D_{60}}}\right)^{-1} \rho V^2 \tag{7}$$

Eq. (7) was, therefore, fitted to the measured V-$\Delta P/L$ data for all three materials using A, B, and a as fitting parameters. Six different fitting approaches were tested: (1) values of A, B, and a were fitted individually for each of the three materials (a total of nine fitting parameters); (2) A and B were fitted individually for each material while one common value of a across all three materials was used (seven fitting parameters); (3) A was fitted individually for each material while common values of B and a were used (five fitting parameters); (4) B was fitted individually for each material while common values of A and a were used (five fitting parameters); (5) a was fitted individually for each material while common values of A and B were used (five fitting parameters); and (6) common values of A, B, and a were used (three fitting parameters). Values of A and B for Eq. (2) and A, B, and a for all six fitting approaches using Eq. (7) are shown in Table 2. Values of the RSE [Eq. (5)] were calculated for each approach both considering each of the three materials individually and all three materials together. These data are also shown in Table 2. Fitted versus measured values of $\Delta P/L$ using approach (1) for all three materials and all gas velocities considered are shown in Fig. 6(a) for granite, Fig. 6(b) for gravel, and Fig. 6(c) for Leca.

The use of Eq. (7) in Approach 1 reduces the RSE by 25% compared to using Eq. (2). The main difference between Eq. (7) in Approach 1 and Eq. (2) is that individual values of D_{eq} for each material are used in the former approach. Thus, although the reduction in RSE is relatively modest, this indicates that improved predictions of $\Delta P/L$ may be achieved by taking into account the effects of particle shape on the value of D_{eq}. Values of A are generally 20–30% higher when using Eq. (7) compared to Eq. (2) while values of B are approximately the same. When using Eq. (7) in Approach 2, there is a clear relationship between A and particle roundness such that A decreases with increasing roundness. For Approaches 1 and 3–6, this tendency is less clear although the lowest values of A are still observed for the highest degree of roundness. Relationships between B, a, and roundness are less clear, although for both parameters the lowest values are observed for the highest degree of roundness indicating that all three parameters A, B, and a are related to particle roundness. Particle roundness may not be the only controlling factor or perhaps not optimal for characterizing particle shape as particles of different shapes may exhibit similar roundness. Also particle characteristics such as surface roughness affect $\Delta P/L$, A, B, and a. Measurement of particle surface roughness on nonspherical particles remains a challenge due to the difficulty in distinguishing particle angularity and particle surface roughness as these two characteristics have similar impact on ΔP.

The data in Table 2, further, show that Eq. (7) can achieve the same (or slightly better) prediction accuracy compared to Eq. (2) using only half the number of empirical fitting parameters [compare Eq. (2) with Eq. (7) Approach 6 in Table 2]. Thus, Eq. (7) offers a much simpler approach for predicting $\Delta P/L$ in granular materials as it only requires one value of A, B, and a regardless of material type, particle shape, and size. The results indicate that $A \approx 562$, $B \approx 51$, and $a \approx 0.7$ are suitable as long as the particle-size distributions of the individual particle-size fractions are uniform. It is very likely that at least some of the empirical parameters A,

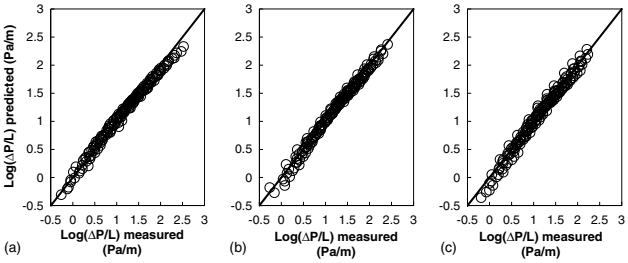

Fig. 6. Measured and predicted [Eq. (7) with A, B, and a fitted individually for each material] values of $\Delta P/L$, for (a) granite; (b) gravel; (c) Leca

B, and a depend on the shape of the particle-size distributions considered, however, more $\Delta P/L$ measurements in media with different particle-size distribution shapes, originating from the same material are needed to verify this.

Conclusions

ΔP as a function of air V was investigated in three different commercially available granular materials, which have very different particle shapes: crushed granite (very angular particles, low roundness); gravel (particles of intermediate roundness); and Leca (almost spherical particles, high roundness). A total of 21 different particle-size fractions were considered, with particle sizes ranging from 2 to 14 mm for each of the three materials.

Overall 1,008 V-$\Delta P/L$ measurements have been carried out. V-$\Delta P/L$ followed a second-order polynomial in agreement with earlier studies. Results showed that $\Delta P/L$ decreased with increasing particle size and that it was inversely correlated with active air-filled porosity. The latter is in contrast to earlier findings for fine-grained materials such as soils and is likely because the pore structure for fine-grained materials is very different from coarse-granular materials used here. Values of $\Delta P/L$ generally decreased with particle roundness. For granite and gravel, $\Delta P/L$ was 1.24 and 1.19 times larger than for Leca on average. Differences in $\Delta P/L$ between the three materials were most prominent for the fractions containing smaller particles. This supports the hypothesis that at least part of the differences in ΔP observed between the three materials used here stems from differences in particle shape (roundness).

An existing model for predicting $\Delta P/L$ as a function of V, developed for Leca, was tested against the V-$\Delta P/L$ values measured in this study, for all three materials. The model performed relatively well although it had a tendency to underpredict small and large while overpredicting intermediate $\Delta P/L$ values. This was the case for the three data sets as a whole but also for the individual particle-size fractions for each material. Thus, an improved model for predicting the V-$\Delta P/L$ relationship was proposed.

This model was able to yield the same accuracy of V-$\Delta P/L$ predictions as the existing model using only half the number of model-fitting parameters (three instead of six) and is, thus, simpler to apply. Results from the modeling further indicated that the material-specific empirical parameters were related to particle shape. Further measurements on other materials with a wider range of particle-size distribution and particle shapes, however, are required to better understand the relationship between the V-$\Delta P/L$ relationship for a given material and its particle size distribution, particle shape, and other characteristics such as particle surface roughness.

References

Ahmed, N., and Sunada, D. (1969). "Nonlinear flow in porous media." *J. Hydr. Div.*, 95(6), 1847–1857.

Andreasen, R. R., Canga, E., Kjaergaard, C., Iversen, B. V., and Poulsen, T. G. (2013). "Relating water and air flow characteristics in coarse granular materials." *Water Air Soil Pollut.*, 224(4).

Andreasen, R. R., Nicolai, R. E., and Poulsen, T. G. (2012). "Pressure drop in biofilters as related to dust and biomass accumulation." *J. Chem. Technol. Biotechnol.*, 87(6), 806–816.

Andreasen, R. R., and Poulsen, T. G. (2013). "Air flow characteristics in granular biofilter media." *J. Environ. Eng.*, 10.1061/(ASCE)EE.1943-7870.0000640, 196–204.

Antohe, B. V., Lage, J. L., Price, D. C., and Weber, R. M. (1997). "Experimental determination of permeability and inertia coefficients of mechanically compressed aluminum porous matrices." *J. Fluids Eng.*, 119(2), 404–412.

Barona, A., Elias, A., Arias, R., Cano, I., and Gonzales, R. (2004). "Biofilter response to gradual and sudden variations in operating conditions." *Biochem. Eng. J.*, 22(1), 25–31.

Barret, P. J. (1980). "The shape of rock particles, a critical review." *Sedimentology*, 27(3), 291–303.

Bowman, E. T., Soga, K., and Drummnond, W. (2001). "Particle shape characterisation using Fourier descriptor analysis." *Geotechnique*, 51(6), 545–554.

Carman, P. C. (1937). "Fluid flow through granular beds." *Trans. Inst. Chem. Eng.*, 15, 150–166.

Chin, D. A., Price, R. M., and DiFrenna, V. J. (2009). "Nonlinear flow in karst formations." *Ground Water*, 47(5), 669–674.

Connell, H., Zhu, J., and Bassi, A. (1999). "Effect of particle shape on crossflow filtration flux." *J. Membr. Sci.*, 153(1), 121–139.

Cornell, D., and Katz, D. L. (1953). "Flow of gases through consolidated porous media." *Ind. Eng. Chem.*, 45(10), 2145–2152.

Cox, E. P. (1927). "A method of assigning numerical and percentage values to the degree of roundness of sand grains." *J. Paleontol.*, 1(3), 179–183.

Darcy, H. (1856). *Les fontaines publiques de la ville de dijon*, V. Dalmont, ed., Paris.

De Oliveira, L. L., Duarte, I. C. S., Sakamoto, I. K., and Varesche, M. B. A. (2009). "Influence of support material on the immobilization of biomass for the degradation of linear alkylbenzene sulfonate in anaerobic reactors." *J. Environ. Manage.*, 90(2), 1261–1268.

Elias, A., Arias, R., Cano, I., Gonzales, R., and Barona, A. (2003). "Effect of sudden variations in operating conditions on biofilter performance." *Air Pollut.*, 13, 523–529.

Endo, Y., Chen, D. R., and Pui, D. Y. H. (2001). "Air and water permeation resistance across dust cakes on filters-effects of particle polydispersity and shape factor." *Powder Technol.*, 118(1–2), 24–31.

Ergun, S. (1952). "Fluid flow through packed columns." *Chem. Eng. Prog.*, 48(2), 89–94.
Fair, G. M., and Hatch, L. P. (1933). "Fundamental factors governing the streamline flow of water through sand." *J. — Am Water Works Assoc.*, 25, 1551–1565.
Forchheimer, P. H. (1901). "Wasserbewegung durch boden." Zeitschrift ver deutscher ingenieure 50, 1782–1788 (in German).
Gadal-Mawart, A., Malhautier, L., Renner, C., and Fanlo, J. L. (2010). "Physicochemical and hydrodynamic characterisation of various packing materials for biofiltration." *Proc., 2010 Duke-UAM Conf. on Biofiltration for Air Pollution Control*, Duke Univ., Durham, NC.
Geertsma, J. (1974). "Estimating coefficient of inertial resistance in fluid-flow through porous-media." *Soc. Pet. Eng. J.*, 14(5), 445–450.
Goldstein, N. (1996). "Odor control experiences: Lessons from the biofilter." *Biocycle*, 37(4), 70–74.
Green, L., and Duwez, P. (1951). "Fluid flow through porous metals." *J. Appl. Mech. Trans. ASME*, 18(1), 39–45.
Hamamoto, S., Moldrup, P., Kawamoto, K., and Komatsu, T. (2009). "Effect of particle size and soil compaction on gas transport parameters in variably saturated, sandy soils." *Vadose Zone J.*, 8(4), 986–995.
Hausrath, E. M., Neaman, A., and Brantley, S. L. (2009). "Elemental release rates from dissolving basalt and granite with and without organic ligands." *Am. J. Sci.*, 309(8), 633–660.
Kim, N. J., Hirai, M., and Shoda, M. (2000). "Comparison of organic and inorganic packing materials in the removal of ammonia gas in biofilters." *J. Hazard. Mater.*, 72(1), 77–90.
Kozeny, J. (1927). "Über kapillare leitung des wassers im boden." *Akad. Wiss. Wien*, 136, 271–306 (in German).
Krumbein, W. C. (1941). "Measurements and geological significance of shape and roundness of sedimentary particles." *J. Sediment. Petrol.*, 11(2), 64–72.
Lage, J. L., Antohe, B. V., and Nield, D. A. (1997). "Two types of nonlinear pressure-drop versus flow rate relation observed for saturated porous media." *J. Fluids Eng. Trans. ASME*, 119(3), 700–706.
Macdonald, I. F., El-Sayed, M. S., Mow, K., and Dullien, F. A. L. (1979). "Flow through porous media—The Ergun equation revisited." *Ind. Eng. Chem. Fundam.*, 18(3), 199–208.
Macdonald, M. J., Chu, C. F., Guilloit, P. P., and Ng, K. M. (1991). "A generalized Blake-Kozeny equation for multisized spherical-particles." *Aiche J.*, 37(10), 1583–1588.
Malhautier, L., Khammar, N., Bayle, S., and Fanlo, J. L. (2005). "Biofiltration of volatile organic compounds." *Appl. Microbiol. Biotechnol.*, 68(1), 16–22.
McNevin, D., and Barford, J. (1998). "Modelling adsorption and biological degradation of nutrients on peat." *Biochem. Eng. J.*, 2(3), 217–228.
Meloy, T. P. (1977). "Fast Fourier transforms applied to shape analysis of particle silhouettes to obtain morphological data." *Powder Technol.*, 17(1), 27–35.
Nicolai, R. E., and Janni, K. A. (2000). "Designing biofilters for livestock facilities." *Proc. 2nd Int. Conf. on Air Pollution from Agricultural Operations*, American Society of Agricultural Engineers, St. Joseph, MI, 376–383.
Omosanya, K. O., Mosuro, G. O., Laniyan, T. A., and Ogunleye, D. (2012). "Prediction of gravity anomaly from calculated densities of rocks." *Adv. Appl. Sci. Res.*, 3(4), 2059–2068.
Pentland, A. (1927). "A method of measuring the angularity of sands." *Royal Soc. Canada Proc. Trans.*, 21(3), Appendix C.
Pugliese, L., Poulsen, T. G., and Andreasen, R. R. (2012). "Relating gas dispersion in porous media to medium tortuosity and anisotropy ratio." *Water Air Soil Pollut.*, 223(7), 4101–4118.
Rouse, P. C., Fannin, R. J., and Shuttle, D. A. (2008). "Influence of roundness on the void ratio and strength of uniform sand." *Geotechnique*, 58(3), 227–231.
Sakuma, T., Hattori, T., and Deshusses, M. A. (2006). "Comparison of different packing materials for the biofiltration of airtoxics." *J. Air Waste Manage. Assoc.*, 56(11), 1567–1575.
Santamarina, J. C., and Cho, G. C. (2004). "Soil behaviour: The role of particle shape." *Proc., Skempton Conf.*, British Geotechnical Association, Imperial College London, London.
Scheidegger, A. E. (1960). *The physics of flow through porous media*, Macmillan, New York.
Sharma, P., and Poulsen, T. G. (2010). "Gas dispersion and immobile gas volume in solid and porous particle biofilter materials at low air flow velocities." *J. Air Waste Manage. Assoc.*, 60(7), 830–837.
Shinohara, K., Oida, M., and Golman, B. (2000). "Effect of particle shape on angle of internal friction by triaxial compression test." *Powder Technol.*, 107(1–2), 131–136.
Sorrentino, J. A., and Anlauf, H. (1999). "Some simple relationships about the influence of particle size distribution on cake permeability." *Adv. Filtrat. Separ. Technol.*, 13A–13B, 917–925.
Sperl, J., and Trckova, J. (2008). "Permeability and porosity of rocks and their relationship based on laboratory testing." *Acta Geodyn. Geomater.*, 5(1), 41–47.
Tickell, F. G. (1931). *The examination of fragmental rocks*, Stanford University Press, London.
Trussell, R. R., and Chang, M. (1999). "Review of flow through porous media as applied to head loss in water filters." *J. Environ. Eng.*, 10.1061/(ASCE)0733-9372(1999)125:11(998), 998–1006.
Wadell, H. (1935). "Volume, shape and roundness of quartz particles." *J. Geol.*, 43(3), 250–280.
Wani, A. H., Branion, R. M. R., and Lau, A. K. (1997). "Biofiltration: A promising and cost-effective control technology for odors, VOCs and air toxics." *J. Environ. Sci. Health Part A: Toxic/Hazard. Subst. Environ. Eng.*, 32(7), 2027–2055.
Ward, J. C. (1966). "Closure to turbulent flow in porous media." *J. Hydr. Div.*, 92(4), 110–121.
Witt, K. J., and Brauns, J. (1983). "Permeability—anisotropy due to particle shape." *J. Geotech. Eng.*, 109(9), 1181–1187.

Paper II

Water Air Soil Pollut (2014) 225:1811
DOI 10.1007/s11270-013-1811-y

Linking Gas and Liquid Pressure Loss to Particle Size Distribution and Particle Shape in Granular Filter Materials

Lorenzo Pugliese · Tjalfe G. Poulsen

Received: 6 August 2013 / Accepted: 7 November 2013 / Published online: 29 November 2013

Abstract The cost efficiency of filtration is often associated with the filter flow velocity (V) and pressure loss (ΔP). Knowledge of the $V-\Delta P$ relationship for a given filter medium–fluid combination is therefore necessary when assessing operation costs. Liquid $V-\Delta P$ measurements are generally much more time-consuming than for gases, thus predicting liquid $V-\Delta$P relationships from corresponding gas data is advantageous. The objective of this work was to identify the relationship between air and water pressure gradients during air and water flow in granular filter media. Three materials: crushed granite, gravel, and Leca® (an insulation material) with very different particle shapes were used. Twenty-one media with different particle size distributions were produced from each material (63 in total) and $V-\Delta P$ measurements carried out using air and water. The results showed that it is indeed possible to predict liquid $V-\Delta P$ relationships from corresponding gas $V-\Delta P$ measurements together with medium physical characteristics. A simple model concept for prediction was proposed. The results also indicated that it is possible to predict both gas and liquid $V-\Delta P$ relationships in coarse granular filter media based simply on knowledge about the particle size distribution and particle shape for the medium in question.

Keywords Pressure loss · Granular filter media · Gas and liquid flow · Particle size distribution · Particle shape · Predictive modeling

L. Pugliese (✉)
Department of Chemistry and Biotechnology,
Aalborg University,
Sohngaardsholmsvej 57, 9000 Aalborg, Denmark
e-mail: lp@bio.aau.dk

T. G. Poulsen
Department of Civil Engineering,
Xi'an Jiaotong–Liverpool University,
Suzhou, China
e-mail: Tjalfe.Poulsen@xjtlu.edu.cn

1 Introduction

Filtration (including biofiltration) is a successful and widely applied technology for removal of unwanted compounds and suspended matter, from gases and liquids. Typical application areas are cleaning of air streams from industrial production, drinking and wastewater treatment, energy, and animal production. A wide selection of literature documenting the application of filtration is available. Examples are O'Neill et al. (1992), Mohammad and Najar (1997), Cohen-Shoel et al. (2002), Erhan et al. (2002), Zouboulis et al. (2002), Den et al. (2004), Wang et al. (2007), Plascak et al. (2008), Chen and Hoff (2009), Balasubramanian et al. (2012), He et al. (2012), and Lee et al. (2013). Filter operation costs are primarily associated with filter energy consumption, which in turn is controlled by filter flow velocity (V) and pressure loss (ΔP) across the filter (Leson and Winer 1991; Scotford et al. 1996; Pugliese et al. 2013).

Investigations of the $V-\Delta P$ relationship in granular filter media were first carried out by Darcy (1856), who linked the pressure loss to filter medium permeability

and proposed a linear relationship between V and ΔP. Forchheimer (1901) improved the Darcy equation, after observing a second-order relationship in porous media at high V. A Forchheimer-based expression was derived by Ergun (1952), linking pressure loss to medium particle specific characteristic length (D_{eq}) using a set of universal empirical constants. Ahmed and Sunada (1969) introduced a relation involving the properties of both the fluid and the porous medium based on the Navier-Stokes equations. Other expressions for the $V-\Delta P$ relationship were proposed by Macdonald et al. (1979), van Genuchten (1980), Alexander and Skaggs (1986), and Poulsen and Moldrup (2007). Common to all these models is that they require knowledge of theoretical and empirical parameters, which are strongly dependent on fluid properties and media physical characteristics (Macdonald et al. 1979), such as porosity, particle size distribution, and particle shape (Trussell and Chang 1999). This means that, for each new medium considered, $V-\Delta P$ measurements are generally necessary in order to use the models, which reduces their usefulness somewhat. Based on the Ergun (1952) equation, Andreasen and Poulsen (2013) proposed a relationship for predicting the $V-\Delta P$ relationship for gas transport in a wide range of media (particle sizes), which needs only knowledge of the $V-\Delta P$ relationship for one single medium as long as all these media consists of particles with the same shape. The model also requires that all media have uniform particle size distributions. There are, however, no requirements with respect to medium porosity or the range of particle sizes (including mean particle size) included in each medium. This model, however, has only been tested against data for a single material (particle shape), and further tests to evaluate its applicability to other materials are therefore required.

Measurements of the $V-\Delta P$ relationship for liquids ($V_l-\Delta P_l$) are generally more time-consuming to carry out than for gases ($V_g-\Delta P_g$) (Andreasen et al. 2013). This is partly because gases flow faster for the same pressure difference and porous medium, and therefore achieve steady-state conditions more rapidly, and partly because the measurement equipment is heavier and more difficult to handle when it comes to liquids. Filtration often involves high fluid velocity and consequently inertial forces in the flow field must be taken into account (Firdaouss et al. 1997; Trussell and Chang 1999; Zeng and Grigg 2006). Based on the experience by the authors, measurements for liquids (water) at such flow velocities take six to ten times longer than corresponding gas (air) measurements. Significant time savings can therefore be achieved if $V_l-\Delta P_l$ can be determined from corresponding $V_g-\Delta P_g$ measurements.

Gas and liquid flow through porous media is controlled by the same parameters and is affected by these parameters in a similar manner. Several studies have focused on relating corresponding $V_g-\Delta P_g$ and $V_l-\Delta P_l$ relationships for a given porous medium. Schjonning (1986) introduced an exponential relationship relating hydraulic conductivity (k_l) and air permeability (k_g), using data from the analysis of 405 undisturbed 100 cm^3 soil cores. A similar relationship was proposed in a later study performed on 229 undisturbed soil samples (Riley and Ekeberg 1989) and again in another study by Loll et al. (1999) using 1,614 soil samples from nine soils. Blackwell et al. (1990) suggested a linear relationship between k_l and k_g. The concept of predicting $V_l-\Delta P_l$ from $V_g-\Delta P_g$ for one of the coarse granular materials (Leca®) as also used here was further investigated by Andreasen et al. (2013). These authors found for a large set of particle size fractions with uniform particle size distribution but different mean particle diameter and particle size range that empirical constants necessary for their model were independent of mean diameter and particle size range, but reliant on the particle shape, and consequently on the used medium. Despite the fact that most of the existing studies focus on soils, they clearly show that $V-\Delta P$ for gas and liquid is medium dependent. As filters generally are made of coarse grained materials, and the number of studies investigating the $V-\Delta P$ relationship for gases and liquids in granular filter materials is very limited, more research is required to investigate the impact of filter medium properties on fluid flow in these materials.

The objective of this paper is therefore to investigate the connection between the $V_g-\Delta P_g$ and $V_l-\Delta P_l$ relationships across porous media with a wide range of particle size distributions, originating from multiple materials with different particle shapes. The aim is to develop an expression for predicting the $V_l-\Delta P_l$ relationship from the corresponding $V_g-\Delta P_g$ relationship for a given medium, based on a limited number of parameters. Three materials with particle shapes ranging from very angular (crushed granite) over intermediate roundness (gravel) to almost spherical (Leca®) were

selected. From these materials, a large set of granular porous media covering a wide range of particle sizes were produced and used in the analyses. Measurements were carried out using atmospheric air and water, as they are inexpensive, readily available, easy to measure, safe to use, and further represent the majority of filter applications in practice.

2 Theory

Darcy's law is traditionally used to describe fluid flow through porous media, at low velocities. For one-dimensional fluid flow, through a section of medium with thickness L (meters), it is given as:

$$\frac{\Delta P}{L} = \frac{\mu}{K} V \tag{1}$$

where ΔP is the pressure loss across the medium (Pascals), L is the distance over which the pressure loss takes place (meters), μ is the fluid viscosity (Pascals per second), K is the medium intrinsic permeability (square meters), and V is the superficial fluid velocity (meters per second) also known as the Darcy velocity, expressed as:

$$V = \frac{Q}{A_c} \tag{2}$$

Where Q is the volumetric flow (cubic meters per second) and A_c is the medium cross-sectional area, perpendicular to the flow direction (square meters). Equation 1 is only valid for Reynolds numbers (Re) below approximately 1 (Trussell and Chang 1999), when flow conditions are laminar and the inertial forces in the flow field are negligible.

Reynolds number (dimensionless) measures the ratio between the inertial and the viscous forces for given flow conditions. For a porous medium, it is defined as:

$$Re = \frac{\rho V d}{\mu} \tag{3}$$

where ρ is the fluid density (kilograms per cubic meter) and d is the mean particle diameter (meters). At $Re>1$ (higher flow velocities), inertial forces are important, the $V-\Delta P/L$ relationship becomes non-linear and Eq. 1 no longer applies. Several non-linear equations relating V and $\Delta P/L$ in this region of Re have been presented (Green and Duwez 1951; Cornell and Katz 1953; Geertsma 1974; Antohe et al. 1997; Lage et al. 1997; Trussell and Chang 1999), but the most widely used is the second-order Forchheimer relationship (Forchheimer 1901):

$$\frac{\Delta P}{L} = \frac{\mu}{K} V + \rho C_f V^2 \tag{4}$$

where C_f is a form coefficient (per meters) which depends on the porous medium characteristics. Equation 4 is valid for both gases and liquids and applies for $1<Re<100$, where the flow is still laminar but inertial effects become increasingly important with increasing Re. Above $Re=100$ (transition regime), Eq. 4 may be used to approximate the $V-\Delta P/L$ relationship, although turbulent forces start appearing (Trussell and Chang 1999; Andreasen and Poulsen 2013).

Ergun (1952) introduced one of the most widely known and used Forchheimer-based equation, describing fluid flow in porous media. This semi-empirical equation is given as:

$$\frac{\Delta P}{L} = A\frac{(1-\varepsilon_{\text{tot}})^2}{\varepsilon_{\text{tot}}^p} D_{\text{eq}}^{-2} \mu V + B\frac{(1-\varepsilon_{\text{tot}})}{\varepsilon_{\text{tot}}^p} D_{\text{eq}}^{-1} \rho V^2 \tag{5}$$

where A, B, and p are empirical constants, D_{eq} is an equivalent particle diameter (meters) and ε_{tot} is the total porosity (cubic meters per cubic meter), expressed as:

$$\varepsilon_{\text{tot}} = 1-\frac{\rho_b}{\rho_p} \tag{6}$$

where ρ_b is the dry bulk density (kilograms per cubic meter) and ρ_p is the particle density (kilograms per cubic meter). In Eq. 5, the Forchheimer parameters K and C_f are expressed as:

$$K = \frac{1}{A}\frac{\varepsilon_{\text{tot}}^p}{(1-\varepsilon_{\text{tot}})^2} D_{\text{eq}}^2 \tag{7}$$

$$C_f = B\frac{(1-\varepsilon_{\text{tot}})}{\varepsilon_{\text{tot}}^p} D_{\text{eq}}^{-1} \tag{8}$$

Ergun (1952) suggested universal values of the empirical constants A, B, and p valid for any fluid and porous medium equal to 150, 1.75, and 3, respectively. The universal applicability of these values was tested later by Macdonald et al. (1979), on a large set of flow-pressure data who found that the constants depended on particle shape. Values of A, B, and p equal to 180, 1.8, and 3.6 for smooth particles and 180, 4, and 3.6 for

rough particles were identified. Macdonald et al. (1979) used D_{eq} for spherical particles as:

$$D_{eq} = \frac{1}{\sum_i Y_i \left(6\frac{V_{p,i}}{A_{p,i}}\right)^{-1}} \quad (9)$$

where Y_i, $V_{p,I}$, and $A_{p,i}$ are the volumetric fraction, the particle fraction, and the particle surface area of the ith particle, respectively. As Eq. 9 is only valid for spherical particles, an alternative and universal expression for estimating D_{eq} was considered (Macdonald et al. 1991):

$$D_{eq} = \left(\frac{M_2}{M_1}\right) \quad (10)$$

where M_2 and M_1 are the first- and the second-order moments of the particle size distribution, with

$$M_i = \int_0^\infty D_p^i n_p^i(D_p)\, dD_p \quad (11)$$

where M_i is the ith moment, $D_p{}^i$ is the particle diameter, and $n_p{}^i(D_p)dD_p$ represents the number of particles with diameters between $D_p{}^i$ and $D_p{}^i + dD_p$.

Andreasen and Poulsen (2013) investigated V_g–$\Delta P_g/L$ relationships for a large set of coarse-grained media with uniform particle size distributions originating from the same material (Leca®) using the Ergun (1952) equation. The authors observed that $\Delta P_g/L$ in these media was almost independent of air-filled porosity and therefore suggested that $\Delta P_g/L$ can be predicted as:

$$\frac{\Delta P_g}{L} = A_\varepsilon D_{eq}{}^{-2}\mu V + B_\varepsilon D_{eq}{}^{-1}\rho V^2 \quad (12)$$

where D_{eq}, A_ε, and B_ε are expressed as:

$$D_{eq} = \frac{2}{\frac{1}{D_m} + \frac{1}{D_{min}}} \quad (13)$$

$$A_\varepsilon = A\frac{(1-\varepsilon_{tot})^2}{\varepsilon_{tot}^p} \quad (14)$$

$$B_\varepsilon = B\frac{(1-\varepsilon_{tot})}{\varepsilon_{tot}^p} \quad (15)$$

where D_m and D_{min} are the mean and minimum particle diameter (meters) in the uniform particle size distribution, respectively.

Andreasen et al. (2013) suggested the use of an empirical constant (f) for air flow (f_g) and for water flow (f_l), to enable prediction of V_l–$\Delta P_l/L$ from V_g–$\Delta P_g/L$ in a given granular material (Leca®). For the Leca® material used by Andreasen et al. (2013), the values of f turned out to be independent of the particle size distribution. Thus, to calculate V_l–$\Delta P_l/L$ for a specific medium by using Eq. 4, K_l and $C_{f,l}$ were expressed as:

$$K_l = K_g\left(\frac{f_l}{f_g}\right)^2 \quad (16)$$

$$C_{f,l} = C_{f,g}\left(\frac{f_g}{f_l}\right) \quad (17)$$

Pugliese et al. (2013) tested Eq. 12 against gas flow data from a set of 63 porous media originating from three different materials and suggested that D_{eq} should be predicted as:

$$D_{eq} = \frac{1}{\left(\frac{a}{D_{10}} + \frac{1-a}{D_{60}}\right)} \quad (18)$$

where a is a weighting factor $0<a<1$ and D_{10}, D_{60} (meters) are the particle diameters at which 10 % and 60 % of the material mass consists of particles with a smaller diameter, respectively. Substituting Eq. 18 in Eq. 12 yields:

$$\frac{\Delta P}{L} = A\left(\frac{1}{\frac{a}{D_{10}} + \frac{1-a}{D_{60}}}\right)^{-2}\mu V + B\left(\frac{1}{\frac{a}{D_{10}} + \frac{1-a}{D_{60}}}\right)^{-1}\rho V^2 \quad (19)$$

3 Materials and Methods

Three commercially available granular materials: (1) crushed granite, (2) gravel, and (3) Leca® (Light Expanded Clay Aggregates) were used in the analyses. The crushed granite has a very angular particle shape and no internal porosity. Gravel has a more rounded particle shape and no internal porosity. Leca® consists of round (in some cases almost spherical) particles which are highly porous. Most of this internal porosity, however, consists of closed vesicles and is therefore not accessible for fluid flow.

Leca® was acquired from Saint-Gobain Weber A/S, Randers, Denmark, while gravel and granite were acquired from JM Service, Nørresundby, Denmark. All three materials were initially sieved into six particle size fractions with uniform particle size distributions. Each of these fractions was characterized by a particle size range (R) of 2 mm, in the range between 2 and 14 mm. Particle diameters (D) in each fraction were $2 \le D < 4$, $4 \le D < 6$, $6 \le D < 8$, $8 \le D < 10$, $10 \le D < 12$, and $12 \le D < 14$ mm, respectively, corresponding to mean particle diameter (D_m) of 3, 5, 7, 9, 11, and 13 mm, respectively. Additional particle size fractions with R=4 mm (D_m=4, 6, 8, 10, 12 mm), R=6 mm (D_m=5, 7, 9, 11 mm), R=8 mm (D_m=6, 8, 10), R=10 mm (D_m=7, 9), and R=12 mm (D_m=8), with uniform particle size distributions, were produced by combining appropriate quantities of the six R=2 mm fractions. Uniform particle size distributions were chosen to ensure well-defined particle size distributions across all particle size fractions used. A total of 63 particle size fractions were produced (21 for each material). Each particle size fraction was packed into a 100-cm long and 14-cm inner diameter clear acrylic column. This column diameter was chosen to avoid effects of preferential flow along the column walls, which may occur if column diameter is too small, compared with the average particle diameter (Pugliese et al. 2012). Packing was done carefully to achieve homogeneity and reduce variation in terms of bulk density (ρ_b) along the length of the column. Columns were fitted with a polyethylene lid and sealed with a rubber O-ring at the bottom. A stainless steel mesh with 2-mm openings and 1-mm thickness was installed to prevent loss of material and to maintain a distance of 10 mm between the lid and the porous medium. Soft Teflon tubing with an inner diameter of 4 mm was used to connect system components. The top of the columns were kept open to the atmosphere.

V–$\Delta P/L$ measurements for air flow (V_g–$\Delta P_g/L$) in the 63 media were carried out in an earlier study by Pugliese et al. (2012). For these measurements, the bottom of each column was connected to a supply of compressed atmospheric air via a valve and a precision ball flow meter (model P450; Porter Instruments). Corresponding values of V and ΔP across the columns were measured for V=0.005, 0.010, 0.016, 0.021, 0.032, 0.043, 0.054, and 0.065 m s^{-1}, equal to Q=5, 10, 15, 20, 30, 40, 50, and 60 l min^{-1}, respectively. The relatively wide Q-range was chosen to get a more reliable determination of the V_g–$\Delta P_g/L$ relationships for the different media. An Alnor AXD 560 digital manometer (Alnor, Ontario, Canada), connected to the bottom and the top of the column, was used to measure ΔP. Following the first round of measurements, all columns were repacked and measurements repeated a second time. A schematic of the air flow setup is shown in Fig. 1a.

V–$\Delta P/L$ liquid measurements, conducted using water (V_l–$\Delta P_l/L$) were carried out (in this study) under constant head conditions. The bottom of each column was connected to a constant-head water tank, in turn connected to a water reservoir via a pump (model E BS 5000 PT11 230 V, Flojet, Hoddesdon, UK). The flow through the column was controlled by changing the elevation of the constant head tank. Prior to measurements, columns were saturated from the bottom over a period of 30 min to achieve equilibrium. That this time period was sufficient was verified several times before starting the experiments via measurements of the effluent volume. Values of V_l were determined by collecting the effluent water from the column over a given period of time followed by weighing. Corresponding values of $\Delta P_l/L$ were determined from the difference in elevation between the water surface in the constant head tank and the water level at the top of the saturated column (Fig. 1b). For each column, one set of V_l–$\Delta P_l/L$ data covering eight water flow rates was collected. Columns were subsequently drained and repacked, and another set of V_l–$\Delta P_l/L$ measurements were carried out. For Leca®, which has a very low ρ_b, a stainless steel mesh was also used at the top of the columns to prevent loss of material via the outlet. A schematic of the water flow setup is shown in Fig. 1b.

Air and water flow rates were selected to cover approximately the same range of Reynolds number ($0 \le Re \le 125$). All measured $\Delta P/L$ values were corrected for the empty column pressure loss (with the metal mesh in place).

When fitting predictive models to the measured data, fitting accuracy, for both air and water measurements, was quantified using the root mean square error (RMSE):

$$RMSE = \sqrt{\frac{1}{N}\sum_{i=1}^{N}\left[\Delta P\Big/L_{\text{measured}}(i) - \Delta P\Big/L_{\text{predicted}}(i)\right]^2} \tag{20}$$

and the relative squared error (RSE), defined as:

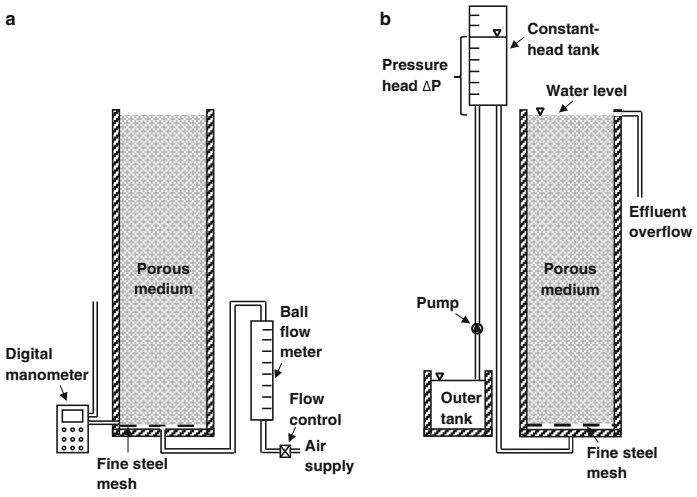

Fig. 1 Experimental setup measuring the $V-\Delta P/L$ relationship in **a** air and **b** water measurements

$$RSE = \sum_{i=1}^{N} \left[\frac{\left(\Delta P \Big/ L_{\text{measured}}(i) - \Delta P \Big/ L_{\text{predicted}}(i) \right)}{\Delta P \Big/ L_{\text{measured}}(i)} \right]^2 \quad (21)$$

where $\Delta P/L_{\text{measured}}$ (i) and $\Delta P/L_{\text{predicted}}$ (i) are the ith observed and predicted (by the predictive model) $\Delta P/L$ values, respectively, while N is the total number of measurements (2016). The minimization procedure was carried out using a non-linear least-square method (the Solver add-in) in Microsoft Excel.

4 Results and Discussion

The $V-\Delta P/L$ and $Re-\Delta P/L$ relationships for both air and water flow all followed second-order expressions in agreement with Eq. 4. Measured $Re-\Delta P/L$ relationships for both air and water flow experiments are shown for selected particle size fractions for all three materials in Fig. 2.

Values of $Re(=\rho Vd/\mu)$ range up to 60 and 125 for air and water measurements, respectively, covering the laminar ($Re<1$), Forchheimer ($1<Re<100$) and part of the transition ($Re\geq 100$) flow regime (Trussell and Chang 1999). As expected, $\Delta P/L$ decreases with increasing particle size for fixed values of Re (or V) across all three materials. The reason is that larger particles results in larger pores which in turn generate lower resistance to both gas and liquid flow and consequently lower pressure losses. For all particle size fractions and for both gases and liquids, there is a tendency that $\Delta P/L$ depends on the particle shape of the used material. For air flow (Fig. 2a), granite (the most angular material) generally exhibits the highest $\Delta P/L$ values for fixed Re and particle size distribution (fixed R and D_m). For water flow (Fig. 2b), however, Leca® (the most rounded material) shows the highest values of $\Delta P/L$, although the tendency is much weaker than for the air flow data. The reason is likely that particle shape affects the flow field and thus the pressure loss. Because the flow fields for air and water in the same medium are not identical (Schjonning 1986; Riley and Ekeberg 1989; Loll et al. 1999), particle shape does not affect the flow of the two fluids in the same manner, thus, the difference. That particle shape (roundness) may affect fluid transport properties in porous media was documented by Pugliese et al. (2012) who observed a dependency between fluid dispersion and roundness, thus, supporting the findings in Fig. 2. Individual values of D_{eq} for each of the 63 particle size fractions for both air and water were determined by fitting Eq. 12 to the measured data using common optimized values of A

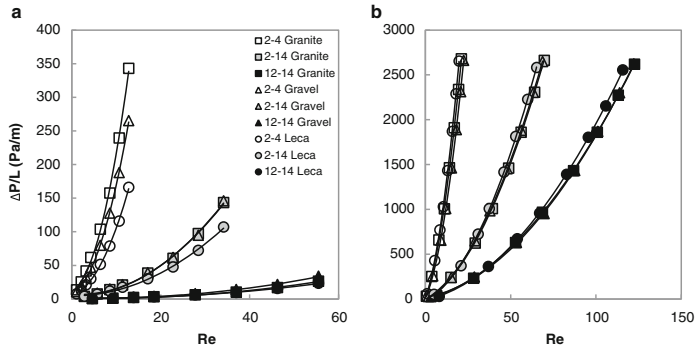

Fig. 2 Measured $\Delta P/L$ values as a function of *Re* for **a** air and **b** water flow measurements, for selected particle size fractions for all three materials

and B across all materials, particle size fractions, and fluids. Fitting accuracy was calculated using the RSE (Eq. 21). Optimal values of D_{eq}, for all combinations of fluid, material, and particle size fraction, are shown in Fig. 3 as a function of D_{10} and $D_{60}-D_{10}$. Optimal values of A and B were 553 and 67, respectively.

For all six combinations of fluid and material (particle shape), D_{eq} increases strongly with D_{10}, and to some degree also with $D_{60}-D_{10}$, although this relation is much weaker than with D_{10}. Andreasen at al. (2013) found that, for a given material, particles with small diameters tend to fill the pores between the larger particles reducing the size of the fluid conducting pores. Thus, the fluid resistance is mainly controlled by the smaller particles in the medium which is why D_{eq} mainly depends on the diameter of the smaller particles in each medium and much less on the total range of particle diameters present in each of the 63 particle size fractions used. Thus, D_{eq} may be viewed as an equivalent diameter of the particles controlling fluid resistance rather than a representative diameter for all particle sizes in the medium. For air flow D_{eq} values range from 0.002 to 0.016 m while, for water flow, values range from 0.002 to 0.003 m. This is in agreement with earlier findings of

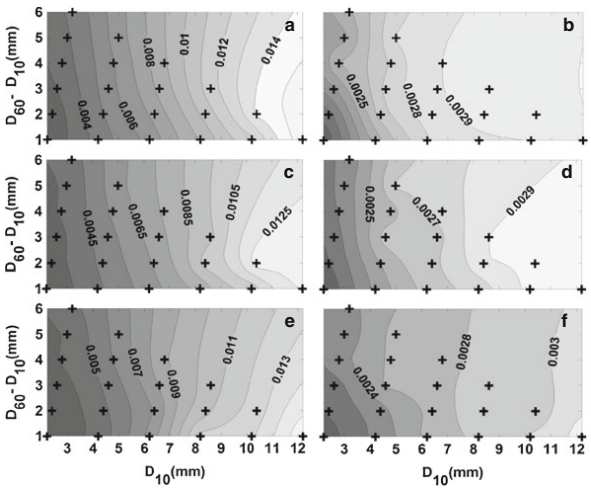

Fig. 3 Contour plots of D_{eq} (identified by fitting Eq. 12 to the measured $V-\Delta P/L$ data) as a function of D_{10} and $D_{60}-D_{10}$, for **a** air flow in granite, **b** water flow in granite, **c** air flow in gravel, **d** water flow in gravel, **e** air flow in Leca®, and **f** water flow in Leca®

Schjonning (1986), Riley and Ekeberg (1989), Loll et al. (1999), and Andreasen et al. (2013), who claim that air and water velocity profiles are different at the pore scale and that this is the main cause of the difference in D_{eq}. Gas slippage has been shown to account for about 10 % of the differences (Schjonning 1986). In general, the water D_{eq} data exhibit more scatter, likely because liquid $V-\Delta P$ relationships are more difficult to measure accurately.

Values of $D_{eq,l}$ are plotted against $D_{eq,g}$ in Fig. 4. It is seen that the data for all three materials follow the same general trend (with the exception of a single measurement for Leca®). An exponential expression was chosen to model the $D_{eq,l}$–$D_{eq,g}$ relationship as:

$$D_{eq,l} = b\left(1-e^{\left(-c*D_{eq,g}\right)}\right) \tag{22}$$

where b (meters) (representing the maximum estimated value of $D_{eq,l}$) and c (per meter) (controlling the rate of increase of the estimated relationship) are fitting parameters. As optimal values of b for all three materials were not significantly different, one common value of b but individual values of c for each of the three materials were used in the modelling. Optimal values of b, $c_{granite}$, c_{gravel}, and $c_{Leca®}$, as quantified by the RSE (Eq. 21) for the data in Fig. 4, were 0.0029 m, 483, 427, and 356 m^{-1}, respectively. It is seen that the value of c is related to particle shape, such that the most rounded particles (Leca®) exhibit the lowest value of c. This again confirms that particle shape does have a marked influence on fluid flow through porous media. It further means that, in order to use Eq. 22 for media other than those considered here, a corresponding value of c must be determined for those media while a value of b= 0.0029 m seems sufficient. A relationship between c and particle shape may be developed, however, that will require additional measurements for several other media (particle shapes) than those used here.

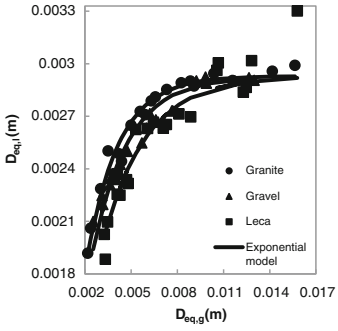

Fig. 4 Relationships based on Eq. 22 between fitted values of $D_{eq,g}$ and $D_{eq,l}$ (from Fig. 3 with b=0.0029, $c_{granite}$=483, c_{gravel}= 427, and $c_{Leca®}$=356)

Optimal fits of Eq. 22 are shown as curves in Fig. 4. In general, Eq. 22 is able to achieve a good fit to the data.

The data in Figs. 3 and 4 suggest that, if $D_{eq,g}$ for a given medium is known, it is possible to calculate the corresponding $D_{eq,l}$ using Eq. 22 and subsequently the $V-\Delta P/L$ relationship for water using Eq. 12.

The feasibility of predicting $V_l-\Delta P_l/L$ from the $V_g-\Delta P_g/L$ in the same medium was tested using six different approaches. All approaches are based on Eq. 12; however, different assumptions are made with respect to the estimation of parameters A, B, and D_{eq}.

Approach 1 is based on the assumption that the parameters A, B, and a are identical for both air and water transport in a given medium and that D_{eq} can be predicted by Eq. 18. Values of $\Delta P/L$ for both air and water transport were therefore calculated using common values of A=562, B=51, and a=0.68 as proposed by Pugliese et al. (2013) based only on gas transport measurements in the same three materials as used in this study.

In approach 2, Eq. 12 is fitted to the $V-\Delta P/L$ data measured in this study for both air and water transport, yielding common values of A, B, and a across all particle shapes (materials) and fluids. D_{eq} estimation was carried out using Eq. 18 (Pugliese et al. 2013). Optimal values of the parameters were identified by minimizing the RSE.

In approach 3, $\Delta P/L$ for both air and water flow were calculated using the fitted D_{eq} values from Fig. 3 together with the optimal common values of A (=553) and B(= 67) determined during the fitting of the D_{eq} values in Fig. 3. Fitting accuracy was estimated by minimizing the RSE. This represents a situation where A, B, and D_{eq} values are known a priori for instance from earlier measurements.

In approach 4, values of $D_{eq,g}$ were fitted using Eq. 12 and corresponding values of $D_{eq,l}$ were then calculated from the $D_{eq,g}$ values using Eq. 22. Values of $\Delta P/L$ for both air and water transport were subsequently calculated from the appropriate D_{eq} values using Eq. 12. One set of common A, B, and b values were used across all particle shapes, particle size fractions, and

fluids while individual values of c were used for each of the three materials. Optimal values of A, B, b, $c_{granite}$, c_{gravel}, and $c_{Leca®}$ were determined by minimizing the RSE between measured and fitted $\Delta P/L$ values for both air and water transport. Approach 4 represents a situation where measurements of $V-\Delta P/L$ for air transport are available, and corresponding $V-\Delta P/L$ data for water transport are estimated from the air transport measurements.

In approach 5, $D_{eq,g}$ is estimated using Eq. 18, while $D_{eq,l}$ is calculated from the estimated $D_{eq,g}$ using Eq. 22. $\Delta P/L$ values were then estimated for both air and water using Eq. 12. Optimal values of A, B, a, and b (assumed identical across all particle shapes, particle size fractions, and fluids) and c (assumed individual for each of the three materials) were determined by minimizing RSE between measured and predicted $\Delta P/L$ values. Approach 5 represents a situation where values of A, B, a, b, and c for the particle shape (for instance via earlier measurements on a single particle size fraction) in question are known a priori.

Approach 6 is identical to approach 5 except that determination of the optimal values of A, B, b, $c_{granite}$, c_{gravel}, and $c_{Leca®}$ was carried out by minimizing the RMSE (Eq. 20) between measured and fitted $\Delta P/L$ values.

Measured versus fitted $\Delta P/L$ data, for both fluids and for each of the six approaches, are shown in Fig. 5. An overview of the optimal values of the parameters A, B, a, b, and c for the six approaches is given in Table 1.

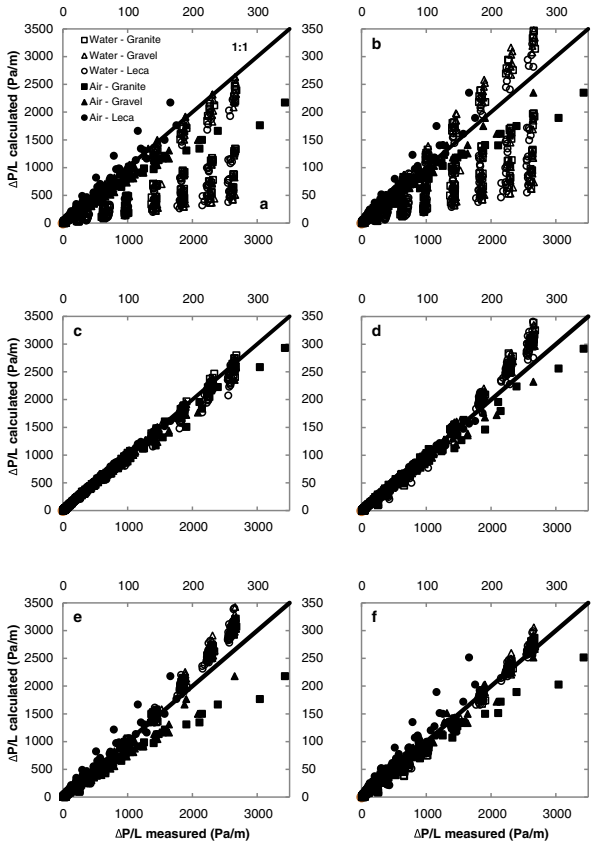

Fig. 5 Measured and fitted/predicted (using Eq. 12) values of $\Delta P/L$ for air and water in all three materials (63 media), for **a** approach 1, **b** approach 2, **c** approach 3, **d** approach 4, **e** approach 5, **f** approach 6. For details about the approaches, please see text

Table 1 Optimal values of the empirical constants A, B, a, b, $c_{granite}$, c_{gravel}, $c_{Leca®}$, and evaluation of the prediction accuracy in terms of the sum of relative (RSE) and root mean square errors (RMSE) for air and water measurements (2,016 measurements in total), following six different approaches

Approach	A	B	a	b	$c_{granite}$	c_{gravel}	$c_{Leca®}$	RSE_{air}	RSE_{water}	RSE_{total}	$RMSE_{air}$	$RMSE_{water}$	$RMSE_{total}$
1	562	51	0.68	–	–	–	–	15.57	179.02	194.59	38.42	2,615.78	2,654.20
2	460	76	0.57	–	–	–	–	28.43	137.48	165.91	33.83	2,184.61	2,218.44
3	553	67	–	–	–	–	–	6.75	3.30	10.05	14.96	203.19	218.15
4	599	58	–	0.0017	340	337	235	5.69	55.22	60.92	25.95	207.58	233.53
5	548	50	0.68	0.0015	326	332	256	15.57	55.16	70.73	13.57	206.88	220.45
6	543	71	0.6	0.0023	332	332	256	30.54	60.09	90.63	11.37	108.48	119.85

For approach 1, values were taken from Pugliese et al. (2013); for approaches 2–5 optimal values were fitted based on RSE (Eq. 21), and for approach 6, optimal values were fitted based on RMSE (Eq. 20)

Approach 1 (Fig. 5a) strongly under-predicts $\Delta P_l/L$ for almost all 63 media (Table 1). Values of $\Delta P_g/L$ are more accurate and shows no bias which is to be expected as the values of A, B, and a were fitted from the $\Delta P_g/L$ data (Pugliese et al. 2013). There is, however, still a fair amount of scatter in the $\Delta P_g/L$ data and the approach overestimates $\Delta P_g/L$ for Leca® and underestimates gravel and granite. This clearly shows that this approach is not capable of taking effects of fluid and medium properties into account. Approach 2 (Fig. 5b) using A, B, and a values fitted to both $\Delta P_g/L$ and $\Delta P_l/L$ data improves prediction of $\Delta P_l/L$ somewhat (Table 1). In this case, $\Delta P_l/L$ values are overestimated for the fine-grained media but underestimated for the coarse-grained media. For $\Delta P_g/L$, the prediction accuracy is somewhat lower than for approach 1.

Approach 3 (Fig. 5c) yields the best prediction accuracy for both $\Delta P_g/L$ and $\Delta P_l/L$. The overall value of RMSE for both air and water is 8 % and 10 % of those found for approaches 1 and 2, respectively. This of course is to be expected as approach 3 is based on individually fitted values of D_{eq} for each medium and fluid combination. To use this approach for estimating both $\Delta P_g/L$ and $\Delta P_l/L$ in practice, knowledge of $D_{eq,g}$ and $D_{eq,l}$ for the medium in question plus the two empirical constants A and B are required as compared with three empirical constants (A, B, and a) for approach 1 and 2. Figure 5c, however, does show the importance of accurate D_{eq} estimates for successful predictions of $\Delta P_g/L$ and $\Delta P_l/L$. Values of A and B can be established based on measurements of V_g–$\Delta P_g/L$ and/or V_l–$\Delta P_l/L$ in a limited set of media with a given particle shape. Hereafter, estimates of any V_g–$\Delta P_g/L$ and V_l–$\Delta P_l/L$ value in any other medium with the same particle shape can be estimated based on a limited set of V_g–$\Delta P_g/L$ and V_l–ΔP_l measurements in the medium of interest.

Approach 4 (Fig. 5d) where $D_{eq,l}$ is predicted from fitted $D_{eq,g}$ by Eq. 22 decreases the prediction accuracy somewhat compared with approach 3 as this approach only uses individually fitted values of $D_{eq,g}$ together with six empirical constants (three c values plus A, B, and b). The total RSE and RMSE for both air and water measurements, however, are still only about 31 % and 9 % of those for approach 1, respectively (Table 1). This shows that it is possible to get an accurate estimation of V_l–$\Delta P_l/L$ from V_g–$\Delta P_g/L$ by using Eq. 22 provided adequate estimates for b and c are available. To use this approach in practice, knowledge of $D_{eq,g}$ as well as the empirical parameters A, B, b, and c for the medium in question is required. Values of A, B, , and c can be established based on measurements of V_g–$\Delta P_g/L$ and V_l–$\Delta P_l/L$ in a limited set of media with a given particle shape. Hereafter, estimates of any V_g–$\Delta P_g/L$ and V_l–$\Delta P_l/L$ in any other medium with the same particle shape can be estimated based on a limited set of V_g–$\Delta P_g/L$ measurements in the medium of interest.

Approach 5 (Fig. 5e) based on estimating $D_{eq,g}$ by Eq. 18 and $D_{eq,l}$ from the estimated $D_{eq,g}$ by Eq. 22 yields prediction accuracies that are comparable to approach 4 in terms of total RSE (16 % higher) and total RMSE (6 % lower), although values of RSE and RMSE for $\Delta P_g/L$ are somewhat higher than for approach 4 (Table 1). Larger values of $\Delta P_l/L$ are slightly overestimated, although still grouped relatively close together. Approach 5 only uses seven fitting parameters (A, B, a, b, and three c values). These results show that the concept of predicting $D_{eq,g}$ from the particle size distribution alone using Eq. 16 followed by predicting

$D_{eq,l}$ from the predicted $D_{eq,g}$ data and subsequently predicting $\Delta P_l/L$ using Eq. 12 is viable provided adequate estimates of the seven fitting parameters are available. Values of A, B, a, b, and c can be established based on measurements of $V_g-\Delta P_g/L$ and $V_l-\Delta P_l/L$ in a limited set of media with a given particle shape. Hereafter estimates of any $V_g-\Delta P_g/L$ and $V_l-\Delta P_l/L$ in any other medium made with the same particle shape can be estimated based on knowledge of the particle size distribution for the medium of interest.

Approach 6 (Fig. 5f) is equivalent to approach 5 but based on fitting using RMSE rather than RSE of course yields increased values of RSE and reduced values of RMSE. The overall value of RSE is about 46 % of that found in approach 1, but the corresponding RMSE value is only about 5 % of that found in approach 1. The advantage of using RMSE in the fitting is that the larger values of $\Delta P_l/L$ data are predicted more accurately (although the prediction of the small values is less accurate). For $\Delta P_g/L$, approach 6 has a weak tendency to overestimate for Leca® and underestimate for granite indicating that $D_{eq,g}$ exhibits a weak dependency on the material properties (for example particle shape). Taking this dependency into account, however, will likely mean that additional fitting parameters are needed.

Altogether the data in Fig. 5 and Table 1 shows that it is possible to predict $\Delta P_l/L$ from measured $\Delta P_g/L$ data with an average error that is less than 26 % of the measured values based on the RSE provided adequate model parameters are available for instance from earlier measurements in media with the same particle shape. The data also indicate that it may be possible to predict both $\Delta P_g/L$ and $\Delta P_l/L$ solely from the particle size distribution of the media, although additional data are required to verify if this is viable. The data in Table 1 further show that, among the model constants A, B, a, b, and c, at least c seems to be dependent on the particle shape (but not the particle size distribution) of the media. In particular, the fitted values of the c parameter for the three materials were inversely proportional to particle roundness (φ) as defined by either Pentland (1927) (φ_p) or Wadell (1935) (φ_w). Values of φ for the three materials used here were determined by Pugliese et al. (2013) as $\varphi_{p,granite}=0.64$, $\varphi_{p,gravel}=0.65$, $\varphi_{p,Leca®}=0.80$ and $\varphi_{w,granite}=0.09$, $\varphi_{w,gravel}=0.51$, $\varphi_{w,Leca®}=0.89$. It is seen that c values for approaches 4, 5, and 6 correlate best with φ_w. Thus, it seems that particle roundness may be a useful parameter in the estimation of c and D_{eq}, although additional data are needed to develop this further. It is emphasized that the approaches for estimating $\Delta P_g/L$ and $\Delta P_l/L$ discussed here have only been tested against data for granular media, having uniform particle size distributions although the media represented a very wide range of uniform particle size distributions and particle shapes.

5 Conclusions

In this study, the relationship between air and water pressure gradients during air and water flow in granular filter media as well as their relationships with media properties was investigated, across three coarse granular porous media (crushed granite, gravel, and Leca®), having different particle shapes. Values of the air velocity–air pressure gradient relationship ($V_g-\Delta P_g/L$, 1008 measurements) from a previous study (Pugliese et al. 2013), while corresponding values of the water velocity–water pressure gradient relationship ($V_l-\Delta P_l/L$, 1008 measurements) in the same media were carried out under identical conditions in this study. Under otherwise identical conditions, $\Delta P_g/L$ values were slightly greater in granite (the most angular material) and lowest in Leca® (the most rounded material). In contrast, $\Delta P_l/L$ values were highest for Leca® but lower and similar for granite and gravel. These dependencies on material type, although small, clearly indicate that particle shape does not affect the flow of the two fluids in the same manner.

Several different approaches for predicting the $V_g-\Delta P_g/L$ and $V_l-\Delta P_l/L$ relationships including some existing approaches based on previously published data for air flow were evaluated. This evaluation showed that the existing approaches although adequate for $V_g-\Delta P_g/L$ predictions were not able to predict $V_l-\Delta P_l/L$ which was to be expected as they have not been developed for water flow.

Results of the evaluation also showed that it is possible to predict of $V_l-\Delta P_l/L$ in a given medium from corresponding $V_g-\Delta P_g/L$ measurements in the same medium with a high degree of accuracy requiring only four empirical parameters. These can be established based on measurements of $V_g-\Delta P_g/L$ and $V_l-\Delta P_l/L$ in a limited set of media with the same particle shape. Hereafter, estimates of any $V_g-\Delta P_g/L$ and $V_l-\Delta P_l/L$ value in any other medium with the same particle shape can be estimated based on measurements of selected

V_g–$\Delta P_g/L$ values in the medium of interest provided the particle size distributions have the same shape.

Results further showed that it is possible to predict the V_g–$\Delta P_g/L$ and V_l–$\Delta P_l/L$ relationships in any medium with good accuracy based only on knowledge about the particle size distribution requiring only five empirical parameters.

Some of the empirical parameters exhibited dependency on material particle shape. This means that improved estimates of parameter values may be achieved by incorporating effects of particle shape in the estimation procedure. This, however, will require further measurements for materials with a larger range of particle shapes than considered here. It is noted that, although the results presented in this study are based on measurements in multiple materials with different particle shapes (roundness) and a large set of particle size fractions, all media used had uniform particle size distributions. To verify the validity of the estimation approaches presented here also for media with non-uniform particle size distributions, further investigations are needed.

References

Ahmed, N., & Sunada, D. (1969). Nonlinear flow in porous media. *Journal of Hydrologic Division-ASCE, 95*(6), 1847–1857.

Alexander, L., & Skaggs, R. W. (1986). Predicting unsaturated hydraulic conductivity from the soil–water characteristic. *Transactions of ASAE, 29*(1), 176–184.

Andreasen, R. R., & Poulsen, T. G. (2013). Air flow characteristics in granular biofilter media. *Journal of Environmental Engineering-ASCE, 139*(2), 196–204.

Andreasen, R. R., Canga, E., Kjaergaard, C., Iversen, B. V., Poulsen, T. G. (2013). Relating water and air flow characteristics in coarse granular materials. *Water Air and Soil Pollut.*, 224(4), doi:10.1007/s11270-013-1469-5.

Antohe, B. V., Lage, J. L., Price, D. C., & Weber, R. M. (1997). Experimental determination of permeability and inertia coefficients of mechanically compressed aluminum porous matrices. *Journal of Fluids Engineering, 119*(2), 404–412.

Balasubramanian, P., Philip, L., & Bhallamudi, S. M. (2012). Biotrickling filtration of VOC emissions from pharmaceutical industries. *Chemical Engineering Journal, 209*, 102–112.

Blackwell, P. S., Ringrosevoase, A. J., Jayawardane, N. S., Olsson, K. A., McKenzie, D. C., & Mason, W. K. (1990). The use of air-filled porosity and intrinsic permeability to air to characterize structure of macropore space and saturated hydraulic conductivity of clay soils. *Journal of Soil Science, 41*(2), 215–228.

Chen, L., & Hoff, S. J. (2009). Mitigating odors from agricultural facilities: a review of literature concerning biofilters. *Applied Engineering in Agriculture, 25*(5), 751–766.

Cohen-Shoel, N., Barkay, Z., Ilzycer, D., Gilath, I., & Tel-Or, E. (2002). Biofiltration of toxic elements by Azolla biomass. *Water, Air, and Soil Pollution, 135*(1–4), 93–104.

Cornell, D., & Katz, D. L. (1953). Flow of gases through consolidated porous media. *Industrial and Engineering Chemistry, 45*(10), 2145–2152.

Darcy, H. (1856). *Les fontaines publiques de la ville de Dijon*. V. Dalmont, ed. Paris, 647.

Den, W., Huang, C. P., & Li, C. H. (2004). Effects of cross-substrate interaction on biotrickling filtration for the control of VOC emissions. *Chemosphere, 57*(7), 697–709.

Ergun, S. (1952). Fluid flow through packed columns. *Chemical Engineering Progress, 48*(2), 89–94.

Erhan, E., Keskinler, B., Akay, G., & Algur, O. F. (2002). Removal of phenol from water by membrane-immobilized enzymes—Part I dead-end filtration. *Journal of Membrane Science, 206*(1–2), 361–373.

Firdaouss, M., Guermond, J. L., & LeQuere, P. (1997). Nonlinear corrections to Darcy's law at low Reynolds numbers. *Journal of Fluid Mechanics, 343*, 331–350.

Forchheimer, P. H. (1901). Wasserbewegung durch boden. *Zeitschrift ver deutscher ingenieure, 50*, 1782–1788 (in German).

Geertsma, J. (1974). Estimating coefficient of inertial resistance in fluid-flow through porous-media. *Society of Petroleum Engineers Journal, 14*(5), 445–450.

Green, L., & Duwez, P. (1951). Fluid flow through porous metals. *Journal of Applied Mechanics—Transactions of the Asme, 18*(1), 39–45.

He, Z. G., Li, J. J., Chen, J. Y., Chen, Z. P., Li, G. Y., Sun, G. P., et al. (2012). Treatment of organic waste gas in a paint plant by combined technique of biotrickling filtration with photocatalytic oxidation. *Chemical Engineering Journal, 200*, 645–653.

Lage, J. L., Antohe, B. V., & Nield, D. A. (1997). Two types of nonlinear pressure-drop versus flow-rate relation observed for saturated porous media. *Journal of Fluids Engineering - Transactions of the Asme, 119*(3), 700–706.

Lee, S. H., Li, C. N., Heber, A. J., Ni, J. Q., & Huang, H. (2013). Biofiltration of a mixture of ethylene, ammonia, n-butanol, and acetone gases. *Bioresource Technology, 127*, 366–377.

Leson, G., & Winer, A. M. (1991). Biofiltration—An innovative air-pollution control technology for voc emissions. *Journal of the Air & Waste Management Association, 41*(8), 1045–1054.

Loll, P., Moldrup, P., Schjonning, P., & Riley, H. (1999). Predicting saturated hydraulic conductivity from air permeability: Application in stochastic water infiltration modeling. *Water Resources Research, 35*(8), 2387–2400.

Macdonald, I. F., Elsayed, M. S., Mow, K., & Dullien, F. A. L. (1979). Flow through porous media—Ergun equation revisited. *I&EC Fundamentals, 18*(3), 199–208.

Macdonald, M. J., Chu, C. F., Guilloit, P. P., & Ng, K. M. (1991). A generalized blake-kozeny equation for multisized spherical-particles. *Aiche Journal, 37*(10), 1583–1588.

Mohammad, A., & Najar, M. (1997). Physico-chemical adsorption treatments for minimization of heavy metal contents in water and wastewaters. *Journal of Scientific & Industrial Research, 56*(9), 523–539.

O'Neill, D. H., Stewart, I. W., & Phillips, V. R. (1992). A review of the control of odor nuisance from livestock buildings 2. The

costs of odor abatement systems as predicted from ventilation requirements. *Journal of Agricultural Engineering Research, 51*(3), 157–165.

Pentland, A. (1927). A method of measuring the angularity of sands. *Royal Soc. Canada, Proc. and Trans.* 21(3), Appendix C.

Plascak, I., Puvaca, V., Jurisic, M., Rapcan, I., & Duvnjak, V. (2008). Influence of mineral and organic fertilizer on primary contamination of the ground waters in eastern Croatia. *Cereal Research Communications, 36*, 151–154.

Poulsen, T. G., & Moldrup, P. (2007). Air permeability of compost as related to bulk density and volumetric air content. *Waste Management & Research, 25*(4), 343–351.

Pugliese, L., Poulsen, T. G., & Andreasen, R. R. (2012). Relating gas dispersion in porous media to medium tortuosity and anisotropy ratio. *Water, Air, and Soil Pollution, 223*(7), 4101–4118.

Pugliese, L., Poulsen, T. G., & Andreasen, R. R. (2013). Biofilter media gas pressure loss as related to media particle size and particle shape. *Journal of Environmental Engineering, 139*(12), 1424–1431.

Riley, H., & Ekeberg, E. (1989). Ploughless tillage in large-scale trials. *Norsk Landbruksforskning, 3*, 107–115.

Schjonning, P. (1986). Soil permeability by air and water as influenced by soil type and oncorporation of straw. *Tidskrift for planteavl* (Special issue).

Scotford, I. M., Burton, C. H., & Phillips, V. R. (1996). Minimum-cost biofilters for reducing odours and other aerial emissions from livestock buildings. 2. A model to analyse the influence of design parameters on annual costs. *Journal of Agricultural Engineering Research, 64*(2), 155–163.

Trussell, R. R., & Chang, M. (1999). Review of flow through porous media as applied to head loss in water filters. *Journal of Environmental Engineering-ASCE, 125*(11), 998–1006.

van Genuchten, M. T. (1980). A closed-form equation for predicting the hydraulic conductivity of unsaturated soils. *Soil Science Society of America Journal, 44*(5), 892–898.

Zeng, Z. W., & Grigg, R. (2006). A criterion for non-Darcy flow in porous media. *Transport in Porous Media, 63*(1), 57–69.

Zouboulis, A. I., Lazaridis, N. K., & Grohamm, A. (2002). Toxic metals removal from waste waters by upflow filtration with floating filter medium I. The case of zinc. *Separation Science and Technology, 37*(2), 403–416.

Wadell, H. (1935). Volume, shape and roundness of quartz particles. *Journal of Geology, 43*(3), 250–280.

Wang, W. D., Yang, H. W., Zhao, H. Z., & Jiang, Z. P. (2007). Transfer and transport of aluminum in filtration unit. *Journal of Environmental Sciences-China, 19*(8), 897–901.

Paper III

Water Air Soil Pollut (2013) 224:1691
DOI 10.1007/s11270-013-1691-1

Gas–Solute Dispersivity Ratio in Granular Porous Media as Related to Particle Size Distribution and Particle Shape

Lorenzo Pugliese · Tjalfe G. Poulsen · Salvatore Straface

Received: 21 May 2013 / Accepted: 7 August 2013 / Published online: 29 August 2013

Abstract Measurements of solute dispersion in porous media is generally much more time consuming than gas dispersion measurements performed under equivalent conditions. Significant time savings may therefore, be achieved if solute dispersion coefficients can be estimated based on measured gas dispersion data. This paper evaluates the possibility for estimating solute dispersion based on gas dispersion measurements. Breakthrough measurements were carried out at different fluid velocities (covering the same range in Reynolds number), using O_2 and NaCl as gas and solute tracers, respectively. Three different, granular porous materials were used: (1) crushed granite (very angular particles), (2) gravel (particles of intermediate roundness) and (3) Leca® (almost spherical particles). For each material, 21 different particle size fractions were used. Gas and solute dispersion coefficients were determined by fitting the advection–dispersion equation to the measured breakthrough curves and in turn used to calculate gas and solute dispersivities as a function of mean particle size (D_m) and particle size range (R) for the 63 particle size fractions considered. The results show that solute and gas dispersivities are related and that their ratio depends on both R and D_m. Based on these observations a simple model for predicting the dispersivity ratio from D_m and R, was proposed.

Keywords Dispersivity · Gas measurements · Solute measurements · Particle shape · Particle size range · Mean particle diameter

L. Pugliese (✉)
Department of Chemistry and Biotechnology,
Aalborg University, Sohngaardsholmsvej 57,
9000 Aalborg, Denmark
e-mail: lp@bio.aau.dk

T. G. Poulsen
Department of Civil Engineering, Xi'an Jiaotong,
Liverpool University, 111 Ren Ai Road,
215123 Suzhou, Jiangsu, China

S. Straface
Department of Ingegneria per l'Ambiente, il Territorio ed
Ingegneria Chimica, Università della Calabria, Via P. Bucci
42B, 87036 Arcavacata di Rende, Italy

1 Introduction

Dispersion of gases and solutes in porous media is a key mechanism controlling transport of various gaseous or dissolved compounds in porous media. Examples of gas phase dispersion arise in processes such as radon migration into buildings (Wang and Ward 2002), remediation and movement of volatile contaminants for instance at contaminated soil sites (Arands et al. 1997; Gidda et al. 2006; Atteia and Hohener 2010), sequestration of CO_2 in saline aquifers and depletion of oil and gas reservoirs (White et al. 2003). Gas dispersion also plays an important role in migration and emission of methane from landfills and wetlands (El-Fadel et al. 1997; De Visscher et al. 1999; Liang et al. 2000; Pangala et al. 2010; Pennock et al. 2010; Schaufler et al. 2010), and during composting of organic material in aerated piles (Fukumoto et al. 2003; Thummes et al. 2007). Solute dispersion is the most important mechanics in the propagation of dissolved contaminants, in both the vadose zone and in groundwater, and knowledge

about it is crucial when estimating contaminant migration or selecting appropriate remediation strategies at a contaminated site (Gerke and van Genuchten 1996; Thomson et al. 1997; Domenico and Schwartz 1998; Silva and Grifoll 2009; Lewis and Sjostrom 2010).

Gas dispersion in porous media has been studied extensively since the late 1960s. Examples are Sinclair and Potter (1965), Evans and Kenney (1966), Edwards and Richards (1968), Suzuki and Smith (1972), Han et al. (1985), Coelho and Guedes de Carvalho (1988), Tan and Liou (1989), Popovicova and Brusseau (1997), Costanza-Robinson and Brusseau (2002), Poulsen et al. (2008), Sharma and Poulsen (2010) and Pugliese et al. (2012). Solute dispersion in porous media has been studied since about 1950. Examples are Bear (1961), Whitaker (1967), Greenkor and Kessler (1969), Rose (1973), Scheidegger (1974), Brenner (1980), Brusseau (1993). Delgado (2006) has published an excellent review of the existing knowledge about dispersion of gases and solutes in homogeneous porous media.

Both gas and solute dispersion generally increases with fluid phase velocity, distance travelled, porous medium particle size range, anisotropy ratio, and pore system tortuosity as confirmed by several earlier studies referred in Delgado (2006), but it is also in agreement with more recent studies such as Gidda et al. (2006), Bromly et al. (2007), Poulsen et al. (2008), and Sharma and Poulsen (2010). Pugliese et al. (2012) observed that dispersion depends on particle shape. In general, it is agreed that gas and solute dispersion are controlled by the same parameters and that they are affected in a similar manner.

For an equal pressure gradient, gases travel much faster than liquids through a given porous medium. It is therefore generally much faster and easier to measure gas dispersion compared to solutes. Solute dispersion measurements, in coarse-grained materials such as sand, usually take 10–100 times longer than gas dispersion measurements performed under identical conditions. In finer materials, such as fine sand or silt, this difference will be even larger. As gas and solute dispersion in porous media are controlled by the same parameters they are likely related. Knowledge of this relation will allow estimating solute dispersion coefficients based on gas dispersion measurements in the same medium which will result in considerable time savings. The main problem in establishing a relationship between gas and solute dispersion is the difference in flow pattern between gases and liquids in porous media. This has been documented by Schjonning (1986), and Loll et al. (1999), who showed that intrinsic gas permeability can be orders of magnitude larger than liquid permeability, depending on porous medium characteristics.

To the knowledge of the authors, however, no studies presenting corresponding measurements of gas and liquid dispersion coefficients under identical conditions, have been published. Thus, knowledge of the link between gas and solute dispersion is at present very limited.

The goal of this paper was, therefore, to measure corresponding gas and solute dispersion coefficients in granular porous media, and to identify a possible connection between them. Measurements were performed under identical conditions, using oxygen and chloride as gas and solute tracers, respectively. These tracers were chosen as they are simple and inexpensive to measure, and safe to use. Dispersion coefficients were measured in three different media: (1) crushed granite (very angular particles), (2) gravel (particles of intermediate roundness), and (3) light expanded clay aggregates (Leca®) (almost spherical particles). For each of the three materials, 21 different particle size fractions were considered.

2 Theory

Gas and solute transport in porous media is traditionally described by the advection dispersion equation (ADE). For one-dimensional transport of a conservative tracer, in homogeneous porous medium, assuming uniform flow and dispersion, and the presence of both a mobile and a stagnant (immobile) fluid phase, the ADE is given as:

$$\frac{\partial C_{\mathrm{m}}}{\partial t} = D\frac{\partial^2 C_{\mathrm{m}}}{\partial x^2} + u\frac{\partial C_{\mathrm{m}}}{\partial x}, \tag{1}$$

where C_{m} is the tracer concentrations in the mobile fluid phases (ML^{-3}), D is the overall dispersion–diffusion coefficient ($\mathrm{L}^2\mathrm{T}^{-1}$) which takes into account effects of molecular diffusion, mechanical dispersion, and fluid mixing in the tubing leading the fluid to and from the column (Poulsen et al. 2008), u is the pore fluid velocity (interstitial velocity) of the mobile phase (LT^{-1}), and x and t are the space (L) and time (T) variables. In this study, no mass transfer between the mobile and immobile fluid phases was assumed (Sharma and Poulsen 2010).

The immobile fluid phase content and the fluid pore velocity were calculated as:

$$\varepsilon_{im} = \varepsilon_{tot} - \varepsilon_m \quad (2)$$

$$u = -\frac{Q}{A\varepsilon_m} \quad (3)$$

where ε_m and ε_{im} are the mobile and immobile volumetric phase contents (L^3L^{-3}) in the porous medium, respectively, ε_{tot} represents the total fluid-filled porosity (assumed equal to medium total porosity), Q is the applied volumetric fluid flow rate (L^3T^{-1}), and A is the column cross-sectional area (L^2) perpendicular to the fluid flow direction. The diffusion/dispersion coefficient D can be expressed as:

$$D = D_{mol} + D_{mech} + D_{mix} \quad (4)$$

where D_{mol} represents the contribution by molecular diffusion, D_{mech} is the contribution from mechanical dispersion and D_{mix} is the contribution from fluid mixing in the tubing leading to and from the porous medium column. D_{mix} is controlled by the experimental apparatus geometry and can be minimized by reducing the travel distances from the tracer injection point to the inlet of the porous medium column and from the outlet to the concentration measurement point. For solute transport, D_{mol} and D_{mix} are generally very small compared to D_{mech}, while for gases both D_{mol} and D_{mech} can be significant. It is well-known (Poulsen et al. 2008; Hamamoto et al. 2009; Hunt and Skinner 2010; Sharma and Poulsen 2010) that D_{mech} increases linearly with increasing fluid pore velocity, except at very low velocities. For a one-dimensional configuration, D_{mech} is expressed as:

$$D_{mech} = u\alpha, \quad (5)$$

where α is the tracer mechanical dispersivity (longitudinal dispersivity) in the mobile fluid phase (L). Combining Eqs. (4) and (5) yields:

$$D = D_{mol} + u\alpha + D_{mix} \quad (6)$$

A plot of D versus u for high flow velocities yields a straight line, identified by the slope α and the intercept $D_{mol} + D_{mix}$ (Poulsen et al. 2008).

The measured breakthrough curves were fitted to Eqs. (1), (2), (3), (4) by optimizing the values of D and ε_m. Initial and boundary conditions for the gas transport simulation were:

$$\text{Initial condition} \quad t = 0, x \geq 0 \quad C = 20.9\%O_2 \quad (7a)$$

$$\text{Boundary condition} \begin{cases} 0 < t \leq t_1, x = 0 & C = 20.9\%O_2 \\ t_1 < t \leq t_2, x = 0 & C = 0\%O_2 \\ t > t_2, x = 0 & C = 20.9\%O_2 \end{cases} \quad (7b)$$

For the solute transport, the corresponding initial and boundary conditions were:

$$\text{Initial condition} \quad t = 0, x \geq 0 \quad C = 0 \quad (8a)$$

$$\text{Boundary condition} \quad t > 0, x = 0 \quad C = C_0 \quad (8b)$$

where t_1 and t_2 are the points in time where the input gas was switched from air to nitrogen and vice versa.

Equations (1)–(3) were solved using an explicit finite difference method, corrected for numerical dispersion. Optimum values of D and ε_m, for each of the 96 measured gas and liquid breakthrough curves (values for gas measurements in gravel and Leca® were taken from a previous study), were determined by minimizing the sum of squared errors (SSE) between measured effluent tracer concentrations and corresponding tracer concentration values predicted by the numerical model as:

$$SSE = \sum_{t=0}^{t_{max}} \left[C_{measured}(t) - C_{predicted}(t)\right]^2, \quad (9)$$

where $C_{measured}(t)$ and $C_{predicted}(t)$ are the observed and predicted (by the model) effluent tracer concentration at time, t, respectively, while t_{max} is the time at which each individual experiment was terminated. The minimization procedure was carried out using a nonlinear least square method.

Particle shape can be characterized by particle roundness. Two very widely applied approaches, used to describe this physical particle characteristic, are those of Pentland (1927) and Wadell (1935). Pentland (1927) defined the roundness as:

$$\varphi_p = \frac{\omega}{\omega_p}, \quad (10)$$

where φ_p (≤ 1) is roundness (dimensionless) based on Pentland (1927), ω is the cross-sectional or projection

area of the grain (L^2) and ω_p is the area of the circle having the largest diameter of the grain projection (L^2). The orientation of the particles is not definite.

Wadell (1935) defined roundness as:

$$\varphi_w = \frac{N}{\sum_N \left(\frac{\Re}{r_N}\right)}, \quad (11)$$

where φ_w denotes the total degree of roundness (dimensionless), N is the number of corners in the given projection plane of the particle, $\mathscr{R}$ the radius of the largest inscribed circle (L) and r the radius of the inscribed circle of the N^{th} corner of the particle in the projection plane (Pugliese et al. 2013).

3 Materials and Methods

Measurements of D_{mech} were performed on three natural and commercially available media: (1) crushed granite, (2) gravel, and (3) Leca®. The crushed granite is characterized by an irregular and very angular particle shape, gravel consists of somewhat rounded rock fragments and Leca® consists of rounded particles. Granite and gravel does not have any internal porosity (single porosity material), while Leca® consists of highly porous particles (double porosity material) although this internal porosity is inaccessible by air as it consists of closed vesicles very much like soap foam.

All three materials were initially sieved into six particle size fractions with uniform particle size distributions. Each of these fractions was characterized by a particle size range (R) of 2 mm, in the range between 2 and 14 mm. Particle diameters (D) were $2 \le D < 4$, $4 \le D < 6$, $6 \le D < 8$, $8 \le D < 10$, $10 \le D < 12$, and $12 \le D < 14$ mm corresponding to mean particle diameter (D_m) of 3, 5, 7, 9, 11, and 13 mm respectively. Additional fractions with R=4 mm (D_m=4, 6, 8, 10, 12 mm), R=6 mm (D_m=5, 7, 9, 11 mm), R=8 mm (D_m=6, 8, 10), R=10 mm (D_m=7, 9), and R=12 mm (D_m=8), with uniform particle distributions, were produced by combining appropriate quantities of the six R=2 mm fractions. Uniform particle size distributions were chosen to ensure well defined particle size distributions across all particle size fractions used. A total of 63 particle size fractions were produced (21 fractions for each material).

Media were packed into 100-cm long and 14-cm inner diameter acrylic columns, taking care to reduce variations and differences in the packing density of each column. A stainless steel mesh with 2-mm openings and 1-mm thickness was installed at both ends of the columns, to support and prevent movements of the media. Polyethylene lids sealed using rubber O-rings were used at both ends. Soft Teflon tubing with an inner diameter of 4 mm was used to connect each component of the system. Different sets of flow rates were applied for both gas and solute dispersion experiments, in order to obtain comparable results for each fluid covering the same range of Reynolds numbers ($Re = \rho V d/\mu$) ($0.004 \le Re \le 2.13$).

Gas dispersion measurements were carried out for granite following the approach of Poulsen et al. (2008). The inlet (at the bottom) end of each column was connected to an air/nitrogen supply via a three-way valve and a precision ball flow meter (model F150, Porter Instruments, Inc., Hatfield, PA) to control gas flow rate. The outlet lid was equipped with an oxygen sensor (KE-12 galvanic oxygen electrode, GS Yuasa Power Supply Ltd., Japan) with a 5-s response time for determination of effluent oxygen concentrations. Readings from the oxygen sensor (sampling every 5 s) were recorded by a data logger (CR-1000, Campbell Scientific, Logan, UT). Atmospheric air and nitrogen were used as tracer gases. A scheme of the experimental setup is shown in Fig. 1a, while details are given in Poulsen et al. (2008).

Columns were initially saturated with atmospheric air (78 % N_2 and 21 % O_2), and the flow adjusted to the desired values. Once the effluent O_2 concentration was stable, the inlet gas was switched to N_2. Care was taken to make sure that gas flow remained constant during the switch. A constant flow of N_2 was maintained until the effluent O_2 concentration reached zero. After that, the gas supply was switched back to atmospheric air and the flow maintained until a stable O_2 concentration was once again observed. Oxygen and nitrogen breakthrough curves were measured in duplicate for granite, at gas flow rates of 0.2, 0.5, 1.0, 1.5, 2.0, and 2.3 L/min. Gas dispersion data for gravel and Leca® measured using an identical procedure, were taken from a previous study (Sharma and Poulsen 2010). All experiments were carried out in duplicates.

For the solute dispersion measurements, the inlet (at the bottom) of the column was connected to a peristaltic pump (model PD 5101, Heidolf). The outlet was connected to a measuring tube holding 12 mL of liquid, equipped with a TETRACON 325 conductometer. A scheme of the experimental setup is shown in Fig. 1b.

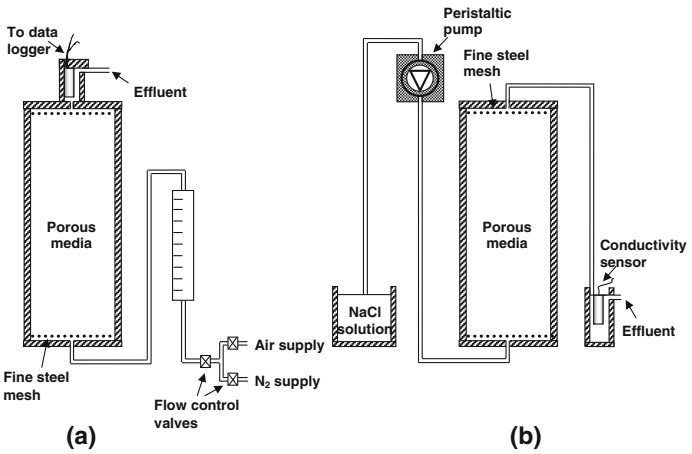

Fig. 1 Experimental setup for **a** gas dispersion and **b** solute dispersion measurements

The column was initially saturated with demineralized water, after which NaCl solution of 5 g L^{-1} was injected continuously at a specific flow rate. Effluent NaCl concentration was measured every 10 s. Experiments were carried out for all three materials at flow rates of 0.015, 0.05, 0.075, 0.1, 0.125, 0.15 L/min, and terminated when inlet and outlet NaCl concentrations were identical. Measurements were conducted for all three porous materials, but only for nine out of 21 particle size fractions for each material as solute dispersion measurements are much more time consuming to carry out than gas dispersion measurements (about 12 times). All experiments were carried out in duplicates.

4 Results and Discussion

For all particle size fractions values of D ($= D_{mol} + D_{mech} + D_{mix}$) increased with u. This was the case for both gas (63 particle size fractions) and solute (27 particle size

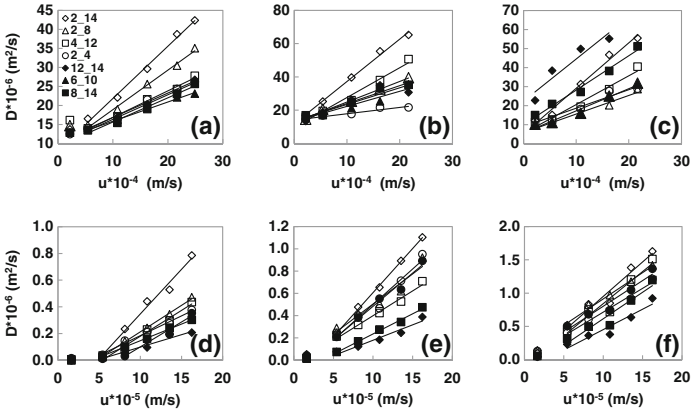

Fig. 2 Calculated values of D from selected gas dispersion measurements in **a** granite, **b** gravel, **c** Leca®, and from selected solute measurements in **d** granite, **e** gravel, **f** Leca®, as a function of pore fluid velocity (u)

fractions). Values of D as a function of u are shown, for both gas and solute measurements, in Fig. 2.

Values of D for gas transport (Fig. 2a, b, and c) are larger compared to solute transport. On average, values of D for gas transport were 20–30 times higher compared to solute transport for identical values of Re. For gas dispersion, the u–D relationship follows a consistent linear trend for $u>5\times10^{-4}$ m s^{-1}. Below this velocity the trend is less clear as there is considerable scatter in the gas dispersion data. This could be because the contribution by D_{mech} becomes small compared to D_{mol}, making it difficult to get a consistent and accurate determination of D_{mech}. Trend lines intercept the D axes at approximately 12×10^{-6} (m^2/s) indicating that D_{mol} has this value. For solute dispersion, the relationship between u–D is also linear for $u>5\times10^{-5}$ (m s^{-1}). Below this velocity, the measurements clearly show that the relationship does not follow the linear trend as the slope of the u–D relationship approaches zero in this region. This may very well also be the case for gas dispersion; however, there is too much scatter in the data to assess if that is the case. The u–D relationships for chloride measurements intercepts the D-axis at a value close to zero, indicating that for the chloride transport D_{mol} is very small which is in agreement with earlier literature. Values of longitudinal dispersivity, α, were determined for each of the six

Table 1 Physical properties of the porous media fractions used in gas and solute dispersion measurements used in this study

Size range (mm)	Granite				Gravel				Leca (R)			
	φ_p		φ_w		φ_p		φ_w		φ_p		φ_w	
	0.64[a]		0.09[a]		0.65[a]		0.51[a]		0.80[a]		0.89[a]	
	ρ_b (g/cm^3)	α_g (mm)	α_s (mm)	α_g/α_s (mm)	ρ_b (g/cm^3)	α_g (mm)	α_s (mm)	α_g/α_s (mm)	ρ_b (g/cm^3)	α_g (mm)	α_s (mm)	α_g/α_s (mm)
2_4	1.51	6.4	3.0	2.2	1.55[b]	3.8[b]	6.4	0.6	0.33	9.7[b]	7.10	1.4
4_6	1.55	4.4			1.54[b]	4.6[b]			0.29	11.4[b]		
6_8	1.52	4.4	3.3	1.3	1.54[b]	5.1[b]	5.6	0.9	0.25	12.9[b]	7.40	1.7
8_10	1.48	5.2	3.2	1.6	1.55[b]	6.1[b]	2.7	2.3	0.25	14.3[b]	7.30	2.0
10_12	1.46	6.0			1.55[b]	11.8[b]			0.24	27.4[b]		
12_14	1.47	6.5	1.9	3.5	1.55[b]	9.4[b]	2.8	3.4	0.23	22.1[b]	6.10	3.6
2_6	1.53	7.8			1.54[b]	7.9[b]			0.31	9.0[b]		
4_8	1.50	5.0			1.53[b]	10.0[b]			0.27	8.9[b]		
6_10	1.53	5.1	3.7	1.4	1.54[b]	9.1[b]	6.0	1.5	0.25	11.7[b]	7.70	1.5
8_12	1.49	5.3			1.56[b]	7.1[b]			0.24	20.1[b]		
10_14	1.46	6.3			1.55[b]	7.8[b]			0.24	20.5[b]		
2_8	1.55	10.4	4.0	2.6	1.56[b]	12.4[b]	5.4	2.3	0.29	9.8[b]	7.90	1.2
4_10	1.50	5.6			1.54[b]	13.4[b]			0.26	11.6[b]		
6_12	1.48	5.6			1.55[b]	7.8[b]			0.24	14.4[b]		
8_14	1.49	6.4	2.5	2.6	1.56[b]	10.7[b]	3.6	3.0	0.24	18.1[b]	8.00	2.3
2_10	1.54	12.7			1.59[b]	18.8[b]			0.27	15.5[b]		
4_12	2.52	7.0	3.9	1.8	1.58[b]	18.0[b]	4.7	3.8	0.26	15.1[b]	9.60	1.6
6_14	1.52	6.1			1.56[b]	13.2[b]			0.24	19.0[b]		
2_12	1.55	12.8			1.58[b]	20.8[b]			0.27	23.1[b]		
4_14	1.53	9.5			1.59[b]	20.3[b]			0.25	19.7[b]		
2_14	1.54	13.7	6.7	2.1	1.61[b]	25.5[b]	7.9	3.2	0.26	23.9[b]	10.30	2.3

Particle roundness (Pentland 1927), φ_p, (Wadell 1935), φ_w; bulk density, ρ_b; gas dispersivity, α_g; and solute dispersivity, α_s

[a] Pugliese et al. (2013)

[b] Sharma and Poulsen (2010)

combinations of fluid type and media used, as the slopes of the linear parts of the *u–D* relationships in Fig. 2. The resulting gas dispersivities, α_g, and solute dispersivities, α_s, values are shown in Table 1. Dispersivity values were generally highest for Leca®, lower for gravel and lowest for granite. This is evident from Fig. 3 that shows the cumulative probability distributions for the difference (residual) in dispersivity values for identical particle size distributions for the three possible material pairs ($\alpha_{Leca®}$–$\alpha_{granite}$, α_{gravel}–$\alpha_{granite}$, $\alpha_{Leca®}$–α_{gravel}) for both gas and solute dispersion. The significance of the difference between the three materials, with respect to dispersivity, was evaluated by testing if the average residual for each material pair was larger than zero using the Mann–Whitney (Mann and Whitney 1947). The results revealed that the following relationships were significant at the 95 % confidence level: $\alpha_{g,Leca®} > \alpha_{g,granite}$, $\alpha_{g,gravel} > \alpha_{g,granite}$ and $\alpha_{s,Leca} > \alpha_{s,gravel} > \alpha_{s,granite}$ for solute dispersion. Although α_{gravel} generally is higher than $\alpha_{granite}$ for gas dispersion (Fig. 3b), the difference between these two materials for gas dispersion was not found significant at the 95 % confidence level.

Despite this, there seems to be a very strong tendency that dispersivity is highest for Leca® and lowest for granite, indicating that particle shape does have a strong influence on dispersivity. Pugliese et al. (2013) determined the roundness (φ) for the three materials used in this study using the Pentland (1927), φ_p, and the Wadell (1935), φ_w, relationships (Eqs. (10) and (11), respectively). The φ values are shown in Table 1 for each material. It is seen that dispersivity generally increases with increasing φ especially for φ_w, again suggesting that particle shape is important in controlling gas and solute dispersivity.

Values of α for each of the three materials as a function of particle size range (R) and mean particle diameter (D_m) are shown in Fig. 4, for both gas and solute dispersion. For all three materials both gas and solute dispersivity tends to increase with increasing values of R. This suggests that increasing R causes an increasing variability of the length of pathways through the pore network which in turn causes increasing dispersion as also discussed by Sharma and Poulsen (2010) and Pugliese et al. (2012). The α - D_m relationship is somewhat more complex across the six combinations of material and fluid, and there is no clear trend. For most of the combinations, α tends to be somewhat larger for small values of D_m (for fixed values of R) although this trend is relatively weak.

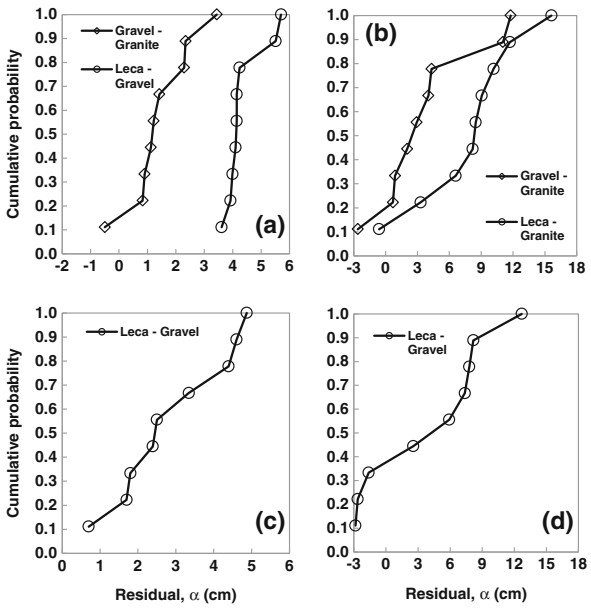

Fig. 3 Cumulative probability plots for the difference (residual) in dispersivities (α) for identical particle size fractions for **a** gravel–granite and Leca®–gravel (α_s), **b** gravel–granite and Leca®–granite (α_g), **c** Leca®-gravel (α_s), and **d** Leca®-gravel (α_g)

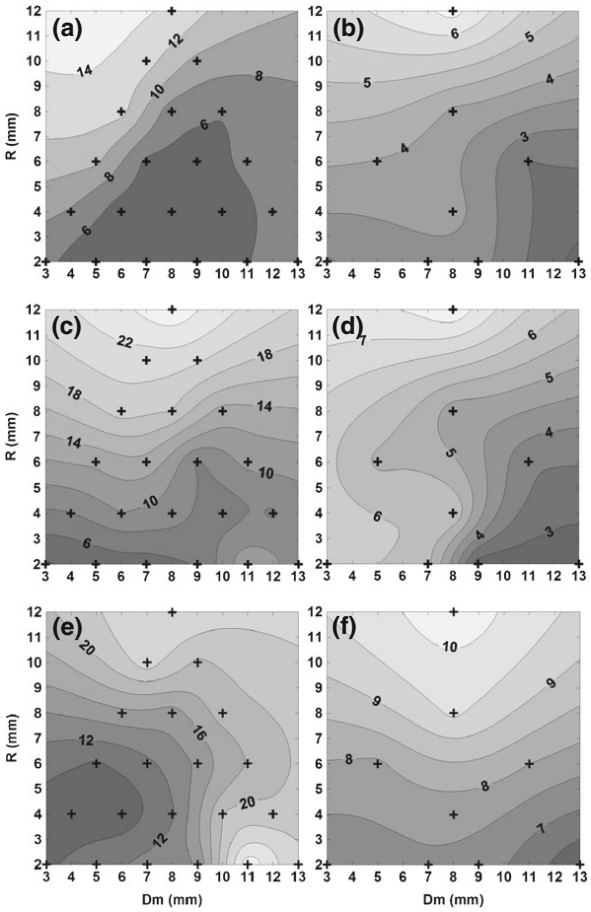

Fig. 4 Contour plots of dispersivity (α) as a function of mean particle diameter (D_m) and particle size range (R) for **a** $\alpha_{g,granite}$, **b** $\alpha_{s,granite}$, **c** $\alpha_{g,gravel}$, **d** $\alpha_{s,gravel}$, **e** $\alpha_{g,Leca®}$, and **f** $\alpha_{s,Leca®}$

Overall, the results indicate that dispersivity is strongly related to the width of the particle size distribution of the medium and the shape of the particles (φ), while the impact of particle size (D_m) is somewhat less marked.

Figure 5 shows the ratio between gas and solute dispersivity, α_g/α_s, as a function of D_m and R, for the three materials. Values of α_g/α_s for granite ranges between about 1 and 4 with gravel exhibiting the largest range. The reason why α_g/α_s is much smaller than the corresponding D ratio is that D_{mol} for gas is orders of magnitude larger than for solute resulting in large D ratios especially at low velocities. In general, α_g/α_s tends to increase with increasing D_m and R although the trends are relatively weak and there is considerable scatter in the data. The scatter is likely a result of the relatively few data points available.

In general, the ranges of α_g/α_s for the three materials are very similar and not significantly different on the 95 % confidence level as tested using ANOVA. Thus, despite the strong dependency of both α_g and α_s on φ their ratio appears independent of particle roundness.

As the ratio α_g/α_s depends on both D_m and R in a nonlinear manner it was chosen here to model this dependency using an empirical exponential relationship.

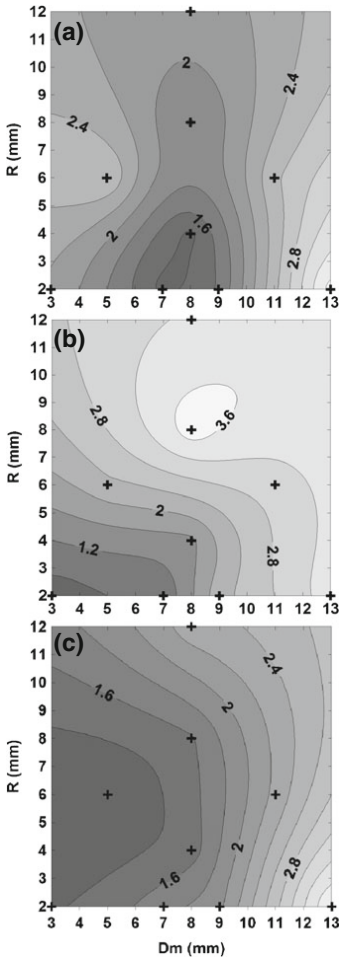

Fig. 5 Contour plot of dispersivity ratio, α_g/α_s, as a function of mean particle diameter (D_m) and particle size range (R) for **a** granite, **b** gravel, and **c** Leca®

Exponential functions are widely applied in science to describe a wide variety of relationships. The following empirical expression for modelling the dependency of α_g/α_s on D_m and R model was selected:

$$\frac{\alpha_g}{\alpha_s} = A\left(e^{BR} + e^{CD_m}\right), \tag{12}$$

where A, B, and C are empirical constants. Equation (12) was fitted to the α_g/α_s data for all three materials using five different approaches: (1) values of A, B, and C were fitted individually for each material, (2) a common value of A across all three materials and individual values of B and C for each material were fitted, (3) common values of A and C across all three materials and individual values of B for each material were fitted, (4) common values of A and B across all three materials, and individual values of C for each material were fitted, and (5) common values of A, B, and C were fitted across all three materials. Measured and fitted values of α_g/α_s using approach 1 are shown in Fig. 6 and values of parameters A, B, and C for all five approaches are given in Table 2.

Fitting accuracy was quantified using the mean squared error (MSE), defined as:

$$\mathrm{MSE} = \frac{1}{N}\sum_i^N \left(\left(\alpha_g/\alpha_s\right)_{\mathrm{measured}} - \left(\alpha_g/\alpha_s\right)_{\mathrm{calculated}} \right)^2 \tag{13}$$

MSE values for all five fitting approaches are also given in Table 2. The MSE values are very similar for approaches 1–3, indicating that coefficients A and C are independent of the medium used. In contrast, MSE increases by about 50 % when using a common value of B indicating that this coefficient at least, to some

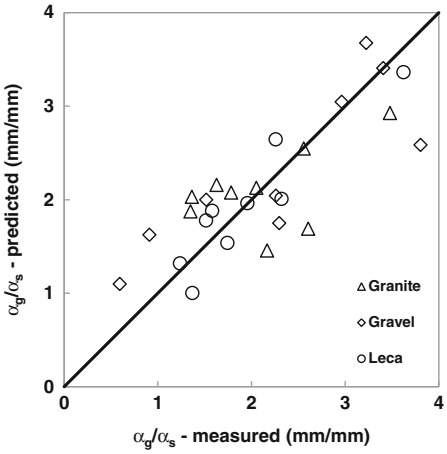

Fig. 6 Measured and predicted (using Eq. (12)) values of α_g/α_s, using individual values of A, B, and C for each of the three materials (approach 1)

degree, is medium dependent and, thus, different for each of three materials.

Figure 6, however, indicates that most of the MSE is related to a limited number of measurements and that the fit in general is able to mimic the α_g/α_s–R–D_m relationship regardless of which of the five approaches in Table 2 that is used.

We therefore suggest, that until more knowledge about the relation between B and medium characteristics becomes available, values of A=0.4, B=0.1, and C=0.15 are used for estimating the α_g/α_s–R–D_m relationship in granular porous media. It is emphasized that these values have only been verified valid for the particle sizes used in this study.

Overall, the results indicate that solute dispersion coefficients in natural porous media may be predicted using gas dispersion measurements although the relationship is not simple and straightforward. To achieve a better understanding of the relationship and its dependency on porous medium characteristics, additional measurements of gas and solute dispersion in a wider range of porous media are required.

5 Conclusions

Gas and solute dispersion in porous materials was analysed using tracer breakthrough data from three commercially available media: (1) crushed granite, (2) gravel, and (3) light expanded clay aggregates (Leca®). A total of 63 particle size fractions were produced (21 fractions for each material), having particle sizes of 2–14 mm. Gas and solute transport measurements were performed at the same range of Reynolds numbers, $0.004 \leq Re \leq 2.13$. Overall, 126 gas and 54 solute tracer breakthrough curves were used in the analyses.

Gas dispersion coefficients were generally larger than for solute. Both gas and solute dispersion coefficients exhibited the well-known linear increase with fluid pore velocity, except at very low fluid velocities. Gas and solute dispersivity (α), determined as the slopes of the linear parts of the u–D relationships, were generally highest for Leca®, lower for gravel, and lowest for granite. As the particle roundness for the three materials follows the same succession, this suggests that α is strongly related to medium particle shape. Results across all three media further indicate that α is strongly related to the width of the particle size distribution (R) and, to a lesser degree, of the actual mean particle diameter (D_m).

In contrast, the ratio between gas and solute dispersivity (α_g/α_s) did not exhibit a strong relationship with particle shape (roundness) but instead depended on D_m and R. Based on these observations, an empirical expression for predicting the dispersivity ratio (α_g/α_s) from D_m and R was suggested. This expression uses three empirical constants and was fitted to the α_g/α_s data using different approaches. The results indicate that at least two of the empirical constants are not medium dependent. As the expression was developed using data from media that are very different with respect to particle size distribution and particle shape, the results are likely robust; however, as the particle size distribution (uniform) and the types of material used here (three) are relatively limited further measurements using materials with a wider range of particle shapes and particle size distributions, are necessary to verify the findings.

Table 2 Optimal values of the empirical constants A, B, and C in Eq. (12), using different fitting approaches

Parameters	Approach 1	Approach 2	Approach 3	Approach 4	Approach 5
$A_{granite}$	0.61	0.42	0.44	0.41	0.40
A_{gravel}	0.37				
$A_{Leca®}$	0.37				
$B_{granite}$	0.02	0.07	0.05	0.10	0.10
B_{gravel}	0.05	0.14	0.14		
$B_{Leca®}$	0.16	0.02	0.02		
$C_{granite}$	0.10	0.14	0.14	0.14	0.15
C_{gravel}	0.16	0.14		0.16	
$C_{Leca®}$	0.16	0.15		0.14	
MSE_{total}	0.24	0.25	0.25	0.32	0.34

References

Arands, R., Lam, T., Massry, I., Berler, D. H., Muzzio, F. J., & Kosson, D. S. (1997). Modeling and experimental validation of volatile organic contaminant diffusion through an unsaturated soil. *Water Resources Research, 33*(4), 599–609.

Atteia, O., & Hohener, P. (2010). Semianalytical model predicting transfer of volatile pollutants from groundwater to the soil surface. *Environmental Science and Technology, 44*(16), 6228–6232.

Bear, J. (1961). On the tensor form of dispersion in porous media. *Journal of Geophysical Research, 66*(4), 1185–1197.

Brenner, H. (1980). Dispersion resulting from flow through spatially periodic porous-media. *Philosophical Transactions of the Royal Society A, 297*(1943), 81–133.

Bromly, M., Hinz, C., & Aylmore, L. A. G. (2007). Relation of dispersivity to properties of homogeneous saturated repacked soil columns. *European Journal of Soil Science Research, 58*(1), 293–301.

Brusseau, M. L. (1993). The influence of solute size, pore water velocity, and intraparticle porosity on solute dispersion and transport in soil. *Water Resources Research, 29*(4), 1071–1080.

Coelho, M. A. N., & Guedes de Carvalho, J. R. F. G. (1988). Transverse dispersion in granular beds: Part I-mass transfer from a wall and the dispersion coefficient in packed-beds. *Chemical Engineering Research and Design, 66*(2), 165–177.

Costanza-Robinson, M. S., & Brusseau, M. L. (2002). Gas phase advection and dispersion in unsaturated porous media. *Water Resources Research, 38*(4), 7.1–7.9.

De Visscher, A., Thomas, D., Boeckx, P., & Van Cleemput, O. (1999). Methane oxidation in simulated landfill cover soil environments. *Environmental Science and Technology, 33*(11), 1854–1859.

Delgado, J. M. P. Q. (2006). A critical review of dispersion in packed beds. *Heat and Mass Transfer, 42*(4), 279–310.

Domenico, P. A., & Schwartz, F. W. (1998). *Physical and chemical hydrogeology* (Vol. 44). New York: Wiley.

Edwards, M. F., & Richards, J. F. (1968). Gas dispersion in packed beds. *Chemical Engineering Science, 23*(2), 109–123.

El-Fadel, M., Findikakis, A. N., & Leckie, J. O. (1997). Environmental impacts of solid waste landfilling. *Journal of Helminthology, 50*(1), 1–25.

Evans, E. V., & Kenney, C. N. (1966). Gaseous dispersion in packed beds at low Reynolds numbers. *Transactions Institute of Chemical Engineers, 44*(6), T189–T197.

Fukumoto, Y., Osada, T., Hanajima, D., & Haga, K. (2003). Patterns and quantities of NH3, N2O and CH4 emissions during swine manure composting without forced aeration—effect of compost pile scale. *Bioresource Technology, 89*(2), 109–114.

Gerke, H. H., & van Genuchten, M. T. (1996). Macroscopic representation of structural geometry for simulating water and solute movement in dual-porosity media. *Advances in Water Resources, 19*(6), 343–357.

Gidda, T., Cann, D., Stiver, W. H., & Zytner, R. G. (2006). Airflow dispersion in unsaturated soil. *Journal of Contaminant Hydrology, 82*(1–2), 118–132.

Greenkor, R. A., & Kessler, D. P. (1969). Dispersion in heterogeneous nonuniform anisotropic porous media. *Industrial and Engineering Chemistry, 61*(9), 14–32.

Hamamoto, S., Moldrup, P., Kawamoto, K., Komatsu, T., & Rolston, D. E. (2009). Unified measurement system for the gas dispersion coefficient, air permeability, and gas diffusion coefficient in variably saturated soil. *Soil Science Society of America Journal, 73*(6), 1921–1930.

Han, N. W., Bhakta, J., & Carbonell, R. G. (1985). Longitudinal and lateral dispersion in packed beds: effect of column length and particle size distribution. *AICHE Journal, 31*(2), 277–288.

Hunt, A. G., & Skinner, T. E. (2010). Predicting dispersion in porous media. *Complexity, 16*(1), 43–55.

Lewis, J., & Sjostrom, J. (2010). Optimizing the experimental design of soil columns in saturated and unsaturated transport experiments. *Contaminant Hydrology, 115*(1–4), 1–13.

Liang, Y. K., Quan, X., Chen, J. W., Chung, J. S., Sung, J. Y., Chen, S., Xue, D. M., & Zhao, Y. Z. (2000). Long-term results of ammonia removal and transformation by biofiltration. *Journal of Hazardous Materials, 80*(1–3), 259–269.

Loll, P., Moldrup, P., Schjonning, P., & Riley, H. (1999). Predicting saturated hydraulic conductivity from air permeability: application in stochastic water infiltration modeling. *Water Research, 35*(8), 2387–2400.

Mann, H. B., & Whitney, D. R. (1947). On a test of whether one or two random variables is stochastically larger than the other. *Annals of Mathematical Statistics, 18*(1), 50–60.

Pangala, S. R., Reay, D. S., & Heal, K. V. (2010). Mitigation of methane emissions from constructed farm wetlands. *Chemosphere, 78*(5), 493–499.

Pennock, D., Yates, T., Bedard-Haughn, A., Phipps, K., Farrell, R., & McDougal, R. (2010). Landscape controls on N(2)O and CH(4) emissions from freshwater mineral soil wetlands of the Canadian Prairie Pothole region. *Geoderma, 155*(3–4), 308–319.

Pentland, A. (1927). A method of measuring the angularity of sands. MAG. MN. A.L. Acta Eng. Dom. Transaction of the Royal Society of Canada. Vol. 21(3), xciii.

Popovicova, J., & Brusseau, M. L. (1997). Dispersion and transport of gas-phase contaminants in dry porous media: effect of heterogeneity and gas velocity. *Journal of Contaminant Hydrology, 28*(1–2), 157–169.

Poulsen, T. G., Suwarnarat, W., Hostrup, M. K., & Kalluri, P. N. V. (2008). Simple and rapid method for measuring gas dispersion in porous media: methodology and applications. *Soil Science, 173*(3), 169–174.

Pugliese, L., Poulsen, T. G., & Andreasen, R. R. (2012). Relating gas dispersion in porous media to medium tortuosity and anisotropy ratio. *Water, Air, and Soil Pollution, 223*(7), 4101–4118.

Pugliese, L., Poulsen, T. G., & Andreasen, R. R. (2013). Biofilter media gas pressure loss as related to media particle size and particle shape. Accepted for publication in *Journal of Environmental Engineering*.

Rose, D. A. (1973). Some aspects of hydrodynamic dispersion of solutes in porous materials. *Soil Science, 24*(3), 285–295.

Schaufler, G., Kitzler, B., Schindlbacher, A., Skiba, U., Sutton, M. A., & Zechmeister-Boltenstern, S. (2010). Greenhouse gas emissions from European soils under different land use: effects of soil moisture and temperature. *European Journal of Soil Science, 61*(5), 683–696.

Scheidegger, A. E. (1974). *The physics of flow through porous media* (3rd ed.). Toronto, Ontario: University of Toronto Press.

Schjonning, P. (1986). Soil permeability by air and water as influenced by soil type and incorporation of straw. *Tidsskrift for Planteavl, 90*, 227–240.

Sharma, P., & Poulsen, T. G. (2010). Gas dispersion and immobile gas content in granular porous media: effect of particle size nonuniformity. *Soil Science, 175*(9), 426–431.

Silva, O., & Grifoll, J. (2009). Non-passive transport of volatile organic compounds infiltrated from a surface disk source. *Transport in Porous Media, 77*(1), 103–129.

Sinclair, R. J., & Potter, O. E. (1965). Dispersion of gas in flow through a bed of packed solids. *Transactions Institute of Chemical Engineers, 43*(1), T3–T9.

Suzuki, M., & Smith, J. M. (1972). Dynamics of diffusion and adsorption in a single catalyst pellet. *AICHE Journal, 18*(2), 326–333.

Tan, C. S., & Liou, D. C. (1989). Axial dispersion of supercritical carbon dioxide in packed beds. *Industrial and Engineering Chemistry Research, 28*(8), 1246–1250.

Thomson, N. R., Sykes, J. F., & Van Vliet, D. (1997). A numerical investigation into factors affecting gas and aqueous phase plumes in the subsurface. *Contaminant Hydrology, 28*(1–2), 39–70.

Thummes, K., Kaempfer, P., & Jaeckel, U. (2007). Temporal change of composition and potential activity of the thermophilic archaeal community during the composting of organic material. *Systematic and Applied Microbiology, 30*(5), 418–429.

Wadell, H. (1935). Volume, shape and roundness of quartz particles. *Journal of Geology, 43*(3), 250–280.

Wang, F., & Ward, I. C. (2002). Radon entry, migration and reduction in houses with cellars. *Building and Environment, 37*(11), 1153–1165.

Whitaker, S. (1967). Diffusion and dispersion in porous media. *AICHE Journal, 13*(3), 420–432.

White, C. M., Strazisar, B. R., Granite, E. J., Hoffman, J. S., & Pennline, H. W. (2003). Separation and capture of CO_2 from large stationary sources and sequestration in geological formations—coalbeds and deep saline aquifers. *Journal of the Air and Waste Management Association, 53*(6), 645–715.

Paper IV

Water Air Soil Pollut (2015) 226:59
DOI 10.1007/s11270-015-2353-2

Relating Non-equilibrium Solute Transport and Porous Media Physical Characteristics

Lorenzo Pugliese · Salvatore Straface · Benito Mendoza Trujillo · Tjalfe G. Poulsen

Received: 3 November 2014 / Accepted: 6 February 2015

Abstract Breakthrough data for solute tracer transport at different velocities, covering a wide range of particle sizes and particle shapes corresponding to 324 breakthrough curves, were used in this study. Analysis was carried out for three granular porous media: crushed granite, gravel, and Leca® (a commercial insulation material). Mobile–immobile phase (MIM) solute transport parameters (dispersivity, mass transfer, and mobile (active) porosity) for non-equilibrium mass transport were determined for each breakthrough curve by fitting a MIM solute transport model to the breakthrough data. The resulting set of solute transport parameters was correlated with porous medium physical properties (particle size distribution and particle shape) to establish a set of simple expressions for estimating the MIM solute transport parameters. Linear expressions for predicting the solute dispersivity, mass transfer, and mobile phase porosity from porous medium particle size distribution (mean particle diameter and width of particle size distribution) and particle shape were developed based on regression analysis. A partial validation of these expressions indicated that the developed expressions are able to accurately predict solute transport parameters from porous medium physical properties.

Keywords Solute breakthrough tailing · Non-equilibrium solute transport · Particle size distribution · Particle shape · Mass transfer coefficient · Solute dispersivity

L. Pugliese (✉)
Department of Chemistry, Biotechnology and Environmental Engineering, Aalborg University, 57 Sohngaardsholmsvej, 9000 Aalborg, Denmark
e-mail: Lorenzo.Pugliese@agro.au.dk

S. Straface
Department of Environmental and Chemical Engineering, University of Calabria, Via P. Bucci 42B, 87036 Arcavacata di Rende, Cosenza, Italy

B. M. Trujillo
Faculty of Engineering, National University of Chimborazo, Km 1, 5 Via Guano, Riobamba, Ecuador

T. G. Poulsen
Department of Civil Engineering, Xi'an Jiaotong-Liverpool University, 111 Ren Ai Road, Suzhou 215123 Jiangsu, China

1 Introduction

Solute transport in porous media is important for a wide range of applications such as groundwater and soil remediation, salt water intrusion, petroleum oil production in oilfields, containment of contaminant plumes, regeneration of reactive beds, drinking water purification, and wastewater treatment. Common to all these applications is the need to develop numerical solutions able to describe the transport mechanisms in all their complexity.

A broad range of models for simulating solute transport in porous media was introduced over the last decades. Initially, studies considered the medium as constituted by a unique (single) porous region (Coats and Smith 1964; Van Genuchten and Wierenga 1976; Cameron and Klute 1977; Rao et al. 1980; Zhang and

Published online: 24 February 2015

Brusseau 1999; Harvey and Gorelick 2000; Gao et al. 2013). Later, this approach was found to be insufficient to reproduce features of preferential flow and transport, caused by non-equilibrium conditions (Brusseau and Rao 1990; Arora et al. 2011). Therefore, porous media were considered as a collection of overlapping mobile and immobile pore subregions, each characterized by their own transport parameters (including porosity). Immobile subregions cause solute storage and delays in solute movement toward mobile subregions, resulting in tailing in overall solute breakthrough. Examples of studies using multiporosity models are those of Valocchi (1990), Haggerty and Gorelick (1995), Ahn et al. (1996), Cunningham and Roberts (1998), Kauffman et al. (1998), and Hollenbeck et al. (1999). The simplest version of the multiporosity model is the dual-porosity model, which considers the medium as a dual-porosity (dual subregions) system constituted of one mobile and one immobile pore regions.

Several studies (Ball and Roberts 1991; Pedit and Miller 1995; Haggerty and Gorelick 1998; Hollenbeck et al. 1999; Haggerty et al. 2000; McKenna et al. 2001) have shown that multiporosity models can achieve better predictions of measured breakthrough data compared to single-porosity models. A performance evaluation of continuum-scale models was carried out for soil columns by Arora et al. (2011). Results confirmed that increasing model complexity improves accuracy of the system dynamics, including depth profiles, temporal trends, and breakthrough curves (BTCs). Multiporosity models, however, require more (fitting) parameters compared to single-porosity models, depending on the number of subregions considered. Moreover, multiporosity models generate difficulties in achieving unique and consistent values of these fitting parameters based on measured breakthrough data, as several parameter value combinations may give a good fit to the data. There is thus a need to attain both good prediction of measured data and correct estimation of the model parameters. Improved consistency may be achieved if the values of the parameters for non-equilibrium transport could be linked to the properties of the porous medium (such as particle size and shape). At present, to the knowledge of the authors, there are no experimental studies on solutes in the published literature attempting to solve these issues for granular media.

The mobile–immobile model (MIM) is a dual-porosity model, which accounts for early arrival and tailing during fluid (gas or solute) transport in porous media (Gao et al. 2010). The MIM has been increasingly used over the last decades to describe transport in porous media. Examples are those of Nielsen et al. (1986), Koch and Fluhler (1993), Piquemal (1993), Haggerty and Gorelick (1995), Knabner et al. (1996), Griffioen et al. (1998), Casey et al. (1999), Van Beinum et al. (2000), Jiang et al. (2010), and Gao et al. (2012). The majority of MIM studies are related to solute transport, and only a limited body of literature on MIM applications for gas transport is available. Despite this, relationships between MIM transport parameters and porous medium characteristics such as particle size distribution and particle shape are mainly available for gas transport, likely because gas transport experiments are much less time-consuming to carry out compared to solute transport experiments. Results from Sharma and Poulsen (2009) showed that the immobile gas volume decreases with increasing velocity and increases with increasing water content. Effects of particle size distribution on MIM gas transport parameters were not addressed. In Sharma and Poulsen (2010b), the same authors investigated dispersion in two different granular materials and observed a strong relationship between gas dispersion and mean particle diameter or particle size range (width of particle size distribution), although no dependency of the mobile gas content on mean particle diameter or particle size range was found. Pugliese et al. (2012) utilized the MIM to investigate gas transport parameters in three granular porous media with different particle shapes and observed a strong dependency of gas transport parameters on particle shape. As gas and solute transport in porous media are controlled by the same mechanisms, the above findings for gas transport indicate that MIM transport parameters for solute transport applications can also be related to porous medium physical properties such as particle size distribution and particle shape. This is important, as knowledge about the relationship between MIM parameters for solute transport and porous medium characteristics can significantly improve the accuracy of MIM solute transport parameter estimates. This will in turn also reduce the need for time-consuming non-equilibrium solute transport experiments which is another important issue, especially when considering solute transport at large scales and in heterogeneous media.

The objective of this paper is, therefore, to evaluate the possibility of relating MIM solute transport parameters to granular porous medium physical characteristics, such as particle shape and particle size distribution.

The evaluation will be based on data from previously conducted solute breakthrough experiments (Pugliese et al. 2013b) for a set of granular media, covering a wide range of particle shapes and particle size distributions.

2 Theory

Transport of conservative solute tracers in porous, granular, and fractured media is often described, at the continuum scale, by the advection dispersion equation (ADE). In case of one-dimensional flow through a column containing a homogeneous porous medium, under assumption of uniform flow and dispersion, in presence of both a mobile and an immobile solute phase, the ADE is expressed as follows:

$$\frac{\partial C_{\mathrm{m}}}{\partial t} = D\frac{\partial^2 C_{\mathrm{m}}}{\partial x^2} - u\frac{\partial C_{\mathrm{m}}}{\partial x} + k(C_{\mathrm{im}} - C_{\mathrm{m}}) \quad (1)$$

where C_{m} and C_{im} are the solute tracer concentrations in the mobile and immobile solute phases (ML^{-3}), respectively, u is the pore velocity (interstitial velocity) in the mobile solute phase (LT^{-1}), k is the tracer mass transfer coefficient (T^{-1}) for mass transfer between the mobile and immobile phases, and x and t are the space (L) and time (T) variables. D is the overall dispersion–diffusion coefficient ($\mathrm{L}^2\ \mathrm{T}^{-1}$), given as follows:

$$D = D_{\mathrm{mol}} + D_{\mathrm{mech}} \quad (2)$$

where D_{mol} is the molecular diffusion coefficient ($\mathrm{L}^2\ \mathrm{T}^{-1}$) and D_{mech} is the contribution by mechanical dispersion ($\mathrm{L}^2\ \mathrm{T}^{-1}$). For one-dimensional flow, D_{mech} is generally expressed as follows:

$$D_{\mathrm{mech}} = \alpha u^m \quad (3)$$

where α is the solute tracer mechanical dispersivity in the mobile phase (L) and m is a dimensionless exponent (Pugliese and Poulsen 2014). For u <0.3 cm min^{-1}, mechanical dispersion approaches 0 and the relation (Eq. (3)) does not hold (Pugliese et al. 2013b).

When simulating solute transport in a porous medium by the MIM, the medium pore space is considered a dual-region system. Therefore, two values of porosity are considered (describing the mobile and immobile region pore volumes, respectively). In this case, solute transport in the mobile region is described by Eq. (1), while tracer concentration in the immobile region is described as follows:

$$\frac{\partial C_{\mathrm{im}}}{\partial t} = -\frac{\varepsilon_{\mathrm{m}}}{\varepsilon_{\mathrm{im}}}k(C_{\mathrm{im}} - C_{\mathrm{m}}) \quad (4)$$

where ε_{m} and $\varepsilon_{\mathrm{im}}$ are the mobile and immobile solute-filled porosities ($\mathrm{L}^3\ \mathrm{L}^{-3}$), respectively. In some cases, the porous medium may contain pores that do not participate in the solute transport, a so-called dead porosity $\varepsilon_{\mathrm{dead}}$. These porosity parameters are linked by the following relation:

$$\varepsilon_{\mathrm{tot}} = \varepsilon_{\mathrm{m}} + \varepsilon_{\mathrm{im}} + \varepsilon_{\mathrm{dead}} \quad (5)$$

where $\varepsilon_{\mathrm{dead}}$ represents a solute-filled porosity ($\mathrm{L}^3\ \mathrm{L}^{-3}$) consisting of isolated (nonconnected or poorly connected) pores which have no solute mass exchange with the rest of the pore system, unlike $\varepsilon_{\mathrm{im}}$ that participates in mass exchange. In practice, $\varepsilon_{\mathrm{dead}}$ represents a pore system subdomain in which mass transfer is too slow to significantly affect solute concentrations over the timescale of the experiment (Zinn and Harvey 2003) and mass transfer is, thus, modeled as being zero.

3 Materials and Methods

The solute BTC data used in this study were all measured previously by Pugliese et al. (2013b) using three commercially available materials: (1) crushed granite, (2) gravel, and (3) Leca® (Light Expanded Clay Aggregates). Crushed granite consists of sharp-cornered particles with a compact internal structure without pores. Gravel consists of more rounded particles also without internal pores. Leca® consists of almost spherical particles which are highly porous with an internal pore structure mainly consisting of closed vesicles.

Measurements of the BTC data by Pugliese et al. (2013b) were conducted as follows: for each of the three materials, nine particle size fractions with uniform particle size distributions were used: 2–4, 2–8, 2–14, 4–12, 6–8, 6–10, 8–10, 8–14, and 12–14 mm. The procedure for creating these particle size fractions is explained in details by Pugliese et al. (2013a, b, c). Each fraction is characterized by a mean particle diameter (d_{m}) and a particle size range (R) (Table 1). Acrylic columns of 100-cm length and 14-cm inner diameter were used to

contain the selected media, which was carefully packed into each column to reduce inhomogeneities in packing density. A stainless steel mesh with 2-mm openings and 1-mm thickness was installed at both ends of the column, to support and prevent movements of the media. Polyethylene lids sealed using rubber O-rings were used at both ends. Soft Teflon tubing with an inner diameter of 4 mm was used to connect each component of the system (Pugliese et al. 2013b).

The inlet was located at the bottom of the column and connected to a peristaltic pump (model PD 5101, Heidolph). The outlet (top of the column) let to a measuring tube capable of containing 12 ml effluent and a TetraCon 325 conductometer. After saturating the columns with demineralized water and adjusting the flow to the desired value, a solution consisting of NaCl dissolved in demineralized water to a concentration of 5 g l^{-1} was injected. Measurements were carried out in duplicate and performed at different flow rates equal to 0.015, 0.05, 0.075, 0.1, 0.125, and 0.15 l min^{-1}. A total of 324 BTCs were measured. More details of the experimental procedure are given by Pugliese et al. (2013b).

Measured BTCs were fitted using Eqs. (1) and (4), by optimizing values of D, ε_m, ε_{dead}, and k. An explicit finite difference method, corrected for numerical dispersion, was used.

The corresponding initial and boundary conditions were as follows:

$$\text{Initial condition} \quad t = 0,\ x \geq 0 \quad C = 0 \tag{6a}$$

$$\text{Boundary condition} \quad t > 0,\ x = 0 \quad C = C_0 \tag{6b}$$

where C_0 is the concentration of the tracer (NaCl).

Optimal values of D, ε_m, ε_{dead}, and k were determined by minimizing the sum of squared errors (SSE) between measured and fitted values of solute concentration as follows:

$$\text{SSE} = \sum [P_{measured} - P_{fitted}]^2 \tag{7}$$

where $P_{measured}$ and P_{fitted} are the original and fitted values of the parameter in question (in this case, solute concentration), respectively.

4 Results and Discussion

Measured BTCs at a solute flow rate of 0.125 l min^{-1}, for the 2–14-mm particle size fraction for all three materials, are shown in Fig. 1. Shown are also the best fitted curves for the MIM (Eqs. (1) and (4)).

All three data sets exhibit the typical sigmoid shape characterizing this type of process. In all three cases, some tailing is evident, with granite showing the least and Leca® the most amount of tailing. This was also the case for the remaining 321 BTCs. The relatively little tailing exhibited by the granite data shows reduced solute exchange between the mobile and immobile phases indicating a quasi-equilibrium condition between the two phases. Conversely, gravel and Leca® exhibit more tailing and thus have larger immobile water contents. Figure 1 shows that the MIM can be accurately fitted to the entire BTC for each of the three materials. This was also the case for the remaining BTCs. These observations are in agreement with previous studies (Zinn and Harvey 2003; Sanchez-Vila and Carrera 2004).

Fitted D values for selected particle size fractions using Eqs. (1) and (4)–(7) are shown in Fig. 2a as a function of u. Granite exhibits the lowest D values, while gravel and Leca® the intermediate and the highest, respectively. The data in Fig. 2a generally show curved relationships in agreement with Eq. (3). Best fit values of α and m for each particle size fraction were determined by fitting Eq. (3) to the D–u data, minimizing the SSE (Eq. (7)) with $P=D$. Granite generally exhibits the highest values of m, while intermediate and lowest m values are exhibited by gravel and Leca®, respectively. This behavior was observed for all particle size fractions. Resulting values of α for each particle size fraction are given in Table 1.

Corresponding k values, for the same particle size fraction data illustrated in Fig. 2a, are shown in Fig. 2b as a function of u. Leca® generally shows the highest k values, while granite shows the lowest. This was also the case for the remaining BTCs and indicates that particle shape affects the flow field, which is in agreement with the findings of Pugliese and Poulsen (2013c). Further analyses of the k–u data showed that k is also proportional to the mean diameter d_m, while particle size range, R, has a minimal effect on k. A power function equivalent to Eq. (3), given as $k=\beta u^n$, was fitted to the k–u data minimizing the SSE (Eq. (7)) with $P=k$. Resulting values of β for the 27 particle size fractions are given in Table 1. The relationships generally exhibit less curvature compared to the D–u relationships, resulting in lower values of n compared to m for all materials and particle size fractions investigated.

Table 1 Physical characteristics of the three media (crushed granite, gravel, and Leca®) and calculated α and β values from the D–u and k–u relationships (Fig. 2), respectively

Size range (mm)	Mean diameter (mm)	Particle size range (mm)	Granite		Gravel		Leca®	
			φ=0.09[a]		φ=0.51[a]		φ=0.89[a]	
			α (cm)	β (cm^{-1})	α (cm)	β (cm^{-1})	α (cm)	β (cm^{-1})
2–4	2	3	0.27	0.0010	0.41	0.0021	0.42	0.0043
2–8	6	5	0.33	0.0012	0.43	0.0019	0.52	0.0047
2–14	12	8	0.37	0.0012	0.61	0.0038	0.61	0.0055
4–12	8	8	0.31	0.0012	0.43	0.0030	0.54	0.0054
6–8	2	7	0.31	0.0012	0.39	0.0023	0.43	0.0052
6–10	4	8	0.22	0.0021	0.44	0.0035	0.50	0.0059
8–10	2	9	0.20	0.0030	0.49	0.0066	0.46	0.0060
8–14	6	11	0.09	0.0016	0.24	0.0039	0.40	0.0056
12–14	2	13	0.07	0.0012	0.17	0.0039	0.30	0.0053

[a] Pugliese et al. (2013a)

It is well known from literature (Delgado 2006) that D increases with the width of the particle size distribution and tends to be greater with packs of non-spherical particles than with packs of spherical particles of the same size (Ebach and White 1958; Hiby 1962; De Carvalho and Delgado 2003). This was later confirmed by Sharma and Poulsen (2010a) and Pugliese et al. (2012), who found that increasing R causes an increasing variability of the length of pathways through the pore network, which in turn increases dispersion. Analysis on the same media as used in this study (Pugliese et al. 2013b) confirmed the previous findings. Moreover, a dependency of transport on particle shape, φ, was observed, although no attempts to relate dispersivity, α, to φ were carried out.

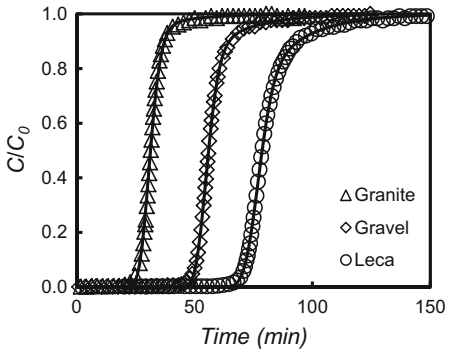

Fig. 1 Measured and fitted solute concentrations for the 2–14-mm particle size fraction for all three materials, at a flow rate of 0.125 l min^{-1}. Fitted values for the MIM (estimated using Eqs. (1) and (4)) are represented by the *continuous line*

These observations suggest that in order to estimate dispersivity, it may be advantageous to consider the contribution of each medium physical characteristic to α separately. It is therefore suggested to model α as a linear combination of contributions by the medium characteristics as follows:

$$\eta = p_1 * d_m + p_2 * R + p_3 * \varphi + p_4 \quad (8)$$

where η represents the parameter to be predicted (in this case α) and p_1, p_2, p_3, and p_4 are empirical constants whose dimension depends on the parameter modeled. d_m is the mean particle diameter (L), R is the particle size range (L), and φ is the particle roundness (dimensionless) as defined by Wadell (1935). Details on roundness measurements for the three materials used here are given in Pugliese et al. (2013a), and values for the three materials are shown in Table 1. Equation (8) was fitted to the α data both across all three materials (27 particle size fractions) and for each material (9 particle size fractions) individually. Best fit values of p were obtained by minimizing the SSE (Eq. (7)) with P=α. Resulting values of p for fitting α are given in Table 2. Fitted (Eq. (8)) versus calculated (Eq. (3)) values of α are shown in Fig. 3a.

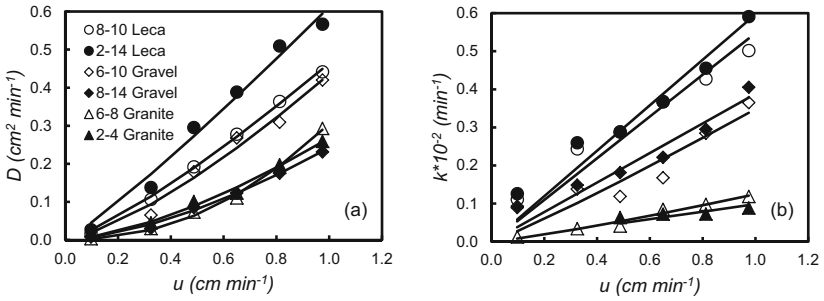

Fig. 2 Fitted **a** D values and **b** k values as a function of pore velocity (u), for selected particle size fractions

One common set of values for p_1 (-), p_2 (-), p_3 (mm), and p_4 (mm) in Eq. (8) valid across all three materials is suggested to limit the number of fitting parameters used. Using individual values of the empirical constants for each material (ten fitting parameters) instead of common values (four fitting parameters) only resulted in an overall reduction in the SSE of 17 %; thus, there is little advantage of using individually fitted p values. To verify the accuracy of Eq. (8) for predicting dispersivity (α), a partial validation analysis was carried for all particle size fractions. The validation procedure was as follows: each time, one α point was set aside and the fitting of p_1, p_2, p_3, and p_4 was done using Eq. (8) together with the remaining 26 data sets. The excluded α value was then predicted using the fitted ps. This procedure was repeated 27 times (each time with a new α point set aside, resulting in 27 predicted values of α), and results are presented in Fig. 3b. Fitting of the calculated α values (Fig. 3a) generates SSE=11.3, while the partial validation (Fig. 3b) approach yields SSE=15.2 (not shown in Table 2)

Table 2 Values of the empirical constants carried out by fitting Eq. (8) for selected scenarios and material combinations

η	Scenario	Materials	p_1	p_2	p_3	p_4	SSE
α			(-)	(-)	(mm)	(mm)	
		All	−0.21	0.18	2.83	3.09	11.3
		Granite	−0.26	0.15	3.17	3.45	9.43
		Gravel	−0.24	0.19	3.06		
		Leca®	−0.13	0.20	1.43		
β			(mm^{-2})		(mm^{-1})		
		All	1.4E−05	–	4.7E−04	–	1.7E−07
		Granite	2.9E−06	–	1.4E−03	–	1.5E−07
		Gravel	2.4E−05	–	3.0E−04		
		Leca®	8.1E−06	–	5.2E−04		
ε_m	1	Granite	−0.001	−0.0003	−0.112	0.423	0.0009
		Gravel	−0.001	−0.0025	−0.039		
		Leca®	0.006	−0.0046	0.050		
	2	Granite	−0.001	−0.002	0.097	0.415	0.0018
		Gravel	−0.001		−0.024		
		Leca®	0.006		0.048		
	3	Granite	0.001	−0.002	0.086	0.399	0.0038
		Gravel			−0.028		
		Leca®			0.103		
	4	All	0.001	−0.002	0.103	0.377	0.0302

Also given are corresponding values of minimum SSE calculated using Eq. (7)

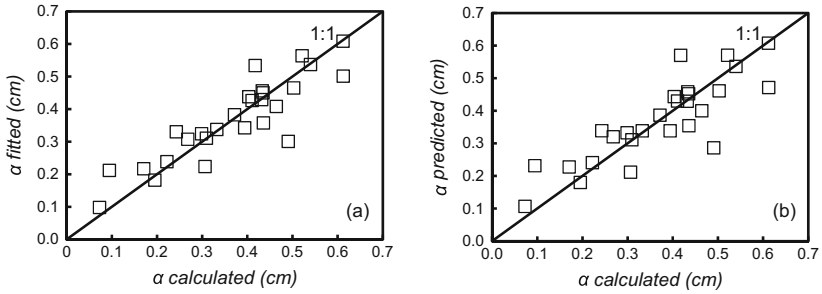

Fig. 3 **a** Fitted (Eq. (8)) vs calculated (Eq. (3)) α values for all materials and particle size fractions using p_1=−0.21, p_2=0.18, p_3=2.83 (mm), p_4=3.09 (mm), and SSE=11.3 and **b** predicted (using partial validation of Eq. (8)) vs calculated (Eq. (3)) α values, SSE=15.2

which corresponds to an increase of 34 %. This relatively limited difference in terms of SSE denotes a good prediction by Eq. (8).

Figure 2a, b indicates that the slope of the D–u relationship (α) and the slope of the k–u relationship (here labeled β) are related. Values of α versus β are plotted in Fig. 4.

The highest values of β are generally obtained for Leca®, while the lowest are obtained for granite. Thus, there seems to be a relationship between β and particle roundness. Round particles such as Leca® seem to have higher mass transfer between the mobile and immobile phases (and thus higher β), than more angular particles such as granite. A reason for this behavior could be differences in the shape of local mobile and immobile pore regions at the pore scale and differences in the amount of interfacial area between the two phases. Despite some scatter in the data especially for the gravel, Fig. 4 further indicates that α and β are proportional to some degree. This means that β likely depends on porous medium characteristics in a manner similar to that of α. It was therefore chosen to describe β using Eq. (8) (with η now representing β). Optimization was performed by minimizing the SSE (Eq. (7) with P=β). Analysis showed that p_2 and p_4 had little or no impact of the fitting accuracy and these parameters were therefore excluded from the analysis. Analyses were carried out considering both one common set of p values across all 27 particle size fractions and p values fitted for each of the three materials individually. Results are given in Table 2.

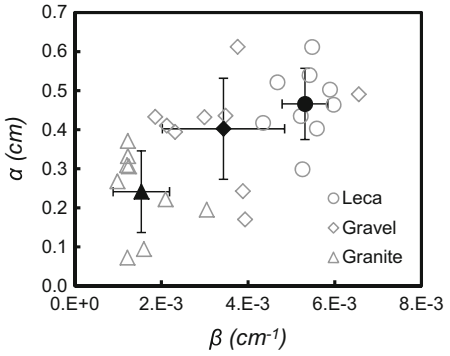

Fig. 4 Relationship between α and β, for all materials and particle size fractions. *Grey* and *black data* represent individual data points and average values, respectively. *Error bars* indicate one standard deviation

Again, one common set of values for p_1 (mm^{-2}) and p_3 (mm^{-1}) in Eq. (8) valid across all three materials is suggested to limit the number of fitting parameters used. Figure 5a shows fitted (Eq. (8)) versus calculated β (slopes of the k–u relationship) values using these two parameters. Using individual p values for each material (six fitting parameters) instead of common values (two fitting parameters) only resulted in an overall reduction in the SSE of 9 % (Table 2).

A partial validation of Eq. (8) following the approach used in Fig. 3b was carried out for the 27 β values, and results are shown in Fig. 5b. Fitting of the calculated β values (Fig. 3a) yields SSE=1.7E−7, while the partial validation approach yields SSE=1.9E−7 (not shown in Table 2) which corresponds to an increase of 14 %. Again, this suggests that Eq. (8) is adequate for describing β.

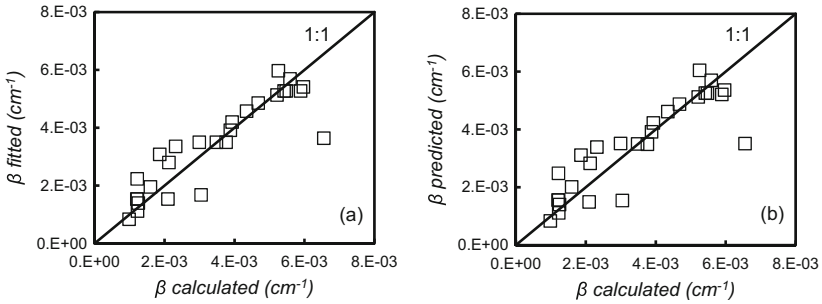

Fig. 5 **a** Fitted (Eq. (8)) vs calculated β values for all materials and particle size fractions with p_1=1.4E−5 (mm^{-2}), p_3=4.7E−4 (mm^{-1}), and SSE=1.7E−7 and **b** predicted (using partial validation of Eq. (8)) vs calculated β values, SSE=1.9E−7

Values of ε_m obtained from the MIM simulations were almost independent of u but did exhibit some dependency on R, d_m, and φ. Therefore, ε_m was assumed constant for each particle size fraction. The relationship between ε_m and R, and d_m and φ was modeled using Eq. (8), where, in this case, η represents ε_m. Equation (8) was fitted to ε_m values, considering all the contributions of the four parameters (p_1, p_2, p_3, and p_4). Four different scenarios were adopted to identify if the empirical constants may be assumed common across all three materials: scenario 1: individual values of p_1, p_2, p_3 and a common value of p_4 (ten fitting parameters); scenario 2: individual values of p_1 and p_3 and common values of p_2 and p_4 (eight fitting parameters); scenario 3: individual values of p_3 and common values of p_1, p_2, and p_4 (six fitting parameters); and scenario 4: common values of all four constants (four fitting parameters). An overview of the resulting constant values is given in Table 2. In comparison with scenario 1, SSE values for scenarios 2, 3, and 4 increased by 101, 310, and 3305 %, respectively. Scenario 2 is therefore suggested as the optimal approach having a moderate value of SSE in combination with a reduced number of fitting parameters.

Figure 6a shows fitted (Eq. (8)) versus calculated average values of ε_m for each of the 27 particle size fractions while Fig. 6b shows fitted (Eq. (8)) versus calculated individual values of ε_m at each combination of velocity and particle size fraction. Note that Eq. (8) does not take the effects of velocity into account and predicts the same value of ε_m for each particle size fraction regardless of velocity. Despite this, Eq. (8) is

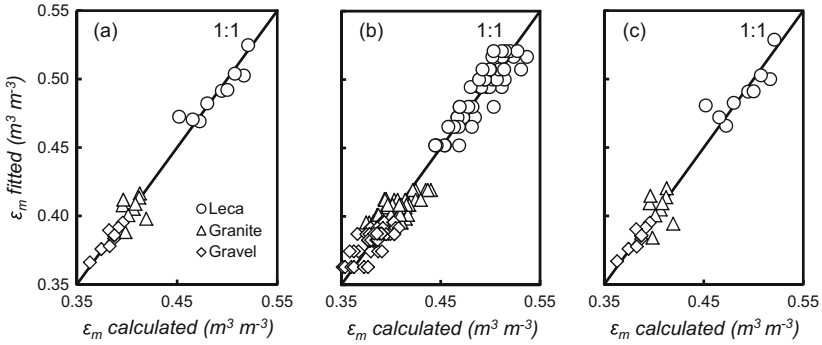

Fig. 6 **a** Fitted (Eq. (8)) vs calculated ε_m values (one average ε_m value across six velocities for each particle size fraction), **b** fitted (Eq. (8)) vs calculated ε_m values (one ε_m value for each combination of velocity and particle size fraction), and **c** predicted (using partial validation of Eq. (8)) vs calculated ε_m values (one average ε_m value for each particle size fraction), yielding SSE=0.0029. All fittings were performed using scenario 2 (Table 2)

still able to predict individual values of ε_m with and accuracy of ±3 % on average.

To estimate the accuracy of Eq. (8) for predicting ε_m, a partial validation analysis on ε_m was carried out using scenario 2 (Table 2). Predicted versus calculated (from the dual-porosity modeling) values are shown in Fig. 6c. This analysis yields SSE=0.0029, an overall increase of 38 % compared to Fig. 6a.

Overall, the results indicate that both α, β, and ε_m are related to porous medium particle size distribution (d_m, R) and particle shape (φ) in a similar way and may be predicted from porous medium characteristics using the same type of expression. The results further suggest that accurate predictions of the tailing end of solute BTCs may be achieved using the MIM. Therefore, it seems feasible to estimate model parameters (α, β, and ε_m) from porous medium physical properties, thus avoiding the necessity for measuring the tailing. This potentially produces significant time savings, especially in connection with in situ experiments, where BTCs often exhibit substantial tailing. To verify the validity of the findings presented here, however, additional measurements for a wider range of media than considered here should be carried out.

5 Conclusions

Solute transport in three different granular porous media (crushed granite, gravel, and Leca®), exhibiting similar particle sizes but different particle shapes, was analyzed in this study. Solute transport data for 27 particle size fractions (nine for each material), at six different pore flow velocities, u, (corresponding to a total of 324 BTCs), using chloride as a tracer, were used in the analysis.

BTC shape suggests the presence of non-equilibrium solute mass transfer between a mobile phase and an immobile phase, in agreement with previous studies. Among the three materials, BTCs for Leca® (having the most rounded particles) exhibit the largest amount of tailing while granite (having the least rounded particles) exhibits the smallest amount of tailing, suggesting that particle shape has a significant impact on mass transfer. The measured BTCs were fitted to the mobile–immobile phase (MIM) model to estimate values of dispersion coefficient (D), mass transfer coefficient (k), and mobile phase porosity (ε_m). Leca® showed the highest k values (a consequence of the higher amount of tailing in the BTCs), while granite showed the lowest values. This indicates that the more spherical the particles, the greater the mass transfer between the mobile and immobile phases. Round particles, in fact, expedite the exchange between mobile and immobile phases, while particles with more angular shapes (mainly granite) hinder it.

The results further indicated that the slope, α, of the D–u relationship (also known as dispersivity), the slope, β, of the k–u relationship, and ε_m (across all three materials and 27 particle size fractions) could be predicted from particle size distribution characteristics and particle shape using a simple linear expression. This means that model parameters (α, β, and ε_m) may be estimated using the porous medium characteristics, which in turn means that significant time can be saved as the time-consuming measurements (especially for measuring BTC tailing) can be avoided.

As the quantity of data used in the analyses presented here is somewhat limited, however, additional measurements on other media, having different particle size distributions and particle shapes, are needed to verify and improve the relationships presented in this study.

References

Ahn, I. S., Lion, L. W., & Shuler, M. L. (1996). Microscale-based modeling of polynuclear aromatic hydrocarbon transport and biodegradation in soil. *Biotechnology and Bioengineering, 51*(1), 1–14.

Arora, B., Mohanty, B. P., & McGuire, J. T. (2011). Inverse estimation of parameters for multidomain flow models in soil columns with different macropore densities. *Water Resources Research, 47*, 1–17.

Ball, W. P., & Roberts, P. V. (1991). Long-term sorption of halogenated organic chemicals by aquifer material 2. Intraparticle diffusion. *Environmental Science and Technology, 25*(7), 1237–1249.

Brusseau, M. L., & Rao, P. S. C. (1990). Modeling solute transport in structured soils: a review. *Geoderma, 46*(1–3), 169–192.

Cameron, D. R., & Klute, A. (1977). Convective-dispersive solute transport with a combined equilibrium and kinetic adsorption model. *Water Resources Research, 13*(1), 183–188.

Casey, F. X. M., Jaynes, D. B., Horton, R., & Logsdon, S. D. (1999). Comparing field methods that estimate mobile-immobile model parameters. *Soil Science Society of America Journal, 63*(4), 800–806.

Coats, K. H., & Smith, B. D. (1964). Dead-end pore volume and dispersion in porous media. *Society of Petroleum Engineers. Journal, 4*(1), 73–84.

Cunningham, J. A., & Roberts, P. V. (1998). Use of temporal moments to investigate the effects of nonuniform grain-size

distribution on the transport of sorbing solutes. *Water Resources Research, 34*(6), 1415–1425.

De Carvalho, J. R. F. G., & Delgado, J. M. P. Q. (2003). Effect of fluid properties on dispersion in flow through packed beds. *AICHE Journal, 49*(8), 1980–1985.

Delgado, J. M. P. Q. (2006). A critical review of dispersion in packed beds. *Heat and Mass Transfer, 42*(4), 279–310.

Ebach, E. A., & White, R. R. (1958). Mixing of fluids flowing through beds of packed solids. *AICHE Journal, 4*(2), 161–169.

Gao, G. Y., Zhan, H. B., Feng, S. Y., Fu, B. J., Ma, Y., & Huang, G. H. (2010). A new mobile-immobile model for reactive solute transport with scale-dependent dispersion. *Water Resources Research, 46*, 1–16.

Gao, G. Y., Zhan, H. B., Feng, S. Y., Fu, B. J., & Huang, G. H. (2012). A mobile-immobile model with an asymptotic scale-dependent dispersion function. *Journal of Hydrology, 424*, 172–183.

Gao, G. Y., Fu, B. J., Zhan, H. B., & Ma, Y. (2013). Contaminant transport in soil with depth-dependent reaction coefficients and time-dependent boundary conditions. *Water Research, 47*(7), 2507–2522.

Griffioen, J. W., Barry, D. A., & Parlange, J. Y. (1998). Interpretation of two-region model parameters. *Water Resources Research, 34*(3), 373–384.

Haggerty, R., & Gorelick, S. M. (1995). Multiple-rate mass-transfer for modeling diffusion and surface-reactions in media with pore-scale heterogeneity. *Water Resources Research, 31*(10), 2383–2400.

Haggerty, R., & Gorelick, S. M. (1998). Modeling mass transfer processes in soil columns with pore-scale heterogeneity. *Soil Science Society of America Journal, 62*(1), 62–74

Haggerty, R., McKenna, S. A., & Meigs, L. C. (2000). On the late-time behavior of tracer test breakthrough curves. *Water Resources Research, 36*(12), 3467–3479.

Harvey, C. F., & Gorelick, S. M. (2000). Rate-limited mass transfer or macrodispersion: which dominates plume evolution at the macrodispersion experiment (MADE) site. *Water Resources Research, 36*(3), 637–650.

Hiby, J. W. (1962). Longitudinal dispersion in single-phase liquid flow through ordered and random packings. In: *Interact between fluid & particles*, London Instn. Chem. Engrs., pp. 312–325.

Hollenbeck, K. J., Harvey, C. F., Haggerty, R., & Werth, C. J. (1999). A method for estimating distributions of mass transfer rate coefficients with application to purging and batch experiments. *Journal of Contaminant Hydrology, 37*(3–4), 367–388.

Jiang, S., Pang, L. P., Buchan, G. D., Simunek, J., Noonan, M. J., & Close, M. E. (2010). Modeling water flow and bacterial transport in undisturbed lysimeters under irrigations of dairy shed effluent and water using HYDRUS-1D. *Water Research, 44*(4), 1050–1061.

Kauffman, S. J., Bolster, C. H., Hornberger, G. M., Herman, J. S., & Mills, A. L. (1998). Rate-limited transport of hydroxyatrazine in an unsaturated soil. *Environmental Science and Technology, 32*(20), 3137–3141.

Knabner, P., Totsche, K. U., & Kogel Knabner, I. (1996). The modeling of reactive solute transport with sorption to mobile and immobile sorbents. 1. Experimental evidence and model development. *Water Resources Research, 32*(6), 1611–1622.

Koch, S., & Fluhler, H. (1993). Solute transport in aggregated porous media: comparing model independent and dependent parameter estimation. *Water, Air, and Soil Pollution, 68*(1–2), 275–289.

McKenna, S. A., Meigs, L. C., & Haggerty, R. (2001). Tracer tests in a fractured dolomite 3. Double-porosity, multiple-rate mass transfer processes in convergent flow tracer tests. *Water Resources Research, 37*(5), 1143–1154.

Nielsen, D. R., van Genuchten, M. T., & Biggar, J. W. (1986). Water flow and solute transport processes in the unsaturated zone. *Water Resources Research, 22*(9), 89S–108S.

Pedit, J. A., & Miller, C. T. (1995). Heterogeneous sorption processes in subsurface systems. 2. Diffusion modeling approaches. *Environmental Science and Technology, 29*(7), 1766–1772.

Piquemal, J. (1993). On the modeling conditions of mass-transfer in porous-media presenting capacitance effects by a dispersion-convection equation for the mobile fluid and a diffusion equation for the stagnant fluid. *Transport in Porous Media, 10*(3), 271–283.

Pugliese, L., & Poulsen, T. G. (2013). Linking gas and liquid pressure loss to particle size distribution and particle shape in granular filter materials. *Water, Air, and Soil Pollution, 225*(1), 1811.

Pugliese, L., & Poulsen, T. G. (2014). Estimating solute dispersion coefficients in porous media at low pore water velocities. *Soil Science, 179*(4), 175–181.

Pugliese, L., Poulsen, T. G., & Andreasen, R. R. (2012). Relating gas dispersion in porous media to medium tortuosity and anisotropy ratio. *Water, Air, and Soil Pollution, 223*(7), 4101–4118.

Pugliese, L., Poulsen, T. G., & Andreasen, R. R. (2013a). Biofilter media gas pressure loss as related to media particle size and particle shape. *Journal of Environmental Engineering, 139*(12), 1424–1431.

Pugliese, L., Poulsen, T. G., & Straface, S. (2013b). Gas-solute dispersivity ratio in granular porous media as related to particle size distribution and particle shape. *Water, Air, and Soil Pollution, 224*(9), 1691.

Rao, P. S. C., Rolston, D. E., Jessup, R. E., & Davidson, J. M. (1980). Solute transport in aggregated porous-media – theoretical and experimental evaluation. *Soil Science Society of America Journal, 44*(6), 1139–1146.

Sanchez-Vila, X., & Carrera, J. (2004). On the striking similarity between the moments of breakthrough curves for a heterogeneous medium and a homogeneous medium with a matrix diffusion term. *Journal of Hydrology, 294*(1–3), 164–175.

Sharma, P., & Poulsen, T. G. (2009). Gas phase dispersion in compost as a function of different water contents and air flow rates. *Journal of Contaminant Hydrology, 107*, 101–107.

Sharma, P., & Poulsen, T. G. (2010a). Gas dispersion and immobile gas content in granular porous media: effect of particle size nonuniformity. *Soil Science, 175*(9), 426–431.

Sharma, P., & Poulsen, T. G. (2010b). Gas dispersion and immobile gas volume in solid and porous particle biofilter materials at low air flow velocities. *Journal of the Air & Waste Management Association, 60*(7), 830–837.

Valocchi, A. J. (1990). Use of temporal moment analysis to study reactive solute transport in aggregated porous media. *Geoderma, 46*(1–3), 233–247.

Van Beinum, W., Meeussen, J. C. L., Edwards, A. C., & Van Riemsdijk, W. H. (2000). Transport of ions in physically heterogeneous systems; convection and diffusion in a column

filled with alginate gel beads, predicted by two-region model. *Water Research, 34*(7), 2043–2050.

Van Genuchten, M. T., & Wierenga, P. J. (1976). Mass transfer studies in sorbing porous-media. 1. Analytical solutions. *Soil Science Society of America Journal, 40*(4), 473–480.

Wadell, H. (1935). Volume, shape and roundness of quartz particles. *Journal of Geology, 43*(3), 250–280.

Zhang, Z. H., & Brusseau, M. L. (1999). Nonideal transport of reactive solutes in heterogeneous porous media. 5 Simulating regional-scale behavior of a trichloroethene plume during pump-and-treat remediation. *Water Resources Research, 35*(10), 2921–2935.

Zinn, B., & Harvey, C. F. (2003). When good statistical models of aquifer heterogeneity go bad: a comparison of flow dispersion, and mass transfer in connected and multivariate Gaussian hydraulic conductivity fields. *Water Resources Research, 39*(3), 1–19.

Paper V

Estimating Solute Dispersion Coefficients in Porous Media at Low Pore Water Velocities

Lorenzo Pugliese[1] *and Tjalfe G. Poulsen*[2]

Abstract: The relationship between solute dispersion coefficient (D_{mech}) and pore water velocity during chloride transport in porous media with different particle characteristics at low pore water velocities ($u < 1$ cm min^{-1}), relevant for ground water flow conditions, was investigated. Data for 29 porous media with very different particle shapes (ranging from almost spherical to very angular) and particle sizes (0.088–12 mm) at different velocities (340 breakthrough curves) were used in the analyses.

The analysis showed that D_{mech} at low u is significantly different from that at higher u. Whereas the u - D_{mech} relationship generally can be assumed linear at higher u (based on observations in earlier studies), the data presented in this study clearly show that this is not the case at low u. The results further indicated that D_{mech} at low u is strongly related to porous medium particle shape and to some degree also to medium particle size range and mean particle diameter. As the current knowledge about dispersion at low u and its dependency on porous medium properties is very limited, the results obtained in this study represent a significant addition to this understanding. A set of expressions for predicting D_{mech} at low u from medium properties was developed. These expressions yield good accuracy across all 29 media, thus providing a means for predicting dispersion at low u across a very wide range of media.

Key Words: Solute transport, dispersion, low pore water velocities, porous media, particle size and shape

(*Soil Sci* 2014;179: 175–181)

Among the mechanisms controlling transport of dissolved compounds in porous media, mechanical dispersion occupies a key role in many practical situations. Examples are migration of contaminants in the groundwater at polluted soil sites, leaching of pesticides from farmland to groundwater and drinking water supply, removal of dissolved contaminants in filters, and migration of dissolved compounds in both saturated and unsaturated soil. Many of the processes, for which dispersion is important, take place in systems such as groundwater aquifers where the liquid flow velocity is relatively low. Understanding the behavior of mechanical dispersion under saturated conditions and low pore water velocities is therefore essential.

A relatively large body of literature relating solute dispersion coefficients to pore water velocity is available, dating back to the 1950s. Examples are Carberry and Bretton (1958), Ebach and White (1958), Liles and Geankoplis (1960), Saffman (1960), Perkins and Johnston (1963), Pfannkuch (1963), Poreh (1965), Miller and King (1966), Chung and Wen (1968), Fried and Combarnous (1971), Klotz (1973), Miyauchi and Kikuchi (1975), Sahimi et al. (1986), Hu and Brusseau (1994), Matsubayashi et al. (1997), and Delgado (2006). In general, the mechanical dispersion coefficient (D_{mech}) has been found to be proportional to pore velocity (u). This relationship is modeled using a power function type of relationship where D_{mech} is proportional to u to a power that generally varies between 1 (a linear relationship) and 2. However, most studies have assumed D_{mech} to be a linear function of fluid velocity (exponent equal to 1), which is now generally used as an approximation.

Investigations of the relationship between D_{mech} and u have mostly been carried out at u ranging between $1*10^{-3}$ and $6*10^{2}$ cm min^{-1} using both natural and artificial media. Groundwater velocities, however, typically range between 10^{-4} and 10^{1} cm min^{-1}, depending on soil type and hydraulic gradient. Thus, the range of u considered in previous studies is generally in the upper end of the typical range for groundwater flow. A limited number of studies (Harleman and Rumer, 1963; Hu and Brusseau, 1994; Padilla et al., 1999; Pugliese et al., 2013b) have investigated dispersion under saturated conditions at velocities lower than 1 cm min^{-1}. Harleman and Rumer (1963) investigated dispersion using an isotropic medium (plastic spheres with an average particle diameter of 0.96 mm) for $u = 0.3$ - 8 cm min^{-1}. The authors presented an equation linking the dispersion ratio (longitudinal over lateral) to a dimensionless coefficient that was presumed dependent on particle shape and particle size distribution. However, no investigations of these relationships were carried out. Hu and Brusseau (1994) measured dispersion using a medium consisting of homogeneous glass beads (diameter, 212–300 μm), at $u = 0.001$ - 1 cm min^{-1}, and found that, for $u < 1$ cm min^{-1}, the u - D_{mech} relationship could be described by a power law function with exponent of 1 - 1.3. Padilla et al. (1999) measured dispersion at two different pore water velocities ($u = 0.03$ and 0.13 cm min^{-1}) for a single porous medium (silica sand with an average particle diameter of 250 μm). Pugliese et al. (2013b) measured dispersion at $u = 0.1$ - 1 cm min^{-1} using an extensive set of granular porous media with a wide range of particle sizes and particle shapes. The authors found that, for $u > 0.3$ cm min^{-1}, the u - D_{mech} relationship was approximately linear regardless of particle size and shape, in agreement with earlier literature. For $u < 0.3$ cm min^{-1}, the u - D_{mech} relationship was not linear but gradually approached a slope of zero with decreasing u. This indicates that the linear relationship is not valid at low u; however, no investigations of the u - D_{mech} relationship and its dependency on particle size and shape in this u-region were carried out by Pugliese et al. (2013b).

Dispersion generally depends on particle characteristics, such as particle size, particle shape, and particle orientation in relation to the direction of flow (Delgado, 2006; Pugliese et al., 2013b). Only a limited number of studies (Ebach and White, 1958; Hiby, 1962; De Carvalho and Delgado, 2003; Pugliese et al., 2013b) have focused on the effects of particle shape on the u - D_{mech} relationship. Results show that D_{mech} is greater for flow through materials consisting of nonspherical particles than through materials consisting of spherical particles of the same size. These studies, however, did not include the behavior of D_{mech} at low u values, relevant for groundwater flow, and their results are

[1]Department of Chemistry and Biotechnology, Aalborg University, Aalborg, Denmark.
[2]Department of Civil Engineering, Xi'an Jiaotong-Liverpool University, Jiangsu, China.
Address for correspondence: Mr. Lorenzo Pugliese, Department of Chemistry and Biotechnology, Aalborg University, 57 Sohngaardsholmsvej, 9000 Aalborg, Denmark. E-mail: lorenzo.pugliese@agro.au.dk
Financial Disclosures/Conflicts of Interest: None reported.
Received December 7, 2013.
Accepted for publication May 6, 2014.

ISSN: 0038-075X
DOI: 10.1097/SS.0000000000000056

therefore not directly applicable to typical groundwater flow situations. To the best knowledge of the authors, no additional studies investigating the specific effects of porous medium physical properties (such as particle size and particle shape) on the u - D_{mech} relationship at low u have been published. At present, knowledge about the u - D_{mech} relationship at u values relevant for groundwater flow and its dependency on porous medium particle size and shape is very limited. There is, thus, a strong need not only to assess the u - D_{mech} relationship at low u values relevant for groundwater flow but also to investigate the impact of particle size and shape on the u - D_{mech} relationship in this range of u across a wider range of particle sizes and shapes.

The objective of this work is, therefore, to evaluate the connection between porous media physical properties (particle size range, mean particle diameter, and particle shape) and the u - D_{mech} relationship including low values of u relevant for groundwater flow using a large set of porous media with different particle size distributions and particle shapes. The aim is to establish a set of expressions for estimating dispersion coefficients from pore water velocity at low velocities, taking into account effects of porous media physical properties. Data for the analyses carried out in this study were taken from three previously published works: Harleman and Rumer (1963), Hu and Brusseau (1994), and Pugliese et al. (2013b). These data cover multiple porous materials exhibiting a wide range of particle sizes and particle shapes.

THEORY

The most widely used expression to describe solute transport in porous materials is the advection-dispersion equation (ADE). In case of one-dimensional solute transport through a homogeneous medium, assuming uniform flow and dispersion, and neglecting mass transfer between the mobile and immobile fluid phase, the ADE is given by:

$$\frac{\partial C_m}{\partial t} = D\frac{\delta^2 C_m}{\partial x^2} - u\frac{\partial C_m}{\partial x} \tag{1}$$

where C_m is the tracer concentration in the mobile fluid phases ($M\,L^{-3}$); D is the overall dispersion-diffusion coefficient ($L^2\,T^{-1}$), which takes into account effects of molecular diffusion, mechanical dispersion, and fluid mixing in the tubing leading the liquid to and from the column (Poulsen et al., 2008); u is the pore fluid velocity (interstitial velocity) of the mobile phase ($L\,T^{-1}$); and x and t are the space (L) and time (T) variables. The liquid u is estimated as:

$$u = \frac{Q}{A\varepsilon_m} \tag{2}$$

where ε_m is the mobile volumetric phase contents ($L^3\,L^{-3}$) in the porous medium, Q is the applied volumetric liquid flow rate ($L^3\,T^{-1}$), and A is the column cross-sectional area (L^2) perpendicular to the liquid flow direction.

The overall diffusion/dispersion coefficient D is expressed as:

$$D = D_{mol} + D_{mech} + D_{mix} \tag{3}$$

where D_{mol} represents the contribution by molecular diffusion, D_{mech} is the contribution from mechanical dispersion, and D_{mix} is the contribution from fluid mixing in the tubing leading to and from the porous medium column. Pugliese et al. (2013b) showed that, at low velocities, D_{mol} can be neglected because it is very small, whereas D_{mix} can be minimized by reducing tracer travel distances outside the porous medium (Pugliese et al., 2012).

For a one-dimensional configuration, D_{mech} is expressed as a power function, such as:

$$D_{mech} = \alpha u^m \tag{4}$$

where α is the tracer mechanical dispersivity (longitudinal dispersivity) in the mobile fluid phase (L), and m is a dimensionless exponent.

Combining Eq.(3) and Eq.(4) yields:

$$D = D_{mol} + \alpha u^m + D_{mix} \tag{5}$$

At larger velocities, m is generally assumed to be equal to 1, and dispersion becomes linearly related to u (Scheidegger, 1961; Bear, 1972; Freeze and Cherry, 1979; Matsubayashi et al., 1997; Pugliese et al., 2013b). In this case, a plot of D versus u yields a straight line, with slope α and intercept $D_{mol} + D_{mix}$ (Poulsen et al., 2008).

Particle shape is usually characterized by particle roundness, defined by Wadell (1935) as:

$$\varphi = \frac{N}{\sum_N \left(\frac{\Phi}{r_N}\right)} \tag{6}$$

where φ represents the total degree of roundness (dimensionless), N denotes the number of corners in the given plane of the particle, Φ is the radius of the largest inscribed circle (L), and r is the radius of the inscribed circle of the N^{th} corner of the particle in the plane (L).

MATERIALS AND METHODS

Assessment of the u - D_{mech} relationship was carried out using breakthrough curves (BTC) previously measured by Pugliese et al. (2013b). Measurements were executed using three commercially available materials: (i) crushed granite, (ii) gravel, and (iii) Leca (Light Expanded Clay Aggregates). Crushed granite consists of very angular particles, whereas gravel particles are more rounded, and Leca particles are almost spherical. A compact internal structure (without pores) characterizes both crushed granite and gravel, whereas Leca has an internal pore structure consisting of closed vesicles. For each of the three materials, nine particle size fractions with uniform particle size distributions were used: 2 to 4, 2 to 8, 2 to 14, 4 to 12, 6 to 8, 6 to 10, 8 to 10, 8 to 14, 12 to 14 mm. Each particle size fraction, created using the procedure of Pugliese et al. (2013a, 2013b, 2013c), is identified by the mean particle diameter (d_m) and the particle size range (R). An

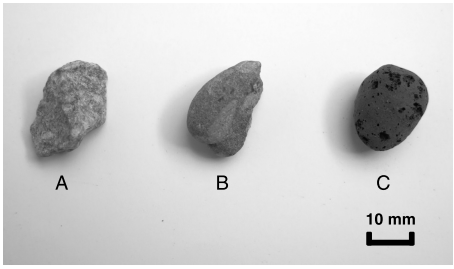

FIG. 1. Illustration of porous materials used by Pugliese et al. (2013b): granite (A), gravel (B), and Leca (C).

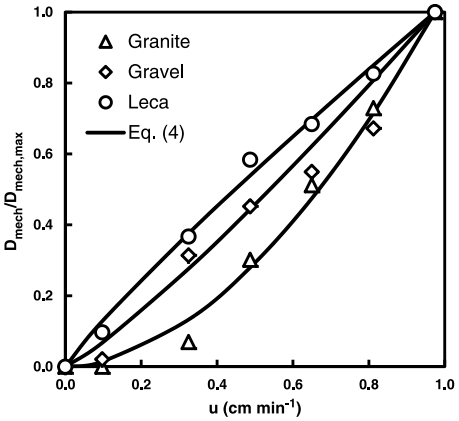

FIG. 2. Relationship between relative dispersion coefficient (D_{mech}/ $D_{mech,max}$) and u for each of the 2- to 8-mm fractions for crushed granite, gravel, and Leca. Symbols indicate values determined by fitting the measured breakthrough data (using Eq.(1)–Eq.(3)), and curves are fitted Eq.(4) to these data.

illustration of typical particles belonging to each of the three materials is given in Fig. 1.

Before measurements, each material was packed into an acrylic column of 100 cm length and 14 cm inner diameter. Packing was done with care to reduce inhomogeneities in packing density. A stainless steel mesh with 2-mm openings and 1-mm thickness was installed at both ends of the column to support and prevent movements of the media. Polyethylene lids sealed using rubber O-rings were used at both ends. Soft Teflon tubing with an inner diameter of 4 mm was used to connect each component of the system (Pugliese et al., 2013b; 2013c).

The inlet was located at the bottom of the column and connected to a peristaltic pump (model PD 5101; Heidolf). The outlet (top of the column) led to a measuring tube holding 12 mL of liquid and a TETRACON 325 conductometer. After saturating the columns with demineralized water, adjusting the flow to the desired value, and achieving constant flow, a NaCl solution was injected. Measurements were carried out in duplicate and performed at six different flow rates equal to 0.015, 0.05, 0.075, 0.1, 0.125, 0.15 L min^{-1}. A total of 324 BTC were measured. More details of the experimental procedure are given in Pugliese et al. (2013b).

The measured BTC were fitted to Eq.(1) to Eq.(3) by optimizing the values of D and ε_m using the following initial and boundary conditions:

$$\text{Initial condition} \quad t = 0, x \geq 0 \quad C = 0 \tag{7a}$$

$$\text{Boundary condition} \quad t > 0, x = 0 \quad C = C_0 \tag{7b}$$

Fitting accuracy was assessed using the relative root mean squared errors (SSE) defined as:

$$\text{SSE} = (P_{\text{data set 1}} - P_{\text{data set 2}})^2 \tag{8}$$

where $P_{\text{data set 1}}$ and $P_{\text{data set 2}}$ are the values of the two data sets that are compared (that being modeled or measured values). Optimum fits were determined by minimizing SSE. Further details on the fitting procedure can be found in Pugliese et al. (2013b).

Two additional data sets (15 BTC) taken from previous studies were also considered in the analysis (Harleman and Rumer, 1963; Hu and Brusseau, 1994). Harleman and Rumer (1963) performed the experiments using plastic spheres, having $\varphi = 1$ d_m = 0.96 mm and R = 0.2 mm. Hu and Brusseau (1994) used glass beads, with $\varphi = 1$ d_m = 0.256 mm and R = 0.088 mm.

RESULTS AND DISCUSSION

Selected u - D_{mech} relationships and corresponding fitted curves representing Eq.(4), for the 2- to 8-mm particle size fraction and for each of the three materials (crushed granite, gravel, and Leca), are shown in Fig. 2. As D_{mech} = 0 for u = 0, an additional point was included in each data set at the origin. In general the u - D_{mech} relationships, based on the breakthrough data from Pugliese et al. (2013b), follow the power function (Eq.(4)) as also found earlier (Hu and Brusseau, 1994; Padilla et al., 1999), throughout the u range investigated. Crushed granite exhibits most curvature, whereas Leca exhibits the least. This was generally also the case for the u - D_{mech} relationships for the remaining eight particle size fractions for each of the three materials.

Values of D_{mech} fitted by Eq.(4) versus calculated from measured breakthrough data using (Eq.(1)–Eq.(3)) are shown in Fig. 3, for crushed granite, gravel and Leca, and for all combinations of particle size fraction and u. For all three materials Eq.(4) correctly estimates D_{mech} along all the u range investigated. The SSE are 0.008, 0.018, and 0.097 for granite, gravel and Leca, respectively. The estimation procedure was carried out considering individual values of α and m for each particle size fraction and

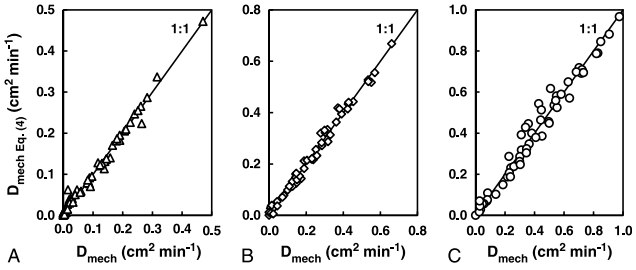

FIG. 3. Values of dispersion coefficient (D_{mech}) fitted by Eq.(4) versus D_{mech} calculated from measured breakthrough data using Eq.(1) to Eq.(3) for crushed granite (A), gravel (B), and Leca (C).

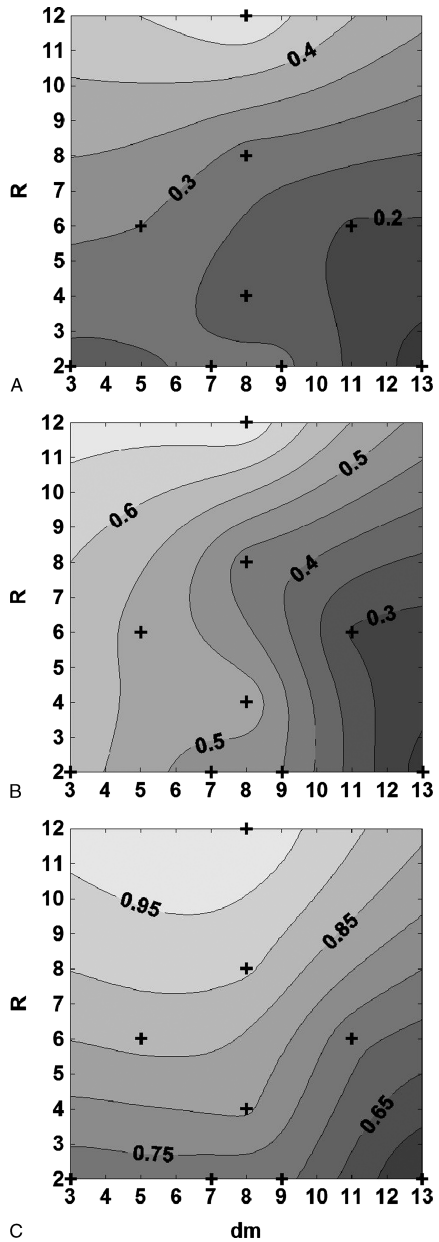

FIG. 4. Contour plots of dispersivity (α), based on Eq.(4), as a function of R and d_m for crushed granite (A), gravel (B), and Leca (C).

material (resulting in 27 α, m data sets). Figure 4 shows the contour plots of α, as a function of R and d_m, for all particle size fractions and materials investigated.

Overall, the plots indicate that α is somewhat dependent on R but almost independent of d_m. Especially Leca (Fig. 4C) clearly shows this behavior. Leca also exhibits higher α values in agreement with previous studies, carried out assuming $m = 1$ (Pugliese et al., 2013b), whereas gravel and granite exhibit the intermediate and lower α values, respectively. Analysis of the particle roundness of the three materials, carried out by Pugliese et al. (2013a) and following the approach of Wadell (Eq.(6)), showed that crushed granite particles had the lowest roundness (0.09), gravel intermediate roundness (0.51), and Leca the highest roundness (0.89). As the main difference between the three materials with respect to transport is the particle roundness, the results indicate that roundness is especially important when estimating α.

To develop a model for estimating α, an expression of the form

$$\alpha = n_0 + n_1 d_m^{n_2} + n_3 R^{n_4} + n_5 \varphi^{n_6} \quad (9)$$

was initially considered, where n_i (for i = 0, 1, 2, 3, 4, 5, 6) are empirical fitting parameters. This type of expression was chosen as it has successfully been used in earlier studies of transport in porous media. The analysis involved the α values for the gravel, granite and Leca presented in Fig. 4 and α values for two additional data sets taken from previous works (Harleman and Rumer, 1963; Hu and Brusseau, 1994). Eq.(9) was initially fitted to the α-data, and the n parameters with little or no impact on fitting accuracy (SSE) were eliminated from the model. The model was then re-fitted with the reduced number of fitting parameters. This procedure was repeated until it was no longer possible to reduce the number of fitting parameters without considerable loss of accuracy as determined by the SSE. This procedure resulted in the following equation for estimating α:

$$\alpha = n_1 (R^{n_2} - 1) + n_3 \varphi^{n_4} \quad (10)$$

where α and R are given in centimeters and millimeters, respectively, and $n_1 = 576$, $n_2 = 0.0003$, $n_3 = 0.56$, and $n_4 = 1.31$ are

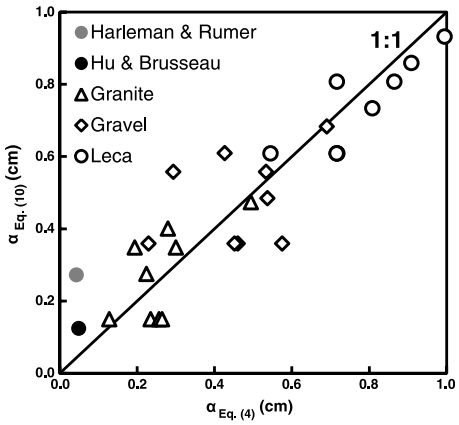

FIG. 5. Values of dispersivity (α) fitted by Eq.(10) versus α values determined by fitting D_{mech} (Eq.(4)) for all particle size fractions and materials. Values of the empirical constants are $n_1 = 576$, $n_2 = 0.0003$, $n_3 = 0.56$, $n_4 = 1.31$.

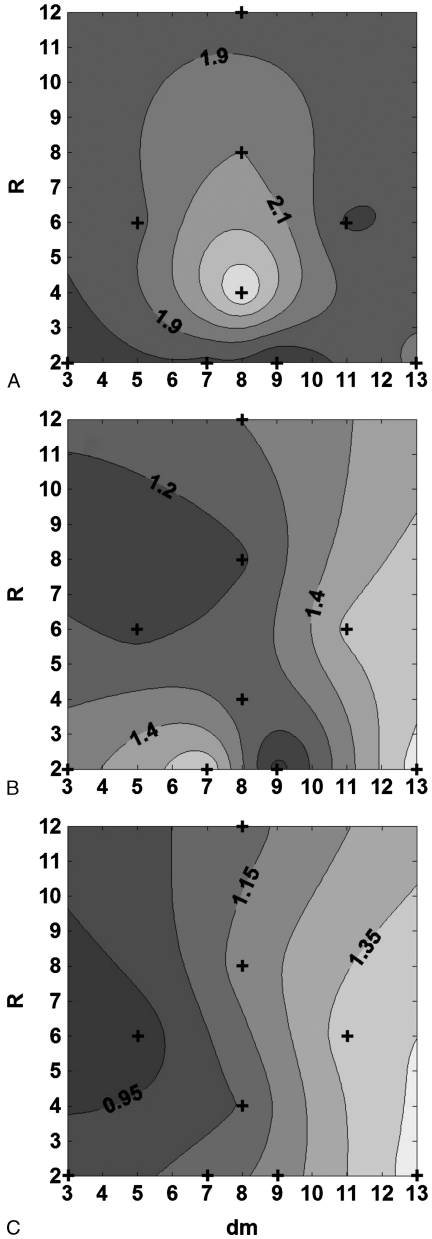

FIG. 6. Contour plots of exponent (m) based on Eq.(4) as a function of R and d_m for crushed granite (A), gravel (B), and Leca (C).

empirical constants, which are identical for all particle size ranges and materials. Eq.(10) shows that a low u dispersivity is proportional to particle roundness, and thus, dispersion seems to be higher in media consisting of spherical particles than those consisting of non-spherical particles. This is a significant finding because current knowledge about the effects of roundness on dispersivity is extremely limited.

Figure 5 shows α values as fitted by Eq.(10) versus α values determined by Eq.(4), for all particle size fractions and materials. The results in Fig. 5 show that Eq.(10) provides a good accuracy across all five materials and 29 particle size fractions in fitting α values based on R, φ, and four empirical constants. As already highlighted in Fig. 4, d_m does not affect the estimation of α at very low pore velocities. This is in contrast with the behavior of α at higher velocities observed in earlier studies, where d_m becomes important (De Carvalho and Delgado, 2003; Delgado, 2006; Pugliese et al., 2013c). The results further indicate that Eq.(10) is applicable for almost all kinds of particle shapes and for particle sizes ranging between 0.088 and 12 mm.

To verify if the α values for granite, gravel, and Leca, calculated from Eq.(4), are significantly different as indicated by Fig. 5, the differences $\alpha_{Leca} - \alpha_{gravel}$, $\alpha_{Leca} - \alpha_{granite}$, and $\alpha_{gravel} - \alpha_{granite}$ were calculated for each particle size fraction. This was done to take into account effects of particle size and shape. It was then tested if the averages of each of the three sets of differences were significantly larger than 0 using percentile bootstrapping (Wilcox, 1997). This is a nonparametric method that is based on generating a large set of artificial data sets with the same distribution as the data that are to be tested (in this case the α differences). These are then used to calculate the confidence interval for the average. Nonparametric statistics were used because the data could not be assumed normally distributed. The test showed that the average differences for the three sets were significantly larger than zero at the 95% confidence level. This means that $\alpha_{Leca} > \alpha_{gravel}$ and $\alpha_{gravel} > \alpha_{granite}$ is significant at the 95% level, confirming that α is strongly dependent on particle roundness.

Values of m obtained from fitting Eq.(4) to the α data are shown in Fig. 6 as a function of R and d_m, for crushed granite, gravel, and Leca, considering all particle size fractions. Figure 6

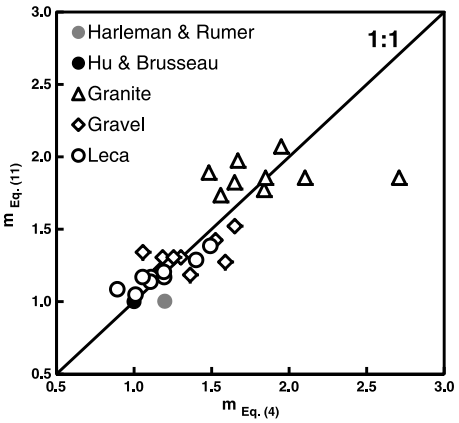

FIG. 7. Values of exponent (m) fitted by Eq.(11) versus m values determined by fitting D_{mech} (Eq.(4)) for all particle size fractions and materials. Values of the empirical constants are $n_1 = 0.003$, $n_2 = 1.89$, $n_3 = -0.22$.

shows that, in contrast to α, m is generally dependent on d_m but almost independent of R. This behavior is clearly visible for Leca (Fig. 6C). The dependency of m on R and d_m is less evident for gravel and granite, and it is probably caused by the limited number of points investigated. Values of m are smallest for Leca, intermediate for gravel, and largest for granite. Values of m are thus inversely proportional to roundness (φ). This tendency is opposite to what was found for α, which is directly proportional to φ. As roundness is the main difference between the three materials, the observations in Fig. 6 suggest that φ is very important when estimating m. Again this is a very significant addition to our current understanding of the relationship between dispersion and particle shape. Figure 6 further indicates that, although m at higher u (as found in previous studies including Pugliese et al., 2013c) may be assumed close to 1, this is not the case for low u where it varies significantly especially in response to roundness. An expression for predicting m based on d_m, R, and φ was developed for all five materials, following the approach used for developing Eq.(10). The following expression was proposed:

$$m = n_1 d_m^{n_2} + \varphi^{n_3} \quad (11)$$

where m and d_m are given in centimeters and millimeters, respectively, and $n_1 = 0.003$, $n_2 = 1.89$, $n_3 = -0.22$, respectively, are empirical constants, which are identical for all particle size ranges and materials. Figure 7 shows m values fitted using Eq.(11 versus m values determined by fitting D_{mech} (Eq.(4)) for all particle size fractions and materials.

Figure 7 shows that there is a good agreement between m values determined by Eq.(4) and Eq.(11). The overall SSE is equal to 0.46, whereas SSE for the granite, gravel, and Leca are 1.13, 0.26, and 0.08, respectively. The SSE for plastic spheres and glass beads was smaller than 0.03 and only generated from one point (only one particle size fraction was considered in those studies).

Percentile bootstrapping was also used in this case to test if values of m were significantly different between granite, gravel, and Leca following the approach used for testing the α values above. The test results showed that the average differences for three sets were significantly larger than zero, which means that $m_{granite} > m_{gravel}$ and $m_{gravel} > m_{Leca}$ is significant at the 95% level, confirming that m is strongly dependent on φ.

CONCLUSIONS

The relationship between pore water velocity (u) and mechanical dispersion coefficient (D_{mech}) at low u was investigated using data for five granular porous materials (crushed granite, gravel, Leca, plastic spheres, and glass beads) with different particle characteristics in terms of particle size and particle shape. A total of 29 different porous media were considered. Analysis of the u - D_{mech} relationships at low u showed that, in opposition to higher u where relationships are generally linear, relationships were generally nonlinear and followed a power function ($D_{mech} = \alpha u^m$). Thus, in contrast to earlier studies of dispersion at higher u where m is generally close to 1, significant deviations from $m = 1$ are observed at low u. Values of dispersivity (α) across the 29 media were strongly dependent on particle shape (roundness, φ) and showed a direct proportionality with φ. Results also indicated that α is proportional to porous medium particle size range (R) but independent of medium mean particle diameter (d_m). This is in contrast to earlier studies of dispersion at high u, where observations show a dependency of α on d_m. In contrast to α, m was inversely proportional to φ but independent of R. Overall, the results show that dispersion at low u behaves significantly different from higher u, and that particle shape is a very important parameter in controlling dispersion at low u. As existing studies of dispersion have focused on its behavior at high u, the results presented here constitute a significant addition to the current knowledge of dispersion behavior at low u and its dependency on porous medium properties.

A set of empirical expressions for estimating α and m from porous medium properties (R, φ, and d_m) was developed. The proposed expression provided good accuracy across all five materials and 29 media involved in the analysis. This indicates that it is possible to estimate α and m from particle size and particle shape across a wide range of particle shapes and sizes. As such models did not exist previously, this fills an important gap in the knowledge about predicting dispersion in porous media at low u. The data used here mainly represent granular media with a relatively large particle size relevant for many filter and aquifer applications. However, to verify and expand the model concepts presented here to soils and similar materials in general, additional measurements for media with smaller particle sizes than used here should be carried out.

REFERENCES

Bear J. 1972. Dynamics of fluids in porous media. New York, NY, American Elsevier.

Carberry J. J., and R. H. Bretton. 1958. Axial dispersion of mass in flow through fixed beds. AIChE J. 4(3):367–375.

Chung S. F., and C. Y. Wen. 1968. Longitudinal dispersion of liquid flowing through fixed and fluidized beds. AIChE J. 14(6):857–866.

De Carvalho J. R. F. G., and J. M. P. Q. Delgado. 2003. Effect of fluid properties on dispersion in flow through packed beds. AIChE J. 49(8):1980–1985.

Delgado J. M. P. Q. 2006. A critical review of dispersion in packed beds. Heat Mass Transf. 42(4):279–310.

Ebach E. A., and R. R. White. 1958. Mixing of fluids flowing through beds of packed solids. AIChE J. 4(2):161–169.

Freeze R. A., and J. A. Cherry. 1979. Groundwater. Prentice-Hall, Englewood Cliffs, NJ.

Fried J. J., and M. A. Combarnous. 1971. Dispersion in porous media, Advances in Hydroscience. Academic Press, Inc., New York, NY, pp. 169–282.

Harleman D. R. F., and R. R. Rumer. 1963. Longitudinal and lateral dispersion in an isotropic porous medium. J. Fluid Mech. 16(3):385–394.

Hiby J. W. 1962. Longitudinal dispersion in single-phase liquid flow through ordered and random packings. *In*: Interaction Between Fluid and Particles. London IChemE. 312–325.

Hu Q. H., and M. L. Brusseau. 1994. The effect of solute size on diffusive-dispersive transport in porous media. J. Hydrol. 158(3–4):305–317.

Klotz D. 1973. Untersuchungen zur dispersion in porosen medien. Z. Deutsch. Geol. Ges. 124:523–533.

Liles A. W., and C. J. Geankoplis. 1960. Axial diffusion of liquids in packed beds and end effects. AIChE J. 6(4):591–595.

Matsubayashi U., L. P. Devkota, and F. Takagi. 1997. Characteristics of the dispersion coefficient in miscible displacement through a glass beads medium. J. Hydrol. 192(1–4):51–64.

Miller S. F., and C. J. King. 1966. Axial dispersion in liquid flow through packed beds. AIChE J. 12(4):767–773.

Miyauchi T., and T. Kikuchi. 1975. Axial dispersion in packed-beds. Chem. Eng. Sci. 30(3):343–348.

Padilla I. Y., T. C. J. Yeh, and M. H. Conklin. 1999. The effect of water content on solute transport in unsaturated porous media. Water Resour. Res. 35(11): 3303–3313.

Perkins T. K., and O. C. Johnston. 1963. A review of diffusion and dispersion in porous media. Soc. Petrol. Eng. J. 3(1):70–84.

Pfannkuch H. O. 1963. Contribution a l'étude des déplacement de fluids miscibles dans un milieu poreux. Rev. Inst. Franc. Pétrol. 18:215–219.

Poreh M. 1965. Dispersivity tensor in isotropic and axisymmetric mediums. J. Geophys. Res. 70(16):3909–3913.

Poulsen T. G., W. Suwarnarat, M. K. Hostrup, and P. N. V. Kalluri. 2008. Simple and rapid method for measuring gas dispersion in porous media: methodology and applications. Soil Sci. 173(3):169–174.

Pugliese L., T. G. Poulsen, and R. R. Andreasen. 2012. Relating gas dispersion in porous media to medium tortuosity and anisotropy ratio. Water Air Soil Pollut. 223(7):4101–4118.

Pugliese L., T. G. Poulsen, and R. R. Andreasen. 2013a. Biofilter media gas pressure loss as related to media particle size and particle shape. J. Environ. Eng. 139(12):1424–1431.

Pugliese L., T. G. Poulsen, and S. Straface. 2013b. Gas-solute dispersivity ratio in granular porous media as related to particle size distribution and particle shape. Water Air Soil Pollut. 224(9):1691.

Pugliese L., S. Straface, B. M. Trujillo, and T. G. Poulsen. 2013c. Relating non-equilibrium solute transport and porous media physical characteristics. Soil Sci. In Press.

Pugliese L., and T. G. Poulsen. 2013d. Linking gas and liquid pressure loss to particle size distribution and particle shape in granular filter materials. Water Air Soil Pollut. 225:1811.

Saffman P. G. 1960. Dispersion due to molecular diffusion and macroscopic mixing in flow through a network of capillaries. J. Fluid Mech. 7(2): 194–208.

Sahimi M., B. D. Hughes, L. E. Scriven, and H. T. Davis. 1986. Dispersion in flow through porous media—1. One-phase flow. Chem. Eng. Sci. 41(8): 2103–2122.

Scheidegger A. 1961. General theory of dispersion in porous media. J. Geophys. Res. 66(10):3273–3278.

Wadell H. 1935. Volume, shape and roundness of quartz particles. J. Geol. 43 (3):250–280.

Wilcox R. R. 1997. Introduction to robust estimation and hypothesis testing. Academic Press, San Diego, CA.

Paper VI

Water Air Soil Pollut (2012) 223:4101–4118
DOI 10.1007/s11270-012-1176-7

Relating Gas Dispersion in Porous Media to Medium Tortuosity and Anisotropy Ratio

Lorenzo Pugliese · Tjalfe G. Poulsen · Rune R. Andreasen

Received: 5 December 2011 / Accepted: 11 April 2012 / Published online: 6 May 2012

Abstract Gas dispersion in a set of three different porous materials with similar particle size, as a function of material tortuosity and anisotropy ratio, was investigated. The materials were packed with different spatial orientations of the individual particles so as to create media with different tortuosity and anisotropy ratios. Three different media (slate chips, wood chips, and pebbles) and four particle orientations have been used to generate a total of nine different porous media mimicking single porosity, dual porosity isotropic, anisotropic, aggregated, or granular materials. Resulting values of tortuosity and anisotropy ratio for each medium were determined via measurements of gas permeability and molecular gas diffusion coefficient. These values were then compared to measured values of gas dispersivity for each medium. The results showed that dispersivity is inversely proportional to tortuosity but directly proportional to anisotropy ratio and that the relations were approximately linear within the range of tortuosities and anisotropy ratios investigated. Wood chips (dual porosity material) yielded higher values of gas dispersivity compared to slate chips (single porosity material). A likely reason is in part the difference in pore structure between the materials and in part a difference in particle surface roughness (which was highest for wood chips) both of which affects dispersion.

Keywords Porous medium tortuosity · Anisotropy ratio · Particle shape · Particle orientation · Mechanical dispersion · Gas permeability

L. Pugliese (✉) · T. G. Poulsen · R. R. Andreasen
Department of Chemistry and Biotechnology,
Aalborg University,
Sohngaardsholmsvej 57,
9000 Aalborg, Denmark
e-mail: lp@bio.aau.dk

1 Introduction

Knowledge of gas transport in porous media and its dependency on media physical properties is essential for understanding and predicting for instance methane emissions from wetlands and landfills to the atmosphere, oxygen and carbon dioxide movement in passively aerated compost windrows, volatile contaminant migration at contaminated soil sites, transport and removal of gaseous contaminants in filters for air cleaning, and radon and volatile organic contaminant transport into buildings. Gas transport in porous media is generally governed by three mechanisms: (1) advection caused by gas pressure gradients within the medium, (2) molecular diffusion caused by gas concentration gradients, and (3) mechanical dispersion caused by spatial variations in the gas velocity and gas transport distances at the pore scale. Advection is in turn controlled by porous medium gas permeability (k_g), molecular diffusion is controlled by the molecular diffusion coefficient in the porous medium (D_{mol}), and mechanical dispersion is controlled by the gas dispersivity of the medium (α). Both k_g and D_{mol} depend strongly on

medium tortuosity (τ) and anisotropy ratio (ξ) for gas migration. While τ defines the transport distance through the porous medium (restricted by the pore system) in comparison to the Euclidean (shortest) distance, ξ quantifies the directional dependency of the porous medium transport properties.

The concept of tortuosity was first introduced by Carman (1939) who found that the microscopic flow path in soil was approximately $\sqrt{2}$ times longer than the thickness of the soil sample. Later it has been shown that τ is related to porous medium properties such as air-filled porosity, particle size distribution, and particle geometry (Prager 1960; Weissberg 1963; Boudreau 1996; Koponen et al. 1997; Moldrup et al. 2001; Nabovati and Sousa 2007; Matyka et al. 2008).

Van Brakel and Heertjes (1974) found that τ could be defined in terms of the average length of the diffusion path through the porous medium. As a result of this and similar findings (Boving and Grathwohl 2001; Weerts et al. 2001; Shen and Chen 2007), τ is now traditionally defined based on the ratio D_{mol}/D_{void} where D_{void} is the molecular diffusion coefficient in free air (Berner 1980; Boudreau 1996; Maerki et al. 2004). Although it is well known that both k_g and D_{mol} depends on medium structure (Kirkham et al. 1958; Millington and Quirk 1964; Schjønning 1989; Blackwell et al. 1990; Poulsen et al. 2001), relatively few investigations of the relation between τ and k_g have been published. The results that have been published, however, agree that k_g in general is inversely related to τ (Kallel et al. 2004; Shen and Chen 2007; Ghassemi and Pak 2011) although no specific relationships for predicting τ from k_g have been suggested. Dispersivity (α) has been shown to increase with travel distance through the porous medium (Gelhar et al. 1992; Schulze-Makuch and Cherkauer 1995; Schulze-Makuch 2005). Dispersion is a result of differences in fluid travel time (due to differences in travel distance and velocity) through the pore system of the porous medium. The wider the range of fluid travel times for a given porous system, the larger the value of α for that system. In larger scale systems, porous medium physical properties such as particle and pore size usually vary over a wider range than in small scale systems resulting in a wider range of fluid travel times and increasing values of α at larger scale. This is especially the case in natural systems such as rock and soil. Effects of scale on α are in general relatively well understood and models for predicting their relationship are available (Schulze-Makuch 2005). Gas dispersivity has specifically been shown to depend on particle size distribution and gas-filled porosity (Sharma and Poulsen 2009; 2010a, b) and it is therefore also almost certainly related to τ; however, no experimental investigations of the relationship have yet been published.

Anisotropy ratio (ξ), which is typically a result of particle, aggregate, or fracture orientation or due to depositional features such as layering, describes the directional dependence of porous medium properties (Hunt et al. 2006). Several publications demonstrating the dependency of ξ on porous medium physical properties such as particle/aggregate shape, particle/aggregate orientation, and particle size distribution are available. Existing studies of anisotropy indicate that in natural systems such as soils and rock, medium properties often differ vertically and horizontally while there is often no dependency between material properties and the specific direction in the horizontal plane. Examples are Chapuis and Gill (1989), Switzer and Kosson (2007), Bagarello et al. (2009), Rowshanzamir and Askari (2010), and Takeda et al. (2011). This means that although anisotropy in theory is considered a three-dimensional tensor, it is in reality often two dimensional. The reason is that in many soils and similar materials, ξ is strongly related to sedimentation, consolidation, and weathering processes (Terzaghi 1943; Marcus and Evenson 1961; Kenney 1963) which act in the vertical direction. For homogeneous materials, Wyllie and Rose (1950) found that ξ only depends on particle (or aggregate) shape and orientation. For sedimentary materials, including sedimentary rocks, the principal directions of anisotropy (the directions where porous medium properties exhibit their largest and smallest values) are the directions parallel and perpendicular to the bedding plane respectively (Chapuis and Gill 1989). In anisotropic materials, both k_g and D_{mol} have been observed to exhibit directional dependence (Terzaghi 1943; Masland 1957; Evans 1962; Basak and Anandakr 1970; Van Loon et al. 2004; Garcia-Gutierrez et al. 2006; Nakashima et al. 2008; Soler et al. 2008; Dorner and Horn 2009; Takeda et al. 2011). As a result of this, ξ is often determined based on measured values of permeability or molecular diffusion coefficient (in the air or water phase) taken in two different directions which are usually vertical and horizontal (Chapuis and Gill 1989; Switzer and Kosson 2007; Bagarello et al. 2009; Takeda et al. 2011).

In contrast, very little is known about the relationship between α and ξ in porous media. The main

reason is likely that experiments for characterizing this relationship are very time consuming to carry out. However, as α is related to porous media physical properties such as air-filled porosity, particle size distribution, and particle shape (Bear 1961; Nikolaevskii 1959; Scheidegger 1960; Greenkorn and Kessler 1969; Nunge and Gill 1969), α is likely also related to ξ. Guin et al. (1972) used a mathematical model to investigate dispersion in hypothetical isotropic and anisotropic media with cylindrical pores and found that the mechanical dispersion coefficient D_{mech} is influenced by ξ the reason being that the flow velocity is different in different directions. There is, however, to the knowledge of the authors no experimental documentation directly linking α and ξ for gas migration in porous media.

The objective of this paper was therefore to investigate if, and how strongly gas dispersivity (α) is related to tortuosity (τ), anisotropy ratio (ξ), and other porous medium properties, in anisotropic porous media aiming at identifying the significance of the correlation, and the similarity of the relationships between these and other parameters in different porous materials. The aim was to provide information about what parameters would be advantageous to use as basis for development of models for estimating α in porous media rather than developing specific models as this will require substantially more data from a much wider range of porous media than is possible to consider in this paper. As most natural systems have been observed to be two-dimensional anisotropic, such systems were also investigated here. The investigation was carried out considering three different porous materials: (1) slate chips (solid particles) representing a single porosity material of variable anisotropy ratio, (2) wood chips (porous particles) representing a dual porosity material of variable anisotropy ratio, and (3) pebbles, representing an isotropic, single porosity material (as a reference material). These three materials were chosen as they approximate both granular (slate chips and pebbles), aggregated (wood chips), and to some degree also fractured materials (wood and slate chips) depending on packing configuration. They also resemble many porous materials of both natural and man-made origin. A further reason for using the wood chips is that it is difficult to acquire especially dual porosity aggregates of traditional materials such as soil or sediments that are stable enough for packing and have an aggregate shape allowing for packing configurations with different tortuosity and anisotropy. It was further chosen not to include effects of system scale in the investigation as effects of scale on dispersivity are relatively well understood as discussed above. Gas transport experiments in the three materials were carried out using oxygen and nitrogen as tracer gases as these are inexpensive, readily available, easy to measure, and safe to use. The significance (strength) of the correlation and the similarity of the relationships between porous medium transport characteristics (including dispersivity) was assessed using statistical evaluation based on a non-parametric approach.

2 Theory

2.1 Advective Fluid Flow

Fluid flow through porous media at low flow velocities is generally described by Darcy's law which in one dimension is expressed as:

$$\frac{\Delta P}{L} = \frac{\mu}{k_{\mathrm{g}}} V \tag{1}$$

where ΔP is the pressure drop (M L^{-1} T^{-2}) across the sample, L is the distance (length of the sample) over which the pressure drop takes place (L), k_{g} is the gas permeability (L^2), μ is the dynamic viscosity of the fluid (M L^{-1} T^{-1}), and V is the superficial gas flow velocity (L T^{-1}). Equation (1) is only valid when inertial forces in the flow field are negligible (which is the case at low flow velocities). At higher flow velocities, when inertial forces are important, the relation between Q and ΔP becomes non-linear and is in such cases often described using the Forcheimer relationship (Forchheimer 1901):

$$\frac{\Delta P}{L} = \frac{\mu}{k_{\mathrm{g}}} V + \rho C V^2 \tag{2}$$

where ρ (M L^{-3}) is the gas density and C is a material specific constant (L).

2.2 Tracer Gas Transport

Transport of a tracer compound in porous media is traditionally described by the advection dispersion equation (ADE). For one-dimensional transport of a conservative tracer gas in a column containing a

homogeneous porous medium, under assumption of uniform flow and dispersion, in the presence of both a mobile and a stagnant (immobile) gas phase, the ADE is given as:

$$\frac{\partial C_m}{\partial t} = D_{tot}\frac{\partial^2 C_m}{\partial x^2} + u\frac{\partial C_m}{\partial x} + k(C_{im} - C_m) \quad (3)$$

where C_{im} and C_m are the tracer concentrations in the immobile and mobile gas phases (M L^{-3}), respectively. D_{tot} is the overall dispersion–diffusion coefficient (L^2 T^{-1}) which takes into account effects of mechanical dispersion, molecular diffusion, and gas mixing in the tubing leading the gas from the point of tracer introduction to the porous medium column, and from the column to the point of tracer breakthrough detection (Poulsen et al. 2008). u is the pore gas velocity (interstitial velocity) in the mobile gas phase (L T^{-1}), k is the tracer mass transfer coefficient (T^{-1}) for mass transfer between the mobile and immobile gas phases, and x and t are the space (L) and time (T) variables.

Assuming that transport by molecular diffusion in the immobile gas phase is negligible compared to the transport in the mobile gas phase when advective gas transport takes place, the immobile gas phase concentration is described as:

$$\frac{\partial C_{im}}{\partial t} = -\frac{\varepsilon_m}{\varepsilon_{im}}k(C_{im} - C_m) \quad (4)$$

where ε_m and ε_{im} are the mobile and immobile gas-filled porosities (L^3 L^{-3}) in the porous medium, respectively. In cases when no advective transport takes place, the entire gas phase is immobile, and molecular diffusion is the only transport mechanism. In this case, gas transport is described as:

$$\frac{\partial C_m}{\partial t} = D_{mol}\frac{\partial^2 C_m}{\partial x^2} \quad (5)$$

where D_{mol} is the molecular diffusion coefficient (L^2 T^{-1}). The immobile gas phase content and the gas pore velocity are calculated as:

$$\varepsilon_{im} = \varepsilon_{tot} - \varepsilon_m \quad (6)$$

$$u = -\frac{Q}{A\varepsilon_m} \quad (7)$$

where ε_{tot} is the total gas-filled porosity. In case of a medium without an immobile gas phase, the tracer transport process is described by Eqs. (3), (6), and (7) with k equal to zero and $\varepsilon_m = \varepsilon_{tot}$. The total gas-filled porosity (ε_{tot}) in a porous medium containing water is given as:

$$\varepsilon_{tot} = 1 - \frac{\rho_b}{\rho_s} - \omega\rho_b \quad (8)$$

where ρ_s is the solids density (M L^{-3}), ρ_b is the dry bulk density (M L^{-3}), and ω is the gravimetric water content (M M^{-1}). In a dual porosity medium consisting of porous particles, the inter-particle (external) porosity is given as:

$$\varepsilon_{ex} = 1 - \frac{\rho_b}{\rho_p} \quad (9)$$

where ρ_p is the dry particle density (M L^{-3}).

2.3 Transport Parameter Relations

The diffusion/dispersion coefficient D_{tot} can be expressed as:

$$D_{tot} = D_{mol} + D_{mech} + D_{mix} \quad (10)$$

where D_{mech} is the contribution by mechanical dispersion (L^2 T^{-1}) and D_{mix} is the contribution from gas mixing in the tubing leading to and from the column (L^2 T^{-1}). D_{mix} generally depends on the geometry of the experimental apparatus and can be minimized by reducing tracer travel distances outside the porous medium. While both D_{mol} and D_{mix} are constant, D_{mech} generally increases linearly with increasing pore gas velocity, except at very low gas flow velocities (Poulsen et al. 2008; Hamamoto et al. 2009; Hunt and Skinner 2010; Sharma and Poulsen 2010a). The reason is that dispersion is a result of differences in travel times for the gas molecules through the porous medium (Delgado 2006) such that a wider range of travel times results in larger values of α. At low velocities, flow mainly occur in the large and often less tortuous pores (having short travel times) while at higher velocities flow will also occur in the smaller and more tortuous pores (having long travel times). This means that as velocity increases the range of travel times for the gas molecules through the porous medium increases, thereby increasing mechanical dispersion. This mechanism is especially important in dual porous materials that often have a very wide range of pore sizes and pore tortuosities, resulting in a very wide distribution of travel times. Particle surface roughness is an additional factor affecting dispersion. Increased

surface roughness will cause increased turbulence in a gas flow passing across the surface. This will in turn cause increased mechanical mixing of the gas stream which results in increased dispersion. For one-dimensional transport, the mechanical dispersion coefficient can be expressed as:

$$D_{\mathrm{mech}} = u\alpha \tag{11}$$

where α is the tracer mechanical dispersivity in the mobile gas phase (L). At very low gas flow velocities, flow dispersion is negligible and the linear relation (Eq. (11)) does not hold (Delgado 2006).

The relationship between dispersivity and transport distance through the porous medium (scale) is often modeled using a power function type model as (Neumann 1990; Schulze-Makuch 2005):

$$\alpha = CL^{e} \tag{12}$$

where C ($L^{(1-e)}$) and e are material specific constants. This means that if α at a given L, together with C and e, for a given porous medium are known, values of α at any other L for that medium can be calculated. Past observations (Schulze-Makuch 2005) indicate that C is on the order of 0.2 $m^{(1-e)}$ while e varies between 0.5 and 1. The diffusion/dispersion coefficient can be defined by combining Eqs. (10) and (11) yields:

$$D_{\mathrm{tot}} = D_{\mathrm{mol}} + u\alpha + D_{\mathrm{mix}} \tag{13}$$

A plot of D_{tot} versus u or $D_{\mathrm{mol}} + D_{\mathrm{mech}}$ versus u should therefore yield a straight line with slope α (Poulsen et al. 2008) except at very low gas flow velocity.

In porous media, tortuosity (τ) expresses the ratio of the travel distance in a free gas volume (L) (in a straight line) to the effective travel distance (Le) through the tortuous pore system of the porous medium (Kozeny 1927):

$$\tau = \frac{L_{\mathrm{e}}}{L} \tag{14}$$

Tortuosity is, thus, a function of the pore system geometry and has been shown in numerous studies to control diffusive gas transport in porous media (Moldrup et al. 2001; Shen and Chen 2007; Zhaowen and Mingzhe 2010) according to the following expression:

$$D_{\mathrm{mol}} = \frac{\varepsilon_{\mathrm{tot}}}{\tau} D_{\mathrm{void}} \tag{15}$$

where D_{void} represent the molecular diffusion coefficient in a free gas volume ($L^2\ T^{-1}$). The quantity $\varepsilon_{\mathrm{tot}} D_{\mathrm{void}}$ in Eq. (15) actually represents the diffusion coefficient in a medium with total (diffusion accessible) gas filled porosity $\varepsilon_{\mathrm{tot}}$ and tortuosity τ=1. As D_{mol} is directly proportional to $\varepsilon_{\mathrm{tot}}$, D_{mol} in a dual porosity medium with a given $\varepsilon_{\mathrm{ex}}$ is larger than in a single porosity medium with the same $\varepsilon_{\mathrm{ex}}$.

In practice, τ is usually determined via measurements of D_{mol} and D_{void} in combination with Eq. (15); however, τ has also been proposed to be predicted based on gas-filled porosity and several expressions for predicting τ from either $\varepsilon_{\mathrm{tot}}$ or ε_{m} have been proposed (Comiti and Renaud 1989; Mauret and Renaud 1997; Barrande et al. 2007; Matyka et al. 2008; Pisani 2011). Most of these expressions, however, are not able to take into account the effect of porous medium particle or aggregate shape on tortuosity. Pisani (2011) proposed a simple geometrical approach to derive tortuosity from porosity that included a shape factor (σ) representing particle or aggregate shape:

$$\tau = \left[1 - \sigma(1 - \varepsilon_{\mathrm{tot}})\right]^{-1} \tag{16}$$

The shape factor is defined by:

$$\sigma = \frac{r\gamma}{V_{\mathrm{p}}} \tag{17}$$

where r (L) is an equivalent particle "radius", γ (L^2) is the particle surface area perpendicular to the direction of flow, and V_{p} (L^3) is the particle volume.

Traditionally the anisotropy ratio (ξ) in two-dimensional anisotropic systems has been defined as (Chapuis and Gill 1989; Switzer and Kosson 2007; Bagarello et al. 2009; Rowshanzamir and Askari 2010; Takeda et al. 2011):

$$\xi = \frac{Z_{\mathrm{parallel}}}{Z_{\mathrm{perpendicular}}} \tag{18}$$

where z is a porous medium transport property such as D_{mol} or k_{g} and subscripts parallel or perpendicular refers to the directions in which the property is measured compared to the direction of interest. For isotropic media, this means ξ=1. In practice, therefore, ξ in a porous medium is determined via measurements of D_{mol}, k_{g}, or other medium transport properties (such as hydraulic conductivity) in combination with Eq. (18).

2.4 Statistical Assessment of Parameter Relationships

When comparing slopes (S) and intercepts (I) of linear regression models, with either known constants or slopes and intercepts of other linear regression models to assess significant differences or similarities, a variety of statistical methods can be used. If a limited number of measurements are used in the regression, a non-parametric statistical test method such as percentile bootstrapping (Wilcox 1997) should be used to get reliable results. When assessing a regression model, the first step is to generate for instance B=1,000 artificial data sets having the same distribution and containing the same number (N) of data points as the set of original measurements used to develop the regression model. Each artificial data set is created by randomly drawing N data points one at a time (with replacement) from the original data set. For each of the B artificial data set, corresponding artificial values of the slope (S*) and intercept (I*) are calculated. The S* and I* values are then ranked from smallest to largest and 95 % confidence intervals for the true slope (S_t) and intercept (I_t) are calculated as:

$$S_{\psi B}{}^* \le S_t \le S_{(1-\psi)B}{}^*,\ \psi = 6 \cdot 10^{-5} N + 0.0102,\ N < 250,\ \psi = 0.025,\ N \ge 250 \tag{19a}$$

$$I_{0.025B}{}^* \le I_t \le S_{0.975B}{}^*,\ \text{for all}\, N \tag{19b}$$

where the subscripts refer to the rank of the relevant S* and I* values in the ranked lists. The statistical assessment is then carried out as follows: if a given constant (for instance zero) is located outside the confidence interval, S_t (or I_t) is significantly different from the constant at the 95 % confidence level. If the 95 % confidence intervals for two slopes or two intercepts do not overlap, the slopes or intercepts are significantly different at the 95 % confidence level. Further details of the statistical method can be found in Wilcox (1997).

3 Materials and Methods

3.1 Materials Used

Assessment of the relations between gas phase dispersivity (α), tortuosity (τ), and anisotropy ratio (ξ) in porous media were carried out using three different commercially available materials. The materials were (1) rounded pebbles (as an isotropic reference material), (2) wood chips made from fir (*Pinus sylvestris*), and (3) slate chips, all air dried for several weeks. Prior to measurements, all three materials were screened and all particles able to pass an 18-mm but retained by a 10-mm sieve (average overall particle diameter 14 mm) were selected for the experiments. This specific particle size range was selected as a trade-off between facilitating ease of packing, which had to be done manually, one particle at a time, and having a particle size that would still mimic relevant natural and man-made systems such as aggregated soils, weathered or fractured rock, and various biofilter and building materials. Both the slate and wood chips were roughly parallelepiped in shape, while the pebbles were more rounded (Fig. 1).

Particle length (L_1) was defined along the longest edge of each particle, the width (L_2) was defined at the widest point of each particle perpendicular to the direction of L_1, and the thickness (L_3) defined at the widest point of each particle perpendicular to the directions of both L_1 and L_2. For each of the three materials, 30 particles were selected randomly and L_1, L_2, and L_3 were measured (see Table 1).

3.2 Porous Media Preparation

Prior to measurements, each of the materials was packed into clear acrylic columns 15 cm in length and 14 cm inner diameter. This column size was chosen in order to avoid effects of preferential flow along the column walls, which may occur if column diameter is too small compared to the average particle diameter. Earlier measurements of gas dispersion indicate that effects of preferential flow is negligible if the mean particle diameter is less than or equal to about 8–10 % of the column diameter (Hiby 1962; Sharma and Poulsen 2010a, b). For slate and wood chips, three separate columns were packed each with a different particle orientation. The columns were packed with the L_1, L_2, or L_3 dimensions being oriented vertically (in the direction of flow), respectively, while the other two particle dimensions were oriented randomly in the horizontal plane. Thus, the anisotropy tensor of the materials in each of the three columns was two dimensional. The particle orientations were labeled A (particle dimension L_1 being vertical), B (dimension L_2 being vertical), and C (dimension L_3

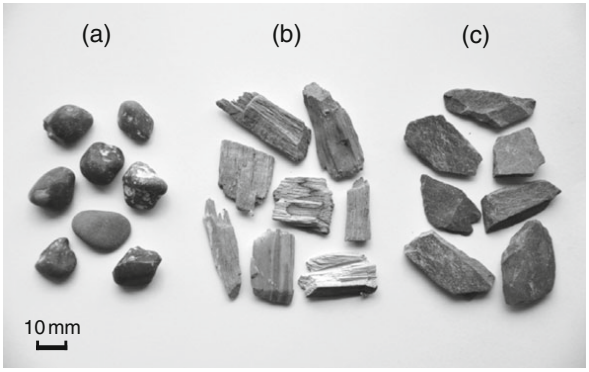

Fig. 1 Illustration of the porous materials used in the gas transport experiments: **a** pebbles, **b** wood chips, and **c** slate chips

being vertical). All columns were packed by manually placing each single particle, one at a time with the correct spatial orientation. Three additional columns were packed using slate chips, wood chips, and pebbles, respectively, with the particles randomly oriented in all three spatial dimensions (labeled D). These columns therefore contained isotropic media. For columns with particle orientation D, particles were not packed one at a time but instead poured into the column to achieve random orientation of particles in all spatial directions. All columns were packed taking care to achieve homogeneous packing and to reduce differences in bulk density between particle orientations A, B, C, and D for each material as much as possible. An illustration of the four particle orientations for the wood or slate chips is given in Fig. 2.

3.3 Porous Media Characterization

For all nine porous media (combinations of materials and particle orientations), dry bulk density (ρ_b), particle density (ρ_b), total air-filled porosity (ε_{tot}), and external air-filled porosity (ε_{ex}) were determined. Initially, the gravimetric water content (ω) of all three air dry materials was measured as the mass loss upon drying at 105°C for 24 h. For the single porosity media slate chips and pebbles, ε_{tot} (=ε_{ex}) was then determined by saturating the media with water and measuring the quantity of water needed for saturation. Dry bulk density (ρ_b) for the single porosity media was determined as the mass of the dry media when packed into the column divided by the column volume. Particle density ρ_p (=ρ_s) for the single porosity media was then determined using Eq. (8). This procedure could not be applied to wood chips as they in contrast to the two other materials expand upon wetting. Instead literature values for ρ_s and ρ_p (Usta 2003; Breyer et al. 2006) were used together with the measured ω in Eqs. (8) and (9) to calculate ε_{tot} and ε_{ex}. All measurements were carried out in duplicate.

3.4 Dispersion/Diffusion Coefficient Determination

Determination of (D_{mol} + D_{mech}) was carried out following the approach of Poulsen et al. (2008). The

Table 1 Physical properties of the three materials (slate chips, wood chips, and pebbles) used for assessing the relationships between gas dispersivity (α), tortuosity (τ), and anisotropy ratio (ξ)

Values in parentheses indicate one standard deviation

[a]Based on Usta (2003) and Breyer et al. (2006)

	Materials		
	Slate chips	Wood chips	Pebbles
L_1 (mm)	36 (7.4)	37 (7.1)	20 (2.9)
L_2 (mm)	19 (5.2)	12 (3.8)	15 (2.7)
L_3 (mm)	5.9 (1.8)	5.4 (2)	11 (2.1)
Solids density ρ_s (g cm^{-3})	2.75	1.50[a]	2.75
Dry particle density ρ_p (g cm^{-3})	2.75	0.57[a]	2.75
Air dry water content, w (g H_2O g solids^{-1})	0	0.095	0

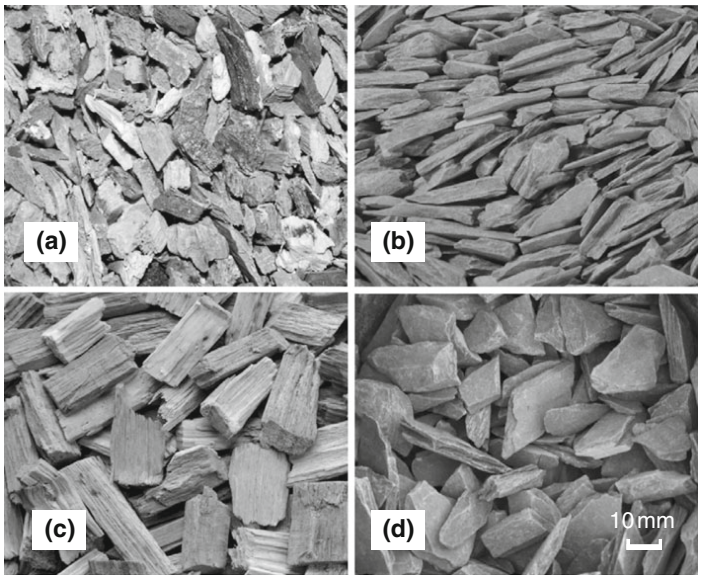

Fig. 2 Illustration of particle orientations used: **a** wood chips orientation A, **b** slate chips, orientation B, **c** wood chips, orientation (C), and **d** slate chips, orientation D

columns were fitted with polyethylene lids at both (inlet and outlet) ends, and sealed using rubber O-rings. Stainless steel mesh with 2-mm openings and 1-mm thickness were installed at the column in- and outlet to support the porous medium. At either end, there was a 10-mm distance between the steel mesh and the lid to allow an even gas distribution. The inlet (at the bottom) end of the column was connected to an air/nitrogen supply via a three-way valve and a precision ball flow meter (model F150; Porter Instruments, Inc., Hatfield, PA, USA) to control gas flow rate. The outlet lid was equipped with an oxygen sensor (KE-12 galvanic oxygen electrode; GS Yuasa Power Supply Ltd., Japan) with 5-s response time for determination of effluent oxygen concentrations. Readings from the oxygen sensor (sampling every 5 s) were recorded by a data logger (CR-1000; Campbell Scientific, Logan, UT, USA). Atmospheric air and nitrogen were used as tracer gases. Soft Teflon tubing with an inner diameter of 4 mm was used to connect the system components. Figure 3a shows a schematic of the experimental apparatus.

Columns were initially saturated with atmospheric air (78 $\%N_2$ and 21 $\%O_2$) and Q adjusted to the desired value. Once the effluent O_2 concentration was stable, the inlet gas was switched to N_2. Care was taken to make sure that Q remained constant during the switch. A constant flow of N_2 was maintained until the effluent O_2 concentration reached zero. At that point, the gas supply was switched back to atmospheric air and Q maintained until a stable O_2 concentration was once again observed. Oxygen and nitrogen breakthrough curves were measured at Q= 0.5, 1.0, 1.5, 2.0, and 2.3 l/min.

The measured breakthrough curves were fitted to Eqs. (3), (4), (5), (6), and (7) by optimizing the values of $D_{mol} + D_{mech}$, k, and ε_m. Initial and boundary conditions for the dispersion simulations were:

Initial condition

$$t = 0,\ x \geq 0 \quad C_m = C_{im} = 21\ \%O_2 \tag{20a}$$

Boundary conditions

$$0 < t \leq t_1,\ x = 0 \quad C_m = 21\ \%O_2 \tag{20b}$$

$$t_1 < t \leq t_2,\ x = 0 \quad C_m = 0\ \%O_2$$

$$t > t_2,\ x = 0 \quad C_m = 21\ \%O_2$$

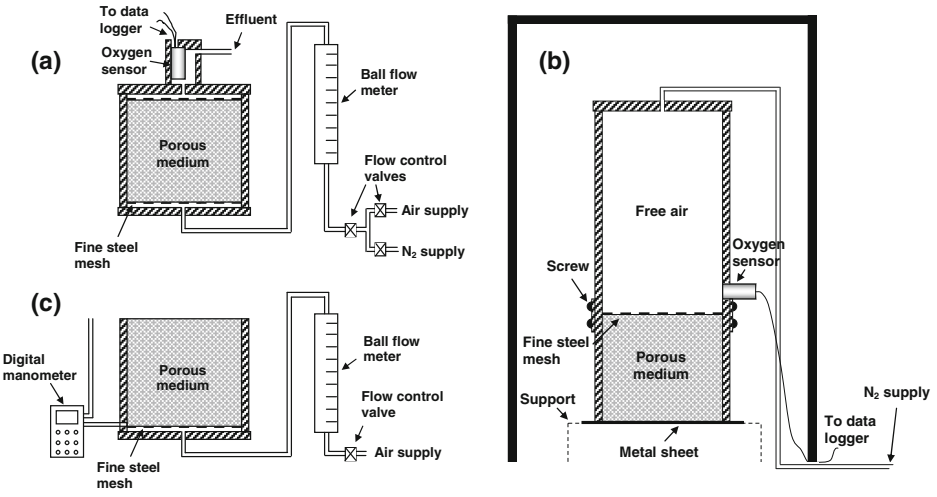

Fig. 3 Experimental set-up for measurements of **a** gas dispersion-diffusion coefficients (D_{tot}), **b** molecular gas diffusion coefficients (D_{mol}), and **c** gas permeability (kg)

where t_1 and t_2 are the points in time where the input gas was switched from air to N_2 and vice versa.

Overall, Eqs. (3), (4), and (5) were solved using an explicit finite difference based model, corrected for numerical dispersion. The solution included simulation of the gas transport in tubing, inlet and outlet chambers, and in the porous media such that effects of D_{mix} were corrected for as part of the modeling. Optimum values of $D_{mol} + D_{mech}$, k, and ε_m for all breakthrough curves were determined by minimizing the sum of squared errors (SSE) between measured and corresponding predicted effluent oxygen concentrations as:

$$\mathrm{SSE} = \sum\nolimits_{t=0,\max} \left[C_{m,\mathrm{measured}}(t) - C_{m,\mathrm{predicted}}(t)\right]^2 \tag{21}$$

where $C_{m,measured}(t)$ and $C_{m,predicted}(t)$ are the measured and predicted (by the model) effluent oxygen concentrations at time, t, respectively. The numerical solution of Eqs. (3), (4), and (5) and the minimization procedure were carried out using Microsoft Excel.

3.5 Molecular Diffusion Coefficient Determination

Determination of D_{mol} was carried out using the same columns as used in the $D_{mol} + D_{mech}$ determination. For D_{mol} determination, however, the top of each 15-cm column was connected to a 25-cm-long empty column of the same diameter fitted with a KE-12 oxygen electrode, closed with a polyethylene lid (with a gas inlet) at the top, and sealed using rubber O-rings. The inlet was connected to the same air/nitrogen supply assembly as used for the $D_{mol} + D_{mech}$ determination. Soft Teflon tubing with an inner diameter of 4 mm was used to connect system components.

The bottom of the 15-cm column was placed on a movable metal sheet such that the sheet could be slid out from under the column leaving it opened to the atmosphere without disturbing the gas inside the column. The connection between sheet and column was not tight but allowed gas to seep out of the column with the sheet in place as long as the pressure inside the column was higher than outside. This allowed for saturating the column with N_2 prior to letting air diffuse into the column. The reason for having the bottom end open to the atmosphere rather than the top was to prevent effects of gravity-driven gas flow as air is slightly heavier than N_2. During measurements the experimental apparatus was placed in a closed chamber to reduce air movement around the apparatus and prevent disturbance to the diffusion process. A schematic of the apparatus is given in Fig. 3b.

Columns were initially saturated with N_2 via the inlet. The flow was then switched off and the metal sheet immediately removed from below the column allowing air to diffuse back in. Gas diffusion values were then determined by fitting Eq. (5) to the measured breakthrough curves using D_{mol} as fitting parameter.

Initial and boundary conditions for the diffusion simulations were:

Initial condition

$$t = 0,\ x \geq 0 \quad C_m = 0 \tag{22a}$$

Boundary condition

$$t > 0,\ x = 0 \quad C_m = 20.9\ \%O_2 \tag{22b}$$

Optimum values of D_{mol} were determined using the same procedure as used for the $D_{mol} + D_{mech}$ determination with k=0 and $\varepsilon_m = \varepsilon_{tot}$.

3.6 Gas Permeability Determination

Determination of gas permeability (k_g) for all nine media was carried out using the same 15-cm column as used for the ($D_{mol} + D_{mech}$) and D_{mol} measurements. For the k_g measurements, however, the columns were fitted with a polyethylene lid and sealed with a rubber O-ring at the bottom. A stainless steel mesh with 2-mm openings and 1-mm thickness was installed to maintain a distance of 10 mm between the lid and the porous medium. The top of the column was kept open to the atmosphere while the bottom was connected to a supply of compressed atmospheric air via a valve and a precision ball flow meter (model P450; Porter Instruments). Soft Teflon tubing with an inner diameter of 4 mm was used to connect system components. Corresponding values of Q and ΔP across the columns were measured for Q ranging between 0 and 50 $l min^{-1}$ using an Alnor AXD 560 digital manometer connected to the bottom and the top of the column. This relatively wide range of Q was used to get a more reliable determination of the Q–ΔP relationship for each medium. A schematic of the experimental set-up is shown in Fig. 3c. Measured ΔP values were corrected for the pressure drop across the empty column with the metal mesh in place. As the Q–ΔP relationship was approximately linear for the range of Q values used in the D_{tot} measurements, values of k_g were calculated using Eq. (1).

4 Results and Discussion

4.1 Transport Parameters

Values of ε_{tot}, ε_{ex}, k_g, and D_{mol} are shown in Table 2 for all materials and particle orientations considered. Although care was taken to ensure similar values of ε_{ex} for each material across all particle orientations, orientations C and D exhibit slightly higher ε_{ex} values than do A and B for both slate and wood chips. The pebbles, having a more rounded shape, show a lower value of ε_{ex} than the wood and slate chips. Values of k_g were highest for particle orientation A and lowest for orientation C for both slate and wood chips (Table 2). Orientation D for both slate and wood chips as well as for pebbles showed intermediate k_g values. The reason is that for particle orientation A, part of the pore system consists of large continuous highly conductive pores (channels) parallel to the direction of flow offering reduced flow resistance while for orientation C these channels are not present resulting in increased flow resistance. Gas permeability is, thus, as expected directly controlled by particle orientation but less so by external porosity which is typically the case in homogeneous soils. Measurements of k_g can therefore be used to characterize the particle or aggregate orientation of aggregated or fractured porous media.

All measured O_2–N_2 breakthrough curves were generally well described by Eqs. (3), and (4) for u >0, and Eq. (5) for u=0 indicating that the experimental conditions used were adequate for measuring D_{mech} and D_{mol}.

Figure 4a shows selected measured and fitted O_2–N_2 breakthrough curves for Q=0.5 $l min^{-1}$ (advective, diffusive, and dispersive gas transport taking place) in wood chips. The four breakthrough curves in Fig. 4a, representing the four different particle orientations (A, B, C, and D), all exhibit the sigmoid shape expected for this type of experiment. This was also the case for the remaining measured breakthrough curves for both wood and slate chips at u >0.

In general, the breakthrough curves exhibited only a small amount of tailing indicating that the presence of an immobile gas phase to which gas exchange takes place was limited ($\varepsilon_{im} \approx 0$). This also means that no significant preferential flow along the column walls occurred as this will result in significant tailing of the breakthrough curves. Fitted values of ($D_{mol} + D_{mech}$) using Eq. (3) were highest for particle orientation A

Table 2 Gas transport parameters: total gas-filled porosity (ε_{tot}), external gas-filled porosity (ε_{ex}), gas permeability (k_g), molecular diffusion coefficient (D_{mol}), tortuosity (τ), anisotropy ratio based on k_g (ξ_k), anisotropy ratio based on D_{mol} (ξ_D), shape factor (σ), and gas dispersivity (α) for the nine combinations of material and particle orientation considered

Material	ε_{tot} ($cm^3\ cm^{-3}$)	ε_{ex} ($cm^3\ cm^{-3}$)	k_g ($10^{-5}\ cm^2$)	D_{mol} ($cm^2\ min^{-1}$)	τ	ξ_k	ξ_D	σ	α (cm)
Slate chips A	0.47	0.47	3.63	5.37	1.19	1.53	1.43	0.30	0.59
Slate chips B	0.47	0.47	3.21	4.70	1.37	0.89	0.87	0.51	0.43
Slate chips C	0.52	0.52	1.53	2.79	2.57	0.42	0.52	1.28	0.22
Slate chips D	0.52	0.52	2.61	3.87	1.84	1.00	1.00	0.95	0.47
Wood chips A	0.75[a]	0.53	5.91	7.74	1.33	1.59	1.78	1.01	1.01
Wood chips B	0.75[a]	0.53	4.50	5.13	2.01	0.76	0.66	2.03	0.79
Wood chips C	0.76[a]	0.54	2.96	3.54	2.95	0.50	0.46	2.78	0.65
Wood chips D	0.78[a]	0.58	3.75	4.36	2.45	1.00	1.00	2.69	0.88
Pebbles	0.41	0.41	2.55	3.61	1.57	1.00	1.00	0.62	0.65

[a] Based on Usta (2003) and Breyer et al. (2006)

and lowest for orientation C. This was the case for both wood and slate chips although wood chips generally exhibited higher (D_{mol} + D_{mech}) values, likely because the surface of the wood chips is somewhat rougher than slate chips (Fig. 1) resulting in increased turbulence and mixing and, thus, increased dispersion.

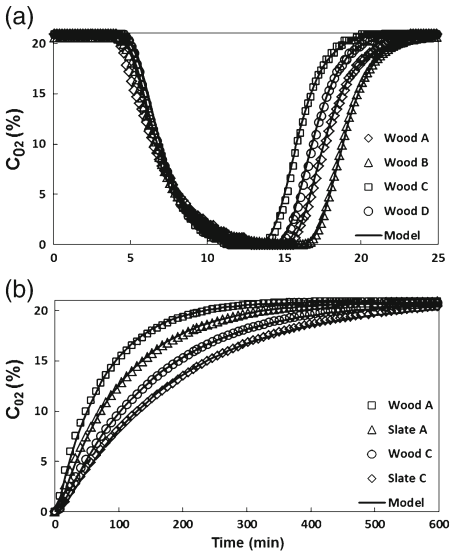

Fig. 4 Measured fitted values of effluent oxygen concentration for selected materials and particle orientations: **a** dispersion, diffusion, and advection at a gas flow rate (Q) of 0.5 $l min^{-1}$ and **b** molecular diffusion. *Symbols* indicate measured data and curves are model predictions

Selected measured and fitted O_2–N_2 breakthrough curves for u=0 (only molecular diffusion taking place) are shown in Fig. 4b for selected materials and particle orientations. All curves asymptotically approach the atmospheric oxygen concentration over time. Diffusion was faster in materials with particle orientation A for both slate and wood chips (the curve approach atmospheric oxygen concentration faster) and slowest in material with particle orientation C. This is a direct consequence of τ being lowest for particle orientation A and highest for orientation C. Wood chips exhibited higher D_{mol} values than slate chips for identical particle orientation (Table 2). Part of the reason is probably that the wood particles are porous allowing for diffusion through the particles meaning that the total gas-filled porosity and, thus, the cross-sectional area available for diffusion is larger in wood chips than in slate chips for the same particle orientation.

For each material and particle orientation, τ was determined using Eq. (15) together with the corresponding D_{mol} values and D_{void}=13.5 $cm^2\ min^{-1}$ (CRC 2011), while ξ was determined using Eq. (18) together with either corresponding values of k_g (labeled ξ_k) or D_{mol} (labeled ξ_D). For particle orientation A, $k_{g,perpendicular,A}$ was defined as the average of $k_{g,B}$ and $k_{g,C}$. A similar approach was used for the other particle orientations for both k_g and D_{mol}. Values of τ, ξ_k, ξ_D, and σ (calculated using Eq. (17)) are shown in Table 2.

Values of (D_{mol} + D_{mech}) were fitted for each material and particle orientation using Eq. (3) corrected for D_{mix}, and (4) together with the measured O_2–N_2 breakthrough curves measured for u >0 for all materials and particle orientations. These are shown in Fig. 5 as a function of u. In all cases, the (D_{mol} + D_{mech})–u relationships are approximately linear in accordance with Eqs. (11) and (13) except at low velocities (indicated by broken curve sections) where the slopes tend to decrease, as also discussed earlier, and intercept the y-axis at D_{mol}. D_{mol} ranges between 2.8 and 7.7 cm^2 min^{-1}, while D_{mech} ranges between approximately 3 and 26 cm^2 min^{-1} depending on medium and gas velocity (Fig. 5). In comparison, model simulations yielded D_{mix} values of about 0.5 cm^2 min^{-1}. For a selected u, wood chips exhibit higher values of (D_{mol} + D_{mech}) compared to slate chips and pebbles. As mentioned above, this could be because the surfaces of the wood chips are rougher than the slate chips and pebbles, and furthermore because this material is dual porous, which as discussed earlier can result in larger D_{mech}. Also, the wood chips have a much higher total porosity than slate chips (due to its high intra-particle porosity) which result in larger values of D_{mol} in accordance with Eq. (15). Linear regression lines were fitted to the (D_{mol} + D_{mech})–u data for u >0. The average regression coefficient (r^2) for all linear regression lines in Fig. 5 was 0.97. Dispersivity (α), represented by the slopes of the regression lines (Eq. (11)), were determined (Table 2). For both slate and wood chips, α was highest for particle orientation A and lowest for particle orientation C. For the pebbles, α was very close to the average dispersivity for all other materials and particle orientations combined (0.65 vs. 0.63 cm, respectively). The α value for pebbles also corresponds well with earlier measurements of α in gravel materials of similar particle size by Sharma and Poulsen (2010a, b) who observed α values of 0.3–0.9 cm. A summary of the data is given in Table 2.

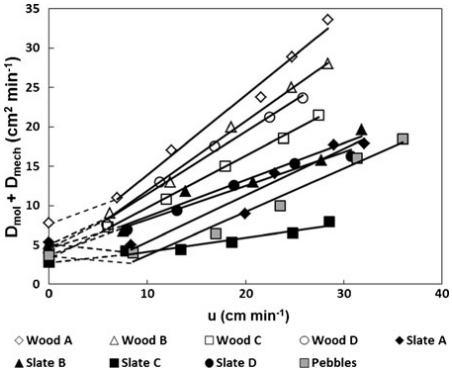

Fig. 5 Calculated values of (D_{mech} + D_{mol}) based on oxygen breakthrough curves, as a function of pore gas velocity (u), for all nine materials and particle orientations considered. Linear relationships represent best fit regression lines to all data for Q >0

4.2 Transport Parameter Relationships

The data in Table 2 indicate a direct proportionality between k_g, D_{mol}, and both ξ_D and ξ_k while σ is inversely related to ξ. This is to be expected as ξ and τ are dependent and that τ is defined based on the magnitude of D_{mol} (Eq. (15)) and are directly defined by the orientation of the particles relative to the direction of transport. It also means that in media consisting of non-spherical particles or aggregates, D_{mol} is strongly dependent on particle or aggregate orientation.

The D_{mol}–k_g, α–k_g, and α–D_{mol} relations are shown in Fig. 6 for all three materials and particle orientations. For both slate and wood chips, D_{mol} is proportional to k_g (Fig. 6a). From Table 2, it is seen that both k_g and D_{mol} for both wood and slate chips are independent of both ε_{tot} and ε_{ex} in contradiction to what is normally observed in isotropic media such as many soils (Poulsen et al. 2006, 2007; Moldrup et al. 2007; Hamamoto et al. 2011). This clearly shows that in anisotropic media both k_g and D_{mol} can depend on particle (or aggregate) orientation to a degree that can mask out effects of variations in gas-filled porosity. Dispersivity (α) is proportional to both k_g and D_{mol} for both wood and slate chips (Fig. 6b, c), which means that α also is strongly dependent on particle orientation. Thus, in anisotropic media it may be possible to predict α based on either D_{mol} or k_g, both of which are much easier to measure than α. It is noted that the k_g–D_{mol}, the k_g–α, and the D_{mol}–α relations in addition to particle orientation likely also depend on particle shape which should, thus, also be taken into account when developing prediction models.

Figure 7 shows α as a function of τ (Fig. 7a), σ (Fig. 7b), ξ_D (Fig. 7c), or ξ_k (Fig. 7d) for all materials and particle orientations. For both slate and wood chips, the relationships are approximately linear within the τ, σ, or ξ ranges investigated, such that α decreases linearly with increasing τ and σ, and increases linearly

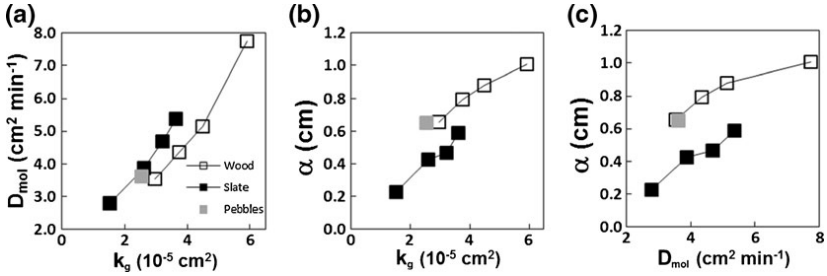

Fig. 6 Relationships between **a** D_{mol} and k_g, **b** dispersivity (α) and k_g, and **c** α and D_{mol} for all materials and particle orientations

with increasing ξ_D and ξ_k. In all four cases, the pebbles fall within the region spanned by the wood and slate chips. Although the α–ξ_k and the α–ξ_D relationships are different, they are both strong, indicating that when developing models for predicting α from ξ, both relationships could be used as a starting point. Seen from an economic and time consumption perspective, ξ_k can with advantage be used as k_g is much simpler and faster to measure than D_{mol}.

The reason why α increases with ξ is that dispersion is caused by differences in the amount of time it takes individual gas particles to pass through the porous medium. Transport time for a given gas particle in turn is controlled by the tortuosity of the individual pore (or succession of connected pores) through which it passes, the average velocity at which it moves through the pore, and the amount of turbulence and mixing within each pore. This means that α in a porous medium depends on both the distribution of tortuosities of the gas conducting pores and the distribution of gas velocities within these pores. The wider the range of transport times (the wider the range of gas

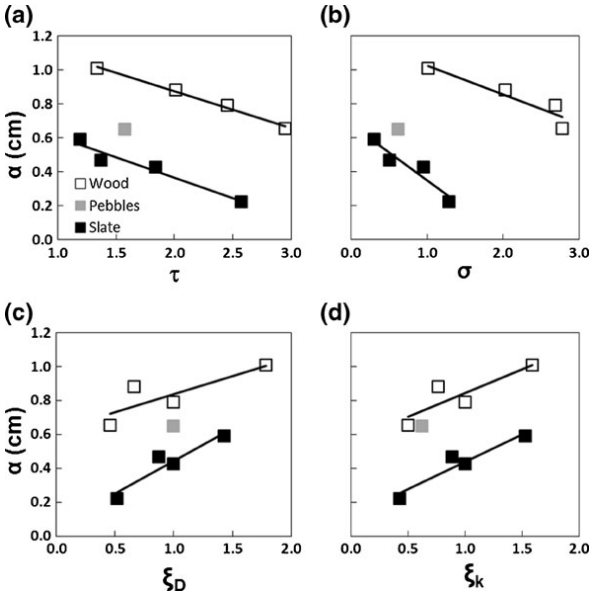

Fig. 7 Calculated values of α as a function of **a** tortuosity (τ), **b** shape factor (σ), **c** anisotropy ratio based on D_{mol} (ξ_D), and **d** anisotropy ratio based on k_g (ξ_k)

conducting pore tortuosities and average pore gas flow velocities) the larger the value of α. In anisotropic media, the widest range in both pore tortuosity and gas pore velocity occur in the spatial direction corresponding to the largest average value of ξ (as defined by Eq. (18)). Consider for instance a medium consisting of layers of coarse and fine materials where the ranges of both individual pore tortuosity and pore gas flow velocity will be larger if gas flow occurs parallel to the layers (where different gas particles pass through different materials) compared to flow perpendicular to the layers (where all gas particles pass through the same materials).

4.3 Statistical Significance of Parameter Relationships

To evaluate whether the α–τ, α–σ, α–ξ_D, α–ξ_k are statistically significant, it was tested whether the slopes (S) of the best fit linear regression lines to the data were significantly different from zero. To evaluate whether the relationships were significantly different for slate and wood chips, it was tested whether the slopes (S) and the intercepts (I) of the best fit linear regression lines for the individual relationships for these two materials were significantly different. Because each data set contains only four values, the non-parametric bootstrapping method (Wilcox 1997) was used. Values of S and I for the α–τ, α–σ, α–ξ_D, α–ξ_k best fit linear regression lines for both wood and slate chips are given in Table 3. In addition, the levels of statistical significance in terms of the p values for test of $S_{\text{wood}} \neq 0$, $S_{\text{slate}} \neq 0$, $S_{\text{wood}} \neq S_{\text{slate}}$, and $I_{\text{wood}} \neq I_{\text{slate}}$ for the α–τ, α–σ, α–ξ_D, and α–ξ_k relationships are given in Table 3. A specific value of p (%) means that the test result is significant at the $(100-p)$ % level.

For all the four relationships in Fig. 6, it is seen from Table 3 that all four slopes are significantly different from zero, confirming that there is a strong and significant relationship between α and τ, σ and ξ and that these parameters with advantage can be used as a starting point for development of models for predicting α. For each relationship slopes for wood and slate chips are not significantly different at the 95 % level (p>2.5 %) but the intercepts are which means that there is a significant difference between the relationships for the two media. As the main differences between the wood and slate chips are associated with particle surface roughness and intra-particle

Table 3 Slopes (S) and intercepts (I) for best fit linear regression lines, and p values: $p(|S|>0)$, $p(S_{\text{wood}} \neq S_{\text{slate}})$, and $p(I_{\text{wood}} \neq I_{\text{slate}})$ for the α–τ, α–σ, α–ξ_D, α–ξ_k, ξ_D–ξ_k, τ–ξ_k, τ–ξ_D, τ–σ, σ–ξ_k, *and* σ–ξ_D *relationships in Figs. 7 and 8*

Relationship	Material	S	I	$p(\|S\|>0)$ %	$p(S_{\text{wood}} \neq S_{\text{slate}})$ %	$p(I_{\text{wood}} \neq I_{\text{slate}})$ %
α–τ	Wood	−0.22	1.31	<0.1*	36	<0.1**
	Slate	−0.24	0.84	<0.1*		
α–σ	Wood	−0.17	1.20	<0.1*	12	<0.1**
	Slate	−0.33	0.67	<0.1*		
α–ξ_D	Wood	0.21	0.62	<0.1*	16	0.7**
	Slate	0.38	0.06	<0.1*		
α–ξ_K	Wood	0.28	0.56	0.3*	39	1.2**
	Slate	0.32	0.12	<0.1*		
ξ_D–ξ_K	Wood	1.25	−0.23	<0.1*	5.5	<0.1**
	Slate	0.83	0.16	<0.1*		
τ–ξ_k	Wood	−1.30	3.44	<0.1*	48	28
	Slate	−1.18	2.87	<0.1*		
τ–ξ_D	Wood	−1.00	3.17	<0.1*	35	48
	Slate	−1.39	3.07	2.4*		
τ–σ	Wood	0.81	0.47	<0.1*	18	23
	Slate	1.36	0.71	<0.1*		
σ–ξ_k	Wood	−1.48	3.55	12	48	28
	Slate	−0.84	1.56	<0.1*		
σ–ξ_D	Wood	−1.17	3.27	15	49	3.6
	Slate	−0.98	1.70	<0.1*		

*Significantly larger than zero at the 95 % confidence level, **significantly different at the 95 % confidence level

(internal) porosity, these two parameters are, as also mentioned earlier, the likely reason for the difference. This means that even if different materials have similar particle shape, size, and orientation, their α values may still be different depending on particle surface properties and particle internal porosity. On the other hand, because the relationship between α and system scale (transport distance) is a monotonously increasing function (Eq. (12)), the nature (correlation strength, differences, and similarities) of the relationships between α and other porous medium properties (such as τ, σ, ξ_D, and ξ_k) is most likely independent of scale.

Figure 8 shows the ξ_D–ξ_k, τ–ξ_k, τ–ξ_D, τ–σ, σ–ξ_k, and σ–ξ_D relationships for all three materials. Corresponding p values for test of $|S|>0$, $S_{\text{wood}} \neq S_{\text{slate}}$, and $I_{\text{wood}} \neq I_{\text{slate}}$ are given in Table 3. While the slopes of the two ξ_D–ξ_k relationships in Fig. 8a are not significantly different, their intercepts are (Table 3). This suggests that values of ξ based on either k_g or D_{mol} cannot be assumed equal for high or low values of ξ and for different materials. The slopes, exhibiting positive values, are significantly larger than zero (Table 3) indicating strong relationships and suggesting a possibility for predicting ξ_k from ξ_D or vice versa. Tortuosity decreases with increasing ξ_k and ξ_D (Fig. 8b, c) with slopes significantly smaller than zero, but neither S nor I for wood and slate chips are significantly different (Table 3). The high p values actually suggest that S and I values for the two materials may be assumed equal although more data are needed to verify if this is the case. Again, this shows that τ and ξ are strongly related and suggests the possibility for predicting τ from ξ or vice versa in anisotropic materials. Tortuosity increases with increasing σ for both wood and slate chips (Fig. 8d), but although S values are significantly larger than zero, neither slopes nor intercepts are significantly different between the two materials. The reason for the lack of difference is likely that the materials used here have similar particle shape, particle size, and external porosity. It is, thus, likely that materials with different particle size and shape will exhibit different relationships. The data, however, also suggests that in materials

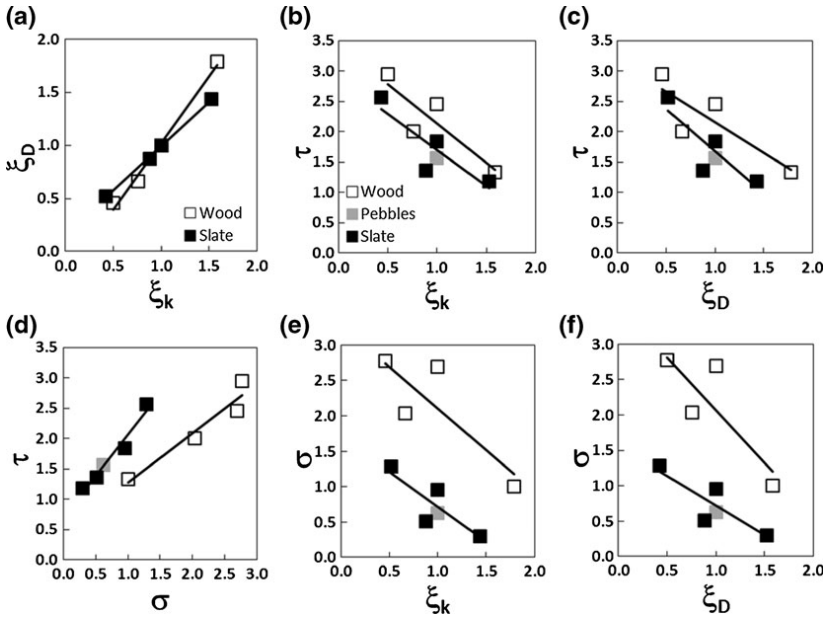

Fig. 8 Relationships between **a** ξ_D and ξ_k, **b** τ and ξ_k, **c** τ and ξ_D, **d** τ and σ, **e** σ and ξ_k, and **f** σ and ξ_D for all materials and particle orientations

of similar particle shape, particle size, and external porosity, the quantity of internal porosity does not affect the relationships.

For both slate and wood chips, σ is inversely proportional to ξ (Fig. 8e, f) as was also the case for τ (a result of the relation between τ and σ given by Eq. (16)). For the same ξ, wood chips exhibit larger values of σ although the data in Table 3 shows that the difference is not statistically significant. In fact, the data suggests that the slopes of the relationships may be identical.

5 Conclusion

Gas permeability (k_g), molecular gas diffusion coefficient (D_{mol}), gas dispersivity (α), porous medium tortuosity (τ), anisotropy ratio (ξ), and particle shape factor (σ) were measured in three different porous media with similar particle size (slate chips, representing a single porosity, anisotropic material, wood chips, representing a dual porosity, anisotropic material, and pebbles, representing a single porosity, isotropic medium). Different levels of these parameters were achieved by packing the materials with different spatial orientation of the particles relative to the direction of transport. A total of nine combinations of material and particle orientation were considered.

For both slate and wood chips, α was directly proportional and linearly related to k_g, D_{mol}, and ξ but inversely proportional (but still linearly related) to τ and σ. The reason for the direct proportionality with ξ is likely that for large ξ, the range of travel path lengths and travel velocities experienced by individual gas molecules is wider than for small ξ. A wide range of travel lengths and travel velocities will result in increased dispersion and thus increased dispersivity. As k_g, D_{mol}, τ, and σ are all governed by ξ, they will of course also be related to α. The direct proportionality between α and k_g, D_{mol}, implies that α may be predicted from either k_g *or* D_{mol}. This is advantageous as both D_{mol} and k_g are significantly easier and simpler to measure than α (this is especially the case for k_g). To develop expressions for such predictions, however, many more measurements of α across a significantly wider range of isotropic and anisotropic media are required; however, this is beyond the scope of this paper. The results presented here in terms of significance of correlation and similarities of the porous media parameter relationships on the other hand are very likely general across different system scales and media types. Thus, the results can very likely be used as a starting point for model development across different media and system scales.

Wood chips generally exhibit higher values of α for identical values of k_g, D_{mol}, τ, ξ, or σ. As particle size and particle shape was similar for the two materials, this difference could be explained by the somewhat rougher surface of the wood chips compared to slate chips, resulting in increased gas turbulence and mixing which results in increased dispersion. This means that in fractured or aggregated media, not only the aggregate shape and orientation but also the roughness of the aggregate surfaces controls dispersion. Values of ξ determined based on either k_g or D_{mol} were similar for wood and slate chips at the same particle orientation although a statistical test of the values indicated that they could not be assumed identical. This means that although ξ can be determined based on either k_g (ξ_k) or D_{mol} (ξ_D), resulting ξ values are not necessarily the same. Whether the directional dependence α as a result of anisotropy is best described by ξ_k or ξ_D is difficult to assess directly based on the data presented here. It could be argued that D_{mol} can be determined with less uncertainty compared to k_g which is more variable and thus ξ_D should be used. On the other hand, as k_g is much faster to measure, the use of ξ_k offers significant time savings. For a more firm conclusion, more data from a larger range of materials than used here are required. Tortuosity and anisotropy ratio were inversely, linearly related and the τ–ξ relationships were not significantly different between materials, likely because the materials used here had similar particle size, particle shape, and external porosity. It is very likely that relationships will differ between materials with different particle size, shape, or external porosity.

References

Bagarello, V., Sferlazza, S., & Sgroi, A. (2009). Testing laboratory methods to determine the anisotropy of saturated conductivity in a sandy-loam soil. *Geoderma, 154*, 52–58.

Barrande, M., Bouchet, R., & Denoyel, R. (2007). Tortuosity of porous particles. *Analytical Chemistry, 79*, 9115–9121.

Basak, P., & Anandakr, M. (1970). Depth dependent hydraulic conductivity. *Journal of Soil Science, 109*, 351–355.

Bear, J. (1961). On the tensor form of dispersion. *Journal of Geophysical Research, 66*, 1185–1197.

Berner, R. A. (1980). *Early diagenesis: a theoretical approach*. Princeton: Princeton University Press.

Blackwell, P. S., Ringrose-Voase, A. J., Jayawardane, N. S., Olsson, K. A., McKenzie, D. C., & Mason, W. K. (1990). The use of air-filled porosity and intrinsic permeability to characterize macropore structure and saturated hydraulic conductivity of clay soils. *Journal of Soil Science, 41*, 215–228.

Boudreau, B. P. (1996). The diffusive tortuosity of fine-grained unlithified sediments. *Geochimica et Cosmochimica Acta, 60*, 3139–3142.

Boving, T. B., & Grathwohl, P. (2001). Tracer diffusion coefficients in sedimentary rocks: correlation to porosity and hydraulic conductivity. *Journal of Contaminant Hydrology, 53*, 85–100.

Breyer, D., Fridley, K., Pollock, D., & Cobeen, K. (2006). *Design of wood structure—ASD/LRFD*. New York: McGraw-Hill.

Carman, P. C. (1939). Permeability of saturated sands, soils and clays. *Journal of Agricultural Science, 29*, 262–273.

Chapuis, R. P., & Gill, D. E. (1989). Hydraulic anisotropy of homogeneous soils and rock: influence of the densification process. *Engineering Geology, 39*, 75–86.

Comiti, J., & Renaud, M. (1989). A new model for determining mean structure parameters of fixed-beds from pressure-drop measurements—application to beds packed with parallelepipedal particles. *Chemical Engineering Science, 44*, 1539–1545.

CRC Handbook of Chemistry and Physics (92nd edition), 2011, Boca Raton: CRC.

Dorner, J., & Horn, R. (2009). Direction-dependent behavior of hydraulic and mechanical properties in structured soil under conventional and conservation tillage. *Soil and Tillage Research, 102*, 225–232.

Delgado, J. M. P. Q. (2006). A critical review of dispersion in packed beds. *Heat and Mass Transfer, 42*, 270–310.

Evans, H. E. (1962). A note on the average coefficient of permeability for a stratified soil mass. *Geotechnique, 12*, 145–146.

Forchheimer, P. H. (1901). Wasserbewegung durch boden. *Zeitschrift ver deutscher ingenieure, 50*, 1782–1788 (in German).

Garcia-Gutierrez, M., Cormenzana, J. L., Missana, T., Mingarro, M., & Martin, P. L. (2006). Large-scale laboratory diffusion experiments in clay rocks. *Physics and Chemistry of the Earth, 31*, 523–530.

Gelhar, L. V., Welty, C., & Rehfeldt, K. R. (1992). A critical review of data on field-scale dispersion in aquifers. *Water Resources Research, 28*, 1955–1974.

Ghassemi, A., & Pak, A. (2011). Pore scale study of permeability and tortuosity for flow through particulate media using Lattice Boltzmann method. *International Journal for Numerical and Analytical Methods in Geomechanics, 35*, 886–901.

Greenkorn, R. A., & Kessler, D. P. (1969). Flow through porous media symposium—dispersion in heterogeneous nonuniform anisotropic porous media. *Industrial and Engineering Chemistry, 61*, 14–32.

Guin, J. A., Kessler, D. P., & Greenkorn, R. A. (1972). Dispersion tensor in anisotropic porous media. *Industrial & Engineering Chemistry Fundamentals, 11*, 477–482.

Hamamoto, S., Moldrup, P., Kawamoto, K., Komatsu, T., & Rolston, D. E. (2009). Unified measurement system for the gas dispersion coefficient, air permeability and gas diffusion coefficient in variably saturated soil. *Soil Science Society of America Journal, 73*, 1921–1930.

Hamamoto, S., Moldrup, P., Kawamoto, K., Wickramarachchi, P. N., Nagamori, M., & Komatsu, T. (2011). Extreme compaction effects on gas transport parameters and estimated climate gas exchange for a landfill final cover soil. *Journal of Geotechnical and Geoenvironmental Engineering, 137*, 653–662.

Hiby, J.W. (1962). Longitudinal dispersion in single-phase liquid flow through ordered and random packings. *Interaction Between Fluid & Particles (London Institution of Chemical Engineers),* 312–325

Hunt, A. G., Blank, L. A., & Skinner, T. E. (2006). Distribution of hydraulic conductivity in single scale anisotropy. *Philosophical Magazine, 86*, 2407–2428.

Hunt, A. G., & Skinner, T. E. (2010). Predicting dispersion in porous media. *Complexity, 16*, 43–55.

Kallel, A., Tanaka, N., & Matsuto, T. (2004). Gas permeability and tortuosity for packed layers of processed municipal solid wastes and incinerator residue. *Waste Management and Research, 22*, 186–194.

Kenney, T. C. (1963). Permeability ratio of repeatedly layered soils. *Geotechnique, 13*, 325–333.

Kirkham, D., De Boodt, M., De Leenheer, L. (1958). Air permeability at the field capacity as related to soil structure and yields. *Proceedings of the International Symposium on Soil Structure*, 377-391.

Koponen, A., Kataja, M., & Timonen, J. (1997). Permeability and effective porosity of porous media. *Physical Review, E56*, 3319–3325.

Kozeny, J. (1927). Uber kapillare leitung des wassers im boden. *Sitzungsberichte der akadämie der wissenschaften in wien abteilung IIa, 136*, 271–301 (in German).

Maerki, M., Wehrli, B., Dinkel, C., & Muller, B. (2004). The influence of tortuosity on molecular diffusion in freshwater sediments of high porosity. *Geochimica et Cosmochimica Acta, 68*, 1519–1528.

Marcus, H., Evenson, D.E. (1961). Directional permeability in anisotropic porous media. *Water Resources Center Contribution* 31.

Masland, M. (1957). Soil anisotropy and land drainage. In J. N. Luthin (Ed.), *Drainage of agricultural lands* (pp. 216–285). Madison: American Society of Agronomy.

Matyka, M., Khalili, A., & Koza, Z. (2008). Tortuosity–porosity relation in porous media flow. *Physical Review E, 78*, 026306.

Mauret, E., & Renaud, M. (1997). Transport phenomena in multi-particle system. Limits of applicability of capillary model in high voidage beds—application to fixed beds of fibers and fluidized beds of spheres. *Chemical Engineering Science, 52*, 1807–1817.

Millington, R. J., & Quirk, J. M. (1964). Formation factor and permeability equations. *Nature, 202*, 143–145.

Moldrup, P., Olesen, T., Komatsu, T., Schjonning, P., & Rolston, D. E. (2001). Tortuosity, diffusivity, and permeability in the soil liquid and gaseous phases. *Soil Science Society of America Journal, 65*, 613–623.

Moldrup, P., Olesen, T., Blendstrup, H., Komatsu, T., de Jonge, L. W., & Rolston, D. E. (2007). Predictive–descriptive

models for gas and solute diffusion coefficients in variably saturated porous media coupled to pore-size distribution: IV. Solute diffusivity and the liquid phase impedance factor. *Soil Science, 172*, 741–750.

Nabovati, A., & Sousa, A. C. M. (2007). Fluid flow simulation in random porous media at pore level using the Lattice Boltzmann Method. *Journal of Engineering Science and Technology, 2*, 226–237.

Nakashima, Y., Kamiya, S., & Nakano, T. (2008). Diffusion ellipsoids of anisotropic porous rocks calculated by X-ray computed tomography-based random walk simulations. *Water Resource Research, 44*, W12435.

Neumann, S. P. (1990). Universal scaling of hydraulic conductivities and dispersivities in geological media. *Water Resources Research, 26*, 1749–1758.

Nikolaevskii, V. N. (1959). Convective diffusion in porous media. *Journal of Applied Mathematics and Mechanics, 23*, 1042–1050.

Nunge, R. J., & Gill, W. N. (1969). Flow through porous media symposium—mechanisms affecting dispersion and miscible displacement. *Industrial and Engineering Chemistry, 61*, 33–49.

Pisani, L. (2011). Simple expression for the tortuosity of porous media. *Transport in Porous Media, 88*, 193–203.

Poulsen, T. G., Iversen, B. V., Yamaguchi, T., Moldrup, P., & Schjønning, P. (2001). Spatial and temporal dynamics of air permeability in a constructed, agricultural field. *Soil Science, 166*, 153–162.

Poulsen, T., Moldrup, P., Yoshikawa, S., & Komatsu, T. (2006). Bimodal probability law model for unified description of water retention, air and water permeability, and gas diffusivity in variably saturated soil. *Vadose Zone Journal, 5*, 1119–1128.

Poulsen, T., Moldrup, G., Thorbjorn, A., & Schjonning, P. (2007). Predicting air permeability in undisturbed, subsurface sandy soils from air-filled porosity. *Journal of Environmental Engineering—ASCE, 133*, 995–1001.

Poulsen, T. G., Suwarnarat, W., Hostrup, M. K., & Kalluri, P. N. V. (2008). Simple and rapid method for measuring gas dispersion in porous media: methodology and applications. *Soil Science, 173*, 169–174.

Prager, S. (1960). Diffusion in inhomogeneous media. *Journal of Chemical Physics, 33*, 122–127.

Rowshanzamir, M. A., & Askari, A. M. (2010). An investigation on the strength anisotropy of compacted clays. *Applied Clay Science, 50*, 520–524.

Scheidegger, A. E. (1960). *The physics of flow through porous media* (pp. 26–30). University of Toronto Press: Toronto.

Schjønning, P. (1989). Long-term reduced cultivation. Soil pore characteristics as shown by gas diffusivities and permeabilities and air-filled porosities. *Soil and Tillage Research., 15*, 91–103.

Schulze-Makuch, D., & Cherkauer, D. S. (1995). Facies dependent scale behaviour of hydraulic conductivity and longitudinal dispersivity. *Groundwater Quality: Remediation and Protection, 225*, 157–164.

Schulze-Makuch, D. (2005). Longitudinal dispersivity data and implications for scaling behavior. *Ground Water, 43*, 443–456.

Sharma, P., & Poulsen, T. G. (2009). Gas phase dispersion in compost as a function of different water contents and air flow rates. *Journal of Contaminant Hydrology, 107*, 101–107.

Sharma, P., & Poulsen, T. G. (2010a). Gas dispersion and immobile gas volume in solid and porous particle biofilter materials at low air flow velocities. *Journal of the Air and Waste Management Association, 60*, 830–837.

Sharma, P., & Poulsen, T. G. (2010b). Gas dispersion and immobile gas content in granular porous media: effect of particle size nonuniformity. *Soil Science, 175*, 426–431.

Shen, L., & Chen, Z. X. (2007). Critical review of the impact of tortuosity on diffusion. *Chemical Engineering Science, 62*, 3748–3755.

Soler, J. M., Samper, J., Yllera, A., Hernandez, A., Quejido, A., Fernandez, M., Yang, C., Naves, A., Hernand, P., & Wersine, P. (2008). The DI-B in situ diffusion experiment at Mont Terri: results and modeling. *Physics and Chemistry of the Earth, 33*, S196–S207.

Switzer, C., & Kosson, D. S. (2007). Evaluation of air permeability in layered unsaturated materials. *Journal of Contaminant Hydrology, 90*, 125–145.

Takeda, M., Hiratsuka, T., Ito, K., & Finsterle, S. (2011). An axisymmetric diffusion experiment for the determination of diffusion and sorption coefficients of rock samples. *Journal of Contaminant Hydrology, 123*, 114–129.

Terzaghi, K. (1943). *Theoretical soil mechanics*. New York: Wiley.

Usta, Ü. (2003). Comparative study of wood density by specific amount of void volume. *Turkish Journal of Agriculture and Forestry, 27*, 1–6.

Van Brakel, J., & Heertjes, P. M. (1974). Analysis of diffusion in macroporous media in terms of a porosity, a tortuosity and a constrictivity factor. *International Journal of Heat and Mass Transfer, 17*, 1093–1103.

Van Loon, L. R., Wersin, J. M., Soler, J. M., Eikenberg, J., Gimmi, T., Hernan, P., Dewonck, S., & Savoye, S. (2004). In-situ diffusion of HTO, $^{22}Na^{+}$, Cs^{+} and I^{-} in Opalinus clay at the Mont Terri underground rock laboratory. *Radiochimica Acta, 92*, 757–763.

Weerts, A. H., Kandhai, D., Bouten, W., & Sloot, P. M. A. (2001). Tortuosity of an unsaturated sandy soil estimated using gas diffusion and bulk soil electrical conductivity. *Soil Science Society of America Journal, 65*, 1577–1584.

Weissberg, H. L. (1963). Effective diffusion coefficients in porous media. *Journal of Applied Physics, 34*, 2636–2639.

Wilcox, R. R. (1997). *Introduction to robust estimation and hypothesis testing*. San Diego: Academic.

Wyllie, M. R. J., & Rose, W. D. (1950). Application of the Kozeny equation to consolidated porous media. *Nature, 165*, 972.

Zhaowen, L., & Mingzhe, D. (2010). Experimental study of diffusive tortuosity of liquid-saturated consolidated porous media. *Industrial Engineering Chemistry Research, 49*, 6231–6237.

Co-authored paper

Chemical Engineering Journal 221 (2013) 292–299

Contents lists available at SciVerse ScienceDirect

Chemical Engineering Journal

journal homepage: www.elsevier.com/locate/cej

Water flow exchange characteristics in coarse granular filter media

Rune R. Andreasen *, Lorenzo Pugliese, Tjalfe G. Poulsen

Department of Biotechnology, Chemistry and Environmental Engineering, Aalborg University, Sohngaardsholmsvej 57, DK-9000, Denmark

HIGHLIGHTS

- We measured the inter media water flow exchange distribution.
- Elution rate decreases at increasing dynamic holdup.
- High surface area and wide particle size distribution cause low elution rate.
- High irrigation velocity cause high elution rate and reduced water utilization.
- We model contaminant elution from particle characteristics and operation settings.

ARTICLE INFO

Article history:
Received 18 October 2012
Received in revised form 30 January 2013
Accepted 1 February 2013
Available online 10 February 2013

Keywords:
Specific surface area related elution velocity distribution
Granular biofilter media
Particle size distribution
Water irrigation rate
Filter moisture content
Liquid holdup

ABSTRACT

Elution of inhibitory metabolites is a key parameter controlling the efficiency of air cleaning bio- and biotrickling filters. To the authors knowledge no studies have yet considered the relationship between specific surface area related elution velocity and physical media characteristics, which constitutes a scientific gap. This study investigates the impact of particle size distribution (considering materials with multiple particle sizes) and irrigation rate on the overall specific surface area related elution velocity distribution in porous granular media. The elution measurements performed in this study are performed at a concurrent airflow of 0.3 m s^{-1}, water irrigation rates of 1–21 cm h^{-1} in materials with particle diameters ranging from 2 to 14 mm to represent media and operation conditions relevant for low flow biotrickling filter design. Specific surface area related elution velocity distribution was closely related to the filter water content, water irrigation rate, media specific surface area and particle size distribution. A predictive model linking the specific surface area related elution velocity distribution to irrigation rate, specific surface area and particle size distribution was developed and predicted the observed specific surface area related elution velocity distributions with a mean error of 9%.

1. Introduction

Biofiltration is a cost effective air pollution control technology [1,2]. A frequent cause of poor biofilter performance is insufficient moisture content and non-uniform moisture distribution within the biofilter medium [3]. Controlling biofilter moisture level is important for biofilter efficiency, as drying of the biofilter medium can reduce biofilter efficiency due to gas flow channeling and localized dry spots with low microbial activity [4–11]. To maintain suitable biofilter moisture content, biofilters often receive pre-humidified air and/or irrigation [6,8,10–12]. Strictly speaking irrigated biofilters becomes biotrickling filters as soon as a moving water phase is present, however, as this study focus on low flow biotrickling filters the term biofilter will be applied to indicate the low irrigation velocity. Irrigation of biofilters can further be utilized for distribution of nutrients, controlling pH and removal of toxic degradation products, all crucial parameters for biofilm activity and biofilter performance [13–15]. In contrast, high volumetric water content (caused by high irrigation rates) can reduce biofilter efficiency by reducing oxygen and substrate supply to the biofilm (especially hydrophobic gaseous compounds) [16–19]. Even in irrigated biofilters, if the water is not evenly distributed in the filter bed, local dry areas or areas with reduced water flow can develop [20], resulting in reduced biomass activity which can lead to decreased overall biofilter performance. Media which facilitates homogeneous distribution of the water flow/water exchange across the complete media specific surface areas therefore seem optimal.

Although water supply to the media specific surface area is known to be a crucial biofilter property relatively little is known about this phenomenon. Distribution of water/air in biofilters is often described through the so-called residence time distribution (RTD), a distribution obtained through tracer tests, where pulses

* Corresponding author. Tel.: +45 9640 8493; fax: +45 9635 0558.
E-mail address: rra@bio.aau.dk (R.R. Andreasen).

1385-8947/$ - see front matter © 2013 Elsevier B.V. All rights reserved.
http://dx.doi.org/10.1016/j.cej.2013.02.002

Nomenclature

a_t	filter medium specific surface area ($L^2\,L^{-3}$)
C	concentration ($M\,L^{-3}$)
C_d	drainage water salt concentration ($M\,L^{-3}$)
$C_{im\text{-}w}$	immersion water salt concentration ($M\,L^{-3}$)
d_p	particle diameter (L)
d	particle diameter (L)
d_m	mean particle diameter (L)
K_0	empirical constant (−)
K_1	empirical constant (−)
L	filter length (L)
MRE	mean relative error (−)
M_d	mass of drained water (M)
M_{wet}	mass of wet filter media (M)
M_{dry}	mass of dry filter media (M)
M_R	mass of residual salt in the filter media at experiment termination (M)
M_E	eluted salt mass (M)
M_0	initial salt mass (M)
RTD	residence time distribution (−)
S-RTD	specific surface area water retention time distribution
n	number of measurements (−)
q	elution quantile (−)
Q	flow rate ($L^3\,T^{-1}$)
R	particle size range (L)
N_q	number of eluted water filled pore volumes at a given quantile, q = 10%, q = 50% and q = 90% (−)
V	superficial liquid velocity ($L\,T^{-1}$)
WFPV	water filled pore volume (−)
$V_{im\text{-}w}$	volume of immersion water (L^3)
P	parameter for empirical fit
q	quantile (eluted salt/total salt) (−)
t	time (T)
t_q, t_{10}, t_{50}, t_{90}	quantile elution time for: any q, q = 10%, q = 50% and q = 90% (T)

Greek letters

α	empirical constant (−)
β	empirical constant (−)
κ_1	empirical constant (−)
κ_2	empirical constant (−)
γ	empirical constant (−)
θ	volumetric water content ($L^3\,L^{-3}$)
μ	viscosity ($M\,T\,L^{-3}$)
ρ	density ($M\,L^{-3}$)
Φ	porosity ($L^3\,L^{-3}$)
Δt	Time interval between measurements (T)

Sub and super scripts

$'$	aggregated empirical constant
N	parameter for N
dyn	dynamic
st	static
b	bulk
w	water
p	particle

of tracer are led through saturated as well as unsaturated columns [21–24]. Simplified RTD in a porous media is an artifact of the presence of mobile and immobile water volumes as well as their internal mass transfer. This means that RTD in theory only depend on these volumes and thereby only indirectly are connected to the media specific surface area. RTD's are therefore independent of inter media dry spots as these do not contribute to the transport nor the retention of tracer. This means that RTD cannot be directly applied for estimating the utilization potential (wetted surface area/total surface area) of the medium. In fact to the authors knowledge no study has addressed specific surface area water retention time distribution (S-RTD) as related to irrigation rate and filter medium particle size distribution in biofilters with air flow based on tracer elution measurements.

The objective of this study is therefore, to develop a method for estimating S-RTD and relate it to media particle size distribution and irrigation rate. The aim is to assess S-RTD as a function of irrigation rate and particle size distribution. S-RTD will be assessed based on breakthrough curves using chloride as a tracer for a range of seven different irrigation rates applied to media with 21 different particle size distributions with particle sizes of 2–14 mm.

As the focus of this study is on the relation between material physical properties and S-RTD, investigations will be carried out under conditions where no biomass is present. This is done to fully understand the link between the S-RTD and the physical properties of the utilized medium. It is recognized that biomass strongly affects biofilter water content as well as pore size distribution [25]. Therefore the results provided in this study cannot be applied directly to biofilters containing biomass, as the presence of biomass is likely to alter the distribution of water. However as this study mainly serves to understand and describe the link between S-RTD and medium physical characteristics, investigations based on clean media were preferred, as uneven distribution of biomass within the filter media will introduce additional uncertainties and complicate the understanding of the relationship.

2. Theory

Irrigation water added to the top of a biofilter will trickle down through the medium creating local regions with different water velocities. The distribution of these velocities depends on the quantity of water held in the filter defined as the total liquid holdup. The total liquid holdup (θ) in irrigated porous media constitutes the dynamic (θ_{dyn}) and static (θ_{st}) holdup. Traditionally the θ_{dyn} in a trickle bed reactor is defined as the drainable volume after gas and liquid flow through the bed are stopped, while the θ_{st} is the remaining volume after drainage [26]. This static holdup consists of the liquid in the intra-particle pores (only for porous particles) as well as the liquid held in the inter-particle pores [26]. Static and dynamic holdup in soils (often labeled water retention) have been investigated extensively [27–29], and a wide selection of predictive expressions are available [27–29]. Soils, however, consists of particles that are typically 2–5 orders of magnitude smaller than for biofilters, thus, flow and retention properties of soils are very different from those found in most biofilter materials. Several correlations relevant for biofilter materials have been proposed [30–35] for predicting these holdups which for materials consisting of spherical particles can be written as:

$$\mathbf{P} = K_1 V^{\alpha} a_t^{\beta} + K_o \tag{1}$$

where **P** is either θ_{dyn} or θ, V is the superficial liquid velocity, a_t is the specific surface area = $6(1-\Phi)\,d_p^{-1}$, where Φ is total porosity and d_p is particle diameter and K_1 is a combined correlation specific constant including various parameters such as gas and liquid viscosity, gas and liquid density and media porosity. Parameters α, β

and K_0 are empirical constants. An overview of the values of α, β and K_0 proposed in various studies can be found in Table 1.

3. Materials and methods

3.1. Media used

Water flow exchange characteristics in biofilter material were investigated using media consisting of crushed granite. This material was chosen because of its very low internal porosity (0.4–1.5%). Granite further has the advantage of being relatively inert and mechanically stable compared to other biofilter media such as straw or woodchips. The granite were provided by a local supplier and sieved into six particle size fractions. These fractions had a particle size range (R) of 2 mm, and particle diameters (d) of $2 \leqslant d < 4$ mm, $4 \leqslant d < 6$ mm, $6 \leqslant d < 8$ mm, $8 \leqslant d < 10$ mm, $10 \leqslant d < 12$ mm and $12 \leqslant d < 14$ mm corresponding to mean particle diameter (d_m) values of 3, 5, 7, 9, 11 and 13 mm, respectively. Additional fractions with $R = 4$ mm ($d_m = 4$, 6, 8, 10, 12 mm), $R = 6$ mm ($d_m = 5$, 7, 9, 11 mm), $R = 8$ mm ($d_m = 6$, 8, 10 mm), $R = 10$ mm ($d_m = 7$, 9 mm) and $R = 12$ mm ($d_m = 8$ mm and uniform particle size distribution were produced by combining appropriate quantities (by weight) of the original $R = 2$ mm size fractions. Uniform particle size distributions were chosen for two reasons: (I) that biofilter materials are usually available in pre-sorted fractions and (II) to have well-defined and identical particle size distribution shapes for all fractions, simplifying the subsequent comparison of media properties. Each fraction was prepared using air dry particles.

3.2. Experimental setup

The experimental set-up consisted of a vertical 38 cm long, 25 cm inner diameter steel ventilation tube connected to a CUBU-FAN 160 EC ventilation pump (Jenk, Brøndby Denmark). Air flow through the media was measured in the inlet to the pump using a VA400 thermal mass flow sensor, (CS instruments Tannheim Germany) calibrated by the manufacturer. A nozzle for spraying irrigation liquid was mounted 51 cm above the filter medium inlet surface. The nozzle was fed with a mixture of liquid and pressurized air in order to achieve adequate liquid distribution across the inlet surface of the filter. Nozzle liquid was supplied by a Iwaki Metering pump C30, (Iwaki pumps, Japan) connected to a supply of both demineralized water (≈25 μS) and NaCl solution (≈30 g L^{-1} - ≈ 50,000 μS) via a 3-way valve enabling instant change of irrigation liquid. The total volume of the tube leading from the valve to the nozzle outlet was 63 mL. The measured breakthrough curves were subsequently corrected for the time delay caused by this volume, assuming plug flow in the tubes. The outlet liquid was collected in a funnel and led through a flow cell with a WTW Tetracon® 925 standard conductivity measuring cell connected to a WTW Multi 3420 digital pH/D.O./conductivity meter logging the conductivity every 30 s. The total liquid filled volume of the outlet catchment system was 8 mL. The measured breakthrough curves were subsequently corrected for the time delay caused by this volume, assuming plug flow. A schematic of the experimental set-up is shown in Fig. 1.

Table 1
Values of α, β and K_0 in (Eq. (1)) for dynamic (θ_{dyn}) and total (θ) water holdups.

P	α	β	K_0	Study
θ_d	0.51	0.81	0	[30]
θ_d	1.3	(included in K_1 and K_0)	≠0, media specific	[31]
θ_d	1/3	1/3	0	[32]
θ_d	0.565	0.695	0	[33,34]
θ	0.11	0.03	0	[35]

3.3. Measurements

Prior to measurement of each breakthrough curve the NaCl solution was prepared and used throughout the measurement. Each particle size fraction was immersed in the NaCl solution for 5 min and drained for 1 min. This procedure was repeated twice with the solution exchanged between the immersions to ensure the inter-particle NaCl concentration was similar to the NaCl solution.

After the 2nd drainage each individual particle size fraction was packed to a height (L) of 30 cm in the filter column and irrigated with the NaCl solution without air flow for 30 min. The measurements were initiated by switching the irrigation pump inlet to clean water, starting the filter airflow and initiating the conductivity measurements at the filter outlet. This procedure was performed to create a gravity equilibrated water saturation level in all particle size fractions at the start of the measurements. Immediately following initiation of the outlet conductivity measurements outlet water flow was measured by collecting the water every minute and measuring the mass until stable flow was observed. Small initial variations in the outlet flow occurred but the flow stabilized within 10 min after initiation of the measurements. As the flow variations were small and lasted only a very short time compared to the total duration of the experiment, they were ignored in the subsequent calculations. Prior to the termination of the air and water flow, three measurements of the outlet water flow were performed to verify that the flow remained stable. Breakthrough curves were measured at irrigation rates, $V = 3$ cm h^{-1} for all 21 particle size fractions and at $V = 1$, 2, 5, 8, 13 and 21 cm h^{-1} for the 2–4 mm, 12–14 mm, 2–14 mm and 6–10 mm particle size fractions (Table 2). This velocity span was chosen as a tradeoff between simulating low trickling velocities and being in-sensitive to the inlet gas humidity level. All measurements were carried out in duplicate at room temperature.

All water draining from the filter immediately following termination of the air and water flow was collected and both the drained filter material and the collected water were weighed (M_{wet} and M_d respectively). After M_{wet} determination the filter material was immersed into 11 L of demineralized water (≈25 μS) to dissolve any salt residue present on the material and then air dried and weighed (M_{dry}). These values were then used to calculate θ as:

$$\theta = \frac{M_{wet} + M_d - M_{dry}}{\text{filter volume}} \quad (2)$$

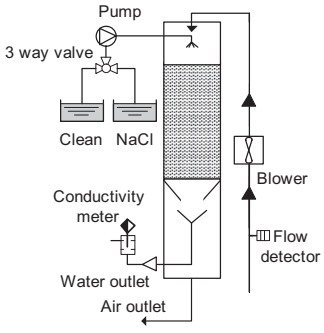

Fig. 1. Experimental set-up.

Table 2
Physical characteristics of the 21 granite particle size fractions with uniform particle size distribution used in this study, in terms of: Particle size, dry bulk density (ρ_b), total porosity (Φ) and specific surface area (a_t).

Fraction (mm)	ρ_b (kg m^{-3})	Φ (m^3 m^{-3})	a_t (m^2 m^{-3})
2–4	1472	0.45	1090
4–6	1622	0.40	721
6–8	1530	0.43	486
8–10	1538	0.43	380
10–12	1496	0.45	302
12–14	1507	0.44	258
2–6	1509	0.44	894
4–8	1516	0.44	578
6–10	1537	0.43	434
8–12	1507	0.44	338
10–14	1502	0.44	280
2–8	1507	0.44	755
4–10	1522	0.44	512
6–12	1518	0.44	388
8–14	1489	0.45	308
2–10	1510	0.44	660
4–12	1544	0.43	467
6–14	1544	0.43	362
2–12	1528	0.43	596
4–14	1558	0.42	431
2–14	1554	0.43	550

and the residual salt mass (M_R) at experiment termination as:

$$M_R = M_d \rho_W^{-1} C_d + V_{im-w} C_{im-w} \quad (3)$$

where C_d is the salt concentration in the drainage water, ρ_w is the drained water density (assumed 1 kg L), $V_{\text{im-w}}$ is the volume of immersion water (11 L) and $C_{\text{im-w}}$ is the measured salt concentration in the immersion water.

Cumulative eluted salt mass from the filter as a function of time during each experiment (M_E) was calculated using the measured water flow rate and outlet salt concentrations.

$$M_E = Q\Delta t \sum_{i=1}^{i=n} C_i \quad (4)$$

where Q is the mean outlet water flow, Δt is the time interval between measurements, n is the number of measurements conducted up to time t and C_i is the ith measured outlet concentration. Total initial salt mass (M_0) in the filter was calculated as the sum of M_R and M_E at the end of each experiment. Based on these data the eluted quantile (q) of M_0 (M_E/M_0) at any given time (t) following initiation of the freshwater irrigation was determined.

3.4. Packed media characterization

Packed media dry bulk density (ρ_b) for each particle size fraction was determined based on M_{dry} and the packed filter bed volume.

Total porosity was determined as:

$$\Phi = 1 - (\rho_b \rho_p^{-1}) \quad (5)$$

where ρ_p is the solids density of the granite particles assumed equal to 2.7 g cm^{-3}. An overview of the measured ρ_b, and Φ of the granite media is given in Table 2.

Estimates of a_t for the particle size fractions were calculated assuming spherical particles as:

$$a_t = \frac{6\sum_1^n \left(\frac{1}{d_{mi}}\right)}{n} \frac{\rho_b}{\rho_p} \quad (6)$$

where d_{mi} is the mean diameter of the ith (R = 2 mm) fraction and n is the number of R = 2 mm fractions used to produce the particle size fraction in question. As the particle shape of crushed granite is quite variable, the spherical surface to volume ratio applied in Eq. (6) is most likely not correct for the media used here. However, the surface to volume ratio of spheres (6 (particle diameter)$^{-1}$) is similar to the surface to volume ratio for various shapes including cubes (6 (side length)$^{-1}$), tetrahedrons ($(6\sqrt{6})$ (side length)$^{-1}$) and octahedrons ($(3\sqrt{6})$ (side length)$^{-1}$). The assumed specific surface area based on spherical particle shape is therefore likely to be directly proportional to the true specific surface area of the media assuming particle shapes across the media particle size fractions to be equal.

3.5. Predictive model evaluation

Model prediction accuracy was quantified using the mean relative error (MRE), defined as:

$$\text{MRE} = \frac{1}{n}\sum_{i=1}^{n}\left(\frac{Abs(\text{Measured} - \text{Predicted})}{\text{Measured}}\right) \quad (7)$$

where n is the number of measured data points.

MRE was chosen as MRE weight all deviations according to their relative size. This weighting of errors was chosen for the data of this study as the temporal duration of the breakthrough curves varied by a factor 20 due to differences in irrigation rate and medium particle size distribution.

4. Results and discussion

Breakthrough curves for elution of salt from the filters are shown for selected particle size distributions and irrigation rates in Fig. 2. The effluent salt concentration for all combinations of media particle size fractions and irrigation rates (V) was observed to decrease with time. The rate of decrease increased with increasing values of d_m and V. For media with R > 2 mm the rate of decrease in concentration with time generally exhibited intermediate values compared to the rates of the decrease for the R = 2 mm fractions used to produce the fraction in question.

This observation was further confirmed when comparing the time required for elution of 90% of the initial salt mass in the filter (t_{90}) for a given particle size fraction with the corresponding d_m and R as can be seen in Fig. 3 where t_{90} for an irrigation rate of 3 cm h^{-1} is shown as a function of d_m and R.

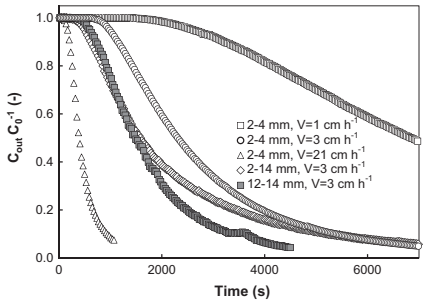

Fig. 2. Relative effluent salt concentration as a function of time during elution of salt from selected filter media particle size distributions and irrigation rates.

In Fig. 3 it is seen that t_{90} increases for increasing R and decreasing d_m, such that t_{90} of a fraction with $R > 2$ mm assumes an intermediate value among the t_{90} values of the $R = 2$ mm fractions used to produce it. Increasing t_{90} for increasing R means that although t_{90} for $R > 2$ mm fractions are intermediates among the t_{90} values for their constituting $R = 2$ mm fractions, t_{90} is more sensitive to the smaller particles (having a high t_{90}) present than to the large particles (having lower t_{90}). Similar observations were also made for the time required to elude 10% (t_{10}) and 50% (t_{50}) of the initial salt mass indicating that this is the case for the time (t_q) to reach any given elution quantile (q). Values of t_{10}, t_{50} and t_{90} were further observed to depend on irrigation rate as shown in Fig. 4 where measured $\log(V) - \log(t_q)$ data for $q = 10\%$, 50%, and 90% are plotted for four different particle size fractions.

$\text{Log}(t_{10})$, $\log(t_{50})$ and $\log(t_{90})$ decrease approximately linearly with increasing $\log(V)$ with slopes of −0.93, −0.91 and −0.80 ($\log(t_q)\ \log(V)^{-1}$) ($R^2 = 0.97$, 0.98 and 0.95) respectively. The relationships indicate an almost hyperbolic relationship between t_q and V especially for lower q ($t_q \sim V^{-1}$). This strongly indicates that the volume of irrigation water ($=Q{\cdot}t_q$) required to reach a given q is almost independent of V at low q ($q < 50\%$) while V is more important at higher q. As t_q is related to particle diameter it is also related to the specific surface area of the medium, a_t. As numerous studies have found a strong correlation between a_t and θ_{dyn} or θ [30,32–35], differences in θ are likely the main cause of the variations in t_q across different particle size distributions. For a given q the corresponding number of eluted water filled pore volumes (N_q) can be calculated as:

$$N_q = \frac{Vt_q}{\theta L} \tag{8}$$

where L is the filter length. Values of N_{10}, N_{50} and N_{90} for all fractions at $V = 3$ cm h^{-1} and for the 2–4 mm, 12–14 mm, 6–10 mm and 2–14 mm fractions at $V = 1$ cm h^{-1} and 21 cm h^{-1} are plotted against a_t in Fig. 5.

It is seen that N_{10}, N_{50} and to some extent also N_{90} are relatively independent of both a_t and V with mean values of 0.10, 0.58, and 2.27 for N_{10}, N_{50}, and N_{90}, respectively (Fig. 5). However N_{90} increases for increasing V, while no direct trend can be seen with respect to a_t. This means that to elude 10%, 50% or 90% of salt, a water volume corresponding to 10%, 58% and 227% of the water filled pore volumes (WFPVs), must be eluded. The elution from 0 to 10% of salt, occurs at 1% salt eluted pr. 1%WFPV added. In contrast the elution from 50% to 90% of salt, occurs at 0.2% salt eluted pr. 1%WFPV added. Thus the elution from 0 to 10% is much more efficient than the from 50% to 90%. This is in agreement with the observations from Fig. 4 where the slopes of the $\log(V) - \log(t_{10})$ and $\log(V) - \log(t_{50})$ are close to −1 (a slope of −1 indicate independency between N_q and V). This observation is somewhat in contrast to observations by Marcandelli et al. [36] who observed the distribution of liquid perpendicular to the flow direction to even out at increasing V. However, although the horizontal mobile liquid distribution (as described by Marcandelli et al. [36]) must be expected to be crucial for media t_q, the horizontal distribution alone is not enough to describe the total liquid distribution as it does not

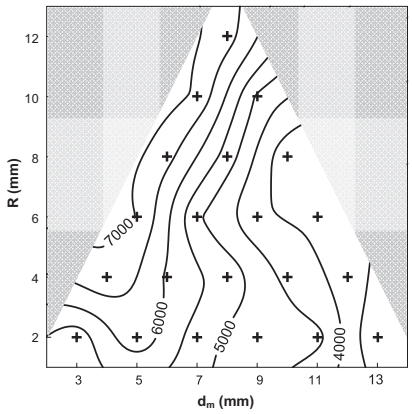

Fig. 3. t_{90} as a function of d_m and R at an irrigation rate of 3 cm h^{-1}. Contours indicate kriged values, black crosses indicate measured values and shaded regions indicate extrapolation.

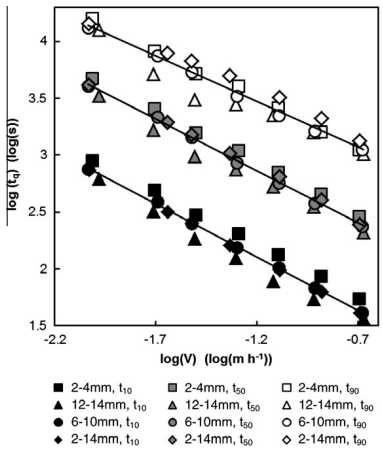

Fig. 4. $\text{Log}(V) - \log(t_q)$ for four different particle size distributions.

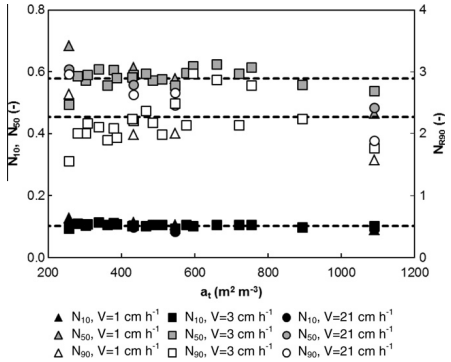

Fig. 5. N_{10}, N_{50} and N_{90} as a function of a_t (Eq. (6)). Dashed lines represent average values of all observed N_{10}, N_{50} or N_{90} values.

include stagnant water. As filter beds contain both stagnant and moving water [26,37] salt present in stagnant (or slowly moving) water will not be removed in direct proportion to the speed of the (fast) moving water. The main impact of water velocity is therefore to be found in the velocity and volume of the moving water phase. This hypothesis would state the main elution of a given q to be directly proportional to the corresponding N_q as long as the removed salt mass are to be found in the moving water phase (affected by velocity). As the initially eluted salt mass must be dominated by the salt mass present in the mobile volumes this hypothesis corresponds well with the found $N_{10} = 0.1$. Once the mobile water volume have been exchanged by freshwater, the main source of eluted salt must be salt transported from the stagnant volumes to the mobile volumes, causing the outlet concentration to drop as it consist of freshwater spiked with salt from the stagnant zones. In this case the elution of salt becomes less affected by the velocity of the mobile water as the dominant parameter is the transfer of mass from the stagnant to the moving water volumes. As this phenomena must be dominating after irrigation of one WFPV (all mobile water exchanged) this hypothesis is supported by the observation of $N_{90} > 0.90$ as well as the observed increase in N_{90} at increasing V.

The filter holdup, θ, depended on both a_t and V (Fig 6a and b). This observation is in agreement with several studies [30,32–35] who linked θ_{dyn} or θ to a_t and V through power functions similar to Eq. (1). Eq. (1) with $K_1 = 0.035$, $\alpha = 0.11$, $\beta = 0.32$ and $K_0 = 0$ was found to describe θ (−) as a function of a_t ($m^2\ m^{-3}$) and V ($m\ s^{-1}$) well with a mean relative error (MRE) of 3% (Fig. 6a and b). Choosing a $K_0 \neq 0$ reduced MRE by <0.01% and K_0 was therefore excluded from the modeling.

Based on the observed relatively constant N_q values and the correlation between θ, a_t and V, we suggest that t_q as a function of a_t and V is expressed as:

$$t_q = \frac{N_q \theta}{V} L = \frac{N_q K_1 V^{\alpha} a_t^{\beta}}{V} L \tag{9}$$

Eq. (9) was found to describe the observed t_{10}, t_{50} and t_{90} data well with a MRE of 6%, 5% and 13%, respectively (Fig. 7).

Fig. 7 indicates that Eq. (9) may in fact be used to describe t_q for any value of V, q, a_t, θ, and N_q across different particle size fractions.

As a first step, an empirical expression for predicting N_q was established based on the following reflections: a) N_q should be proportional to q at low q and increase at higher q (obtained by the $(q + \kappa_1 q^{\kappa 2})$. As the expression of N_q will be applied together with the expression for θ addition of a constant (K_{1_N}), V^{α_N} and $a_t^{\beta_N}$ can be done without increasing the total amount of aggregated empirical parameters and R^{γ} was added as inhomogeneity is known to be a parameter of impact regarding preferential flow and thereby the relationship between moving and stagnant volumes [38–40]. As the effect of stagnant volumes are significant only at higher q, the R parameter was placed inside the brackets of the first right-side term of Eq. (10)).

$$N_q = (q + \kappa_1 q^{\kappa_2} R^{\gamma}) K_{1_N} V^{\alpha_N} a_t^{\beta_N} \tag{10}$$

where κ_1 and κ_2 are empirical constants describing the relationship between N_q and q, γ describes the impact of R, α_N the impact of V, and β_N the impact of a_t.

Combining Eqs. (9) and (10) yields:

$$t_q = \frac{\left((q + \kappa_1 q^{\kappa_2} R^{\gamma})\right) K_{1_N} V^{\alpha_N} a_t^{\beta_N}\right)(K_1 V^{\alpha} a_t^{\beta})}{V} L \quad \text{or simply}$$

$$\vdots \quad \frac{\left((q + \kappa_1 q^{\kappa_2} R^{\gamma}) K_1' V^{\alpha'} a_t^{\beta'}\right)}{V} L \tag{11}$$

where $K_1' = K_1 K_{1R}$, $\alpha' = \alpha + \alpha_R$ and $\beta' = \beta + \beta_R$.

To test Eq. (11) q and corresponding t_q values were calculated from each effluent concentration measurement considering all particle size fractions and irrigation rates (a total of 18,370 data points). Eq. (11) was then fitted to these data using with κ_1, $\kappa 2$, γ, K_1', α' and β' as fitting parameters while minimizing the MRE for all data combined. Resulting values of the model constants were $\kappa_1 = 9.7$, $\kappa_2 = 5.75$, $\gamma = 0.28$, $K_1' = 0.072$, $\alpha' = 0.13$ and $\beta' = 0.25$ (corresponding to $K_{1_N} = 2.1$, $\alpha_N = 0.016$ and $\beta_N = -0.075$). With these parameter values, the model was found to describe the measured data well with a MRE of 9.0% (Fig. 8). In addition the robustness of Eq. (11) was tested by excluding one parameter at a time (V in the denominator was not removed as this parameter is not included in the original empirical equations for θ and N_q, see Eq. (9)). This was done by fitting Eq. (11) with one of the following fixed constants: $\kappa_1 = 1$, $\kappa_2 = 0$, $\gamma = 0$, $K_1' = 1$, $\alpha' = 0$ and $\beta' = 0$. Resulting MRE were then: 11%($\kappa_1 = 1$), 28%($\kappa_2 = 0$), 13%($\gamma = 0$), 13%($K_1' = 1$), 12%($\alpha' = 0$) and 10% ($\beta' = 0$).

The positive value of γ given above indicates that N_q increases for increasing R. This correlation could be caused by stagnant/semi-stagnant liquid volumes created by an increased variety of pore sizes. Large pore size variation is known to facilitate preferential flow in the macropores even as film flow at unsaturated conditions [38–40]. It is therefore likely that the presence of preferential flow causes a smaller part of the possible pathway area (constituted by a_t) to conduct a relatively large fraction of the total water flow and thereby bypassing/establishing stagnant/semi-stagnant zones. However, it should be noted that as other studies have found macropore flow to affect solute transport only at saturated

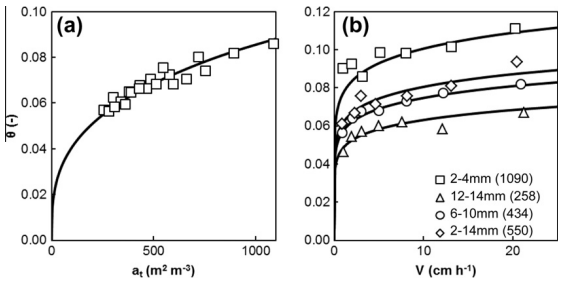

Fig. 6. (a) θ as a function of a_t for all 21 particle size fractions used in this study at $V = 3$ cm h^{-1}. (b) θ as a function of V for the 2–4 mm, 2–14 mm, 6–10 mm and 12–14 mm particle size fractions. Numbers in brackets indicate a_t for the fractions and solid lines represents Eq. (1) with $K_1 = 0.035$, $\alpha = 0.11$, $\beta = 0.32$ and $K_0 = 0$.

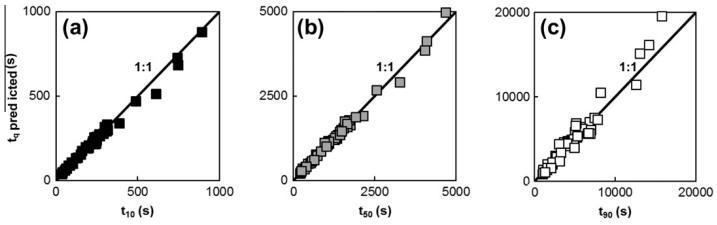

Fig. 7. 1:1 plots of observed versus predicted t_{10} (a) t_{50} (b) and t_{90} (c) using Eq. (9) with K_1 = 0.035, α = 0.11, β = 0.32 (Fig. 6) and N_{10}, NR_{50}, and N_{90} equal to their observed average (0.10, 0.58 and 2.27, respectively, (Fig. 5)).

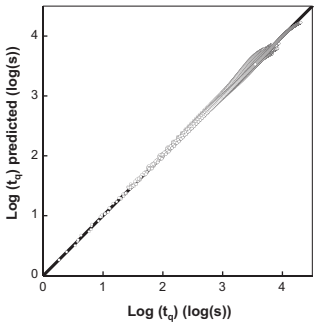

Fig. 8. Measured and predicted (Eq. (11)) values of t_q for all measured breakthrough data across all particle size fractions and irrigation rates (18,370 data points).

conditions [41], the direct effect of pore size could be questioned. Another explanation could be found in the correlation between the quantity of stagnant water and the number of particles present, as inter particle contact points are known to create static liquid menisci [42] and thereby increase the volumetric static water fraction. An increased R could also be assumed to affect the elution through an increased a_t as $a_t^{1/3}$ have been found directly proportional to the static water holdup (θ_{st}) in packed bed reactor studies [32]. Increasing a_t resulted in decreasing N_q as reflected in the negative value of β_N. The reason could be that the stagnant water content is controlled by the number of particles present and the heterogeneity of the media while the total (including the mobile) water content is more dependent on a_t. Higher a_t therefore means that a larger fraction of the water present in the filter is mobile which means that a given q is reached in a shorter time yielding a lower N_q. However as the a_t–N_q relationship observed in this study was observed over a relatively small range of a_t's a verification of this trend should be based on a wider range of a_t's. In addition it should be noted that the term mobile and stagnant water in this study is a relative term applied to describe the observed effect of various water film velocities in the inter-particle pores. Hence, a high N_q is in reality caused by a wide volumetric water flow velocity distribution causing great variety between the fastest flowing and slowest flowing water volumes, rather than the presence of true immobile water.

Finally the positive although small value of α_N supports the previously discussed (in connection with Fig. 5) effect of V on t_q at higher q. This means that it is possible to calculate t_q in a known biofilter medium for any q based on a six empirical constants relating N_q to media characteristics as well as biofilter operation conditions. It should further be noted that both t_q and N_q decrease for decreasing R. This suggests that a better removal of metabolites will occur when using materials with a narrow particle size distribution. The most optimal would be to use media consisting of uniformly sized particles, which besides ensuring optimal water utilization also is known to reduce biofilter pressure drop, a crucial parameter for the biofilter operation cost [43]. As increasing V similar decrease t_q but increase N_q increasing V can be applied to reduce t_q. However as increasing V also decrease the water effectiveness (elution/water volume), this should be done with caution.

To apply knowledge of media t_q distribution to full-scale biofilters, biomass activity as a function of surface water residence time should be known. Assuming q to be proportional to the quantile of specific surface with a replaced water phase, the t_q distribution becomes equal to the residence time distribution of the complete media specific surface area, (in contrast to traditional RTD). Knowing this distribution and the equivalent biomass activity will enable engineers and researchers to calculate an activity coefficient stating how active the media specific surface area will be as related to its S-RTD. This can then be used to select the appropriate level of irrigation for a given filter material. It should further be noticed that the presence of biofilm probably will alter the results gained in this study as these are based on clean media. Based on the procedure presented in this paper, new S-RTD describing constants for media with biomass could be determined. However as biofilm is a water accessible medium, the presence of biofilm will produce stagnant water accessible volumes beneath surfaces with a newly exchanged water film. This means that the presence of biofilm will increase t_q even if the true specific surface area related water retention time remains unchanged.

5. Conclusion

In this study the elution of contaminant from irrigated reactors (such as biotrickling filters) were investigated using solid granite particles of 2–14 mm of diameter. Elution was measured based on freshwater breakthrough curves through salt water soaked porous filter media. Measurements were carried out for media of 21 different particle size distributions and at seven velocities. Elution time, defined as the time for a given fraction (quantile) of the initial salt mass to be eluted (t_q), was found proportional to the elution quantile, irrigation velocity, hydraulic holdup, specific surface area, and particle size range for the medium. It was further noticed that the total irrigated liquid volume to reach a given elution quantile was almost constant for elution quantiles below 50% regardless of particle size distribution and irrigation velocity. A predictive model based on these observations were proposed and found to fit all data (18370 t_q data points) well with a mean relative error

of 9.0% based on six empirical parameters. The most optimal medium was found to be consisting of uniformly sized particles.

Acknowledgements

Helle Blendstrup and Jesper Svenningsen who carried out 95% of the operable measurements, involving washing, packing and excavating granite in 20 kg batches.

References

[1] L. Chen, S.J. Hoff, Mitigating odors from agricultural facilities: a review of literature concerning biofilters, Appl. Eng. Agric. 25 (5) (2009) 751–766.
[2] D.H. O'Neill, I.W. Stewart, V.R. Phillips, A review of the control of odour nuisance from livestock buildings: Part 2. The costs of odour abatement systems as predicted from ventilation requirements, J. Agric. Eng. Res. 51 (1992) 157–165.
[3] J.S. Devinny, J. Ramesh, A phenomenological review of biofilter models, Chem. Eng. J. 113 (2–3) (2005) 187–196.
[4] I. Datta, D.G. Allen, Biofilter Technology, in: Z. Shareefdeen, A. Singh, (Eds.), Biotechnology For Odor And Air Pollution Control, Springer-Verlag, 2005, pp. 125–145.
[5] M.C. Delhomenie, M. Heitz, Biofiltration of air: a review, Crit. Rev. Biotechnol. 25 (1–2) (2005) 53–72.
[6] H. Van Langenhove, E. Wuyts, N. Schamp, Elimination of hydrogen sulphide from odorous air by a wood bark biofilter, Water Res. 20 (12) (1986) 1471–1476.
[7] P.A. Gostomski, J.B. Sisson, R.S. Cherry, Water content dynamics in biofiltration: the role of humidity and microbial heat generation, J. Air Waste Manag. Assoc. 47 (9) (1997) 936–944.
[8] H.H.J. Cox et al., Influence of the water content and water activity on styrene degradation by Exophiala jeanselmei in biofilters, Appl. Microbiol. Biotechnol. 45 (6) (1996) 851–856.
[9] S. Krailas et al., Effect of inlet mass loading, water and total bacteria count on methanol elimination using upward flow and downward flow biofilters, J. Chem. Technol. Biotechnol. 75 (4) (2000) 299–305.
[10] B. Sheridan et al., Biofiltration of odour and ammonia from a pig unit – a pilot-scale study, Biosyst. Eng. 82 (4) (2002) 441–453.
[11] R. Auria, A.C. Aycaguer, J.S. Devinny, Influence of water content on degradation rates for ethanol in biofiltration, J. Air Waste Manag. Assoc. 48 (1) (1998) 65–70.
[12] S. Revah, J.M. Morgan-Sagastume, Methods of Odor and VOC Control, in: Z. Shareefdeen, A. Singh, (Eds.), Biotechnology For Odor And Air Pollution Control, Springer-Verlag, 2005, pp. 29–63.
[13] M.J. Gribbins, R.C. Loehr, Effect of media nitrogen concentration on biofilter performance, J. Air Waste Manag. Assoc. 48 (3) (1998) 216–226.
[14] Y. Cohen, Biofiltration – the treatment of fluids by microorganisms immobilized into the filter bedding material: a review, Bioresour. Technol. 77 (3) (2001) 257–274.
[15] T. Yamamoto et al., Odor Pollution Control, in: L.K. Wang, N.C. Pereira, Y.-T. Hung (Eds.), Advanced Air and Noise Pollution Control, Humana Press, 2005, pp. 273–334.
[16] A. Singh, O. Ward, Microbiology of Bioreactors for Waste Gas Treatment, in: Z. Shareefdeen, A. Singh (Eds.), Biotechnology For Odor And Air Pollution Control, Springer-Verlag, 2005, pp. 101–121.
[17] B.H. Davison et al., Influence of high biomass concentrations on alkane solubilities, Biotechnol. Bioeng. 68 (3) (2000) 279–284.
[18] M.B. Bagherpour et al., Effects of irrigation and water content of packings on alpha-pinene vapours biofiltration performance, Biochem. Eng. J. 24 (3) (2005) 185–193.
[19] S.C. Popat, M.A. Deshusses, Analysis of the rate-limiting step of an anaerobic biotrickling filter removing TCE vapors, Process Biochem. 45 (4) (2010) 549–555.
[20] M.J. Mysliwiec et al., Dynamic volume-averaged model of heat and mass transport within a compost biofilter: I. Modal development, Biotechnol. Bioeng. 73 (4) (2001) 282–294.
[21] M. Martinov, D. Hadjiev, S. Vlaev, Liquid flow residence time in a fibrous fixed bed reactor with recycle, Bioresour. Technol. 101 (4) (2010) 1300–1304.
[22] S. Sharvelle, E. McLamore, M.K. Banks, Hydrodynamic characteristics in biotrickling filters as affected by packing material and hydraulic loading rate, J. Environ. Eng. – Asce 134 (5) (2008) 346–352.
[23] M. Salazar, M. Morales, S. Revah, Biodegradation of methyl tert-butyl ether by cometabolism with hexane in biofilters inoculated with Pseudomonas aeruginosa, J. Environ. Sci. Health Part A – Toxic/Hazard. Substances Environ. Eng. 47 (7) (2012) 1017–1026.
[24] Y.W. Hutomo, K.L. Pinder, Effects of residence time distribution and packing on methanol oxidation in biotrickling filter, J. Air Waste Manag. Assoc. 56 (3) (2006) 334–342.
[25] R.R. Andreasen, R.E. Nicolai, T.G. Poulsen, Pressure drop in biofilters as related to dust and biomass accumulation, J. Chem. Technol. Biotechnol. (2012).
[26] S. Goto, J.M. Smith, Trickle-bed reactor performance. 1. Holdup and mass-transfer effects, AIChE J. 21 (4) (1975) 706–713.
[27] M.T. van Genuchten, A closed-form equation for predicting the hydraulic conductivity of unsaturated soils, Soil Sci. Soc. Am. J. 44 (5) (1980) 892–898.
[28] M.G. Schaap, F.J. Leij, Improved prediction of unsaturated hydraulic conductivity with the Mualem-van Genuchten model, Soil Sci. Soc. Am. J. 64 (3) (2000) 843–851.
[29] H. Vereecken, J. Maes, J. Feyen, Estimating unsaturated hydraulic conductivity from easily measured soil properties, Soil Sci. 149 (1) (1990) 1–12.
[30] T. Otake, K. Okada, Liquid holdup in packed towers, Kaguku Kogaku (Chem. Eng. Japan) 17 (1953) 176.
[31] C.N. Satterfield, P.F. Way, Role of liquid-phase in performance of a trickle bed reactor, Aiche J. 18 (2) (1972) 305–311.
[32] V.G. Rao, M.S. Ananth, Y.B.G. Varma, Hydrodynamics of 2-phase co-current downflow through packed-beds. 2. Experiment and correlations, AIChE J. 29 (3) (1983) 473–483.
[33] A.J. Colombo, G. Baldi, S. Sicardi, Solid–liquid contacting effectiveness in trickle bed reactors, Chem. Eng. Sci. 31 (12) (1976) 1101–1108.
[34] V. Specchia, G. Baldi, Pressure-drop and liquid holdup for 2-phase concurrent flow in packed-beds, Chem. Eng. Sci. 32 (5) (1977) 515–523.
[35] G.J. Stiegel, Y.T. Shah, Backmixing and liquid holdup in a gas–liquid cocurrent upflow packed-column, Ind. Eng. Chem. Process Des. Develop. 16 (1) (1977) 37–43.
[36] C. Marcandelli et al., Liquid distribution in trickle-bed reactor, Oil Gas Sci. Technol. – Rev. IFP 55 (4) (2000) 407–415.
[37] L. Baussaron et al., Wetting topology in trickle bed reactors, AIChE J. 53 (7) (2007) 1850–1860.
[38] S.E. Allaire-Leung, S.C. Gupta, J.F. Moncrief, Water and solute movement in soil as influenced by macropore characteristics – 1. Macropore continuity, J. Contam. Hydrol. 41 (3–4) (2000) 283–301.
[39] J.R. Nimmo, Preferential flow occurs in unsaturated conditions, Hydrol. Process. 26 (5) (2012) 786–789.
[40] G.W. Su, J.R. Nimmo, M.I. Dragila, Effect of isolated fractures on accelerated flow in unsaturated porous rock, Water Resour. Res. 39 (12) (2003).
[41] E. Lamy et al., Modeling the influence of an artificial macropore in sandy columns on flow and solute transfer, J. Hydrol. 376 (3–4) (2009) 392–402.
[42] I. Iliuta, F. Larachi, M.H. Al-Dahhan, Multiple-zone model for partially wetted trickle flow hydrodynamics, Chem. Eng. Res. Des. 78 (A7) (2000) 982–990.
[43] R.R. Andreasen, T.G. Poulsen, Air flow characteristics in granular biofilter media, J. Environ. Eng. 139 (2) (2003) 196–204.